Climate change impacts and mitigation measures on floods in urbanising areas

Submitted in partial fulfilment of the requirement for the award of the degree of

Doctor of Philosophy

by

Seenu P Z

Roll No. 716106

Supervisor

Prof. K.V. Jayakumar

DEPARTMENT OF CIVIL ENGINEERING
NATIONAL INSTITUTE OF TECHNOLOGY
WARANGAL-506004, INDIA

November 2021

Dedicated

To

My Son

THESIS APPROVAL FOR PH.D.

This Thesis entitled "**Climate change impacts and mitigation measures on floods in urbanising areas**" prepared by **Ms Seenu P Z** (Roll No. 716106) is approved for the degree of Doctor of Philosophy.

Examiners

_____

_____

_____

Supervisor

_____

Chairman

_____

Date:

Place:

DECLARATION

This is to certify that the work presented in the thesis entitled "**Climate change impacts and mitigation measures on floods in urbanising areas**" is a bonafide work done by me under the supervision of **Prof. K.V. Jayakumar** and was not submitted elsewhere for the award of any degree.

I declare that this written submission represents my ideas in my own words and where others' ideas or words have been included, I have adequately cited and referenced the original sources. I also declare that I have adhered to all principles of academic honesty and integrity and have nor misrepresented or fabricated or falsified any idea/data/fact/source in my submission. I understand that any violation of the above will be a cause for disciplinary action by the Institute and can also evoke penal action from sources which have thus not been properly cited or from whom proper permission has not been taken when needed.

Seenu P Z

Roll No. 716106

Date: 24/11/2021

NATIONAL INSTITUTE OF TECHNOLOGY

WARANGAL

CERTIFICATE

This is certify that the thesis entitled "**Climate change impacts and mitigation measures on floods in urbanising areas**" being submitted by **Ms. Seenu P Z** for award of the degree of Doctor of Philosophy to the Faculty of Engineering and Technology of **National Institute of Technology Warangal** is a record of bonafide research work carried out by her under my supervision and it has not been submitted elsewhere for award for any degree.

(K.V. JAYAKUMAR)
Thesis supervisor
Emeritus Professor
Department of Civil Engineering
National Institute of Technology Warangal

ABSTRACT

Urban flood is one of the significant and frequently occurring catastrophic events in the recent era. Urbanisation is one of the causes of climate change, and climate change results in high-intensity rainfall, which produces urban floods. Major causes of urban floods can be extreme short-term rainfall, the improper design of the drainage systems, and increased imperviousness. The areas vulnerable to flood disaster can be identified using appropriate technologies for flood vulnerability mapping and visualisation. The knowledge about the changes in extreme rainfall is considerable in planning flood mitigation activities and water resources management.

Amaravati, the area taken up for the study, is a part of the Kondaveeti Vagu catchment. Amaravati is situated at the banks of the Krishna River, on the upstream side of Prakasam barrage. The area has a history of flooding.

Monthly, seasonal and annual maximum rainfall trends were analysed in this study, using Mann Kendall (MK1), Modified Mann Kendall (MK2) trend tests and Innovative Trend Analysis (ITA) technique. Variations in seasonal and annual maximum rainfall trends across Kondaveeti Vagu were analysed with MK1 and MK2 tests and compared with the ITA technique. Using ITA Technique, monotonic and non-monotonic trends are identified in data with or without any condition of the serial correlation, size of the dataset and distributions. Results conclude that rainfall trends showed variability from the ITA technique to MK tests. For monsoon season, no trend was detected in MK1, MK2 whereas ITA technique detected trends. During post-monsoon season, trends were seen for all grid points using MK1, MK2 and ITA techniques. The result obtained from the ITA technique agreed with the result obtained from MK1 and MK2 tests. It was also observed that the ITA technique detected trend better than MK tests.

Homogeneity of precipitation series was tested by Pettitt's test, von Neumann's test, Buishand's test, and Standard Normal Homogeneity Test (SNHT). Stationarity and non-stationarity of precipitation time series are determined using Kwiatkowski– Phillips–Schmidt–Shin (KPSS), Phillips-Perron (PP) and Dickey-Fuller (ADF) methods. Parametric linear regression analysis of annual precipitation exhibited a positive trend in most of the stations. In the non-parametric test for annual average precipitation series, 47% of the stations showed a positive trend, in which the significant trend was detected in Vijayawada urban station. Sen's slope values varied from -1.233

mm/year (at Kanchikacherala) to 1.744 mm/year (in Vijayawada Urban). Most of the stations showed homogeneity and stationarity.

Frequency analysis of rainfall data (1961-2020) provided the estimates of the rainfall depth for different return periods. Hydrological modelling was carried out with the help of HEC-HMS, and the surface runoff of urban sub-catchments are estimated. For 2-year, 5-year, 10-year, 50-year, and 100-year design storms (rainfall) of 84.475mm, 119.95mm, 145.25mm, 206.5mm, and 234.9mm data input into Kondaveeti Vagu, HEC-HMS model generated runoff (peak flood discharges) of 107m^3/s, 192.4 m^3/s, 238.3 m^3/s, 398.7 m^3/s, and 460 m^3/s magnitudes respectively at the Undavalli outlet. The model output results of HEC-HMS are the computed runoff floods that resulted from input rainfall data. These hydrographs generated are given as input for unsteady flow data in HEC-RAS. Results obtained indicated that the methodology developed in the study for developing flood inundation maps with the combination of HEC-GeoHMS to ArcGIS, HEC-HMS and HEC-RAS, is very robust.

Studies on the impact due to climate change on water resources are typically evaluated for regional scale, and the evaluation is carried out at site-specific or local scale. General Circulation Models (GCMs) and Regional Climate Models (RCMs) are used to understand future climate changes. RCMs show critical biases in precipitation. Six RCMs are considered and analysed in this study to reduce the errors in RCMs. Four statistical bias correction techniques are used: linear scaling, cumulative distributive transformation, quantile mapping using parametric transformation, and quantile mapping using smooth spline methods. These bias-corrected datasets are compared with observed datasets using different relative errors, viz. standard error, mean absolute error, root mean square error and mean square error. Relative errors showed the performance of simulated data with observed data. The results showed that quantile mapping using the parametric transformation technique gave optimum values for the results with minimum error compared to the other three methods. However, there is no generalised optimised technique available, at present, to reduce the bias in the datasets of the RCMs, and there is a need to reduce the errors for reducing the uncertainties in the climate impact studies either at the local or regional scale.

RCM ensemble was done for the six RCM models with 2 different parameters using the multi-model mean method. Historic (1970 – 2005), RCP 4.5 future 1 (2014-2056), RCP 4.5 future 2 (2057-2099), RCP 8.5 future 1 (2014-2056) and RCP 8.5 future 2 (2057-2099) are the ensemble RCM time series. Rainfall depths for different return periods using GEV for historical data (RCM), RCP 4.5 future 1, RCP 4.5 future 2, RCP 8.5 future 1 and RCP 8.5 future 2 were calculated. For the

respective rainfall depth, peak discharges were calculated, and it was found that RCP 8.5 future 1 showed maximum peak discharge.

Three LID scenarios, viz., biological BMPs, structural BMPs and a combination of biological and structural BMPs, were considered for the study. Biological BMPs chosen are Bioretention, Rain Garden and Grass swale. Structural BMPs used are Permeable pavement, Infiltration trench and Rain barrel. The three scenarios are simulated for 5-year return period in five sub-catchments for 50% of the catchment area. Based on the results obtained, it was observed that the performance and potential of biological BMPs were higher in controlling and reducing the runoff volume compared to those of structural BMPs.

The results of this study will help to make decisions in planning, management and development of water resources under climate change scenarios in the Amaravati region.

TABLE OF CONTENTS

List of Tables

List of Figures

Abbreviation Notation and Nomenclature

1D	One Dimensional
2D	Two Dimensional
3D	Three Dimensional
4D	Four Dimensional
A	Cross-sectional area
AC	Agreement by Chance
ACCESS	Australian Community Climate and Earth System Simulator
ADF	Augmented Dickey-Fuller
AHP	Analytical Hierarchy Process
AMSL	Above Mean Sea Level
APCRDA	Andhra Pradesh Capital Region Development Authority
ArcGIS	Aeronautical Reconnaissance Coverage Geographic Information System
BMP	Best Management Practice
c	Historic training period
C	Runoff coefficients
CA	Cellular Automaton
CCSM	Community Climate System Model
CCTV	Closed-Circuit Television
CDF	Cumulative Distributive Transformation Function
CA	Cellular automation
CNRM	Centre National de Recherché Meteorologiques
CPS	Computational Point Spacings
CORDEX	Coordinated Regional Climate Downscaling Experiment
CV	Coefficient of variation

DEM	Digital Elevation Model
DSM	Digital Surface Models
DSRO	Direct Surface Runoff
EIM	Enhanced Inundation Method
EPA	Environmental Protection Agency
ESRI	Environmental Systems Research Institute
F	CDF of either the modelled values or observed values
FCC	False Colour Composite
FEMA	Federal Emergency Management Agency
G	Grid
GARCH	Generalised Autoregressive Conditional Heteroscedasticity
GCM	General Circulation Model
GCS	Geographic Coordinate System \
GEOGCS	Coordinate system based on latitude and longitude
GEV	Generalised Extreme Value
GFDL-CM3	Geophysical Fluid Dynamics Laboratory Climate Model version 3
GIS	Geographic Information System
HEC	Hydrologic Engineering Centre
HEC-HMS	Hydrologic Engineering Centre - Hydrologic Modeling System
HEC-RAS	Hydrological Engineering Centre – River Analysis System
IDF	Intensity duration frequency
ILLUDAS	Illinois Urban Drainage Area Simulator
IMD	Indian Meteorological Department
IPCC	Intergovernmental Panel on Climate Change
ITA	Innovative Trend Analysis
IUH	Instantaneous Unit Hydrograph

IWD	Inverse Distance Weighting
J	Junction
KNN	K-Nearest Neighbors
KPSS	Kwiatkowski– Phillips–Schmidt–Shin
L	Hydraulic length of the watershed
Lag	Basin lag time
Landsat	Land Remote-Sensing Satellite
LID	Low Impact Development
LiDAR	Light Detection and Ranging
LR	Logistic Regression
LULC	Land Use Land Cover
M	Modelled Values
MAE	Mean absolute error
MRL	Manning's roughness layers
MK1	Mann Kendall test
MK2	Modified Mann Kendall
ML	Machine Learning
MLC	Maximum Likelihood Classification
MNDWI	Modified Normalized Difference Water Index
MPI-ESM-LR	Max Plank Institute Earth System Model at Base Resolution
MSE	Mean Square Error
n	Manning Roughness Coefficient
NDBI	Normalized Difference Built Index
NDISI	Normalized Difference Impervious Surface Index
NDMA	National Disaster Management Authority
NDVI	Normalized Difference Vegetation Index

NEXARD	Next Generation Weather Radar
NFPI	National Flood Insurance Program
NorESM	Norwegian Earth System Model
O	Observed precipitation
OA	Overall Accuracy
Obs	Observed values
OLI	Optical Line Interface
p	Future projection period
P	Probability of exceedance
$P_{corrected}$	RCM daily precipitation data
PDF	Probability Distribution Function
P_{mod}	Modelled values
PP	Phillips-Perron
PPWM	Partial Probability Weighted Moments
Q	Flow rate
Qmap.P	Quantile mapping parametric transformation
Qmap.S	Quantile mapping smoothing splines
R	Hydraulic radius
RADARSAT	Radar Satellite
RAS	River Analysis System
RCM	Regional Climate Model
RCP	Representative Concentration Pathway
RF	Random Forest
r_i	Rank
RMSE	Root Mean Square Error
r_t	Random walk

RUFIDAM	Rapid Urban Flood Inundation and Damage Assessment Model
SCS CN	Soil Conservation Service Curve Number
SE	Standard error
SNHT	Standard Normal Homogeneity Test
SPOT	Satellite for observation of Earth
SRTM	Shuttle Radar Topography Mission
SWMM	Storm Water Management Model
Tc	Time of concentration
TLS	Terrestrial Laser Scanner
USACE	United States Army Corps of Engineers
USGS	United States Geological Survey
USISM	Urban Storm Inundation Simulation Method
UTM	Universal Transverse Mercator
W	Subbasin
WCRP	World Climate Research Program
WGS	World Geodetic System
Xt	Rainfall depth
y	Year
Y	Basin slope
Z	Standardised test statistics
α	Significance level
αt	Deterministic trend
ε_t	Sum of stationary error
μ	Mean
τ	Kendall's Tau
$\hat{\tau}$	Test statistic of ADF

$H0$	Null hypothesis
$H1$	Alternate hypothesis
NIR	Near Infrared
S	MK1 - Test statistic
$SWIR$	Short-wave infrared
TIR	Thermal Infrared
n	Length of data
S^*	Adjusted partial sum in Buishand Range test
S_i	Magnitude of Sen's slope
T_y	SNHT statistic
$V^*(S)$	Corrected variance
Y_j	Observations at times j
Y_k	Observations at times k
n_s^*	'Effective' number of data to account for autocorrelation
x_i	Rank for i^{th} observations
x_j	Rank for j^{th} observations
$\check{y}_{adjst}$	Corrected climate variable
ρ_k	Autocorrelation function of ranks of the data
σ^2	Variance

CHAPTER 1

INTRODUCTION

1.1. General

Urban flooding is one of the severe disasters, and various studies show that its effects are intensifying due to climate change which can cause changes in the hydrologic cycle. Changes in the hydrological cycle can cause significant impacts to both environment and the economy, such as flooding of urban areas, overflowing of sewers, damage to stormwater drainage infrastructure, disruption to day-to-day life, etc. Furthermore, as urbanisation continues, high rainfall intensities during the rainy season also become more common. The urban drainage infrastructure network is one of the most vulnerable systems due to the adverse effects of heavy rainfall. Climate change magnifies the problems that are already existing in the ageing infrastructure. Besides the climatic variabilities, the increasing perviousness due to urbanisation and land-use changes are other relevant issues. Therefore, the impact of climate change on the existing drainage infrastructure is a significant focus of many hydrological studies.

In the most recent decades, significant flood events have seriously affected and harmed many areas worldwide. Urban flooding frequently occurs with short notice and in regions not clearly inclined to flood, making it challenging to oversee and foresee. Urban flood inundation mapping has become more significant due to the frequent and unexpected occurrence of urban floods. The purpose of flood hazard/flood inundation mapping is to identify and visualise areas at different level of risk from flood hazards.

Flood modelling is an important activity to examine the impact of floods on urbanised areas. It helps to create inundation maps to determine the areas susceptible for floods by determining the depth of water levels. Flood risk management strategies must be employed to optimise flood protection measures and minimise harmful effects on the life and property of human beings. This can be achieved either by reducing the likelihood of flooding or by reducing the negative impacts when flooding occurs. A flood is an event that cannot be stopped, but its after-effects can be minimised. Mitigation is a long-term and ongoing process that should be carried out before the occurrence of floods to minimise the damages caused by flooding. Considering the cost as the determining factor, there are a few hurdles in mitigating the flood risk through engineering measures. It is the process of making humanity to survive sensibly with floods and its consequences. To mitigate floods, the first step should be creating public awareness followed by the political support that results in the proper drafting of schemes by law and order. Many urban stormwater management techniques can be used to reduce the effects of urban runoff and its flooding. Stormwater Best Management Practice (BMP) is one of the surface runoff mitigation and treatment technique at the source to control stormwater overland runoff, to controls flood volume and its flow rate.

1.2. Urban Floods

Flood is caused by various factors such as precipitation, the flow in the streams and rivers and tidal surge, topography and infrastructural modifications. There are considerable variations in flood events; some floods build up and discharge over a longer time, while others can occur in a short time and recede quickly. Though floods have been occurring since time immemorial, deeper study of urban floods started only during the last few decades.

Urban areas are densely populated areas. High population results in an increased number of residences, paved surfaces, parks, paved parking lots etc., which overlay the natural ground, increasing the imperviousness and reducing the time of concentration. Construction activities further modify the natural slope of the ground and alter the existing drainage pattern. Properly designed drainage systems can help control floods up to a specific limit. Lack of proper maintenance of the drainage and disposal of solid wastes and sewage into the storm drains reduces the carrying capacity of the drains, adding to the severity of the floods. Industrialisation and consequent urbanisation were perhaps the major causes for global

warming and the consequent climate changes have resulted in high-intensity rainfall with shorter return periods. If there exists a green belt boundary surrounding the urban area in question, the system acts as a heat island creating difference in air temperature, resulting in heavy rains downstream.

Urban flooding has attracted significant attention and consideration from hydrologists in the last few decades as it is one of the foremost principle challenges encountered in modern cities. Rapid urbanisation disturbed the natural drainage system, resulting in an increase in the runoff to the drainage networks. There is a rise in the flood peaks upto 1.8 to 8 times and flood volumes are escalated up to 6 times because of the increase in paved and impervious surfaces in the developed regions.

Urban flooding often leads to significant economic losses and devastating social and environmental impacts. Unlike other types of flooding, urban flooding is a direct, quick and localised consequence of rainfall. It often occurs with minimum warning and in areas not prone to flooding, making it difficult to manage and predict the consequences. Extreme or prolonged rainfall events can also occur in rural areas and urban areas, but compared to rural areas, the same amount of rainfall can cause more pronounced and damaging losses in urban areas.

Urban flood risk is expected to increase significantly in the future as a result of climate changes and demographic shifts: the climate change is likely to increase the magnitude and frequency of extreme storm events, the driving force of urban flooding, while the demographic shift will increase exposure and hence, risk.

1.2.1. Causes of Urban Floods

The drainage and sewerage networks in most parts of the country are old and their present conditions are very poor. They cannot adapt to the increased volume of water or are hindered by refuse and by non-biodegradable plastic wastes dumped into them. Due to the increased developments on the pervious lands, the quantity of the runoff from the surface into the drainage and sewerage systems rises rapidly. Unplanned development impacts floodplains, blocking the flood-ways and reducing the natural flood storage.

Urbanisation leads to some major hydrological effects. They are listed below:

- Due to the densely populated clusters, the water demand rises which is generally higher than the availability of water at the various sources.
- The wastewater generated from the urban area is also more, which burdens the receiving water systems like streams, rivers and lakes. This can also endanger the ecology and cause imbalances in the eco-system.
- The increased percentage of imperviousness results in faster and higher peak flow into the drainage channels.
- Reduction in infiltration of the water causes reduction in the groundwater recharge, increment in the use of groundwater, and diminished base flow.

1.2.2. Consequences of Urban Floods

Many of the recent studies show that the flood is considered as one of the severe massive natural hazards. The consequences of floods can be understood at different levels causing social disturbances, large economic and environmental losses. These effects can be broadly classified into (i) primary effects; and (ii) secondary effects as discussed below.

(i) Primary effects

- Urban areas being densely packed are more adversely affected by the floods. The occurrence of floods over an area primarily affects the life and property, which in turn, will affect the economy.
- Flood causes damage to the buildings and structures resulting in shortage or lack of shelter for the people who are residing in the flooded and flood-prone areas. It can also cause damage to the heritage structures.
- Extreme floods result in disruption of the stormwater drainages, sewerage systems, roadways, railway tracks, and also airways. Some of the recent examples of airport disruption are due to the Kolkata and Delhi floods which resulted in the stagnation of huge amount of water on the airport.
- Disruption of the sewerage systems can lead to the mixing of the clean waters to the sewerage resulting in contamination of water, causing waterborne diseases such as typhoid, giardia, cryptosporidium, cholera, etc.

- Power transmissions and power generation are also affected, resulting in long hours of power shortages. Further, the fire due to short circuit in the affected regions can cause major accidents leading to loss of human lives as well as affecting the economy.
- Educational institutions are affected resulting in a shutdown.
- Flood makes it difficult for flood relief teams to mobilise the aids to the affected people or in providing the emergency health treatments due to the damage to the roads and the transport infrastructure. Road accidents due to open pits, and manholes hidden under accumulated water add to the problem.
- It becomes a major challenge to maintain the supply of essential services and telecommunication, which affect the industrial productions. The escalation of prices of the essential commodities causes difficulties, especially for the urban poor, to survive the situation.

(ii) Secondary effects

Secondary effects can be understood as the long-term damages resulting from the occurrence of extreme flood events. Economic hardships faced by society and administrations can be considered as the long-term effect of floods. Disturbance in tourism, rehabilitation of residents and rebuilding of the damaged structures or maintenance of roads, food shortages are a few factors that hit the economy real hard. Urban flooding can cause persistently wet houses, resulting in the growth of indoor mould, which can lead to adverse health effects, particularly respiratory illness. There are uncertainties of the safe returns of the family members in flood-hit areas resulting in psychological stress and damages. Extreme flood events in a country can result in the damage of the agricultural harvest. Prolonged stagnated water in the farms and fields makes them unworkable for harvesting or cropping, resulting in the shortage of food for human as well as the cattle.

1.3. Need for Urban Flood Studies

Urban development increases flood risk in cities due to local changes in hydrological and hydrometeorological conditions. Large concentration of people in urban areas increases the vulnerability to floods. Urbanisation results in significant increase in the proportion of paved surfaces, which increases flood risk up to three times. Increased runoff and early peak

discharge results in floods within short durations which can be minutes. Urban areas being densely populated, the floods affect large numbers of people, causing severe economic and infrastructural losses. The unauthorised and dense construction in the vicinity of coastline regions results in frequent flooding even for a short duration rainfall.

The study of urban floods is needed for carrying out flood risk management activities prior to the occurrence of the hazard. The damages caused by the urban floods can be minimised if prior to floods, some measures like maintenance of the existing drainage networks, providing different drainage paths (including underground), controlling the entry of non-biodegradable solid wastes like plastics, etc. into the drainage systems, constructing permeable and porous pavements to allow infiltration of rainwater, application of stormwater management techniques etc. are taken up to mitigate the losses.

1.4. Climate Change Impact on Urban Flood

A warmer climate is already causing extreme weather events that affect the lives of millions of people around the world (Schiermeier, 2011). Specifically, as per IPCC (2014), extreme climate events are likely to occur more frequently in different parts of Asia during different seasons in the future. Brunner et al. (2017) indicated that climate change impacts the peak, the volume of runoff and the shape of the flood hydrograph. Hence, assessment of climate change impacts on floods should consider all the flood characteristics (i.e. peak, volume and duration) rather than only the flood peak. Urbanisation is one of the causes of climate change, and climate change results in high-intensity rainfall, which produces urban floods.

General Circulation Models (GCMs) are very helpful in understanding the future evolution of the global climate. However, they have too coarse a spatial resolution (100–300 km) for assessing regional or local changes (Turco, 2017). To get a better spatial resolution (10–50 km), Regional Climate Models (RCMs) are obtained by dynamically downscaling the GCM data (Hostetler, 2011). However, these models are unable to accurately reproduce the historical climate since they suffer from systematic biases in the simulated variables (e.g., precipitation and temperature); a correction is therefore needed to obtain reliable local-scale results (Christensen, 2008; Teutschbein, 2012). GCMs and RCMs are used to understand

future climate changes. RCMs have a higher resolution to understand the reliable estimation of local-scale climate variables.

1.5. Flood Modelling

Flood modelling is becoming a fundamental process to examine the impact of floods on urbanised territories. It helps create inundation maps to determine the susceptibility of the flood-hit areas by determining the depth of water levels. However, advances in computational methods, coupled with broad and more wide-ranging meteorological data observation and topographic data acquisition practices, have permitted simulation models to solve the principal equations to define the hydraulic transport processes and generate the inundation map (Marko et al. 2019). The flood inundation map demonstrates the spatial extent of possible flooding under various circumstances and can be utilised quantitatively or qualitatively. Nowadays, good computer software is available for carrying out the 1D, 2D or integrated 1D/2D flood inundation modelling such as SWAT, SWMM, HEC-RAS, MIKE 11, etc.

The hazard assessment using flood modelling is carried out to know the probability of occurrence of an explicit hazard, in an obvious future time, as well as its intensity and area under influence. Hazard is hypothetically a destructive physical occurrence, an event that may cause death or injury, property harm, natural debasement, social and monetary interruption.

1.6. Flood Mitigation

A flood is an event that humans cannot stop, but its after-effects can be minimised. Mitigation can be understood as a long-term and ongoing process that should be carried out before the occurrence to minimise the damages caused due to flooding. Considering the cost as the determining factor, there are a few hurdles in mitigating the flood risk through engineering measures. It is the process of making humanity to survive sensibly with floods and their consequences. To mitigate floods, the first step should be the creation of public awareness followed by the political support that results in the proper drafting of schemes to be followed in the event of floods. Proper education and training are required to reduce physical vulnerability.

The following activities are to be considered prior to planning of flood mitigation:

- Activation of emergency response strategies for communities to be readied.

- Defining the properties of the watershed or coastline.
- Climatological interpretations and forecast statistics on precipitation should be done.
- Hydrological observations and flood forecasts should be made.

A flood inundation map can help in the flood mitigation work. Urban flood mitigation is of high priority concern, because urban areas are the centers of economic activities with vital infrastructure that needs to be protected 24x7. The flood mitigation approach can be divided into structural and non- structural approaches. The purposes of urban flood management are to obtain specific results that have to be achieved in a predetermined time frame. These are: reducing exposure of people and property to flood hazards, reducing the existing level of flood damages, minimising receiving water pollution, enhancing recreational opportunities and improving overall urban amenities. Best Management Practices (BMPs) are used to describe both structural or engineered control devices and systems to reduce both pollution and runoff from stormwater. On the other hand, Low Impact Development (LID) is also used to describe a land planning and engineering design approach to manage stormwater runoff through various techniques such as infiltrating, filtering, storing, evaporating, and detaining runoff close to its source (NDMA, 2012).

Structural measures can reduce the post-development runoff peak. Structural measures are physical in nature and include redesigning the existing drainage system or providing suitable interventions in the form of storage at suitable locations in the upstream catchment, which may include detention ponds, grass swales, grass filter strip, and activating inline storage. The storage reduces the peak, but not the volume of runoff, and this contributes to increased runoff flows over long time periods. Non-structural measures attempt to keep people away from the flood waters by means of Early Warning System and other mitigation measures. (Ivan and Jelkovic, 2001; NDMA, 2012)

1.7. The Problem and its Significance

Urban floods represent a significant risk to settlements and the environment in many areas and results in significant monetary losses. Further, failure of electric power due to floods in the urban areas are common. Development of the rural areas into urban areas causes increased percentage of imperviousness leading to the early and higher peak of the floods. There has been almost no advancement in the provision of drainage infrastructure for the urban

communities. This results in various issues like flooding, spreading of waterborne sicknesses, and disruption to routine life.

Amaravati city, in the state of Andhra Pradesh, is under rapid development, resulting in increased impervious surfaces due to the construction of new roads, path walks, parking lots, rooftops, and other infrastructure. Kondaveeti Vagu, also known as the 'Sorrow of Streams' and flowing through the city, and Pala Vagu, undergo seasonal flood extremities every year. Low lying areas are inundated even in a matter of a few hours when extreme rainfall occurs in the region. Climate change intensifies the rainfall resulting in severe floods. Thus, the study and modelling of the urban floods are required for proper management to reduce the losses as much as possible. The relief for flood risks can be effectively provided when point by point information is gathered about the frequency, character, and magnitude of the hazard in the area.

The efficiency of the present drainage networks should be checked to predict and manage the consequences created by the excess runoff. Flood inundation mapping is required to check the overflow of the drainage or the streams due to the high-intensity rainfall, thereby providing the solutions like the construction of bunds or improving the drainage network and stormwater management using BMPs and LIDs.

1.8. Objectives of the Study

The main objectives of the study is to determine the impact of climate change on urban flood, develop flood inundation maps, and determine strategies for mitigation for urban floods using Best Management Practices. Specific objectives of the research work are to:

- Perform precipitation trend analysis for observed, gridded and climate data and carry out extreme rainfall variation analysis.
- Determine the Land Use Land Cover changes in the study area.
- Apply a selected flood model for the study area.
- Study the impact of climate change on the urban flood.
- Develop a sustainable solution for managing urban floods (BMP).

1.9. Organisation of the Thesis

The problem taken up for the study and discussion on the significance of the problem and the objectives of the study are presented in this Chapter. A detailed review of the literature related to various trend analysis methods, stationarity and homogeneity, flood frequency analysis, hydrological modelling, flood hazard mapping, climate change impact on urban flooding and mitigation is carried out and presented in Chapter 2.

Chapter 3 presents the methodology related to the trend analysis, stationarity and homogeneity analysis, LULC changes, hydrological modelling, flood inundation, bias correction, climate change impact analysis and mitigation of urban flood. Further, the description of the study area, data needed and available for the study are also presented in this Chapter. The result and discussion of the work carried out are given in Chapter 4.

The summary of the work, conclusions arrived from the study and some recommendation for further research activities based on the conclusions from study on the impact of climate change on flood risk are presented in Chapter 5. A comprehensive list of the various references used in the study follow Chapter 5.

CHAPTER 2

LITERATURE REVIEW

2.1. General

Urban flood has become an intensifying and constant danger throughout the world due to the impacts of continuous urbanisation and climate changes. Hence, better analytical comprehension, visualisation and mitigation of such floods are essential to prepare to limit the consequences of urban flooding. In this Chapter, a review of the existing literature relevant to the present work has been carried out. This review covers topics related to rainfall analysis, frequency analysis of extreme events, land use land cover, hydrological and hydraulic modelling, and climate change impact on urban flood and mitigation.

2.2. Trend Stationarity and Homogeneity

Trends in precipitation have been extensively studied around the world (Nair and Mirajkar, 2021; Núñez-González 2020; Bartels et al. 2019; Asfaw et al. 2018; Langat et al. 2017; Verma and Swain 2016; Javari 2017 and Alahacoon et al. 2018). These studies reveal both increasing and decreasing trends with the behavioural changes in seasonal precipitations at various spatial scales across India (Singh et al. 2021; Pathak et al. 2020; Bisht et al. 2018; Kumar and Jain 2011; Duhan and Pandey 2013 and Krishnakumar et al. 2009). For effective planning, development, and efficient water resources management, it is very important to analyse the trends in precipitation and interpret appropriately.

Significant research has been carried out in detecting daily, monthly, seasonal and annual rainfall trends using different parametric/non-parametric trend methods like the Mann-

Kendall (MK) test (Jain et al. 2013; Kendall 1975; Mann 1945), linear regression (Meshram et al. 2018), Spearman's Rho test (Spearman 1904), Sen's slope (Sen 1968) and cumulative sum approaches (Karpouzos et al. 2010). Non-parametric tests are appropriate for distribution-free (non-normally distributed) datasets compared to parametric tests. The most extensively applied trend detection tests are the Spearman Rho and Mann- Kendall tests, followed by trend rate evaluation tests using the approaches used by Theil (1950) and Sen (1968). Kumar et al. (2010) calculated the long-term rainfall trends for India using the MK test. Trend analyses for temperature and rainfall datasets using MK and Sen's slope tests over India were carried out by Jain and Kumar (2012). Patra et al. (2012) applied the MK and linear regression trend tests for the rainfall dataset over Orissa, India. Palizdan applied average MK test, MK test coupled with bootstrap, and discrete wavelet transform to study rainfall trends over the Langat River Basin, Malaysia (Palizdan et al. 2014; Palizdan et al. 2017). Huang et al. (2014) evaluated the trend in rainfall on a monthly and seasonal basis using Holt's method. These methods have some assumptions like (i) no seasonal dependence, (ii) time series structure to be independent and (iii) normality of distribution.

Zekâi (2012) proposed a graphical trend evaluation technique named innovative trend analysis (ITA) technique representing low, medium and high values for the time series. Analyses of trends in meteorological and hydrological variables using the ITA technique and its different modifications have been carried out in some of the recent studies (Singh et al. 2021; Kumar and Kumar 2020; Güçlü et al. 2020; Wang et al. 2020; Marak et al. 2020; Farrokhi et al. 2020; Caloiero 2020; Serencam 2019; Malik and Kumar 2020; Al Balasmeh et al. 2019; Zhou et al. 2018; Wu et al. 2018; Mohorji et al. 2017; Cui et al. 2017; Dabanli et al. 2016). Ay and Kisi (2015) carried out the monthly total rainfall trend analysis by MK test and ITA technique. The studies concluded that the ITA technique could be effectively applied to estimate maximum and minimum values of rainfall data for trend analysis. Compared with other non-parametric tests, the ITA technique has broad applicability, regardless of distribution assumptions, size and serial correlation of a dataset. Because of these advantages, the ITA technique has been extensively applied in detecting trends for meteorological and hydrological variables. Kisi (2015) and Tabari and Willems (2015) used the ITA technique for annual maximum, monthly pan evapotranspiration and streamflow data. Graphical representation in ITA shows hidden sub-trends of time-series that overcome the assumptions of dependency of dataset, distribution normality, and data length.

The precipitation data are subjected to homogeneity identification as a precursor to modelling the precipitation series under various climate change scenarios. Precipitation data with non-homogeneity indicates sudden and unexpected discontinuities in the original time-series data, mainly due to variations in the precipitation pattern at the stations in the immediate vicinity. The output from the model becomes less reliable if the input hydrological time-series data contain non-homogeneity. Several tests already exist in the literature to identify the homogeneity in the time-series data (Buishand 1982 and Yozgatligil and Yazici 2016). Based on whether the homogeneity test is applied for each station at a time or to multiple neighbouring stations, the methods of homogeneity analysis are classified into two broad categories, viz., absolute and relative. Among these, the absolute methods are mostly preferred for analysing precipitation time-series homogeneity (Buishand 1982; Tomozeiu et al. 2005; Huss et al. 2009 and Byakatonda et al. 2018). Yozgatligil and Yazici (2016) recommended that the Standard Normal Homogeneity Test (SNHT) was more suitable for identifying non-homogeneity in precipitation data. Machiwal and Jha (2012) pointed out that more than one method should be considered for improved identification of non-homogeneity in precipitation time-series data. Machiwal et al. (2016) and Jaiswal et al. (2015) used the Pettitt homogeneity test developed by Pettitt (1979) to determine rapid changes in precipitation pattern over the Indian sub-continent,

In the domains of hydrology and meteorology, some studies preferred the stationarity test to identify the statistical characteristics of the original dataset. However, such tests are widely used in econometric studies to evaluate time-series data (Phillips and Xiao 1998; Fuller 1996 and Dickey and Fuller 1979). In hydrological studies, non-stationarity tests and trend analysis are more commonly used for non-stationarity detection (Rosenberg et al. 2010 and Wang et al. 2005). Kwiatkowski et al. (1992) presented an easy and direct method to find the stationarity null hypotheses to distinguish the types of time series, whereas, for other tests, it was necessary to use the unit root null hypotheses that indicated the non-stationarity of data. A set of new stationarity tests has also been applied to evaluate the time-series data in hydrology and meteorology (Tan and Gan 2015 and Villarini et al. 2009). Modarres and Ouard (2013) used the Philips-Perron test and the Augmented Dickey-Fuller (ADF) test to study the stationarity of runoff series at two gauged stations and four precipitation stations around Quebec, Canada. They also used these tests at two stations in Iran to determine the stationarities in the atmospheric indices and drought indices before the analysis of data were

carried out using the multivariate generalised autoregressive conditional heteroscedasticity (GARCH) models.

2.3. Frequency Analysis of the Extreme Events

The design and assessment of flood risk for hydraulic structures, water resources planning, reservoir management, and flood hazard maps involve identifying the flood events with a low probability of exceedance. Flood frequency analysis seeks to connect the magnitude of extreme events with their frequency of occurrence using an appropriate probability distribution. The objective of frequency analysis is to estimate the return period associated with a flood of a given magnitude (Castellarin et al. 2012). The use of return period as a standard criterion is common in designing hydraulic structures and flood control. In most cases, it is necessary to obtain the frequency curve fitting the Probability Distribution Function (PDF) to the observed data to estimate flood quantiles associated with given return periods. Many PDFs have been considered in different situations for the probability modelling of flood events. Malamud and Turcotte (2006) and El Adlouni et al. (2008) divided the widespread distribution in frequency analysis into four groups as the Generalised Extreme Value (GEV) family, the Normal family, the Pearson Type III family and the Generalised Pareto Distribution family. Several approaches are available to analyse the data, including probability plots and probability plot regression, weighted-moment estimators, maximum likelihood estimators, conditional probability models, and partial probability weighted moments. Methods for the maximum likelihood estimate of a GEV distribution from samples have been suggested by Prescott and Walden (1983) and Phien and Fang (1989). Wang (1990a, 1996a, 1996b) introduced the concept of Partial Probability Weighted Moments (PPWMs) to analyse monitored data samples and a derived unified expression for the GEV distribution.

Extreme events, such as floods, hurricanes, earthquakes etc., can damage infrastructure, cause harm to life and affect the economy. These events cannot be prevented but can be managed so that the damage is minimised as much as possible with the relief measures taken before and during these events. Thus, the study and visualisation of the frequency of occurrence of extreme events are essential. Bisht (2016) carried out frequency analysis based on the L-moments method being employed to estimate the design storm for a small urbanised area in West Bengal, India, using daily annual maximum rainfall.

The frequency analysis of rainfall and streamflow data was conducted by Leonard et al. (2008) for the seasonal and climatic situation in Murray-Darling Basin, Australia. Different seasonal and annual rainfall data were analysed for various neighbourhoods throughout Australia, and an in-depth analysis was presented for the daily streamflows in the study area. The urban design scenario of the for Scott Creek in the Adelaide Hills, South Australia was analysed. The strong influence of seasonal and climatic variability in the occurrence of extremes was illustrated using streamflow data. They showed a wide variety of potential applicability for incorporating seasonal and climatic scenarios into the design concepts for water resources arrangements as:

i. Examining whether the simulation models appropriately replicate the seasonal composition of extreme.
ii. Validating, for similar recurrence interval, whether the seasonal rainfall extremes give the streamflow extremes.
iii. Inferring seasonal/climatic conditional levels of risk and necessary draw-down levels.
iv. Dual-purpose watersheds for water retention and flood mitigation can be designed.
v. Allowing for in-stream processes in a design such as placing aquifer-storage pumps in a flood detention basin.
vi. For the regions where seasonal flood is susceptible, the design of the structures and channels can be done.

By carrying out hydrological frequency analysis, Chebana et al. (2013) assessed the non-stationarity hypothesis. They used two different types of non-parametric trend tests and applied their multivariate extensions to multi-variable and multi-site flood attributes. For the development of the model, the importance of trends in multivariate distributions (copula and margin) was highlighted. The generalised additive model is valuable for regional frequency analysis in the expressions of performance and practical phases.

By using the Archimedean copulas, Li et al. (2019) presented the study for non-stationary frequency analysis of extreme rainfall for Eastern China. The study highlights integrating non-stationarity in multivariate hydrological analysis and incorporating compatible data sets for improving copula inference.

Jeffrey and Edward (2019) worked on the challenges that emerged out with the availability of the limited data for the study area of Weser River basin, Germany. The data

was analysed and processed: (a) for the data of average daily discharge evaluating the instantaneous peaks (the adjustments from daily to instantaneous discharges reach as high as 1.39 for gauges with smaller drainage areas), (b) to eliminate unrepresentative data for cases in which reservoirs may have changed flow conditions because mean annual maximum discharges were 21% lower after reservoir construction for the longest gauge record. In order to calculate the flood discharges for various return periods, the processed data were utilised for the regional frequency analysis using L-moments.

Zamir et al. (2021) studied the use of the Gumbel-logistic model for the analysis of the bivariate rainfall frequency for two correlated events - the annual extreme monthly rainfall and the corresponding total amount of rainfall. They found out that the Gumbel logistic model has been used to improve the extreme rainfall assessment of univariate and bivariate by analysing the distributions of two positively correlated extreme random variables which are Gumbel distributed. The fit of the logistic model applied in this study was also examined through the fitness test of the data. The fit of the distribution was determined by comparing the empirical probability value with the theoretical probability value of the distribution. Based on the comparison, the result of the estimation of the combined duration of the analysis of the rainfall variability showed a similar pattern to the univariate rainfall data.

2.4. Hydrological Modelling

Hydrological modelling is considered an essential tool for water resources planning and management. A hydrological model is a valuable tool for studying the impact of climate change on water resources from present and future scenarios. Many urban areas have experienced a change in the frequency and magnitude of extreme hydrological events (Praskievicz and Chang, 2009; Wang et al. 2020). Numerous hydrological models have been developed and applied to assess the impact of climate change on water resources, particularly for floods. This section is devoted to a comprehensive review on hydrological models.

Rainfall-runoff models can be classified into several categories based on model input parameters and the physical principles used within the models. They can also be classified based on the model parameters as a function of time and space (i.e. lumped and distributed). Besides, the model is considered deterministic if a set of input values will always produce the same output values. A model is stochastic if the input values do not produce the same output

values. The event and continuous simulation models are distinguished based on the specific and continuous period of output respectively (Wheater et al. 2008). Table 2.1 presents the brief characteristics of three types of hydrological models, viz., empirical, conceptual and physically-based models.

Table 2. 1 Characteristics of hydrological models (Devia et al. 2015)

Empirical model	Conceptual model	Physically-based model
• Metric or black box model • Describe by mathematical structure using time series information • Do not need prior knowledge about hydrology process • High predictive power but low explanatory capacity • Cannot be generated to another catchment	• Parametric or grey box model • Based on modelling of reservoir and include semi empirical equations with a physical basis • Model parameters are calibrated • Simple and easily calculated using computer code • Require large hydro-meteorological data	• Mechanistic or white box model • Based on spatial distribution, evaluation of parameters describing physical characteristics • Model parameters can be measured • Complex model and requires high computational demand • Suffer from extreme data demand, scale related problems and over-parameterization

Rainfall-runoff modelling had its origin during the middle of the 20th century. In 1932, Sherman introduced the concept of "unit-graph" or unit hydrograph. This method not only concentrated on predicting the peak flow and time to peak instead, but also, for first time, the whole hydrograph was predicted. Hydraulic models are complex tools, requiring large amounts of input data for their specification to a particular application and produce a huge amount of output data. The data requirements for distributed hydraulic models are grouped into topographic and hydrologic data (Cunge, 1980). An important role of hydrologic design has been to quantify and mitigate the risks of flooding that arise from the variability of extreme rainfall and streamflow values (Michael et al. 2007). Many software like ILLUDAS, SWMM, HEC-RAS, LISFLOOD, MIKE FLOOD, MIKE URBAN etc. are available for urban storm drainage modelling (Patro et al. 2009; Sen 2013; Bisht et al. 2016; Patel et al. 2017; Teng et al. 2017).

The EPA's Storm Water Management Model (SWMM) is used extensively throughout the world for planning, analysis, and design related to stormwater runoff, combined and sanitary sewers, and other drainage systems. The runoff component of SWMM works on a

combination of sub-catchment areas that receive rainfall and generate runoff and pollutant loads (Rossman and Huber, 2016). SWMM is dynamic rainfall-runoff simulation model which is mainly used for quantitative as well as qualitative simulations of both single and long-term continuous runoff events. The work carried out by Bisht et al. (2016), Vemula et al. (2018), Rai et al. (2018), Ranger et al. (2011), Sahoo and Sreeja (2016) and Dasgupta et al. (2013) are some of the studies conducted in urban flood modelling using SWMM in India.

HEC-1 was developed in the 1960s by the Hydrological Engineering Centre, U.S. Army Corps of Engineers. Later, HEC-1 came to be known as HEC-HMS with the addition of new user interface and spatial data input and analysis features. Jain and Ramsastry (1990) effectively utilised the HEC-1 model for modelling the rainfall-runoff response of Hemavati river basin up to Sakleshpur within the constraints of data availability. HEC-1 along with Nash IUH model was used by Chatterjee et al. (2001). For the generation of the direct surface runoff (DSRO) hydrograph, they compared the performances of HEC-1 model and Nash model for the catchment considered in the study. Coupling of HEC-HMS with an atmospheric model was performed for the estimation of the resulting runoff in the catchment of Sierra Nevada Mountains California, USA by Anderson (2002). Integration of GIS, HEC-HMS and HEC-RAS was successfully carried out by Knebl et al. (2005) using the Next Generation Weather Radar (NEXARD) data for the development of flood polygons for the basin of San Antonio River. A successful tool was suggested for the regional scale hydrological forecasting of floods which will be beneficial in future. Ranaee et al. (2009) carried out the routing of floods for two branches of Zoshk River by using HEC-GeoHMS extension in ArcMap, HEC-HMS and MIKE 11. HEC-GeoHMS was employed to successfully develop the statistics that were required for rainfall-runoff modelling in HEC-HMS.

2.5. Flood Inundation Mapping

By 1976, the techniques used for solving the Saint-Venant equations were found adequate with mathematical models found to be satisfactory for the wide range of applications (Priessmann, 1976). Bates et al. (2000) developed the model, LISFLOOD-FP, which was tested for the estimation of flood inundation for the river reach of 35 km of the River Meuse in the Netherlands. This model comprised of a one-dimensional kinematic wave approximation for the channel flow which was solved using explicit finite difference and a diffusion wave scheme for 2D representation of flow in the floodplain.

Best outcomes were obtained by the combination of GIS and remote sensing with urban storm drainage model (Talukdar et al. 2021; Jamali et al. 2018., Zhang and Pan, 2014., Mokhtar et al. 2018)., The urban flood inundation maps display the water flow paths in detail during extreme events based on high-resolution DEM. Four-dimensional GIS (4D GIS) analyses, manages and integrates, spatial and temporal information, providing quality communication, simulation, and visualisation, which will be useful for the spatial extension of the flood with respect to time. (Kumar and Reshma, 2017).

Demonstration of the applicability of SOBEK, the 2D hydrodynamic model for rebuilding characteristics of a higher magnitude outburst flood was done by Carrivick et al. (2006). The study depicted a better understanding of spatial and temporal hydraulics as well as higher magnitude flow phenomenon.

Patro et al. (2009) used the coupled 1-D and 2-D hydrodynamic model, MIKE FLOOD, to simulate the flood inundation range and flooding intensity in the watershed of Mahanadi River, India. They performed the bathymetry survey of the watershed using SRTM-DEM and used it as an input data to the 2-D model, MIKE 21. Using parallel links in MIKE 11 and MIKE 21 models, flood inundation mapping was prepared. They analysed the results with real inundated stretch downloaded from IRS-1D WiFS image.

Sarchani et al. (2020) used a combination of 1D/2D hydraulic model to determine the extent of flooded area and concluded that the 2D model delivered more accurate flood mapping during the maximum flood depths as well as for flow velocities and peak discharge.

MIKE FLOOD model was prepared and successfully simulated by Timbadiya et al. (2014) for the Lower Tapi River basin. It was concluded from the study that in comparison to 1D and 2D models, the results generated by an integrated 1D/2D model was better.

Papaioannou et al. (2016) found that it is advantageous to use terrestrial laser scanner (TLS) that can direct to a high-resolution digital elevation model (DEM). They employed several hydraulic-hydrodynamic modelling methodologies and numerous types of river and riparian area spatial resolution for implementing the sensitivity analysis to the floodplain mapping and flood inundation modelling process at ungauged watersheds. Flood hazard maps have been produced for each modelling approach and landscape alignment at the lower part of Xerias River reach Volos, Greece, and analysed for evaluating the sensitivity of input data and model structure uncertainty. Different models that were used and compared were MIKE

ZERO, MIKE 11 and HEC-RAS for floodplain mapping. The study concluded that the accuracies in flood inundation mapping by different approaches can be better by using higher spatial resolution data.

2.5.1 HEC-RAS

The HEC-2 computer model was introduced by the Hydrologic Engineering Centre (HEC) of the US Army Corps of Engineers in 1964 in order to help the hydraulic engineers to deal with river channels and floodplains (USACE, 2010). Due to the increase in the use of Windows operating systems by 1990, the HEC-2 was upgraded to be used in the operating system and the software was renamed as HEC-River Analysis System (RAS).

Martin et al. (2012) carried out a study to generate flood inundation maps from which the flood hazard zones within the area can be recognised. The detailed objectives of the study for the River Sironko basin comprised of three stages namely: (i) performing rainfall-runoff analysis (hydrological modelling); (ii) performing hydraulic modelling; and (iii) preparing flood inundation maps. Hydrological modelling was carried out using HEC-HMS software, after watershed delineation and generating the catchment basin model (325km^2) using HEC-GeoHMS in ArcGIS environment, populating the meteorological model input with design storm data, and assigning the control specifications. Flood hazard zones and inundation maps were produced by exporting the output from the HEC-RAS model to ArcGIS where they were processed to recognise the flood-prone areas. From the flood hazard zoning maps, it was concluded that the areas around the middle reach of Sironko River were mostly affected.

Ahmad et al. (2010) carried out the hydraulic modelling and produced the flood inundation maps for Nullah Lai River, Rawalpindi using HEC-GeoRAS extension with GIS and HEC-RAS model. Correlation among the immersion depth and flow runoff values was established. Adnan et al. (2012) conducted the bathymetry mapping based on remotely sensed imagery coupled with ancillary datasets utilising the hydraulic model HEC-RAS for River Kelantan, Malaysia. Comparison and analysis of the predicted flood inundation extent using HEC-RAS were carried out with the flood predicted from a RADARSAT image. The areas were marked as upstream; midstream and downstream and thus the accuracy assessment was applied for identifying the spatial variation in the error between above-mentioned areas.

Geographic Information System (GIS) and HEC-RAS were integrated and used by Fosu et al. (2012) for the modelling of Susan River basin. Contour data was processed in ArcGIS to produce DEM. The geometric inputs desired for modelling were obtained from the DEM, topographic map and field dimensions. Land use land cover maps were generated for classifying different land-use types and thus estimating the manning's roughness coefficient. The outputs produced by the model were analysed in ArcGIS environment. The delineation of the affected buildings and assets were carried out by superimposing the results of the flood simulation with the topographic map. The map generated gave the clear picture of the spatial distribution of the inundated regions which were essentially the areas with relatively high risk.

Silva et al. (2014) mapped the extent of flood in the urban region of Rio dos Cedros city, Medium Itajaí River Valley – Santa Catarina, with HEC-RAS, supported by a GIS. Simulation was carried out to find out the region that will result in inundation for the events of 2, 5, 10, 100 and 200-year return periods and a past flood event. The study showed the appropriateness and capability of HEC-RAS in flood plain mapping when the higher resolution spatial data was used.

One dimensional steady flow analysis was carried out by Ahmad et al. (2016) using HEC-RAS for the watershed of Jhelum River, Jammu and Kashmir, India. The steady flow analysis showed the suitability of HEC-RAS model. The area was susceptible for inundation by 50-year and 100-year floods. The area lying towards the left bank was found to be more susceptible for floods and thus mitigation measures were needed.

Probabilistic flood inundation mapping to evaluate the uncertainty introduced by the roughness coefficient values in hydraulic models and for the ungauged Xerias stream reach, Volos, Greece was carried out by Papaioannou et al. (2017). They performed manual calibration by trial-and-error method for the simulation of a historical flood event and estimated average value of Manning’s n for the study. They proposed the applicability of HEC-RAS software for hydraulic modelling at ungauged streams.

Patel et al. (2017) carried out the assessment of the flood inundation due to the past event that occurred in the Surat city, situated 100km downstream of the Ukai dam. The study included the breaching of the dam. 1D/2D hydrodynamic model was developed and simulated to determine the inundation extent in the low-lying areas. The authors demonstrated the

applicability of HEC-RAS for flood modelling. In the study, the extents of depths and area were found that were most likely to be inundated and those needed the mitigation measures.

Yalcin (2020) studied the impact of land cover and topography resolutions on the calculation of flood coverage, flow velocities, depths, and time of concentration of the 2D HEC-RAS model for differently sized mesh structures. To determine these properties for a large variety of data conditions, Manning's roughness layers (MRL) and digital surface models (DSM) with different resolution were formed for the floodplain by processing the high-quality DSM. In addition, different computational point spacings (CPSs) were tested to estimate variations in the model outputs depending on the dimensions of mesh grids. The simulation executed for the most detailed model configuration was utilised as the base model simulation to compare the performances of other simulations. The model simulation configured with the 2 m cell size DSM, 10 m cell size MRL, and 10 m × 10 m CPS showed performance comparable to the base model simulation with a small loss in the accuracy of the estimates, indicating that very-fine-resolution (less than 2 m) topography and high-resolution (less than 10 m) land cover data may not be indispensable to produce reliable simulations with 2D urban flood modelling using HEC-RAS software.

2.5.2. Urban flood inundation model

An urban flooding analysis simulated by one-dimensional hydrodynamic modelling incorporating the interaction between, the buried pipe system, the streets with open channel flow and the areas flooded with stagnant water was proposed by Mark et. al (2004). The study handled both urban flooding with and without flood water entry into houses. The modelling results were presented in the form of flood inundation maps produced in GIS. Local rainfall was considered together with the impact in terms of flood extent, flood depth and flood duration. The data requirement for verification of urban flood models together with an outline of a simple cost function for estimation of the cost of the flood damages were explained.

Zhu et al. (2016) proposed an approach to quantitatively and qualitatively estimate flood risks in urban drainage network based on a stormwater management model. The K-means clustering technique and the projection pursuit technique were verified using a residential area in Guangzhou, China. Seven evaluation indices were considered and twenty rainfall-runoff events were selected to calibrate and validate the parameters of the rainfall-

runoff model. The flood risks in the drainage system in the study region were assessed for various rainfall conditions. A SWMM model inundation risk evaluation approach was used with the observed rainfall and runoff data. This method could estimate the inundation risk of the present urban drainage network. By this method, the flooded area could be derived at various scales and the results were transferable to other scales without methodological limitations. This paper proposed a successful and novel method to find out the risk in urban drainage network and gives guidance for improving urban drainage network and flood awareness.

Jamali et al. (2018) developed a rapid urban flood inundation and damage assessment model (RUFIDAM), using GIS technology with the intention of rapidly estimating flood extent, depth and its associated damage. RUFIDAM integrates a 1D hydraulic drainage network model (SWMM or MOUSE) with an adapted version of rapid flood inundation models. Surcharge volumes from the 1D drainage network model were fed statically into the rapid inundation model. The model was tested on three urban catchments located in southeast Melbourne. Results of flood depth, extent and damage costs were compared with those produced using MIKE FLOOD. Results showed that RUFIDAM can predict flood extent and accumulated damage cost with acceptable accuracy. Although some variations in the simulated location of flooding were observed, simulation time was reduced by two orders of magnitude compared to MIKE FLOOD. As such, RUFIDAM is suitable for large-scale flood studies and risk-based approaches that rely on a large number of simulations.

An efficient and flexible cellular automaton (CA) model to simulate stormwater runoff and the flood inundation process during extreme storm events was developed by Liu et al. (2015). The process of infiltration, inlet discharges and flow dynamics can be simulated with a little preprocessing of commonly available basic urban geographic data. In this model, a set of gravitational diverging rules were implemented to govern the water flow in a rectangular template of three cells by three cells of a raster layer. The model was calibrated using one storm event and validated by another event in a small urban catchment in Guangzhou of southern China. The depth of accumulated water at the catchment outlet was interpreted from street-monitoring closed-circuit television (CCTV) videos and verified by on-site survey. A satisfactory level of agreement between the simulated process and the reality was attained for both storm events. The model reproduced the changing extent and depth of flooded areas at

the catchment outlet with an accuracy of 4 cm in water depth. Comparison with a physically based 2-D model (FloodMap) showed that the model was capable of effectively simulating flow dynamics. The high computational efficiency of the CA model can meet the needs of city emergency management.

Mei et al. (2020) developed a numerical flood model of Xiamen Island in China. Simulations were conducted for 12 design rainstorm events with different return periods, rainfall patterns, and durations. The results indicated that, in the case of an equal rainfall amount, the rainfall intensity is the key factor that influences the inundated area, depth, and damages. However, the rainfall intensity was not the only determining factor, but the rainfall pattern also affected the inundations. Considering the rainfall pattern, a higher rainfall peak coefficient usually leads to severe urban inundation and damage. As a result, the lag time would be shorter, which may further aggravate the impact of urban flood disasters. The results of this study provided the insights into managing flood risks, developing urban flood prevention strategies, and designing flood prevention measures.

Tsubaki and Fujita, (2010) developed a comprehensive method to conduct detailed inundation flow simulations for a populated area with complex topographical features using LiDAR data. Detailed geospatial information including the location and shape of each building was extracted from the LiDAR data and used for the grid generation. The approach developed could distinguish buildings from vegetation and treat them differently in the flow model. With this method, a fine unstructured grid could be generated which represented the complicated urban land features precisely without much labour for data preparation. The accuracy of the generated grid with different grid spacing, grid type and the optimal range of grid spacing for direct representation of urban topography were investigated. The developed method was applied to the estimation of inundation flows in the basin of the Shin-minato River. A detailed inundation flow structure was represented by the flow model, and the flow characteristics with respect to topographic features were discussed.

Both 2D and 3D hydrodynamic models were built separately to quantify the flood danger to a coastal city and studied by Rong et al. (2020). A digital city model was generated by integrating building information modelling (BIM) and GIS technology based on digital aerial photogrammetry for the 3D hydrodynamic model. The results revealed that 2D hydrodynamic assumptions and approximations weaken if the vertical fluctuations were

enormous, especially in urban environments. In comparison, a 3D model coupled with high-resolution topographic data could provide a more realistic and accurate result for the complex flow field. Furthermore, comparisons between using the digital city model and a standard digital elevation model (DEM) in a 3D model were carried out. The flood inundation was simulated step-wise using the standard DEM, while the wave front propagated in a more realistic manner based on high-resolution topography data. Thus, a 3D hydrodynamic model coupled with the digital city model was recommended for urban flood simulation, since it would improve the ability of flood prediction and prevention.

Hou et al. (2021) established a rapid forecasting model of urban flood inundation based on machine learning (ML) algorithms and a hydrodynamic-based urban flood model. The ML model is obtained by training the simulation results of the hydrodynamic model and rainfall characteristic parameters. Part of Fengxi New Town, China, was used to validate the forecasting model. A comparison of ML predictions and hydrodynamic model simulations showed that when using one ML algorithm (random forest (RF) or K-nearest neighbour (KNN)) for inundation prediction, the accuracy of the inundation water volume and area was not satisfactory, the maximum error being 28.56%. Combining the RF and KNN models can effectively improve the prediction accuracy and overall stability. The mean relative errors of the inundation area and depth were less than 5%, and the mean relative error in the estimation of the inundation volume was within 10%. The simulated time of a single rainfall event can be controlled within 20 seconds, which could provide sufficient lead time for emergency decision-making, thereby helping decision-makers to take more appropriate measures against inundation.

An enhanced inundation method (EIM) for urban flood hazard mapping at the large catchment scale is proposed by Zhao et al. (2019). EIM can be easily coupled with urban hydrological models and the coupled framework can be considered both source flooding and non-source flooding in floodwater generation. In EIM, the floodwater spreading order in the positive process is based on the topological relationship between depression outlets; the floodwater from lower depression elements is considered as a feedback process. These improvements made the proposed method suitable for inundation estimation in large urban catchments. Dahongmen (DHM) catchment in Beijing, China was selected as the case study area to illustrate the applicability of the proposed method. Historical inundation records of one

heavy storm were applied to test the performance of the method. EIM is compared with USISM (urban storm inundation simulation method) on the flood hazard map in the DHM catchment, which reveals the effectiveness of the improvements. The results show that all inundation locations were successfully identified by EIM and distributed in flooding areas (water depth greater than 0.15 m) in the catchment. The average relative error of simulated inundation depths was 15%, which indicated that EIM can successfully simulate flooding scopes and depths in the study area. The results revealed that EIM can be a valuable tool for mapping urban flood hazards at the large catchment scale based on GIS techniques.

2.6. Land Use Land Cover (LULC) Changes

Land cover modifications generally associated with the infrastructure development, such as removal of vegetative surface, replacement of raw land with impervious pavements, clearance and filling of natural ponds and streams, could induce increased number of pollutants and harm the quality of urban water systems (Arora et al. 2013., Hardy et al. 2005., Jayasuriya et al. 2007, Elliott and Trowsdale, 2007). LULC changes play a significant part in the runoff generation due to the modification in various hydrological processes such as erosion, interception, evapotranspiration, and infiltration (Melesse and Shih 2002). To attain an improved sustainable development and management of the watershed, knowledge, proper understanding and evaluation of the effects of LULC changes on the watershed hydrological process are of great importance to forecast the flood risk, flood hazard and flood potential (Riebsame et al. 1994; Vorosmarty et al. 2000; Beighley et al. 2004; Chen et al. 2009; Ali et al. 2011; Suriya and Mudgal 2012; Potter 1991; Wang et al. 2007). Analysis of LULC changes is essential to quantify the changes in the runoff generation at different spatial and temporal scales. LULC changes also determine the human-induced changes on the watershed. Several studies (e.g., Lopez et al. 2001; Lorup et al. 1998; Saghafian et al. 2008; Lambin 1997) have suggested combining traditional statistical tests and hydrological models to determine the impact of LULC changes on runoff on a catchment scale. A large number of studies have attempted to examine land use and land cover changes using remote sensing and GIS techniques. The need for greater attention towards monitoring the changes in land use and land cover in urban areas was understood, since past studies had shown that anthropogenic activities influence the urban environment considerably (Stow and Chen, 2002; Alberti et al. 2003; Andersson 2006; Lundholm et al. 2010).

A combination of Markov Chain models, cellular automata (CA), and logistic regression (LR) was used to find the future land use land cover changes based on historical data. Flood risk assessment was made at present and for future and land use land cover changes scenarios (Mohammed et al. 2020)

Zope et al. (2017) analysed the LULC change using the toposheets and satellite images for the watershed of Poisar River in Mumbai, India. For the assessment of flood, a combination of HEC-RAS, HEC-GeoHMS and HEC-HMS with HEC-GeoRAS was used. These models were integrated with remote sensing and GIS data to make a regional model for the flood hazard analysis and estimation of flood plain extent. The effect of LULC change and impacts of detention ponds on flood plain extent as well as surface runoff for different return periods were calculated and flood plain maps and flood inundation maps were created. The results showed that for low return period rainfall events, the hydrological impacts were higher due to geographic features of the region.

An indicator based on the runoff coefficient, which allowed quantifying the impact on runoff due to the increase of green infrastructure, was presented by Zimmermann et al. (2016). This study suggested a method to identify the indicator with the flood risk. Four scenarios were evaluated: baseline scenario (current scenario), three hypothetical (future) scenarios, considering moderate and severe waterproofing situations, respectively, and one green scenario with increased green infrastructure. The results showed that the moderate and severe waterproofing scenarios increased flooding risk from 1.9 times to 4 times, respectively. This implied a necessary reinvestment to be made in urban stormwater infrastructure in order to maintain the original security levels. The green scenario would maintain the runoff coefficient, even considering the major increases in population and urbanisation. Improving the green infrastructure constituted a strong strategy to adapt to climate and urban changes and cope with upcoming increase in the precipitation and rate of urbanisation.

Idowu and Zhou (2021) introduced a map-matrix-based, post-classification LULC change detection method to evaluate multi-year land cover changes. Seven conditions were recognised as potential contributing factors accountable for the increasing flood hazards in the study area. Their weights were evaluated using a combined (hybrid) Shannon Entropy weighting method and Analytical Hierarchy Process (AHP). The resulting flood hazard categories were very low, low, moderate, high, and very high hazard levels. Investigation of

the LULC change in the framework of flood hazard showed that most LULC changes resulted in the conversion of wetland areas into developed areas and unplanned development in very high to moderate flood hazard zones. The study concluded that the changes in LULC were responsible for the rise in flooding in the study region.

Nguyen et al. (2021) developed an innovative method integrating hydraulic models and land-use change to discover future urban flood risk, intending to decrease it in different exposure and vulnerability situations. Sentinel-2 and SPOT-3 images were processed to generate land cover maps, which were then used to forecast the land cover using the Land Change Modeler Module of Terrset. Flood risk was calculated by integrating vulnerability, exposure, and hazard using hydrodynamic modelling and the AHP method. Although flood risk increases with urbanisation and population density, especially in the coastal region, the area exposed to high and very high risks decreased due to a reduction in the poverty rate. This study provided a theoretical framework supporting climate change related to risk assessment in other metropolitan regions. The importance of using satellite imagery and the continuity of data in the planning-related decision-making process was highlighted in the study.

2.7. Climate Change Impact on Urban Flood

From recent studies, it was observed that climate change affected the intensity of precipitation in urban areas (Kang et al. 2021; Hosseinzadehtalaei et al. 2020; Sun et al. 2017; Li et al. 2019; Han et al. 2015; Shahid et al. 2015; Kug and Ahn 2013 and Sun et al. 2014).

Climate change has been widely acknowledged as a global issue due to its anticipated impacts on urban water systems in terms of changes in water runoff and urban flooding (Ranger et al. 2011, Willems et al. 2012, Hallegatte et al. 2011). General Circulation Models (GCMs) and Regional Climate Models (RCMs) are used to understand future climate changes. RCMs have a higher resolution to understand the reliable estimation of local-scale climate variables. Many studies have reported that the expected increase in design intensities due to climate change can reach 20%–80%, depending on the region (Willems et al. 2012, Arnbjerg-Nielsen, 2012, Ekström et al. 2005). This has posed a considerable challenge to the current drainage system designed based on a specific return period. The stormwater management system, therefore, faced severe capacity problems in coping with the increasing amount of water due to climate change impacts. More importantly, future drainage design needs to

consider the increased frequency and intensity of precipitation to maintain an acceptable frequency of system overloading (Mailhot et al. 2010., Burrell et al. 2007).

2.7.2. Bias correction

In spite of the significant improvements in the results obtained by using RCMs in replicating the regional climate scenarios, systematic errors were still present in them (Frei et al. 2003; Suklitsch 2008; Suklitsch et al. 2011). The precipitation simulations produced by RCMs are biased due to limited understanding of the process or due to inadequate spatial resolution. It is, therefore, statistically needed to adjust with post-processing before it could be used for the assessment of climate variables (Maraun et al. 2010; Winkler et al. 2011). Various studies used daily precipitation data obtained from climate models that were then bias-corrected and matched with the precipitation statistics already observed for modelling applications. Appraising the impact of climate change over hydrological systems lies in evaluating the effects of variations in the precipitation frequencies that may occur in the future. This is a major challenge since climate models do not always simulate the daily precipitation values very accurately.

Various bias correction methods were used in climate change impact studies. Quantile mapping is one of the widely used methods (Panofsky and Brier, 1968; Thrasher et al. 2012). Quantile mapping corrects the model variable by creating quantiles of the distribution of model onto those of the observations. This method has been used worldwide to analyse the output of climate models (Thrasher et al. 2012). Another technique used for bias correction is the cumulative distribution transformation method (Michelangeli, 2019), assuming that the modelled and observed CDF mappings affect future data.

2.8. Flood Mitigation

Flood mitigation comprises of the various actions that alter the exposure of life and property due to flooding. For mitigation of the floods in urban areas, some of the established best management practices (BMP) are preferred. These BMPs are the non-structural measures which are used in the developing regions to minimise or reverse the impacts of urbanisation. The suggested BMPs should be economically justifiable and environmentally sustainable. The two basic requirements that BMP should ensure is: (i) it should result in the reduction of the

flood volume; and (ii) the flood peak discharge should be attenuated by implementing the BMPs.

An approach was presented for low impact development type of BMP for stormwater management to manage the urban runoff for the region of Beijing Olympic Village (Jia et al. 2012). Coupled SWMM-BMPDSS model was used to evaluate the runoff peak rate and the reduction in flood volume after defining the low impact development (LID) approach and BMPs into the model. Analysis of low impact development were carried out for BMPs such as green roofs, green spaces and porous pavements. They recommended the BMP plan resulted in the reduction of flood volume by 27% with the optimisation of the cost.

Te Xu et al. (2017) developed a new methodology based on SWMM for block scale low impact development (LID) best management practices (BMP). For the study, SWMM 5.1 was to identify the BMPs and these are simulated for Haihe River in Tanggu Bay, Tianjin, China. They referred "Technical Guide for the Construction of the Sponge City" for setting the parameters for LID-BMPs.

Meena et al. (2018) described a modelling approach to incorporate four types of BMPs in the study site and estimated the impacts of BMPs on flood volume and peak flow reduction. They showed the effects of the suggested BMPs in reducing floods using PCSWMM, for the urban area of the Bengaluru city. The evaporation was assumed to be negligible; the runoff over the catchment was infiltrated, flowed away or stored on the surface. The model was simulated for the conditions of pre-BMP and post-BMP. Post BMPs included the installation of permeable pavement, infiltration trench, and rain barrel storage and bioretention cell. The study showed that by adopting BMPs, that there was around 40% reduction in the flood volume.

2.9. Summary

In this Chapter, a comprehensive review of the literature on trend, stationarity, homogeneity, frequency analysis of extreme events and LULC changes are presented. The literature review also provided the clarity of the appropriateness and applicability of the software available which can be used in the study. Detailed review of literature on climate change impact on urban flood and flood mitigation has also been reported. Some ideas, which were derived from the review of the literature, and used in the study are presented below.

- Performing the frequency analysis on the basis of L-moments to estimate the design storms of different return periods for the watershed, using daily annual maximum rainfall.
- The watershed delineation in the study considering flow direction and flow accumulation in the catchment using HEC-GeoHMS extension in ArcGIS.
- Determination of peak discharges and flow hydrographs for various duration rainfall events using the HEC-HMS and SWMM software.
- Integration of GIS to HEC-HMS, HEC-RAS and SWMM for the urban flood inundation mapping. The applicability of software used can be established from the above-mentioned studies.
- Climate change impact on urban flood carried out using RCM models.
- Use of BMPs as flood mitigation measures.

CHAPTER 3

STUDY AREA AND METHODOLOGY

3.1. Introduction

This Chapter gives details of the area taken up for the study and data collected during the visit to the Andhra Pradesh Capital Region Development Authority (APCRDA) in the proposed legislative capital city region. The Chapter also explains the methodologies including rainfall-runoff modelling adopted in the study to estimate the influence of rainfall on runoff. Flood inundation maps are generated by hydraulic modelling to locate the depth and area that are susceptible to flooding. The frequency analysis of rainfall data was carried out to estimate rainfall depth for different return periods prior to any model application. The methodology used for calculating land use and land cover changes and different indices is explained. Methods used for climate change impact and mitigation for urban flooding are also included in this Chapter.

3.2. Study Area

Based on the Andhra Pradesh Reorganisation Act, 2014, the state of Andhra Pradesh was bifurcated into the states of Telangana and Andhra Pradesh, initially with a common capital city, Hyderabad. Later, a new capital city for Andhra Pradesh, Amaravati, was proposed. The administration created the Andhra Pradesh Capital Region Development Authority (APCRDA) to plan, develop, and manage the capital city. Amaravati is situated at the banks of the Krishna River, on the upstream side of Prakasam barrage. Development is proposed over an area covering about 217 km^2, spread across 25 villages of Guntur district. The capital city zone has rich natural features, including hillocks, stream islands, abundant

water, fertile soil and greenery. While the abundance of water is a boon for the capital city, seasonal flooding of the Krishna River and the Kondaveti Vagu pose a threat to the capital city region. Amaravati is proposed to be developed as a capital city with a vision of building up a sustainable and green capital city. Due to the seasonal floods of Kondaveeti Vagu occurring every year and causing floods in the low-lying areas, Kondaveeti Vagu has also come to be known as Stream of Sorrows. The capital city region has four reservoirs, viz., Ananthavaram, Sakhamuru, Neerukonda and Krishnayapalem.

3.2.1. Boundary map of the study area

The study area, shown in Fig 3.1, shows the geographic location of Andhra Pradesh in India and the location of the Kondaveeti Vagu catchment in Andhra Pradesh. Geographically, Amaravati lies between the latitudes 16°17'30" N and 16°34'55" N and between longitudes 80°15'30"E and 80°39'00 "E. The elevation of the study area ranges from 13 m in the SE to 22m, AMSL (above mean sea level) in the north.

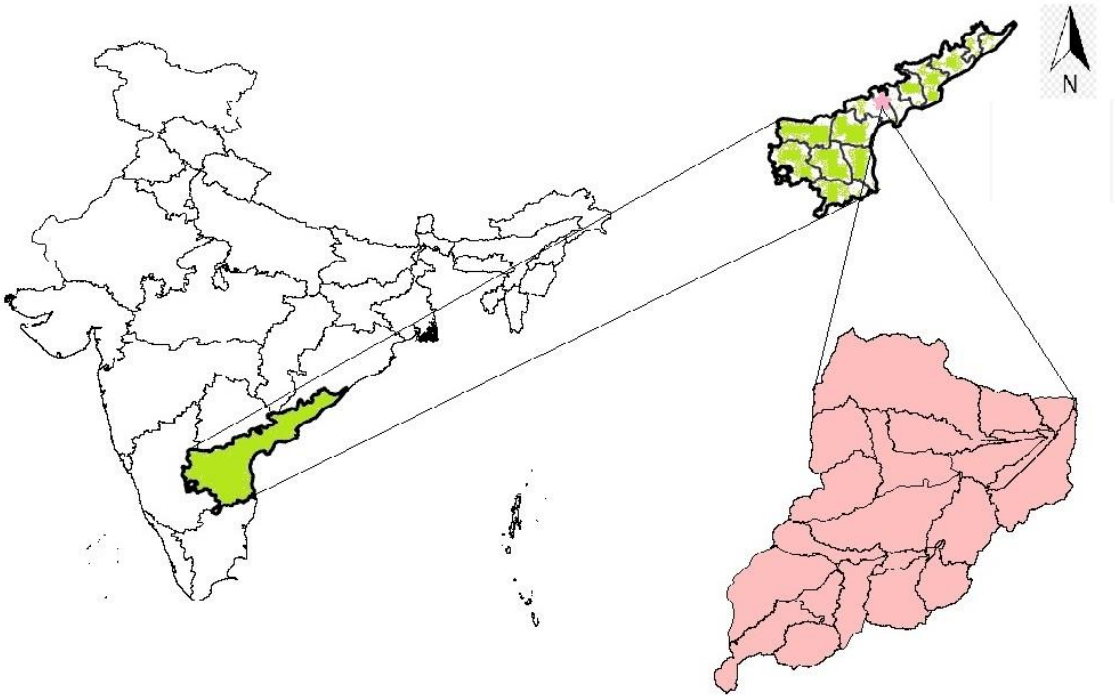

Fig 3. 1 Map of the study area showing Kondaveeti Vagu catchment

3.2.2. Kondaveeti Vagu and its tributaries

Perecherla village of Guntur district, which has the Kondaveedu hill ranges, the originating point of Kondaveeti Vagu, is situated on the south of the proposed capital city, Amaravati. The vagu (a small stream) passes through Achampeta, Tadikonda, Mangalagiri and Amaravati over a length of 29.5 km before its confluence with Krishna River near the upstream of Prakasam Barrage. The major tributaries which join Kondaveeti Vagu at different points are Paala Vagu, Kotella Vagu, and Erra Vagu. Pala Vagu is spread over a length of 16.3km. To overcome the issue of flooding in Kondaveeti Vagu, a lift system is built to handle the floodwater. The pump house is built in the low-lying region; Undavalli of Amaravati near the upstream of Prakasam barrage is installed with 16 pumps, each capable of lifting 350 m^3/sec of water to transfer it back to the Krishna River. One of the pumps is kept as a standby in case, any of the pumps fail any time.

3.2.3. Climatic condition

The temperature of the warmest month, May, in the region has an average high temperature of 42°C and an average low temperature of 27°C. Most of the rainfall occurs in the month of July in Amaravati. The average annual rainfall in the region is about 870 mm. The average high and average low temperatures range between 28°C and 15°C during the coldest months of December and January.

Humidity

The humidity in the study area is the highest during July to September and the least from March to April. The relative humidity in the district around Guntur ranges from 63% to 81%. The most extreme moistness is seen during September. This is because, before the end of August, this area would have received significant rainfall, and all the tanks would be full, and waterways and streams would be streaming in rapids. These make the relative humidity in the district as high as 81%. In the dry and hot months of April and May, when practically all the tanks and water resources are dry, the most extreme humidity is about 63%.

3.2.4. Land Use Land Cover (LULC)

The landscape of the city of Amaravati is dominated by hills, tanks, forests and rock formations. From the land use and land cover map of the Kondaveeti Vagu catchment, it can be seen that the built-up area in the catchment is 25.2%, while the barren land covered 16.76% of the catchment area. As the catchment comprises of fertile soil, around 51.4% is the cropland, and the vegetation cover over the catchment is around 6.17% with the water bodies over 0.4% of the total area.

3.3. Data Collection

The various data required for carrying out the flood inundation modelling include the Digital Elevation Model (DEM), rainfall data of the study area, geometric and cross-sectional data of the streams and reservoirs present in the watershed, topographical details, hydro-meteorological data like infiltration, base flow etc.

Rainfall data was collected from the Indian Meteorological Department (IMD) for the past 59 years (from 1961 to 2020) as gridded data (0.5^0 x 0.5^0). Hourly rainfall data from Gannavaram Airport and daily rainfall data from APCRDA were also collected. Shuttle Radar Topography Mission (SRTM) DEM with 30m x 30m resolution, downloaded from United States Geological Survey (USGS), is used in the study to delineate the watershed as well to generate the terrain for the hydrodynamic modelling. Toposheets, cross-sectional data of the Kondaveeti Vagu, Pala Vagu, Anathavaram, Sakhamuru, Neerukonda and Krishnayapalem were collected from APCRDA. The land use and land cover map, and soil map were downloaded from Bhuvan website. Discharge data or water stages for the Vagu were not available. From the reports of APCRDA, the only recorded data known about the discharge was that for 100-year return period the peak discharge was 460 m^3/s at the confluence point of Kondaveeti Vagu with Krishna River. Table 3.1 shows the different satellite images that were collected for the study.

Table 3. 1 List of satellite images collected

Satellite	Date
Landsat 5 TM	03 June 1990
Landsat 5 TM	27 April 2000
Landsat 5 TM	09 May 2010
Landsat 8 OLI	01 May 2013
Landsat 8 OLI	17 March 2014
Landsat 8 OLI	20 March 2015
Landsat 8 OLI	22 March 2016
Landsat 8 OLI	25 March 2017
Landsat 8 OLI	31 May 2018
Landsat 8 OLI	15 March 2019
Sentinel 2A	26 April 2016
Sentinel 2A	11 April 2017
Sentinel 2A	16 April 2018
Sentinel 2A	26 April 2019

Regional climate model data was obtained from Coordinated Regional Climate Downscaling Experiment (CORDEX) which is of 50km x 50km resolution simulated under RCP 4.5 and RCP 8.5 scenarios. Based on the availability of climate data, five models were selected for the impact studies (Table 3.2). RCP 4.5 is a scenario with stabilized radiative forcing of 4.5 W m−2 i.e., approximately 650 ppm CO_2-equivalent, which considers the long-term global emissions of greenhouse gases on short-lived species. Thomson et al. (2011) suggested that RCP4.5 scenario in climate models investigated the remote future response of climate system by stabilizing the anthropogenic components of radiative forcing. RCP 8.5 is characterized as high greenhouse gas emissions scenario over time with increased concentration levels of greenhouse gases (Riahi et al. 2011). Climate model data has bias when compared with observed data.

Table 3. 2 List of climate models

Acronym	Expansion	Modelling Centre
ACCESS	Australian Community Climate and Earth System Simulator	Commonwealth Scientific and Industrial Research Organization and Bureau of Meteorology, Australia
CCSM4	Community Climate System Model	National Center for Atmospheric Research
CNRM_CM5	Centre National de Recherché Meteorologiques	Centre National de Recherches Meteorologiques, Centre Europeen de Recherche et de Formation Avancee en Calcul Scientifique
NorESM 1	Norwegian Earth System Model 1	Bjerknes Centre for Climate Research, Norwegian Meteorological Institute
MPI-ESM-LR	Max Plank Institute Earth System Model at Base Resolution	Max Planck Institute for Meteorology
GFDL-CM3	Geophysical Fluid Dynamics Laboratory Climate Model version 3	Geophysical Fluid Dynamics Laboratory

3.4. Methodology

3.4.1. Trend analysis

There are mainly two types of statistical tools that are being used to identify the trends in time-series: parametric and nonparametric. Parametric trend test of the annual average precipitation series was carried out using the linear regression method. This method is extensively used in the research since it gives results that are simple and easy to interpret, analytically as well as graphically, considering the parameters and shape of the trend equation (Wibing and Gloicki 2002; Feidas et al. 2004). The value of the slope determines the sign of the trend for temperature. In this interpretation, a slope which is greater than zero indicates a positive or increasing trend, a slope which is less than zero indicates a negative or decreasing trend and a slope that is equal to zero indicates no trend (no change).

The occurrence of monotonic negative or positive trends was identified using the non-parametric MK1 trend test. The MK1 test was considered for monotonic series, and therefore, it was not appropriate for cases with periodic or sequence data. The Modified Mann Kendall (MK2) trend test was used to obtain better results of the trend from the autocorrelated series.

Using Innovative Trend Analysis (ITA) technique, monotonic and non-monotonic trends in the data were identified with or without any pre-condition of the serial correlation, size of the dataset and distributions. Trends in low, medium and high ranges in the rainfall data were checked using ITA technique. For finding the proper slope of a linear trend, Sen's slope technique, which uses a linear model for the estimation of residual's variance and trend's slope, was used. The Kolmogorov-Smirnov test was used to identify the normality of maximum monthly, seasonal and annual rainfall data (Deepesh and Jha 2012; Kanji 2006). It should be noted that single data error or outliers will not produce a considerable impact on Sen's slope technique (Gilbert 1987). The spatial distribution of the trends in monthly, seasonal and annual maximum rainfall series was interpolated using the inverse distance weighting (IWD) method in ArcGIS 10.3 environment. The MK1, MK2 and ITA approaches have many advantages which make them valuable in analysing hydrological variables.

3.4.1.1. Mann-Kendall Test (MK1)

MK1 trend analysis is a rank-based non-parametric test (Kendall 1975; Mann 1945). The MK1 test statistic S is computed using equation (3.1), and the sign function is calculated using equation (3.2).

$$S = \sum_{j=1}^{n-1} \sum_{i=j+1}^{n} sign(x_i - x_j) \tag{3.1}$$

$$sign(x) = \begin{cases} 1 & \ldots. \ for \quad (x > 1) \\ 0 & \ldots. \ for \quad (x = 1) \\ -1 & \ldots. \ for \quad (x < 1) \end{cases} \tag{3.2}$$

where n - length of data

x_j - rank for j^{th} observations ($j = 1,2,3 \ldots . n-1$),

x_i - rank for i^{th} observations ($i = j+1, 2, 3 \ldots . n$)

For the time series, S is the test statistic considered where the length of observation $n > 10$ is usually asymptotically allocated with variance given in equation (3.3) and mean $E(S) = 0$.

$$V(s) = \frac{n(n-1)(2n+5)}{18} \tag{3.3}$$

The standardised Z value is calculated as shown in equation (3.4)

$$Z = \begin{cases} \frac{S-1}{\sqrt{V(s)}} & when \;\; S > 0 \\ 0 & when \;\; S = 0 \\ \frac{S+1}{\sqrt{V(s)}} & when \;\; S < 0 \end{cases} \quad (3.4)$$

Z follows the standard normal distribution with mean zero ($\mu = 0$) and variance equal to 1.0 ($\sigma^2 = 1$). The null hypothesis (Ho) indicates that there is no significant trend, and the alternate hypothesis ($H1$) indicates that there is a significant trend. Therefore, in a two-sided test, the hypothesis Ho and $H1$ are verified at significance levels (α), i.e., α= 10% with Z = ± 1.645, α = 5% with Z = ± 1.96 and α = 1% with Z = ± 2.33. If $\pm Z > \pm Z\ \alpha/2$, then $H1$ is accepted, and Ho is rejected. Positive Z indicates an increasing trend and negative Z indicates a decreasing trend.

3.4.1.2. Modified Mann Kendal (MK2)

To detect a trend in the time series with autocorrelation, pre-whitening is used, which is likely to decrease the significant trend detection rate in MK1 test (Cunderlik and Burn 2004; Kumar and Rathnam 2019; Yue et al. 2003; Wang et al. 2020). Hence MK2 test (Hamed and Rao 1998) was also applied to the autocorrelated series for better detection of the trend. Initially, the Theil and Sen's median slopes were calculated and subtracted from the data. Then the ranks of the observations ρ_k were analysed, and the autocorrelation between these ranks was evaluated. To arrive at the variance correction factor n/n_s^*, only the significant values of ρ_k were evaluated. The variance correction factor for positive n is required since the variance of S is underestimated when autocorrelated positively charged data is used (equation (3.5)).

$$\frac{n}{n_s^*} = 1 + \frac{2}{n(n-1)(n-2)} \times \sum_{k=1}^{n-1} (n-k)(n-k-1)(n-k-2)\rho_k \quad (3.5)$$

where n is the actual length of data

n_s^* - 'effective' number of data to account for autocorrelation

ρ_k - autocorrelation function of ranks of the data.

Corrected variance, $V^*(S)$ is given by

$$V^*(S) = V(S) \times \frac{n}{n_s^*} \quad (3.6)$$

where $V(S)$ is given as

$$V(S) = \frac{n(n-1)(2n+5) - \sum_{i=1}^{m} t_i(t_i-1)(2t_i+5)}{18} \quad (3.7)$$

The standardised test statistics Z (N (0,1)) is calculated by

$$Z_{MK} = \begin{pmatrix} \frac{S-1}{\sqrt{V^*(S)}} \; when\, S > 0 \\ 0 \qquad when\, S = 0 \\ \frac{S+1}{\sqrt{V^*(S)}} \; when\, S < 0 \end{pmatrix} \quad (3.8)$$

3.4.1.3. Innovative Trend Analysis

The ITA technique, proposed by Sen (2012), was used to analyse the rainfall trends for maximum monthly, seasonal and annual time series. The advantage that ITA technique possesses over other trend analysis methods is, that, it does not involve assumptions like non-normality, serial correlation and sample number. For ITA, the dataset was divided into two equal lengths. Both parts were arranged in increasing order. The first half of the dataset were plotted on the X-axis, and on the Y-axis- the second half of the dataset were plotted. When the points are plotted on the 45° line (1:1 ideal line), no trend was observed. An increasing trend existed for the points in the upper triangular area of the 45° line. If points are in the lower triangular area of the 45° line, then a decreasing trend was observed (Zekâi 2012). In some situations, non-monotonic trends occur for the variable concerned, which indicated decreasing as well as increasing trends which occurred within the series temporally. In such cases, for detailed interpretation, points that are plotted on the 45°line graphs are separated into clusters called low, medium and high. The main advantage of ITA technique is that the MK trend test assumptions are avoided here and further, square area plots can calculate the trend magnitudes. Therefore, the trends of low, medium and high values of hydro-climatic or hydro-meteorological variables can accurately be recognised through this technique.

3.4.1.4. Sen's slope

The magnitude of Sen's slope (Sen 1968) is calculated as using equation (3.9)

$$S_i = median\left(\frac{(Y_j - Y_k)}{(j-k)}\right) for\ i = 1,2,3 \ldots\ldots N, \text{ (j > k)} \quad (3.9)$$

where, Y_j and Y_k are observations at times j and k. The median of the $N = \frac{n(n-1)}{2}$ where n is the number of time-periods.

3.4.2. Stationarity and homogeneity analysis

Homogeneity of precipitation series is calculated by Standard Normal Homogeneity Test (SNHT), Buishand's test, Pettitt's test and von Neumann's test. Stationarity and non-stationarity of precipitation time-series were determined using Kwiatkowski– Phillips–Schmidt–Shin (KPSS), Phillips-Perron (PP) and Dickey-Fuller (ADF) methods.

3.4.2.1. Stationarity analysis

The main objective of trend analysis is to understand whether the data set has general decreasing or increasing trend characteristics. But, this behaviour of the time series does not show non-stationarity always. To find out the non-stationarity in series, further analyses are required. In this study, three statistical analyses are used identify the non-stationarity in the annual average precipitation series. These are ADF, KPSS and PP approaches. These methods are considered because they are commonly used in hydrological research (Yoo, 2007; Wang et al. 2005; Wang et al. 2006).

Phillips-Perron test is based on the equation (3.10)

$$X_t = \mu + \alpha t + \pi X_{t-1} + u_t \quad (3.10)$$

where, μ and α are the first-order polynomial regression parameters and u_t is not considered as white noise. PP test is the modification of ADF test (Dickey and Fuller, 1979), by correcting the heteroskedasticity and serial correlation present in the error. The unit root null hypothesis is verified with H0: $\pi = 1$ in contrast to the alternate Ha: $\pi < 1$.

KPSS method was introduced by Kwiatkowski et al. (1992). It matches the unit root test by finding the null hypothesis of stationarity either around a deterministic trend or a fixed level against the alternate of difference stationary series. The series $\{X_t\}$ is stated as the sum of stationary error (ε_t), random walk (r_t), deterministic trend (αt) and the test is Lagrange Multiplier Test of the hypothesis (equation (3.11))

$$X_t = \alpha t + r_t + \varepsilon_t \tag{3.11}$$

$r_t = r_{t-1} + u_t$, where u_t are $iid(0, \sigma^2)$ (3.12)

The null hypothesis H_o: $\sigma u2 = 0$ and $\propto = 0$ against the alternative H_a is the same as that of deterministic trend (trend stationarity), to find the stationarity around a trend stationarity, in AR (1) model and ADF test, as shown in equation (3.13)

$$y_t = \theta y_{t-1} + \varepsilon_t \tag{3.13}$$

The stationarity against the unit root null hypothesis alternative corresponds to: H_A: $\theta < 1$ against H0: $\theta = 1$. The model can be also formulated as (equation (3.14))

$$\Delta y_t = (\theta - 1) y_{t-1} + \varepsilon_t = \pi y_{t-1} + \varepsilon_t \tag{3.14}$$

where $\pi = \theta - 1 = \theta(1)$. The unit root hypothesis converts to H0: $\pi = 0$ against HA: $\pi < 0$.

The test statistic of ADF ($\hat{\tau}$) is calculated by equation (3.15)

$$\hat{\tau} = \frac{\hat{\theta} - 1}{se(\hat{\theta})} = \frac{\hat{\pi}}{se(\hat{\pi})} \tag{3.15}$$

The asymptotic distribution of $\hat{\tau}$ is not normal. This distribution depends on the deterministic components. In the simple case, the 5% critical value (one-sided) is −1.95 and not −1.65.

PP and ADF tests show non-stationarity in the time-series when the result shows null hypothesis H0, while the KPSS test show stationarity in the time-series data for null hypothesis H0. A confidence level of 0.05 was considered for the stationarity test in this study. The null-hypothesis H0 is rejected when the confidence level is higher than the Probability (P-value) of

the statistics. van Gelder et al. (2007) and Sen and Niedzielski (2010) explained these tests in details.

3.4.2.2. Homogeneity and change point analysis

In this study, change point analysis was done for the annual average precipitation time series to determine the time period showing the discontinuity in the data for this study. This can be due to the effects of various factors like climate change, human interference or observational error while monitoring or recording. Four methods are selected in this study to determine the homogeneity of the precipitation series and to find the change point. These methods are: the Buishand range test (Buishand, 1982), the SNHT (Alexandersson, 1986), the von Neumann ratio test (von Neumann, 1941) and the Pettitt test (Pettitt, 1979). The SNHT, Pettit test and Buishand range test identify the year of change point, while von Neumann ratio test shows only the presence of change point in the series (Winjngaard et al. 2003). The SNHT test detects change point near the starting and end of the time-series while Buishand test and Pettitt test identify change point in the middle of the series. (Hawkins 1977, Kang and Fadhilah 2012, Costa and Soares 2009).

In SNHT a statistic T_y, as shown in equation (3.16), is used to relate the average of the first y years with the last of (n-y) years:

$$T_y = y\overline{z}_1 + (n-y)\overline{z}_2 \ , y = 1,2,3,\dots,n \tag{3.16}$$

where

$$\overline{z}_1 = \frac{1}{y}\sum_{i=1}^{n}\frac{Y_i-\overline{Y}}{s} \tag{3.17}$$

$$\overline{z}_2 = \frac{1}{n-y}\sum_{i=y+1}^{n}\frac{(Y_i-\overline{Y})}{s} \tag{3.18}$$

The year y has break if value of T is maximum. To reject null hypothesis, the test statistic,

$$T_0 = maxT_y \tag{3.19}$$

must be greater than the critical value, which depends on the sample size.

In Buishand Range test, the adjusted partial sum is defined as given in equation (3.2).

$$S_o^* = 0 \quad \text{and} \quad S_y^* = \sum_{i=1}^{y}(Y_i - \overline{Y}) \quad y = 1,2,3,\dots,n \tag{3.20}$$

When the series is homogeneous, then the value of S^*_y will rise and fall around zero. The year y has break when S^*_y has reached a maximum (negative shift) or minimum (positive shift). Rescaled adjusted range, R is obtained by (equation (3.21)

$$R = \frac{\max\limits_{0\le y\le n} S_y^* - \min\limits_{0\le y\le n} S_y^*}{s} \tag{3.21}$$

The $\frac{R}{\sqrt{n}}$ is the critical values used by Buishand (1982).

Pettitt Test is based on the rank, r_i of the year, y_i and ignores the normality of the series.

$$X_y = 2\sum_{i=1}^{y} r_i - y(n+1), y = 1,2,3,\dots,n \tag{3.22}$$

The change is observed in year k when

$$X_k = \max_{1\le y\le n} |X_y| \tag{3.23}$$

The result is then related with the critical value by Pettitt (1979). The ratio of mean square of successive year to year difference to the variance is used in Von Neumann Ratio Test. The test statistic is shown in equation (3.24)

$$N = \frac{\sum_{i=1}^{n-1}(Y_i - Y_{i+1})^2}{\sum_{i=1}^{n}(Y_i - \overline{Y})^2} \tag{3.24}$$

The null hypothesis H0 is considered as homogeneous series and the alternative hypotheses Ha is non-homogeneous.

3.4.3. Land Use Land Cover changes

3.4.3.1. Land Use Land Cover classification

Supervised classification technique was used to classify the images into five classes, namely, cropland, barren land, built up area, vegetation, and water. Supervised classification

is the process of sorting pixels into a finite number of individual classes or categories based on their digital values. If a pixel satisfies a certain set of criteria, then the pixel is assigned to the class that corresponds to that criterion. In this process, the pixels that represent certain patterns are selected or can be identified with the help of other sources. Knowledge of the data, the classes desired and the algorithm to be used are required to be planned before selecting the training samples. In this study, Maximum Likelihood Classification (MLC), was the algorithm used for supervised classification, which is one of the most popular supervised classification methods used with remote sensing image data. This method is based on the probability that a pixel belongs to a particular class. The basic theory assumes that these probabilities are equal for all classes and that the input bands have normal distributions (Erdas Inc, 1999). Training sets were given as input to as signature files to classify the FCC image. ArcGIS 10.3 software was used for supervised classification.

3.4.3.2. Accuracy assessment

Error matrix (or) Confusion matrix was used for accuracy assessment. Producer's accuracy, user's accuracy, overall accuracy and kappa coefficients were calculated for the data. Google Earth images were used as reference data to compute the accuracies and kappa coefficient.

The producer's accuracy is defined as the ratio of correctly classified pixels to the total reference pixels. The user's accuracy is referred to as the ratio of correctly classified pixels to the total classified pixels. Overall accuracy represents the ratio of a total number of correctly classified pixels to the total number of pixels. All the three types of accuracies are expressed as the percentage. Kappa coefficient quantifies the level of information represented in the main diagonal of the table and later these values are adjusted for the amount of agreement that could be expected due to chance alone. Kappa coefficient, given in equation (3.25) is always less than or equal to 1. A value of 1 indicates perfect agreement between the classified data and the actual data (Gwet, 2002; Viera and Garrett, 2005).

$$\textbf{\textit{kappa coefficient}} = \frac{OA-AC}{1-AC} \tag{3.25}$$

where OA = Overall Accuracy and AC = Agreement by Chance.

3.4.3.3. Indices

NDVI, MNDWI, NDBI, and NDISI, were calculated for Landsat images from 2013 – 2018. NDVI, NDBI, and MNDWI were calculated for sentinel images from 2016 – 2019. NDISI was not possible to be calculated for sentinel images as there was no thermal band for sentinel data. Raster calculator in QGIS 3.4 was used to calculate the indices for the corresponding data. Corresponding bands in different satellites are shown in Table 3.3. The following expressions have been used to calculate different indices.

(i) Normalized Difference Vegetation Index (Lucas 1995):

$$NDVI = \frac{NIR - RED}{NIR + RED} \tag{3.26}$$

(ii) Normalized Difference Built Index (Zha et al. 2003):

$$NDBI = \frac{SWIR1 - NIR}{SWIR1 + NIR} \tag{3.27}$$

(iii) Modified Normalized Difference Water Index (Xu, 2006):

$$MNDWI = \frac{GREEEN - SWIR1}{GREEN + SWIR1} \tag{3.28}$$

(iv) Normalized Difference Impervious Surface Index (Xu, 2010):

$$NDISI = \frac{TIR - \left(\frac{MNDWI + NIR + SWIR1}{3}\right)}{TIR + \left(\frac{MNDWI + NIR + SWIR1}{3}\right)} \tag{3.29}$$

Table 3. 3 Corresponding bands in different satellites

Sl No:	Band	Landsat 8	Sentinel 2
1.	Green	Band 3	Band 3
2.	Red	Band 4	Band 4
3.	Near Infrared	Band 5	Band 8
4.	Shortwave Infrared	Band 6	Band 11
5.	Thermal Infrared	Band 10	-

3.4.4. Rainfall data analysis of extreme events

For the frequency analysis of the rainfall data, 24-hour maximum annual series was generated from the collected rainfall data. Fig 3.2. shows the rainfall variation. 24-hour maximum rainfall events in the years 1969, 1977, 1989, 1994, 1996, 2005, 2006, 2012, 2013 and 2017 are 185.95mm, 138.43mm, 182.63mm, 135.83mm, 151.22mm, 175.05mm, 146.83mm, 152.70mm and 157.21 respectively.

Frequency analysis was carried out in the study with the help of EasyFit software. EasyFit is effectively used by business analysts, engineers, researchers and scientists for different purposes like risk analysis, economics, market research, reliability engineering, hydrology, forestry, image processing, and many other areas where the users need to deal with random data. The ranking by three goodness of fit test approaches, viz., Kolmogorov Smirnov, Anderson Darling and Chi-Squared method was obtained. The distribution with the best fit rank was chosen for the estimation for 24-hour maximum rainfall for different return periods. The analysis of the precipitation data showed the Generalised Extreme Value (GEV) distribution as the best fit. Therefore, one-day maximum rainfall depth was estimated for various return periods of 2, 5, 10, 50, 100 and 200 years using GEV.

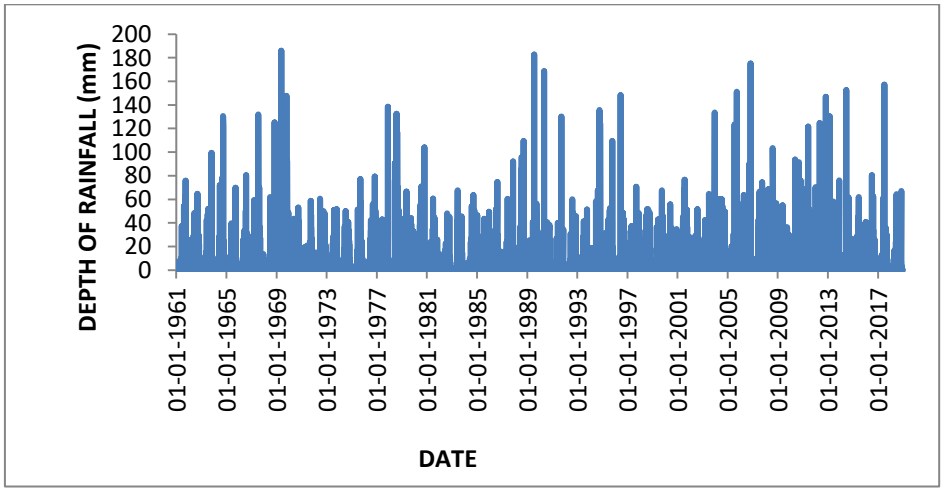

Fig 3. 2 Depth of rainfall from 1961-2020

3.4.5. Hydrologic modelling

3.4.5.1. HEC-HMS

HEC-HMS is one of the models used for carrying out the hydrological modelling in the catchment area. HEC-HMS is a differential surface - water model that is reliable for the simulations of rivers, watersheds, channels, and water-control structure behaviour, thus predicting flow, stage, and timing. The model carries out the computation of the rainfall losses into the soil and the excess rainfall is converted to runoff and routing (Maidment and Seth, 1999). HEC- HMS version 4.2.1 is used in the study to carry out the hydrologic modelling.

Fig 3.3 shows the user interface of the HEC-HMS model comprising of the basin model, meteorological models, control specifications and time-series data. All the sub-basin, junction and reaches can be identified in the Kondaveeti Vagu catchment.

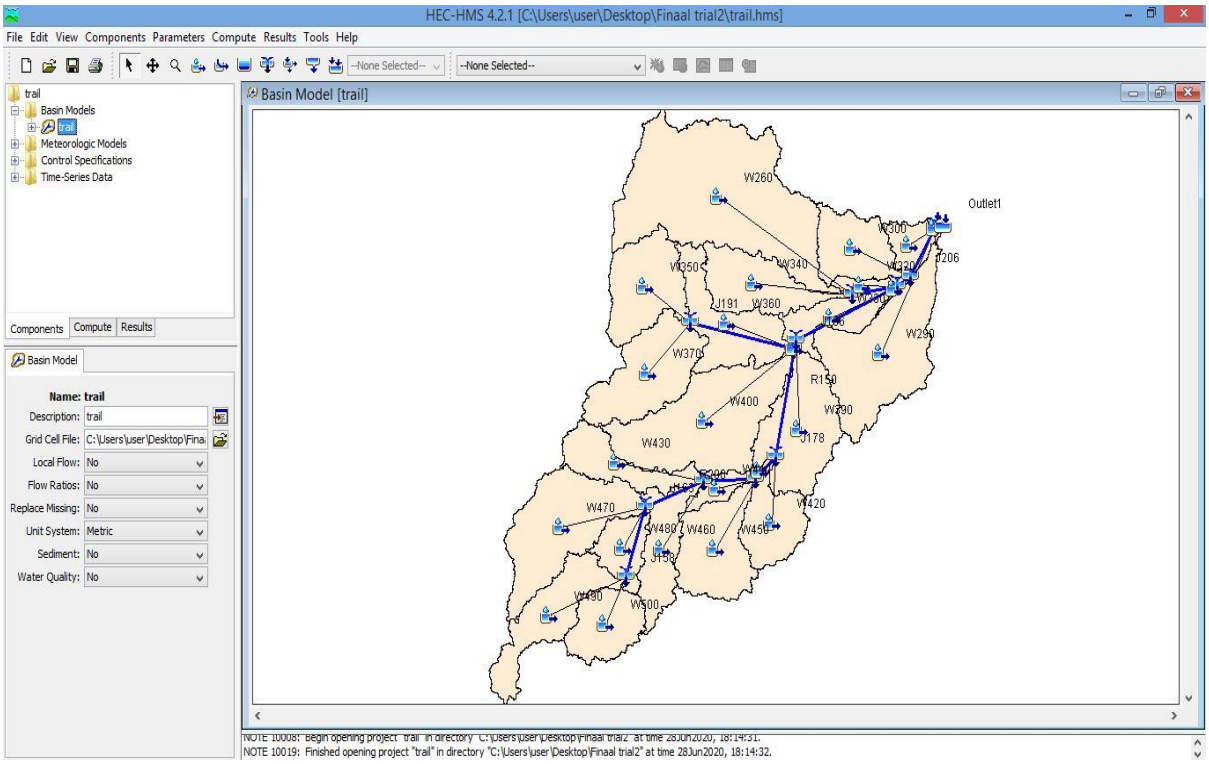

Fig 3. 3 User interface of HEC-HMS showing basin model file

HEC-HMS has three major components i.e.

i. Basin Model: The basin model component contains descriptions associated to the physical characteristics of the basin. Basin model consists of the sub-basins, junction and river reach.

   Sub-basin: Various inputs that are to be provided for a sub-basin are the area of the sub-basin, downstream of the sub-basin, loss method and the transform method. The area of the sub-basins is given as obtained in ArcGIS during the terrain processing.

ii. Loss model - SCS Curve Number method

   a) Different loss methods available in HEC-HMS are Green and Ampt, Deficit and Constant, Exponential, Initial and Constant, SCS Curve Number, Smith Parlange, and Soil Moisture Accounting. In the study, the SCS CN method is used as the loss method for estimating the initial abstraction parameters for the sub-basins.
   b) Basin Curve Number depends on the physical property of the sub-basin. While data processing of the DEM using HEC-GeoHMS extension in the ArcGIS environment, the basin Curve Number values were estimated for every sub-basin. These values of sub-basin Curve Number were then obtained from the attributes table of the sub-basin layer.
   c) Percentage of imperviousness for each sub-basin is considered as 60.0% for the city area in the Kondaveeti Vagu catchment since the urban area is still under development.

iii. Transform method - Modified Clark Method

   a) For Modified Clark method, Kirpich formula (Eq.3.30) (Subramanya 2018) is used to calculate the time of concentration. One of the basin parameters is time of concentration Tc (in minutes) which represents the physical characteristics of the basin, the time taken to travel to the outlet from the farthest point in the watershed. It depends on length travelled (L) in metres and slope S of the watershed.

$$Tc = 0.01947\left(\frac{L^{0.77}}{S^{0.385}}\right) \quad (3.30)$$

   The land use and land cover digital maps were utilized to find the spatially varying roughness coefficient and CN values for the floodplain.

b) Basin Lag time in hours for each sub-basin was computed using equation (3.31) (USACE, 2000) and then is multiplied by 60 for converting into minutes.

$$\text{Lag}= \frac{L^{0.8}(S+1)^{0.7}}{1900*Y^{0.5}} \quad (3.31)$$

where S = Maximum retention

Lag = basin lag time (hours)

L= hydraulic length of the watershed (the longest flow path in feet)

Y = Basin slope (%)

Reach: For routing, Muskingum–Cunge method is applied to the handle the water movement in the reach.

Junction: The downstream reach to the junction is given as the input for a junction in the model.

iv. Precipitation model consists of precipitation data input files of a past flood event and for return periods of 2, 5, 10, 50, 100 and 200 years.

v. Control specifications is the section that comprises information related to the date and time of the occurrence of a storm event or the time interval for which the simulation is to be carried out.

The simulation is run to obtain the peak runoff hydrographs at the outlet as well as for each junction. The hydrographs generated are used as the input flow hydrographs in the unsteady flow data in HEC-RAS.

Data Processing Tools

HEC-RAS is used for the modelling of flood in the Kondaveeti Vagu catchment. To delineate the watershed, ArcGIS 10.3 containing ArcInfo, ArcCatalog, ArcToolbox and extensions such as 3D analyst, spatial analyst, ArcHydro tools and HEC-GeoHMS was used. In the present work SRTM 30m x 30m DEM in ESRI format has been used in developing the HEC- HMS basin model.

Terrain processing is carried out in ArcGIS by using the HEC-GeoHMS extension. It involves the following procedure for pre-processing, project setup, characteristics, and HMS:

Pre-processing

i. Fill Sinks: Resampling and interpolating of the grid can cause errors in the DEM which may result in pits or depression. Thus, to create a depressionless DEM, filling of the

depression was done by increasing the elevation of lower elevated cells to the level of the neighbouring terrain. Raw DEM is the input given for generating fill sinks.

ii. Flow Direction: It defines the direction of the steepest descent for each terrain cell. Hydro DEM is given as input data for generating the flow direction map.

iii. Flow Accumulation: It defines the number of upstream cells which will be draining into a given cell. By multiplying the flow accumulation value to the grid cell area, upstream drainage area can be determined. Flow direction data is given as input for generating the flow accumulation of terrain.

iv. Stream Definition: This progression arranges all cells with a flow accumulation greater than the user-defined threshold as cells belonging to the stream network. The flow accumulation for a specific cell must surpass the user-defined threshold for a stream to be started. Flow accumulation grid and the number of cells are given to define the stream as input data for generating stream definition.

v. Stream Segmentation: For dividing the stream grid into segments, stream grid and flow direction grid are used as input data. Streams segments are the parts of a stream that combines two successive junctions, a junction and an outlet, or a junction and the drainage divide.

vi. Catchment Grid Delineation: Knowing the input of flow direction grid and stream link grids for all of the stream segments, the watershed is delineated into sub-basins.

vii. Catchment Polygon Processing: Using the catchment grid delineation as input, the polygon sub-basin layer of the catchment is produced.

viii. Drainage Line Processing: Giving the input of stream link and flow direction, the stream vector layer of drainage line is generated.

ix. Adjoint Catchment Processing performed in the sequential order.

Project setup

i. Start a new project: Project is defined by giving the name of the project and thus input of the location to save the project. Project area and project point are defined. Then the watershed is provided with an outlet or inlet by adding project points.

ii. Generate project: After adding the project point and defining the project, generate project is done.

Characteristics

River length, river slope, longest flow path, basin centroid and the centroidal longest flow path are the characteristics used in the study.

Parameters

River name, basin name, grid cell processing and sub-basin parameters from raster are the parameters used.

HMS

i. Basin model file
ii. Grid cell processing
iii. HMS Schematic
iv. Meteorological model file
v. Creation of an HEC-HMS project.

3.4.5.2. Storm Water Management Model (SWMM)

The SWMM (Huber,1984; Metcalf and Eddy Inc, 1971; Peterson and Wicks, 2006; Burger et al. 2014) is a dynamic rainfall-runoff simulation model based on momentum, mass and energy conservation laws. This model is used in the design, analysis and planning of drainage systems and for the simulation of runoff quality and quantity in urban areas (Rossman, 2010, Martínez-Solano et al. 2016; Rabori and Ghazavi, 2018). Additionally, SWMM can simulate the quality and quantity of runoff generated in each catchment and through each pipe during a simulation period. Compared with other models, SWMM results indicated that runoff reached a peak in the shortest time, and the calculated values were closer to the measured values (Lee et al. 2010). In this study, each catchment (containing both impervious and pervious areas) was regarded as a nonlinear reservoir, and its net rainfall was delivered from or overflowed to other catchments. Runoff that changes over time was calculated using the combined continuity equation and Manning's equation. According to the specific circumstances of the study area, infiltration was calculated using the Horton model. For the hydraulic calculations of the pipeline network, the dynamic wave method is used because it considers the counter-flow, pressure flow and storage of the drainage system.

SWMM is used all over the world, for planning, analysis and design related to stormwater runoff, combined and sanitary sewers, and other drainage systems in urban areas. There are many applications for drainage systems in non-urban areas as well. The model tracks

the quantity and quality of runoff made within each sub catchment. It also tracks the flow rate, flow depth, and quality of water in each pipe and channel during a simulation period made up of multiple time steps.

(a) Applications

Since its release, SWMM has been used in several sewer and stormwater studies throughout the world. Typical applications include the following:

- Designing and sizing of drainage system components for flood control
- Sizing detention facilities and their appurtenances for flood control and water quality protection
- Mapping flood plains of natural channel systems (SWMM 5 is a FEMA approved model for National Flood Insurance Program (NFPI) studies)
- Designing control strategies for minimizing combined sewer overflows
- Evaluating the impact of inflow and infiltration on sanitary sewer overflows
- Generating non-point source pollutant loadings for waste load allocation studies
- Controlling site runoff using LID practices
- Evaluating the effectiveness of BMPs for reducing wet weather pollutant loading

In this study, drainage network is created in SWMM with the help of flow accumulation developed from the DEM. The flood occurrence points are determined by providing input data such as intensity from IDF curve, continuous rainfall from historic rainfall data, and runoff by rational method. Other sub-catchment parameters like percentage imperviousness and slopes are also given as input.

Overland flow from each sub-catchment is calculated using the rational formula. Runoff coefficients (C) for each sub-catchment are taken based on land use of the study area. Each sub-catchment has a heterogeneous land use, and hence the C values are taken as weighted average of the area. Open conduits are selected for the study area. Design storms with return periods 2, 5, 10, 25 and 100 years are simulated by giving historical rainfalls in the SWMM model with no combined sewer overflow.

Sub-catchment areas may either be pervious or impervious. Pervious areas contribute to runoff losses due to infiltration. Impervious areas have losses due to depression or detention storage. Infiltration is modelled using the Horton infiltration method. Surface runoff is calculated using Manning's equation. Flow routing in channels and pipes is simulated by Saint

Venant equation through the conservation of mass and momentum for unsteady flow. To arrive at the most theoretically accurate results, dynamic flow routing was used to solve the complete one-dimensional Saint Venant flow equations (EPA, 2013).

SWMM conceptualizes a drainage system as a series of water and material flows between several major environmental compartments. The sub-catchments are perceived as a land surface compartment. SWMM uses rain gauge readings to represent rainfall inputs to the system. The land surface compartment sends outflow in the form of infiltration to the groundwater compartment and also as surface runoff and pollutant loadings to the transport compartment. In this study, pollutant loads are not considered. The transport module contains a network of conveyance elements (channels, pipes, pumps, and regulators) and storage/treatment units that transport water to outfalls or to treatment facilities. Inflows to this module can come from surface runoff, groundwater interflow, sanitary dry weather flow, or from user-defined hydrographs. The components of the transport compartment are modelled with node and link objects.

The study area was divided into 25 sub-catchments by watershed delineation. Outlet points of each sub-catchment were identified. Discharge outlet points can be either nodes of the drainage system or other sub-catchments. Infiltration of rainfall from the previous area of a sub-catchment into the unsaturated upper soil zone can be described using the Horton infiltration equation, Green-Ampt infiltration equation or the SCS Curve Number approach. In this study, Green-Ampt infiltration model is adopted.

The other principal input parameters for sub-catchments include:

- Rainfall from assigned rain gauges;
- Outlet node or sub-catchment;
- Assigned land uses;
- Tributary surface area;
- Imperviousness;
- Slope;
- Characteristic width of overland flow;
- Manning's n for overland flow on both pervious and impervious areas;
- Depression storage in both pervious and impervious areas; and
- Percentage of impervious area with no depression storage.

Invert elevation and height to ground surface are two important parameters to the junction nodes, where invert elevation is found with the help of DEM. SWMM has 20 common conduit shapes includes irregular open channels, custom closed conduits. SWMM uses the Manning's equation, given in equation (3.32), to express the relationship between flow rate (*Q*), cross-sectional area (*A*), hydraulic radius (*R*), and slope (*S*) in all conduits.

$$Q = \frac{1}{n} AR^{\frac{2}{3}}S^{\frac{1}{2}} \tag{3.32}$$

where *n* is the Manning roughness coefficient. The slope *S* is interpreted as either the conduit slope or the friction slope (i.e., head loss per unit length).

The principal input parameters for conduits are:

- Names of the inlet and outlet nodes;
- Offset height or elevation above the inlet and outlet node inverts;
- Conduit length;
- Manning's roughness;
- Cross-sectional geometry.

(b) Sub-catchment Parameterisation

For every sub-catchment in the drainage network, there is an outlet node (junction) to which it is connected. Twenty-five sub-catchments with different areas, shapes based on the conduits and drainage grid, are located on the natural flow paths and named (S1 to S25) matching the names of the drainage basins. The channels (link) are designed in such a way that the water is redirected to the outlets, along the riverside by gravity. The runoffs from both impervious and pervious fractions of sub-catchments are connected to a single junction.

For the accurate calculation of rainfall-runoff, it is important that the characteristics of the sub-catchments are also considered. The factors that affect the accuracy of surface water runoff modelling using SWMM are (a) width of the overflow path in meters, and (b) the percentage impervious area.

The widths of the sub-catchments are considered as a ratio of the area of sub-catchment (A) to the length of the longest overland flow path of the sub-catchment (L). The Manning's roughness coefficient (n), was assumed based on literature, i.e., for smooth asphalt, n was set to 0.015 for impervious areas and for the pervious area, n was taken as 0.02. The depth of the depression storage was taken as 1.52 mm and 3.81 mm for impervious and pervious surfaces

respectively (Rossman, 2010). For this study, the calibration of model was done with the observed 100-year return period discharge data.

3.4.6. Flood inundation

Flood models can be categorised into several types depending upon their data requirements, level of complexity of the underlying equation and the resolution. 1D models can solve problems of flood flows in open channels with assumptions that vertical acceleration is not significant and that water level in the channel cross-section is approximately horizontal are valid. However, problems arise when the channel is embanked and water levels are different in the flood plain than in the channel and in such situations, 2D models are needed. 2D numerical models solve full shallow water equations, which are able to simulate timing and duration of inundation with high accuracy. 2D flood inundation models are now important parts of flood risk management practices because they are capable of adequately predicting water depth, velocity and flood risk with high level of accuracy (Lamb et al. 2009, Teng et al. 2017). However, 2D modelling has some limitations such as taking a long time to set up and run 2D model, particularly for the large area.

3.4.6.1. HEC-RAS

HEC-RAS is a one-dimensional/ two dimensional steady/unsteady flow hydraulic model designed to support the hydraulic engineers in river flow analysis and floodplain zoning (USACE, 2010). HEC-RAS version 5.0.3 is used in the present study to carry out the hydraulic modelling of the Kondaveeti Vagu catchment.

RAS Mapper is the GIS integration to HEC in which the terrain of the work area is generated from clipped DEM by specifying the project spatial reference system and the input is given for ESRI Projection file of WGS_1984_UTM_Zone_44N", GEOGCS ["GCS_WGS_1984", DATUM["D_WGS_1984]. Different map layers such as Google map, Google satellite, Open street maps, Google terrain streets water, etc. can be enabled in the background from Web Imagery option present in the tools, to get the better understanding of the terrain or work area. The places or the attributes can easily be identified with the help of map layers by adjusting the transparency from the properties of the map layers. The user interface of RAS Mapper is shown in the Fig 3.4.

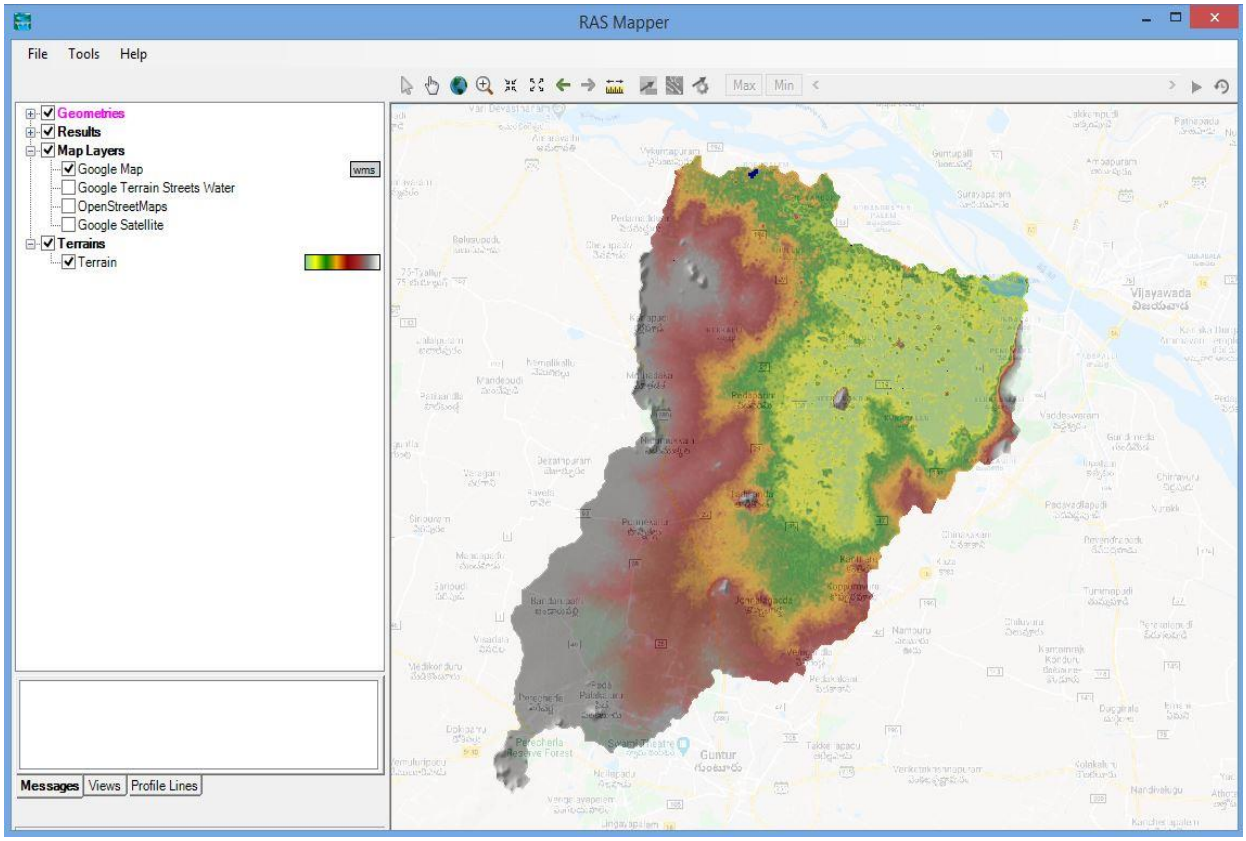

Fig 3. 4 User interface of RAS Mapper showing the catchment area with google map layer

HEC-RAS consists of three main components: -

i. Geometry data: The geometry data contains the information regarding the dimension, shape, and connectivity of stream cross-sections. The Amaravati region consists of four reservoirs in the capital area region namely, Anathavaram, Sakhamuru, Neerukonda and Krishnayapalem. Cross-sectional details of all the reservoirs, Kondaveeti Vagu and Pala Vagu present in the study area are defined and given as input in the geometry data.

   The downstream boundary is provided at the Undavalli outfall where the discharge confluences with the Krishna River and the upstream boundary is located near the Thullur region as the stream from the south of the Kondaveeti Vagu watershed brings the water near Neerukonda reservoir. (Fig 3.5 and Fig 3.6).

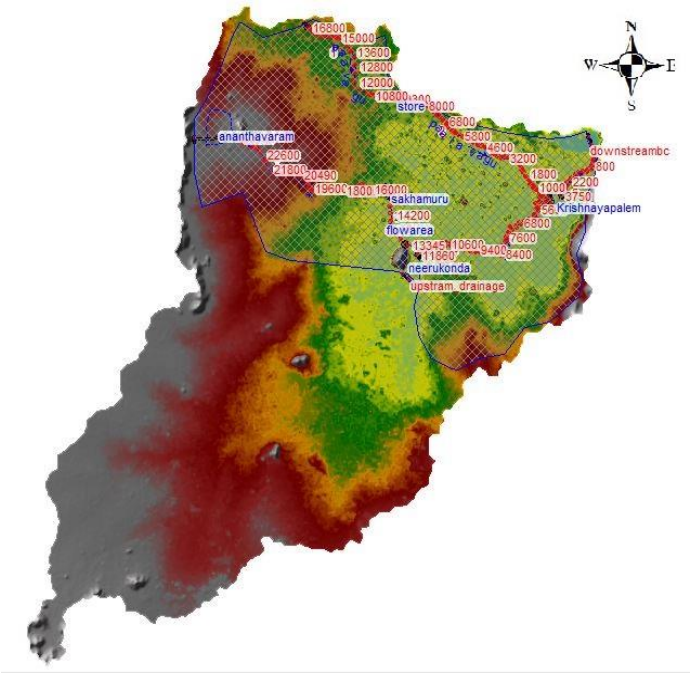

Fig 3. 5 Geometric data input in HEC-RAS

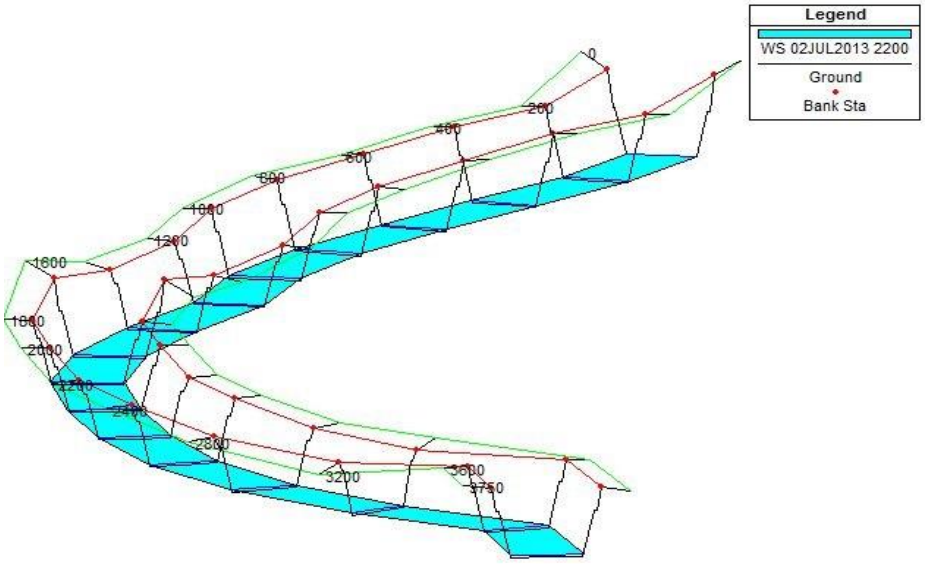

Fig 3. 6 Cross sectional view for the part of the Kondaveeti Vagu

ii. The flow data containing discharge rates: The runoff hydrographs generated in HEC-HMS are given as input for flow data. The model is simulated for the unsteady flow data. Fig 3.7 shows the user interface for unsteady flow data input in HEC-RAS.

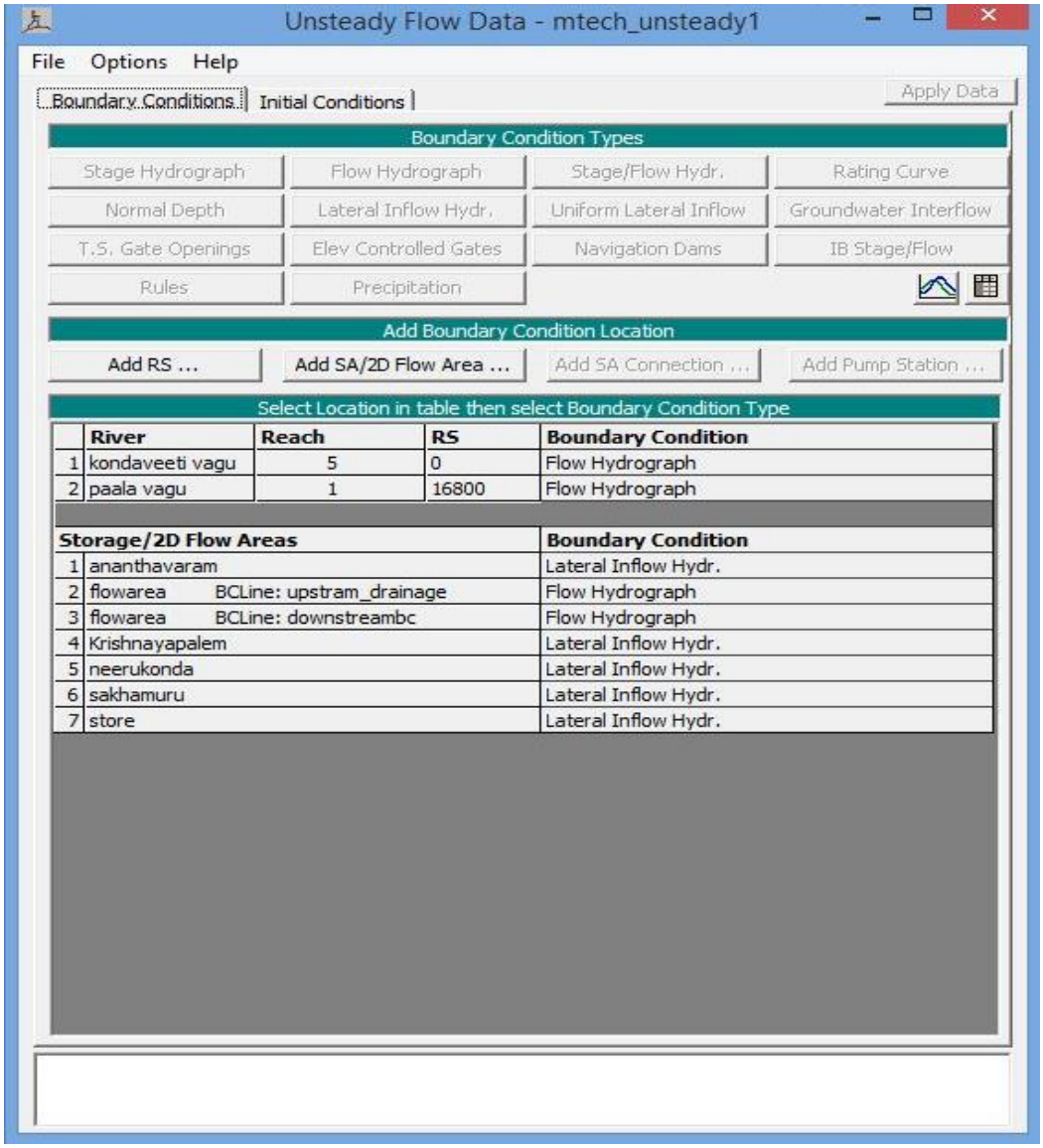

Fig 3. 7 User interface for unsteady flow data input in HEC-RAS

iii) The plan data consists of the information related to the run specifications like simulation time, computation settings and information of the flow regime of the model. The primary method used by HEC-RAS to estimate the water surface profiles assumes a steady, gradually varied flow scenario. The program is then run for geometry processor, unsteady flow simulation and floodplain mapping.

3.4.6.2. Flood inundation study using SWMM

Urban flood inundation studies require high-resolution DEM, land use and soil map, rainfall, topographical details, channel characteristics and hydro-meteorological data like

evaporation, infiltration etc. Preparation of flood inundation map requires runoff resulting from a stormwater management model. All the surface water that is flowing on the terrain drains out through a common outlet. Awareness on the mechanism of drainage basins is the starting point in understanding how vulnerable an area is to floods, as their varying properties have a greater impact on hydrology. Watersheds can be delineated both manually on paper maps and digitally in a GIS environment. Delineation of drainage basins present in this study area was performed by applying the basin tools in ArcGIS and the characteristics of the flow of water on the surface of these basins are studied.

The reference coordinate system of the DEM was transferred to geographic coordinate system WGS1984 (Janssen, 2009). The fill option in ArcGIS helped to remove peaks. Flow direction map was created from the filled DEM. For the study area, flow accumulation and existing drainage network were found to be similar. Thus, pour points were given in the outlets based on the flow accumulation details and watershed delineation was done. After watershed delineation, the total area was divided into 25 sub-basins. The flowchart of the procedure to attain the visualisation of the flood is presented in Fig 3.8.

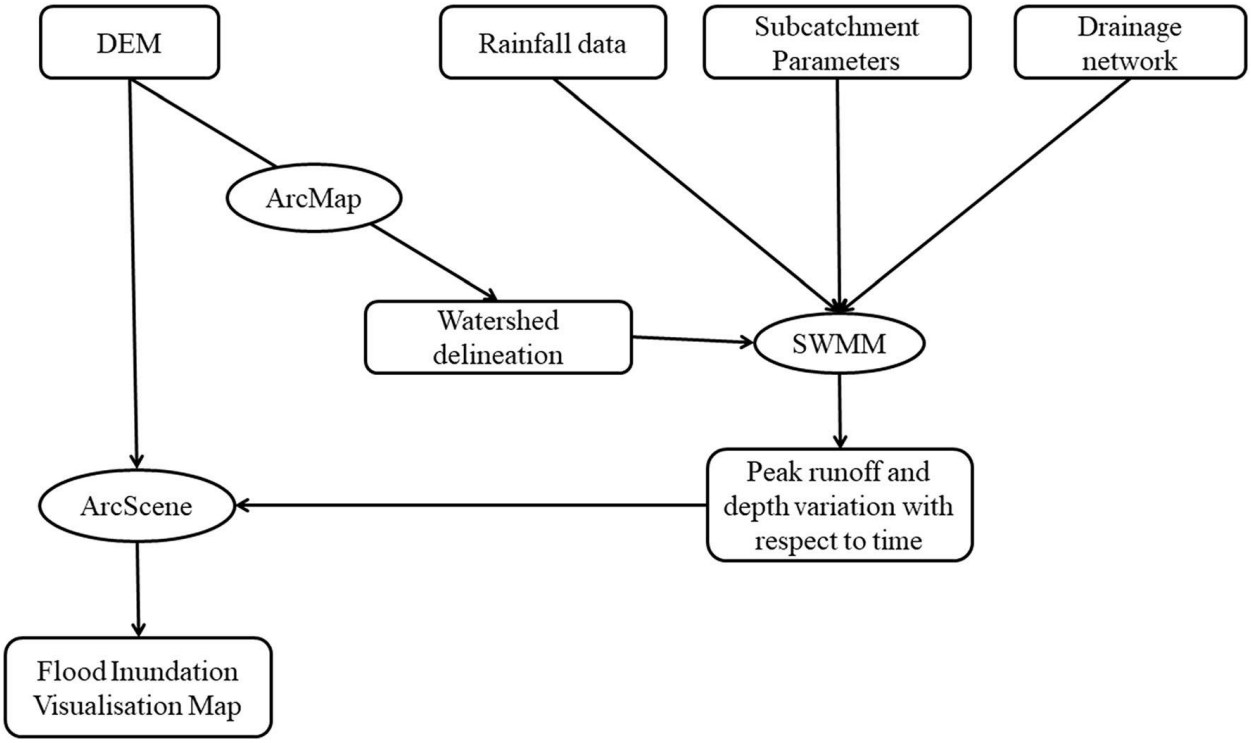

Fig 3. 8 Flowchart of the methodology used for the flood inundation map using SWMM and ArcGIS

Flood inundation visualisation

Based on the results from the SWMM (peak discharge and discharge depth with respect to time), shapefiles with respect to the discharge were prepared. Flood inundation visualisation is the spatial-temporal geographic information system which can be used for the spatial extension of the flood with respect to time. The 4D tool provides a graphical representation of the overall flood inundation which makes it easy for the analysis of floods and decision-making process. ArcScene 10.1 was used to convert DEM into 3-Dimension. Flood-prone areas were identified with the help of SWMM. Using GIS, flood inundation maps were prepared by considering the elevation and discharge depth of those places. 4-D flood inundation visualisations were carried out using ArcScene time slider visualisation tool.

3.4.7. Bias correction

RCMs show critical biases in precipitation, and therefore, it is mandatory that bias correction is to be carried out so that they are usable for research. Nine grid points, from in and around Amaravati, were selected for this study. The CORDEX simulated RCM outputs for South Asia such as CNRM-CM5, ACCESS, CCSM4, GFDL-CM3, NORESM1-M and MPI ESM LR were selected for bias correction. The observed precipitation data obtained from the Indian Meteorological Department (IMD) with a resolution of 0.5° × 0.5° observed gridded data were used to obtain the optimise method for bias correction. Four statistical bias correction techniques were applied to each observation stations separately.

3.4.7.1. Bias correction methods

Bias correction is carried out by (i) Linear scaling, (ii) Cumulative distributive transformation function (iii) Quantile mapping parametric transformation and (iv) Quantile mapping smoothing splines. These are briefly discussed below.

(i) Linear scaling: In this approach, the RCM daily precipitation data, $P_{,}$ are transformed into $P_{corrected}$ such that

$$Pcorrected = \alpha Pmod \tag{3.33}$$

where α is a scaling factor, $\alpha = O/ P_{mod}$, O is the observed precipitation values and P_{mod} is modelled values. For every modelled precipitation value, the scaling factor is applied and the

corrected time-series is generated. Linear scaling methods include delta change methods and factor change methods which belong to the same family (Hay et al. 2000). This method is simple with modest data requirement. But correction applied to the monthly mean rainfall data can adversely affect the relative change in the distribution of rainfall in different months and may distort other moments of daily rainfall distribution models.

(ii) Cumulative distributive transformation function (CDF): The basic principle of this approach is to first arrive at a statistical connection between observed data and outputs of models on the basis of historical data. The transfer function, thus derived, was then applied to future model projections and the track of future observations was obtained. The distribution of monthly RCM precipitation variables was mapped onto that of the observed gridded data by the quantile-based mapping method. Quantile-based mapping is a simple and efficient method that has been used successfully in various climate impact studies as well as in hydrology (Cayan et al. 2008; Maurer and Hidalgo, 2008). The method can be mathematically represented for a climate variable y, which is corrected to $\check{y}_{adjst}$ as shown in equation (3.34)

$$\check{y}_{adjst} = F^{-1}{}_{obs-c}(F_{obs-c}(y_{m-p})) \tag{3.34}$$

Here F denotes the CDF of either the modelled values (m) or observed values (obs) for the current climate or future projection period (p) or a historic training period (c). The bias correction of future model values was done by first calculating the percentile values for the future projection points in the CDF of the model for the period. Next, for that CDF, the observed values were traced to arrive at the bias-corrected model values. An important advantage of the method is that the rank correlation between observations and models is maintained and all the moments are adjusted in such a way that the distribution of the observations used for the training period agree with the modelled distribution. However, the method is based on an important assumption that there is no significant change in climate distribution over time. In other words, only the mean changes and the skew and variance of the distribution remain constant. This will not hold true if there are variations in the higher moments (Meehl and Thomas, 2007). It would be better, if, instead of assuming that the historic data distribution can be applied to the future period, information from model projection CDF is incorporated. It is assumed that for a given percentile, the adjustment

function is a constant, that is, the difference between the observed and model values also applies to the future.

(iii) Quantile mapping parametric transformation (Qmap.P). The quantile-quantile relation can be directly modelled by using parametric transformations. The appropriateness of the parametric transformations given below (equations: (3.35) to (3.39)) are studied.

$$\tilde{P}_{obs} = aP_{mod} \tag{3.35}$$

$$\tilde{P}_{obs} = b + aP_{mod} \tag{3.36}$$

$$\tilde{P}_{obs} = aP_{mod}{}^{c} \tag{3.37}$$

$$\tilde{P}_{obs} = a(P_{mod} - x)^{c} \tag{3.38}$$

$$\tilde{P}_{obs} = (b + aP_{mod})\,(1 - e^{-(P_{mod}-x)/\tau}) \tag{3.39}$$

Here, $\tilde{P}_{obs}$ denotes the estimate of P_{obs} and a, b, c, x and τ are free parameters that are subject to calibration. The direct scaling, Eq. (3.35), is very much related to linear scaling (Widmann et al. 2003; Schmidli et al. 2006) and is often used to correct RCM precipitation (Maraun et al. 2010). Piani et al. (2010) used the transformations Eq. (3.36) to Eq. (3.39), which have also been used in some studies that followed (Rojas et al. 2011). By reducing the residual sum of squares, all parametric mappings were matched to the part of CDF correlated to wet days in observed series ($P_{obs} > 0$). The modelled values set to zero correspond to dry part of the empirical CDF observed.

(iv) Quantile mapping smoothing splines (Qmap.S): Non-parametric regression can also be used in modelling the transformation, Eq. (3.40). Even though there are other non-parametric methods which are equally efficient, the use of cubic smoothing splines is more popular as it is the only method suited for part of CDF correlated to wet days in observed series. In order to identify the spline's smoothing parameter, generalized cross matching was used.

$$P_{obs} = h(P_{mod}) \tag{3.40}$$

3.4.7.2. Evaluation methodology

By comparing the differences between observed, corrected and RCM datasets, the overall performance of each method used for bias correction can be analysed. But quantitative analysis of the robustness of the methods have not been carried out. The assessment of the robustness of each method was done by quantifying the relative errors such as standard error, mean absolute error, root mean square error and mean square error.

3.4.8. Climate change impact on urban flood

Climate change studies have been carried out using Regional Climate Downscaling Experiment-South Asia (CORDEX-SA) data under RCP 4.5 and RCP 8.5. CORDEX is a World Climate Research Program (WCRP) developed to produce an improved set of regional climate change projections worldwide. CORDEX considers an ensemble of different dynamical and statistical downscaling models that consider multiple forcing GCMs. In this study, an ensemble of 6 RCM models under 2 representative concentration pathways (RCP 4.5 and RCP 8.5) are used. The ensemble of climate models was carried out using the multi-model mean method. The climate data is then divided into two series as Future 1, F1 (2021-2060) and Future 2, F2 (2061-2099).

The ranking for the time series was obtained by three goodness of fit tests, viz., Kolmogorov Smirnov, Anderson Darling and Chi-Squared method. The distribution with the best fit rank was carefully chosen for the estimation for 24-hour maximum rainfall for different return periods. The analysis of the data showed the Generalised Extreme Value (GEV) distribution as the best fit. So, one-day maximum rainfall depth was estimated for various return periods of 2, 5, 10, and 20 year using GEV. Peak discharge was calculated for the RCP 4.5 F1, RCP 8.5 F1, RCP 4.5 F2 and RCP 8.5 F2 series for the respective one-day maximum rainfall depth.

3.4.9.Mitigation of urban flood

Low Impact Development (LID) is a stormwater management strategy that seeks to mitigate the impacts of increased runoff and stormwater pollution by managing runoff as close to its source as possible. LID comprises a set of site design strategies that minimise runoff and

distributed small scale structural practices that mimic natural or predevelopment hydrology through the processes of infiltration, evapotranspiration, harvesting, filtration and detention of stormwater. These practices can effectively reduce the volume and intensity of stormwater flows. There are several different types of LID controls available for implementation. For each LID control, different scenarios are created with their respective level of implementation. LID is a decentralised small-scale measure module which is included in SWMM. It is environmentally friendly, easy to construct, small in size, economical, and ornamental as landscape. In SWMM, several LID modules are created, which are then added to the corresponding sub-area by changing the parameters according to the actual situation. Based on the principle of water balance, the SWMM calculates real-time inflow and outflow of the sub-area (Rossman, 2014). Three scenarios considered for the study were: Biological BMPs, Structural BMPs and Combination of biological and structural BMPs. Biological BMPs are Bioretention, Rain Garden and Grass swale. Structural BMPs considered are permeable pavement, infiltration trench and rain barrel. The three scenarios are simulated for 5-year return period in five sub-catchments for 50% catchment area.

During the simulation, SWMM performs a moisture balance that keeps track of how much water moves between and stored within each LID layer. Representation of the water pathway in LIDs of SWMM is shown in Fig 3.9. Surface layer is the ground surface that receives direct runoff from upstream land areas, stores excess inflow and generates surface outflow. Pavement layer is the layer of porous concrete used in continuous porous pavement systems. Engineered soil mixture is used in bioretention cell to support vegetative growth. Storage layer is the bed of crushed rock or gravel that provides storage in bioretention cells, infiltration trench, and porous pavement. Under drain conveys water out the gravel storage of Bio retention cells, infiltration trench, into an outlet pipe.

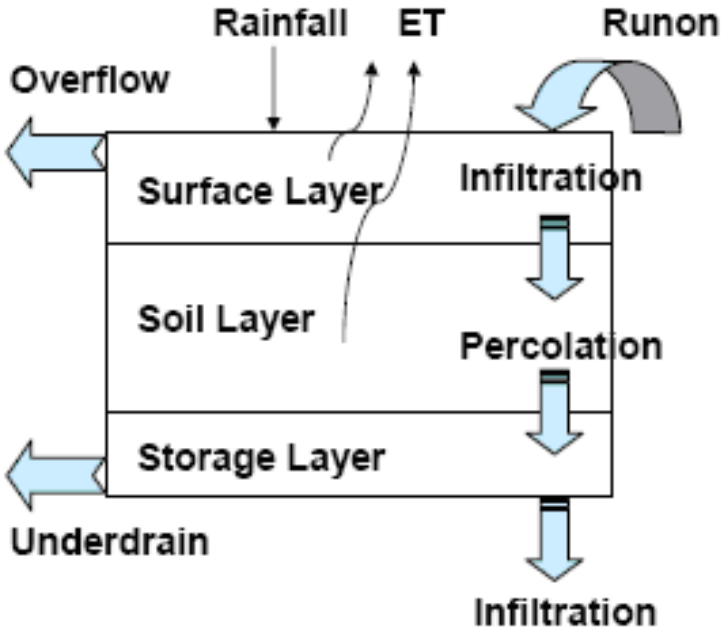

Fig 3. 9 Representation of the water pathway in LIDs of SWMM

CHAPTER 4

RESULTS AND DISCUSSION

4.1. General

Rapid changes of climate and land use result in the increase of the flood risk. Flood inundation mapping and proper flood mitigation measures are required for the management and mitigation of floods. This chapter contains the application of methodology and the results of the analysis carried out in the study for the flood inundation mapping, climate change impact on flood for the study area and the best management practices that can be used in the study area to reduce the impact of flood.

4.2. Rainfall Characteristics

Observed rainfall data from 1985-2020 for 17 rain gauge stations were collected from APCRDA (Andhra Pradesh Capital Region Development Authority). The gauged stations are located in and around the study area. Table 1 gives the locational details of the rain gauge stations and the periods for which data are available. All the stations, except Mangalagiri, Guntur and Pedakurapadu, have some missing data. Missing data of the annual precipitation series were estimated using multiple imputation methods, suggested by Sovilj et al. (2016). Multiple imputation is considered much better than single methods or case deletion as it imputes M times and returns M complete datasheets (Scheffer, 2002). The missing data were filled in by a set of values. They are, later, analysed using standard statistical methods explained by Rubin (1987,1988). Basic statistical properties of time-series of maximum values of daily rainfall data for the 17 rainfall stations in and around Kondaveeti Vagu from 1985 to 2020 are presented in Table 4.2. The gauge station at Ibrahimpatnam showed the highest mean (122.1 mm) with a standard deviation of 44.20 mm in maximum values of daily rainfall data

among all the stations, while the lowest mean (91.4mm) and standard deviation (25.28 mm) was observed at Tadikonda. Maximum values of daily rainfall varied from 145.60 mm (Pedakakani) to 263.200 mm (Guntur). The lowest coefficient of variation (CV) was seen at Medikonduru where the lowest maximum rainfall observed in a day during a year was 161 mm/day and highest CV was seen at Pedakurapadu with a highest in daily annual maximum rainfall of 230.40 mm/day. These indicate that the highest CV of rainfall had lowest value in maximum values of daily rainfall and this agrees with the study conducted by Bewket & Conway (2007). Fig 4.1 shows the box-whisker plots of temporal variation extension of maximum values of daily rainfall over the 17 gauged stations. Vatticherukuru had the widest variations among all other station with 25.60 mm/day to 256.40 mm/day.

Table 4. 1 Latitude and longitude of gauged stations and number of years of missing data

Gauge station number	Name	Latitude (N)	Longitude (E)	Number of years where data is missing
1	Amaravati	16°34'33.68"	80°21'27.27"	4
2	Thullur	16°31'26.84"	80°28'30.00"	3
3	Thadepalli	16°28'54.73"	80°38'41.45"	4
4	Mangalagiri	16°25'05.28"	80°33'59.56"	0
5	Tadikonda	16°25'14.41"	80°27'23.89"	4
6	Medikonduru	16°21'04.47"	80°18'09.54"	9
7	Guntur	16°17'25.83"	80°26'46.03"	0
8	Pedakakani	16°29'39.48"	80°29'39.54"	9
9	Duggirala	16°19'27.10"	80°37'38.72"	1
10	Pedakurapadu	16°28'12.10"	80°15'27.27"	0
11	Phirangipuram	16°17'32.63"	80°16'03.30"	1
12	Prathipadu	16°10'54.48"	80°20'6.72"	2
13	Vatticherukuru	16°10'55.2"	80°26'52.08"	3
14	Ibrahimpatanam	16°34'55.83”	80°30'55.71”	3
15	Vijayawada Urban	16°30'19.00”	80°38'54.26”	8
16	Penamaluru	16°28'5.52"	80°43'10.2"	3
17	Kanchikacherla	16°41'0.24"	80°23'25.44"	4

Table 4. 2 Minimum, maximum, mean and standard deviation of maximum daily precipitation time-series during the year (1985-2020)

Variable	Minimum (mm/day)	Maximum (mm/day)	Mean (mm/day)	Std. deviation (mm/day)	CV (%)
Amaravati	40.00	194.20	115.84	41.06	35.44
Thullur	49.80	183.00	105.73	34.33	32.46
Thadepalli	52.60	211.60	111.28	37.10	33.33
Mangalagiri	53.60	203.00	112.45	33.27	29.58
Tadikonda	50.40	166.00	91.41	25.28	27.65
Medikonduru	40.20	161.00	96.66	23.64	24.46
Guntur	54.60	263.20	98.29	42.40	43.13
Pedakakani	42.30	145.60	92.66	25.76	27.80
Duggirala	31.00	150.20	94.35	32.11	34.03
Pedakurapadu	47.60	230.40	96.39	45.20	46.89
Phirangipuram	37.20	216.30	99.04	43.04	43.45
Prathipadu	22.60	200.00	91.89	40.36	43.92
Vatticherukuru	25.60	256.40	99.89	52.74	52.79
Ibrahimpatanam	65.40	230.00	122.06	44.20	36.21
Vijayawada Urban	50.00	190.80	120.27	37.68	31.33
Penamaluru	58.60	211.60	117.91	40.00	33.92
Kanchikacherala	28.20	220.60	117.99	49.46	41.91

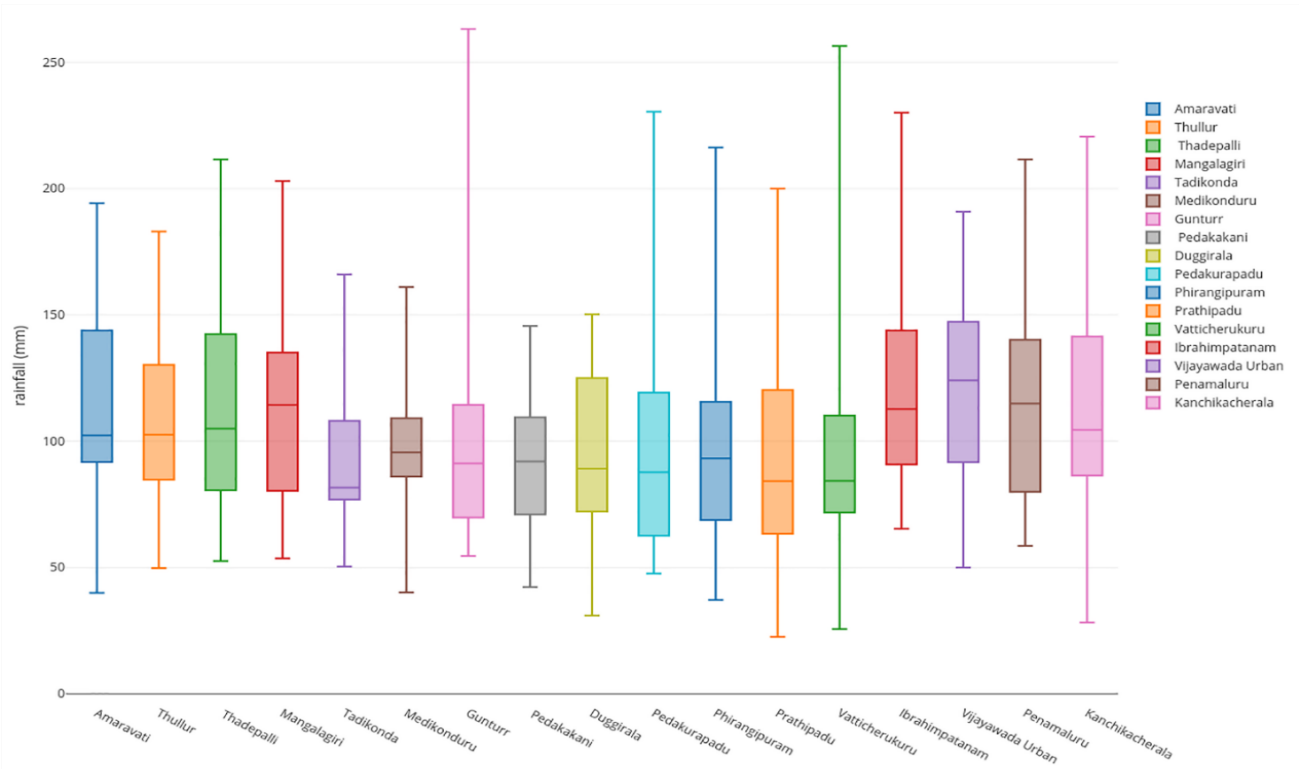

Fig 4. 1 Box-whisker plot illustrating median and extremes of maximum daily precipitation time-series of 17 stations.

4.3. Trend Analysis

In this study, maximum of monthly, seasonal and annual trends for rainfall are analysed using MK1, MK2 and ITA techniques and the trend magnitudes are calculated using Sen's slope estimator for 15 grid points in the study area. Kolmogorov–Smirnov test was used to determine if the maximum monthly and seasonal rainfall data for the entire period (1961–2018) was following the normal distribution. It was found that none of the rainfall series used in the study was following the normal distribution. Results of the MK1, MK2 and Sen's slope approaches are tabulated for all 15 grid points. ITA technique was employed for annual and seasonal rainfall for the period 1961–2018. Trend detection using the ITA technique was performed to plot the sub-series of the dataset. While doing so, no assumptions regarding the statistical distribution were made. For the discussion and comparison, results of the ITA technique for annual, winter, pre-monsoon, monsoon, and post-monsoon seasons represented in Figs. 4.5, 4.6, 4.7, 4.8 and 4.9. Due to large volume, the results are presented only for six grid points (G2, G4, G7, G8, G13 and G14). Results from the ITA technique are compared with MK1 and MK2 test only for these six grids.

4.3.1. Monthly maximum trends for rainfall

The Z statistics of monthly maximum rainfall data obtained from MK1 and MK2 are presented in Table 4.3 and Table 4.4. These represent both the negative and positive significant trends. Out of the 180 cases, 21 cases (11.6%) displayed positive trends in MK1 while 22 cases (12%) displayed significant positive trends in MK2 considering the three significant levels. In this study, no significant negative trends are exhibited for monthly maximum rainfall. For the MK1 test, significant positive trends were detected in January, February, May, August and November, whereas for the MK2 test, most of the trends were observed in May, August, November and December. Compared to MK1, the MK2 test exhibited similar significant positive trends. Among the 15 grids, G5 and G10 in the MK1 test and G5, G10 and G13 in the MK2 test did not have any significant trend, while the remaining grids exhibited significant trends for some months as seen from Tables 4.3 and 4.4. From MK1 and MK2 tests, more significant positive trends are seen in the month of May followed by August and November.

Table 4. 3 Z statistic of MK1 test for monthly maximum rainfall

	Mann Kendall test (MK1)											
Grid	Jan	Feb	Mar	Apr	May	Jun	Jul	Aug	Sep	Oct	Nov	Dec
G1	0.89	1.14	0.53	-0.94	0.58	-0.36	-0.06	0.16	-0.12	-0.49	0.24	**1.69[a]**
G2	**1.66[a]**	**1.67[a]**	0.92	0.45	0.66	-0.05	0.61	0.45	0.74	0.65	1.19	1.19
G3	**1.79[a]**	1.00	0.58	-0.12	**2.57[c]**	0.40	0.06	0.05	-0.21	-1.01	0.85	0.33
G4	1.12	0.44	1.32	0.39	**2.59[c]**	0.78	0.34	0.91	-0.07	-0.68	1.11	0.73
G5	1.09	1.10	0.21	-0.55	1.27	0.93	0.08	0.80	-0.65	-0.30	0.92	1.00
G6	0.64	0.93	-0.36	-0.82	**2.14[b]**	0.59	-0.78	0.96	-0.23	-0.33	1.30	0.28
G7	1.40	0.83	0.18	-0.31	**2.41[c]**	0.71	-0.87	0.91	-0.13	-0.85	**1.83[a]**	0.27
G8	0.46	0.23	0.86	0.07	**2.56[c]**	1.04	0.03	1.39	-0.07	-0.58	**1.90[a]**	0.63
G9	**1.80[a]**	1.10	0.30	-0.28	0.82	0.97	-0.15	1.59	0.36	-0.40	1.46	0.99
G10	1.39	0.99	-0.18	-0.37	1.21	0.54	-0.96	1.34	-0.12	-0.94	1.45	0.12
G11	1.25	0.70	0.02	0.01	1.47	0.75	-1.25	1.02	0.05	-0.81	**1.84[a]**	0.03
G12	1.06	0.70	0.62	0.22	**1.91[a]**	0.79	-0.83	1.15	0.33	-0.53	**2.23[b]**	0.33
G13	0.80	0.35	0.33	-0.23	1.43	0.79	-0.41	**1.99[b]**	0.21	-0.83	1.54	-0.34
G14	1.51	0.79	0.44	-0.10	**1.65[a]**	0.78	-0.68	1.39	0.35	-0.51	**1.93[a]**	-0.47
G15	0.46	0.70	0.62	0.12	**1.73[a]**	0.90	-0.37	**1.70[a]**	0.64	-0.11	**2.39[c]**	-0.13

(Numbers with symbol ‘a’,’b’,’c’ shows the significance level at 1%, 5%, 10% respectively.)

Table 4. 4 Z statistic of MK2 test for monthly maximum rainfall

	Modified Mann Kendall Test (MK2)											
Grid	**Jan**	**Feb**	**Mar**	**Apr**	**May**	Jun	Jul	Aug	Sep	Oct	Nov	Dec
G1	1.03	0.97	0.71	-0.95	0.52	-0.33	-0.06	0.17	-0.13	-0.50	0.25	**2.63[c]**
G2	0.86	1.04	0.74	-1.43	**2.08[b]**	0.13	-0.52	0.18	-0.16	-0.91	0.89	0.56
G3	1.31	1.00	0.50	-0.17	**2.58[c]**	0.54	0.09	0.07	-0.18	-1.02	0.85	0.33
G4	0.82	0.45	1.18	0.35	**2.94[c]**	1.27	0.45	1.39	-0.07	-0.84	1.11	0.73
G5	1.25	0.94	0.22	-0.56	1.27	0.86	0.08	0.80	-0.66	-0.31	1.00	1.46
G6	0.64	0.80	0.12	-0.82	**2.15[b]**	0.59	-0.78	1.18	-0.28	-0.43	1.51	0.28
G7	1.40	0.83	-0.19	-0.31	**2.41[c]**	0.71	-0.91	**2.69[c]**	-0.15	-0.85	**1.94[b]**	0.26
G8	0.47	0.24	0.21	0.07	**3.20[c]**	1.05	0.03	1.40	-0.07	-0.81	**1.91[a]**	0.60
G9	**1.81[a]**	0.96	0.32	-0.28	0.82	0.97	-0.16	1.60	0.36	-0.40	1.57	1.35
G10	1.40	0.99	-0.30	-0.38	1.22	0.64	-0.96	-0.09	-0.15	-0.94	1.55	0.13
G11	1.25	0.71	0.31	0.01	1.47	0.93	-1.25	**2.26[b]**	0.06	-1.08	**1.85[a]**	0.04
G12	1.06	0.70	1.01	0.22	**1.91[a]**	0.99	-0.83	1.07	0.33	-1.68	**2.23[b]**	0.33
G13	0.80	0.35	1.10	-0.23	1.43	0.98	-0.44	0.21	0.21	-0.83	1.54	-0.34
G14	1.51	0.79	0.62	-0.10	**1.65[a]**	1.09	-1.03	**2.69[c]**	0.35	-0.51	-0.47	**1.93[a]**
G15	0.46	0.80	**1.69[a]**	0.12	**1.73[a]**	1.21	-0.37	**2.66[c]**	0.64	-0.14	**2.39[c]**	-0.13

(Numbers with symbol ‘a’,’b’,’c’ shows the significance level at 1%, 5%, 10% respectively)

4.3.2. Seasonal and annual trends for rainfall

The monthly maximum rainfall was grouped into four seasons. The Z statistics attained from MK1 and MK2 tests for seasonal and annual rainfall are presented in Table 4.5. In this study, no significant negative trends are exhibited for seasonal and annual rainfall. It is observed from Table 4.5, that out of the four seasons, the post-monsoon season showed no trend at all the grid points. In contrast, the monsoon season exhibited a significant positive trend only at G1for the MK1 test. Winter season displayed positive significant trend at all grid points for both MK1 and MK2 as seen in Table 4.5. The significant trend for annual series was observed only at G8 for both tests, while no trend was observed at the remaining 14 grids. The number of positive significant cases (out of 180) and their percentages for seasonal and annual rainfall at 1%, 5% and 10%significance levels are presented in Table 4.6. Seasonal trends at 1% significance level have 12 positive significance cases in MK1 and 22 in MK2 (0.16% for MK1 and 0.29% for MK2) tests. For 5% significance level, 8 positive significance cases for MK1 and 2 cases for MK2 and at 10% significance level, 8 positive significance instances in MK1 and 2 cases in MK2. Seasonally more trends were observed at a 1% significance level compared to 5% and 10% significance levels. Table 4.7 presents the significant positive trend cases at different significance levels for four seasons. Winter season exhibited more positive trend cases followed by pre-monsoon season. No significant trend was detected in post-monsoon seasons at any of the selected significance levels. At a 1% significance level, winter season showed more significant positive trends.

Table 4. 5 Z statistic of MK1/MK2 tests for seasonal and annual maximum rainfall

Grid	Winter	Pre-monsoon	Monsoon	Post-monsoon	Annual
G1	**2.50^{c}/2.51^{c}**	0.94/1.13	**-1.72^{a}**/-1.61	-0.15/-0.17	-0.59/-0.65
G2	**2.69^{c}/2.70^{c}**	1.34/**2.75^{c}**	0.11/-0.35	0.79/-0.62	1.24/-0.11
G3	**2.49^{c}/2.50^{c}**	**2.95^{c}/2.95^{c}**	0.17/0.23	-0.48-0.49	0.34/0.28
G4	**2.39^{c}/3.28^{c}**	**3.22^{c}/2.84^{c}**	-0.01/-0.01	-0.23/-0.32	1.12/0.89
G5	**2.63^{c}/3.64^{c}**	**1.87^{a}/2.34^{c}**	0.20/0.20	0/0	0.17/0.20
G6	**2.41^{c}/3.24^{c}**	**2.26^{b}/2.26^{b}**	-0.03/-0.03	0.32/0.32	0.64/0.65
G7	**2.16^{b}/2.79^{c}**	**2.84^{c}/2.46^{c}**	-0.46/-0.43	-0.05/-0.05	0.61/0.61
G8	**2.05^{b}/2.69^{c}**	**3.12^{c}/3.12^{c}**	-0.13/-0.16	0.33/0.29	**1.69^{a}/1.69^{a}**
G9	**2.55^{c}/3.65^{c}**	1.21/1.21	1.006/1.01	-0.11/-0.12	1.02/1.33
G10	**2.00^{b}/2.75^{c}**	**1.68^{a}/1.68^{a}**	0.56/0.56	-0.19/-0.24	1.02/1.42
G11	**1.87^{a}/2.98^{c}**	**1.7^{a}**/1.4	-0.18/-0.21	0.18/0.24	0.74/0.73
G12	**1.89^{a}/3.01^{c}**	**2.32^{b}/2.31^{b}**	0.06/0.06	0.39/0.42	1.43/1.43
G13	**2.17^{b}/3.55^{c}**	**1.83^{a}**/1.45	1.09/1.24	-0.28/-0.37	0.96/0.97
G14	**1.99^{b}/3.52^{c}**	**2.01^{b}**/1.59	0.72/0.59	0.01/0.01	1.01/0.95
G15	**1.88^{a}/3.34^{c}**	**2.74^{c}/2.37^{c}**	0.71/0.70	0.38/0.34	1.37/1.37

(Numbers with symbol ‘a’,’b’,’c’ shows the significance level at 1%, 5%, 10% respectively.)

Table 4. 6 Mann Kendall trend statistics for monthly rainfall

Significance level	Monthly Significant positive trend		Seasonal and Annual Significant positive trend	
	Cases (180)	Percentage	Cases (75)	Percentage
1% (values > 2.33)				
MK1	5	2.78%	12	16%
MK2	9	5%	22	29.33%
5% (values >1.96)				
MK1	3	1.67%	8	10.67%
MK2	5	2.78%	2	2.67%
10% (values >1.645)				
MK1	13	7.22%	8	10.67%
MK2	8	4.44%	2	2.67%

Table 4. 7 Mann Kendall trend statistics for seasonal and annual rainfall

Significance Level	Season	Significant Positive Trend cases
1% (values > 2.33) MK1/MK2	Winter	7/15
	Pre-monsoon	5/7
	Monsoon	0/0
	Post-monsoon	0/0
	Annual	0/0
5% (values >1.96) MK1/MK2	Winter	5/0
	Pre-monsoon	3/2
	Monsoon	0/0
	Post-monsoon	0/0
	Annual	0/0
10% (values >1.645) MK1/MK2	Winter	3/0
	Pre-monsoon	4/1
	Monsoon	1/1
	Post-monsoon	0/0
	Annual	1/1

4.3.3. Comparison of spatial changes in trends of MK1 and MK2

Comparisons of spatial distribution of Z statistics of MK tests for the monthly, seasonal and annual maximum rainfall are shown in Fig. 4.2, Fig. 4.3 and Fig.4.4. From the Fig. 4.2 and Fig. 4.3, the similarities between the spatial distributions of trend can be observed, except in the month of March. The Z values of MK2 show a more significant trend than MK1 which is not visible in the spatial distribution. Fig. 4.4 shows the comparison of Z values in MK1 and MK2 in seasonal and annual maximum rainfall; from the figure, it can be seen that winter and pre-monsoon seasons show significant difference since MK2 showed a more significant trend.

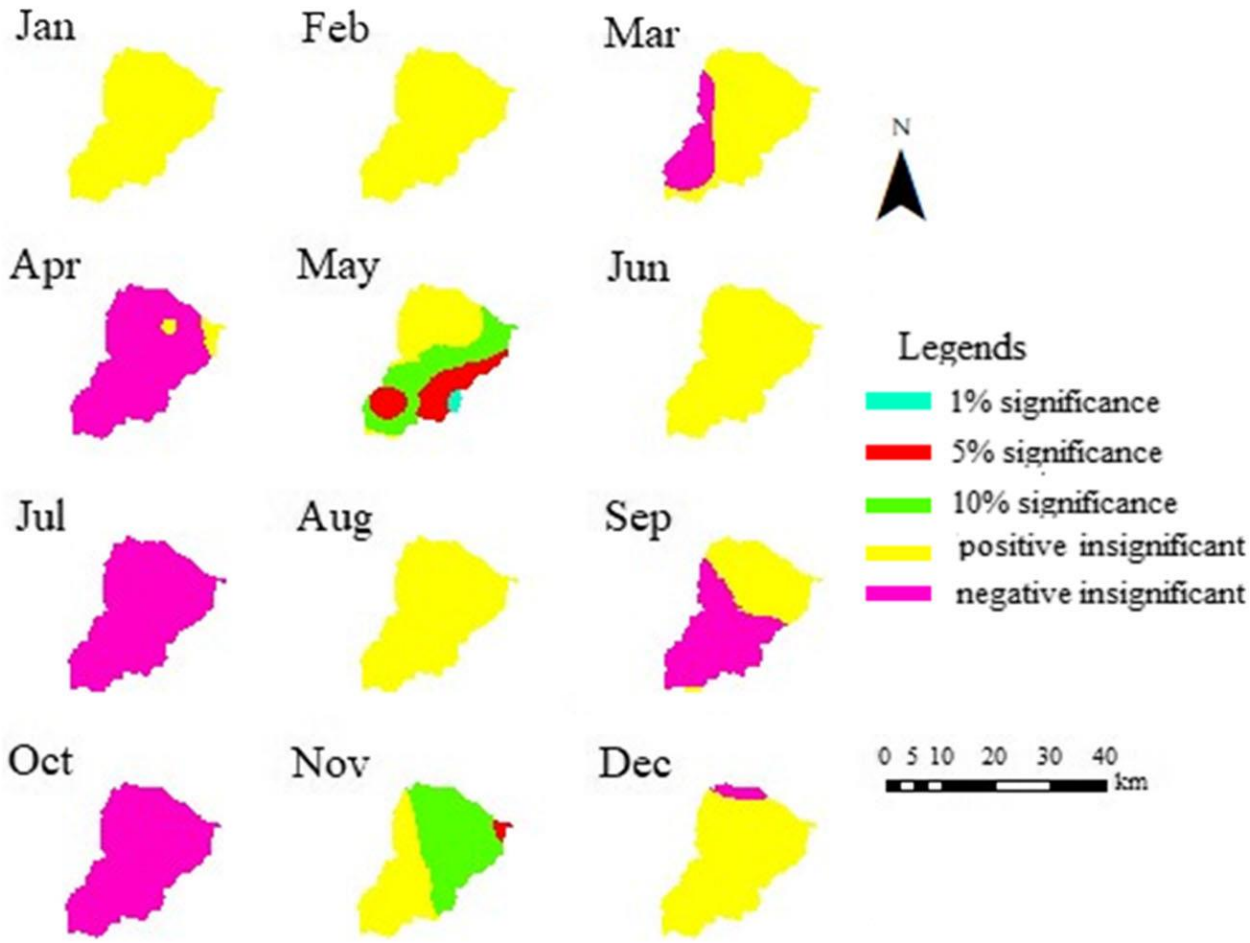

Fig 4. 2 Spatial distribution of Z statistics of MK1 test for the monthly maximum rainfall

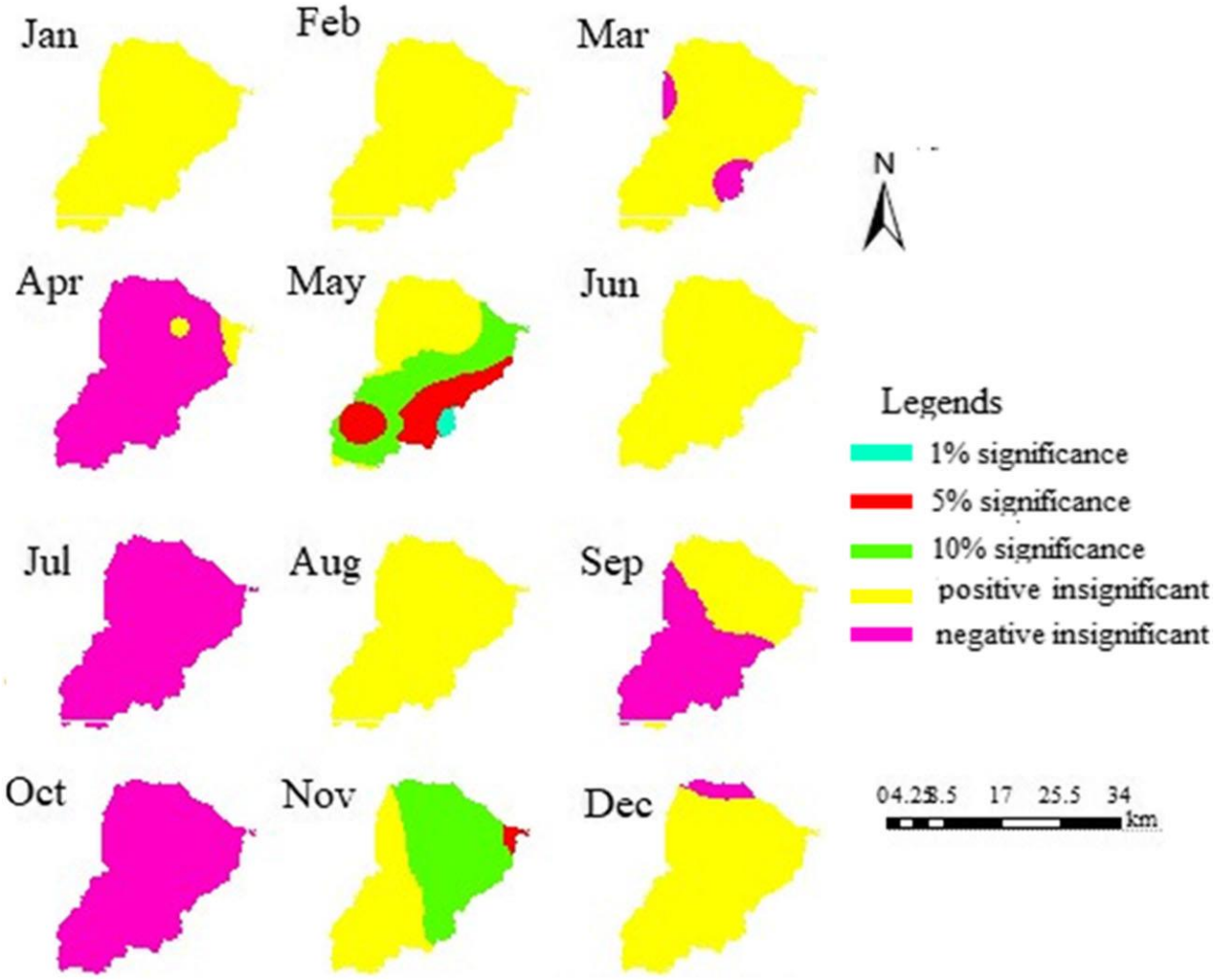

Fig 4. 3 Spatial distribution of Z statistics of MK2 test for the monthly maximum rainfall

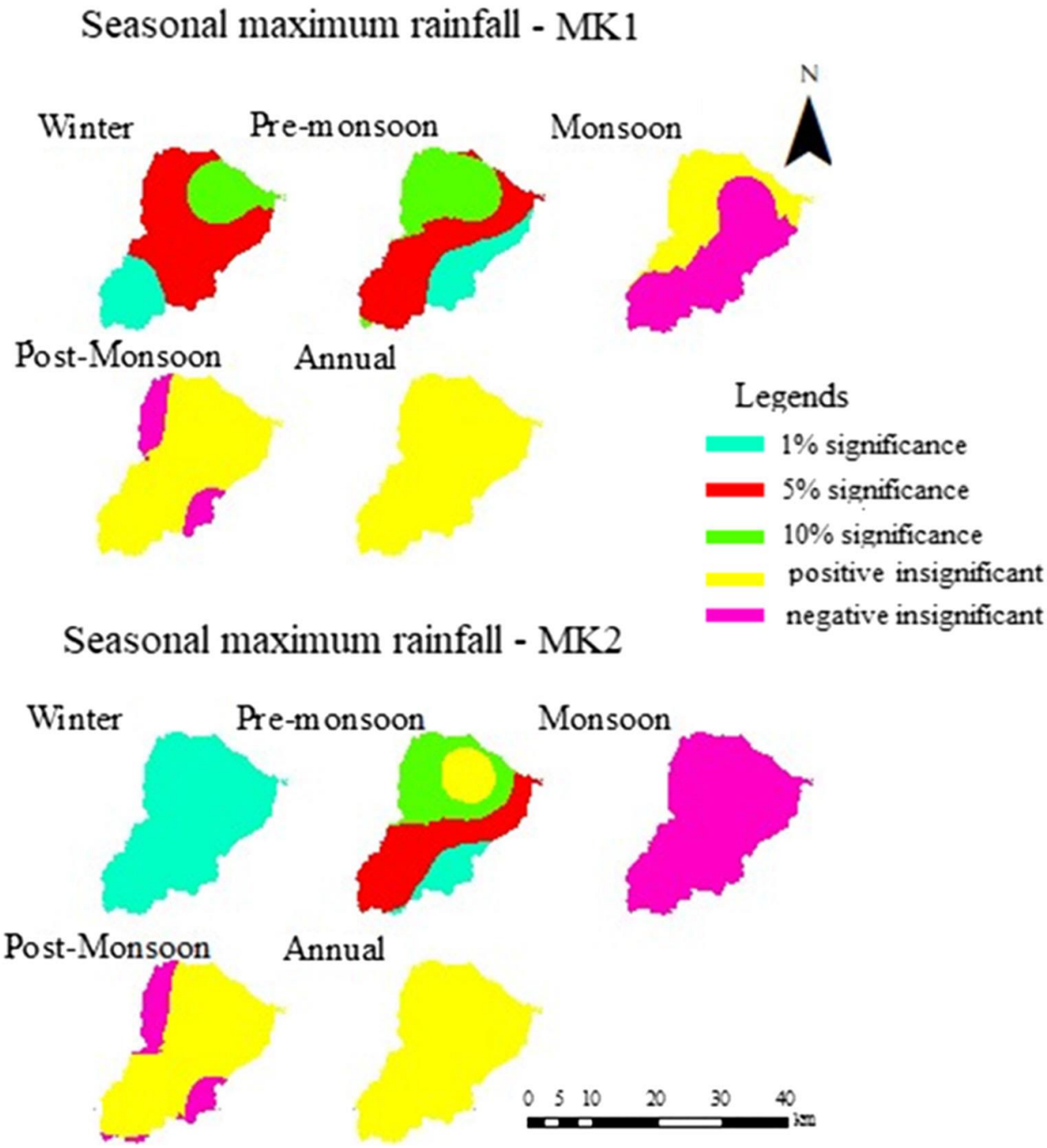

Fig 4. 4 Spatial distribution of Z statistics of MK1 and MK2 test for seasonal and annual rainfall

4.3.4. ITA technique for annual rainfall

The results of the ITA technique for the annual maximum series are presented in Fig. 4.5. As mentioned earlier, the results of 6 grid points out of 15 are only presented and explained. ITA plots are divided into three clusters as low, medium and high to examine the

trend variations. Explanations for the ITA technique are given for these three clusters. Plots G2, G13 and G14 showed no trend and increasing trend in the low phase, while in the medium phase, all grids are showing an increasing trend except for G13; in the high phase a declining trend is exhibited for G7 and G8; grid points G2 and G4 are detected with a growing trend. A monotonically increasing trend was observed only at G4, while all the remaining grids showed non-monotonic trends as shown in Fig. 4.5.

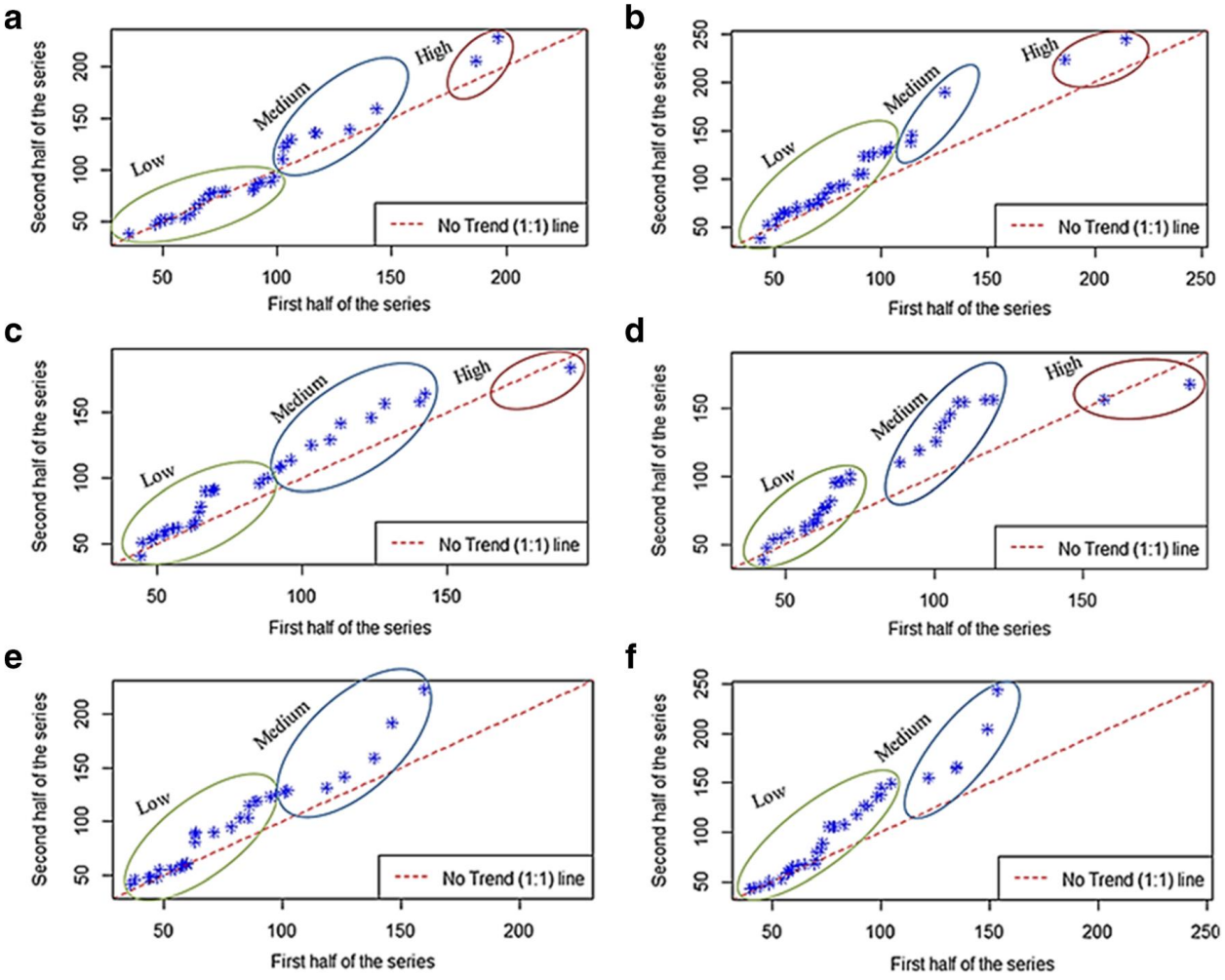

Fig 4. 5 ITA technique results for annual maximum rainfall for (a) G2, (b) G4, (c) G7, (d) G8, (e)G13 and (f) G14

4.3.5. ITA technique for seasonal rainfall

The results of the ITA technique for four seasons are presented in Fig. 4.6 to Fig. 4.9. Seasonal results are also explained for the same 6 grid points out of 15 grid points. Rainfall dataset of pre-monsoon season (Fig. 4.6) displayed an increasing trend in low and medium phases for all the selected 6 grids, whereas in the high phase, increasing trend for three grids

(G2, G8 and G4) and a decreasing trend for grids 4 and 7 were observed as shown in Fig. 4.6. In the monsoon season (Fig. 4.7), for all 6 grids, dataset points are spread over low, medium and high phases. In the low phase, no trend was observed in all the 6 plots except for G8 and G13 (no trend followed by increasing trend), whereas in medium and high phases, an increasing trend was exhibited for all grids except for grid 2. Grid G2 exhibited no trend in low and high phases and a non-monotonic trend was observed in the medium phase as shown in Fig. 4.7. For the post-monsoon season, rainfall dataset of plots G2 and G4 are spread in low, medium and high phase. For all the grids, either no trend or increasing trends were observed in all three phases. G8 exhibited no trend, whereas, for G13 and G14, an increasing trend was observed in the medium phase with no trend in low and high phases. G7 displayed an increasing trend only in the high phase as shown in Fig. 4.8. For the winter season, for the dataset points of G2, G4, G7, G8, G13 and G14 no trend was detected at starting subseries plot, and furthermore, a continuously increasing trend was observed as shown in Fig. 4.9.

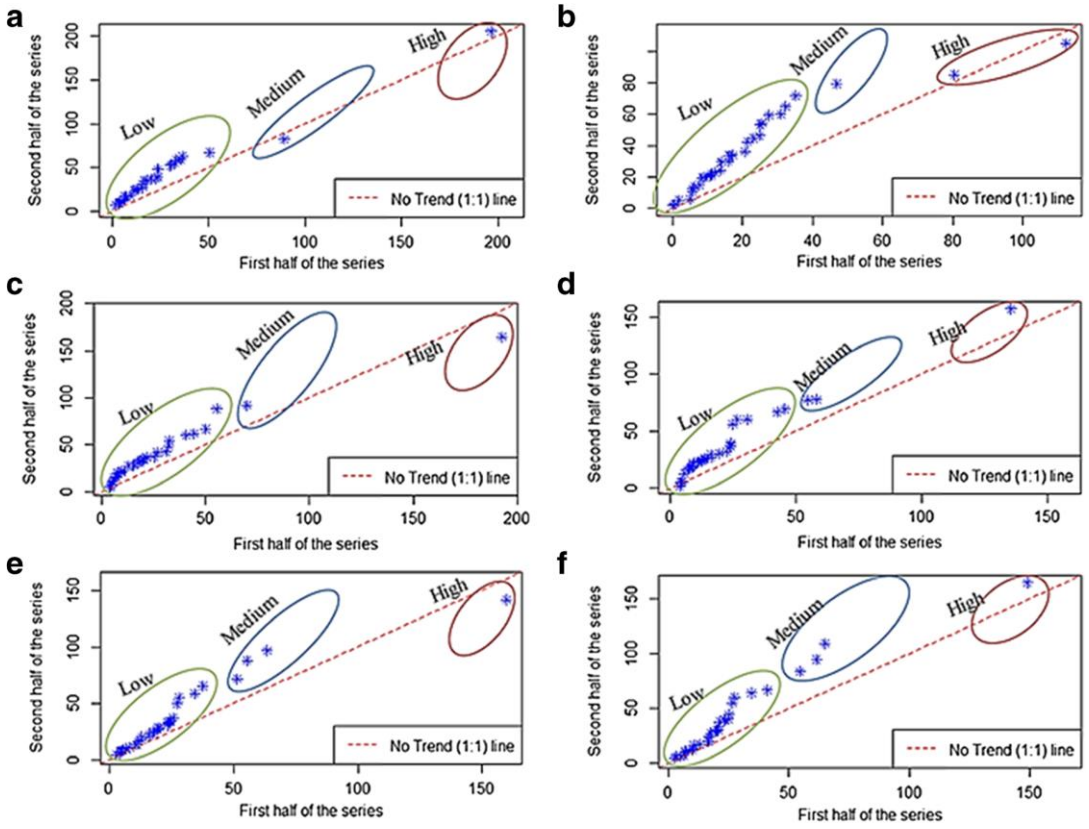

Fig 4. 6 Results of the ITA technique for the pre-monsoon season maximum rainfall for (a) G2, (b) G4, (c) G7, (d)G8, (e) G13 and (f) G14

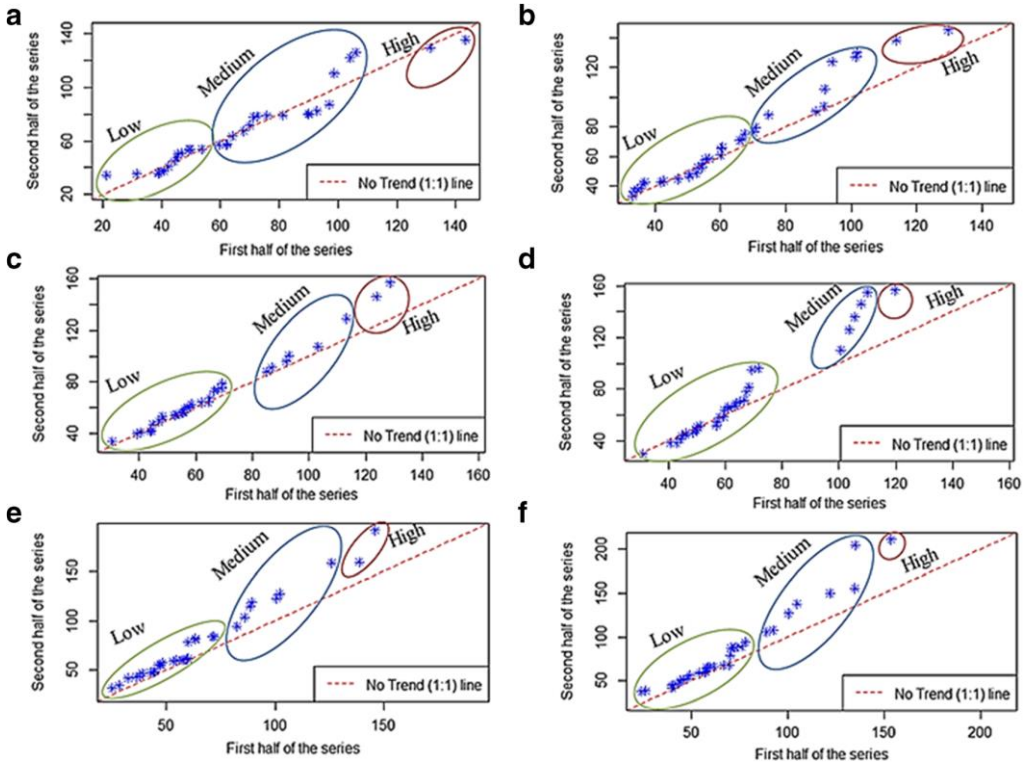

Fig 4. 7 ITA technique results for the monsoon season maximum rainfall for (a) G2, (b) G4, (c) G7, (d)G8, (e) G13 and (f) G14

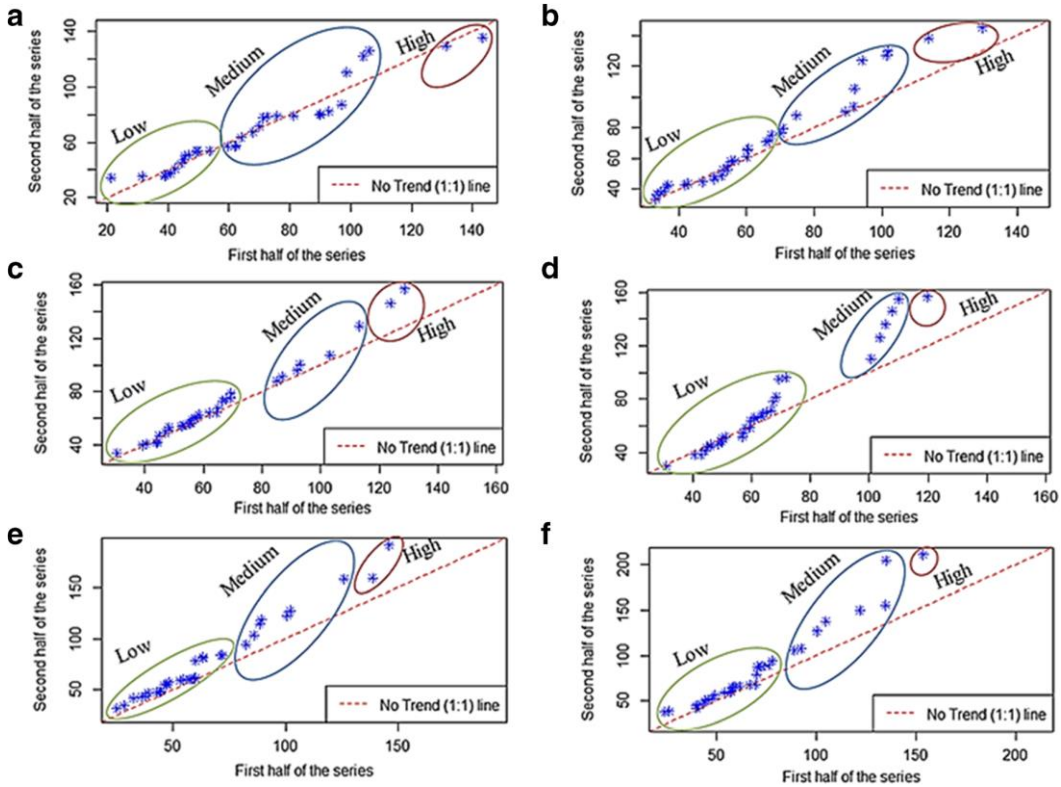

Fig 4. 8 ITA technique results for the post-monsoon season maximum rainfall for (a) G2, (b) G4, (c) G7, (d)G8, (e) G13 and (f) G14

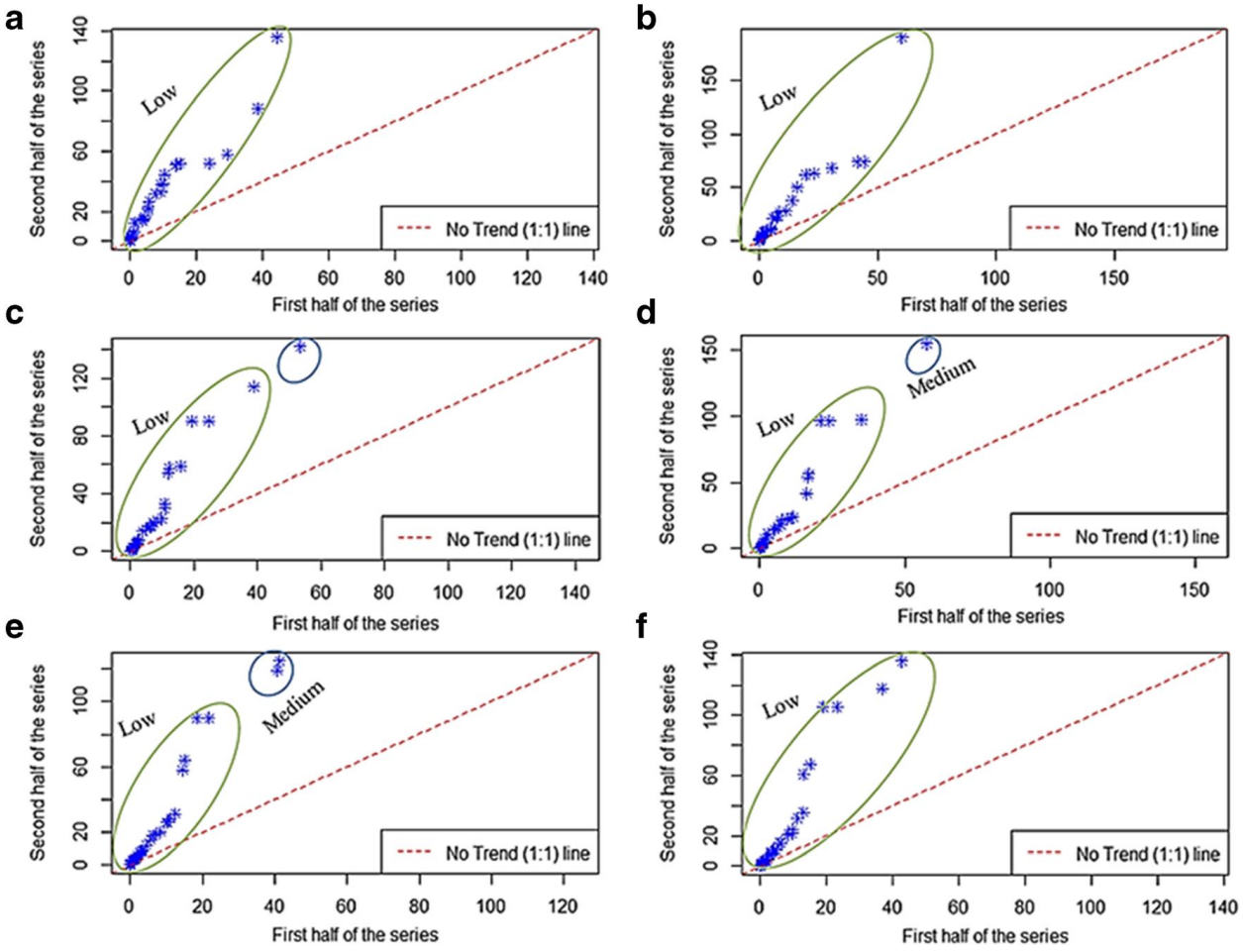

Fig 4. 9 Results of the ITA technique for the winter season maximum rainfall for (a) G2, (b) G4, (c) G7, (d)G8, (e) G13 and (f) G14

4.3.6. Comparison of seasonal and annual trends

As expected, rainfall trend showed large variability in ITA technique compared to MK1 and MK2 trend tests. For annual series, using MK1 and MK2 tests, trends were detected only for G8 as shown in Table 4.5, whereas, in the case of the ITA technique, trends were detected for all grid points as shown in Fig. 4.5. The ITA technique does not have any assumptions like that of MK tests, due to which, the graphical test is more appropriate in detecting monotonic and non-monotonic trends.

In the pre-monsoon season, similar trends were detected for MK1 and MK2 tests compared to the ITA technique. But, for the ITA technique, all trends were limited only to low phase. In the monsoon season, no trend was noticed for MK1 and MK2, whereas, by ITA technique, increasing trends were observed at G4, G7, G8, G13 and G14. During the post-

monsoon season, no trends were detected for all grid points using MK1 and MK2, while for ITA technique, increasing trends were observed for G4, G13 and G14. In the winter season, trends were detected for all the 15 grid points using MK1 and MK2 tests, whereas an increasing trend was noticed for all 15 grid points in the low phase using the ITA technique. So, the ITA technique showed a tendency for more increasing trends compared to MK1 and MK2 tests without any assumptions.

4.3.7. Sen's slope for maximum monthly rainfall

Monthly maximum rainfall trend magnitudes are calculated using Sen's slopes and plotted using box plots as shown in Fig. 4.10. In the box plots, the central thick horizontal line of all the months represents the median. Vertical lines (whiskers) with lower and upper ends signify the magnitudes of lowest and highest rainfall values. The upper and lower ends of the boxes represent the 25th and 75th percentiles respectively. For the months of January, February, March, April and December, the median passes through the origin as there were no trend magnitudes for these months. From May to November, the trend magnitudes were positive and negative, falling above and below the origin. Among all vertical lines, only one month, i.e. October, signifies the lowest negative magnitude, i.e. nearly - 0.08 mm/year followed by July with 0.05 mm/year. Similarly, the highest magnitude occurred in May (nearly 0.17 mm/year) followed by November (nearly 0.14 mm/year).

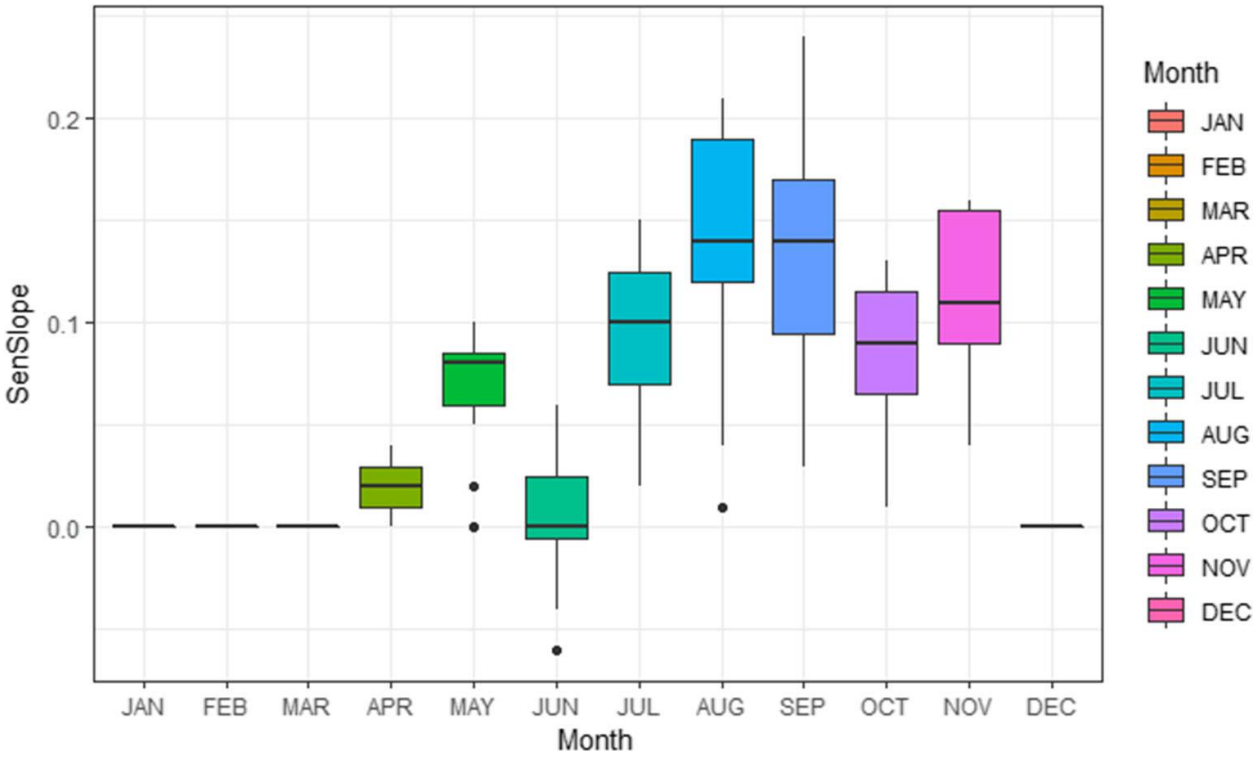

Fig 4. 10 Maximum monthly rainfall trend magnitudes

4.3.8. Sen's slope for seasonal and annual rainfall

Sen's slope approach was used in estimating the magnitudes for seasonal and annual rainfall as shown in Fig. 4.11. All the four seasonal and annual magnitudes exhibited positive slopes with a peak of 0.23 mm/year in the pre-monsoon season and annually at 0.18 mm/year. The highest and lowest magnitudes were observed in pre-monsoon (nearly 0.23 mm/year) and post-monsoon seasons respectively. The magnitudes Sen's slope of seasonal and annual rainfall varied between 0.00 and 0.23 mm/year. The seasonal magnitudes were decreasing from pre-monsoon to post-monsoon and then magnitude increased in winter season as shown in Fig. 4.11.

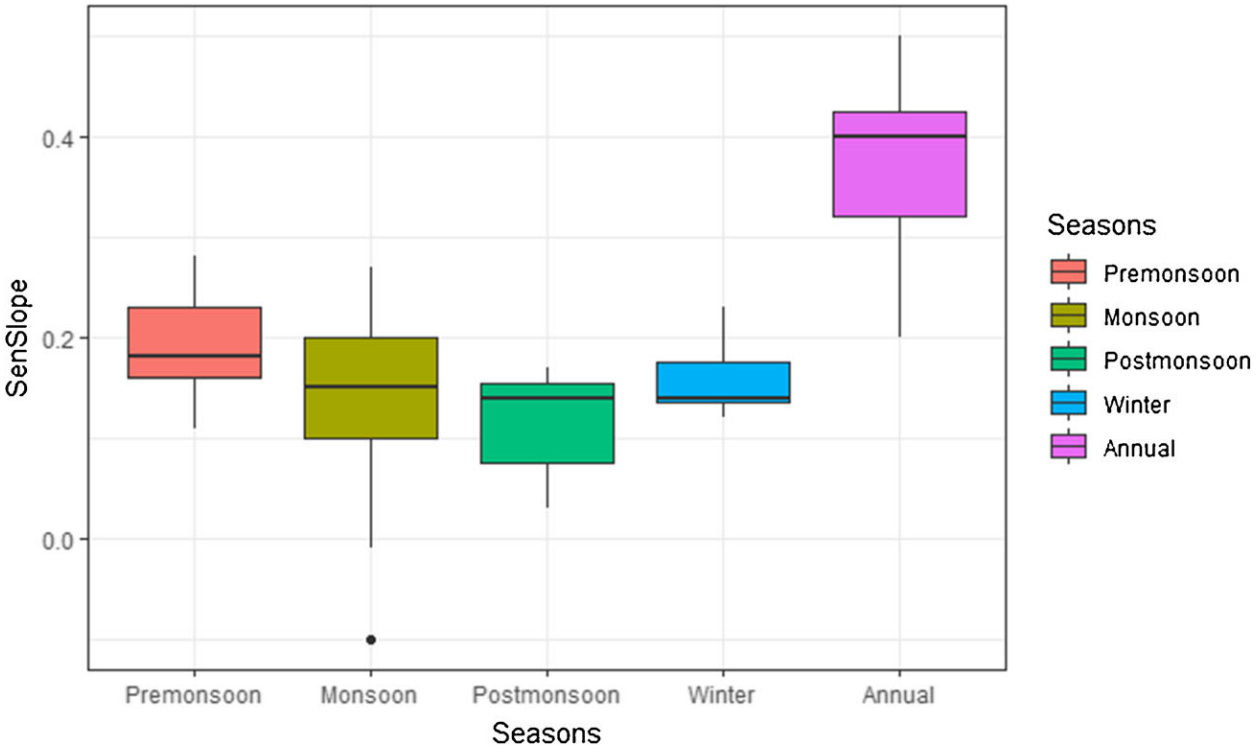

Fig 4. 11 Seasonal and annual maximum rainfall trend magnitudes

4.3.9. Parametric trend (regression analysis)

Trends, along with model equations of annual average rainfall over a period of 30 years (from 1985 to 2014) of seventeen gauged rainfall stations in and around Kondaveeti Vagu using linear regression analysis. Because of space constraint, details of only 8 stations with visible trends are shown in Fig.4.12 (A-H). Rainfall at stations at Amaravati, Thadepalli, Mangalgiri, Pedakurapadu, Vijayawada Urban and Penamaluru showed positive trends while the rainfall at Tadikonda, Guntur, Vatticherukuru, Ibrahimpatanam and Duggirala showed negative trends. Rainfall at rest of the stations, namely Kanchikacherala, Phirangipuram, Prathipadu, Medikonduru, Thullur, Pedakakani showed no trend. From these, it can be inferred that, even though the rainfall series at the six gauged rainfall stations showed positive trends and that at five gauged stations showed negative trends, the trends were very insignificant, as their R^2 values were less than 0.12.

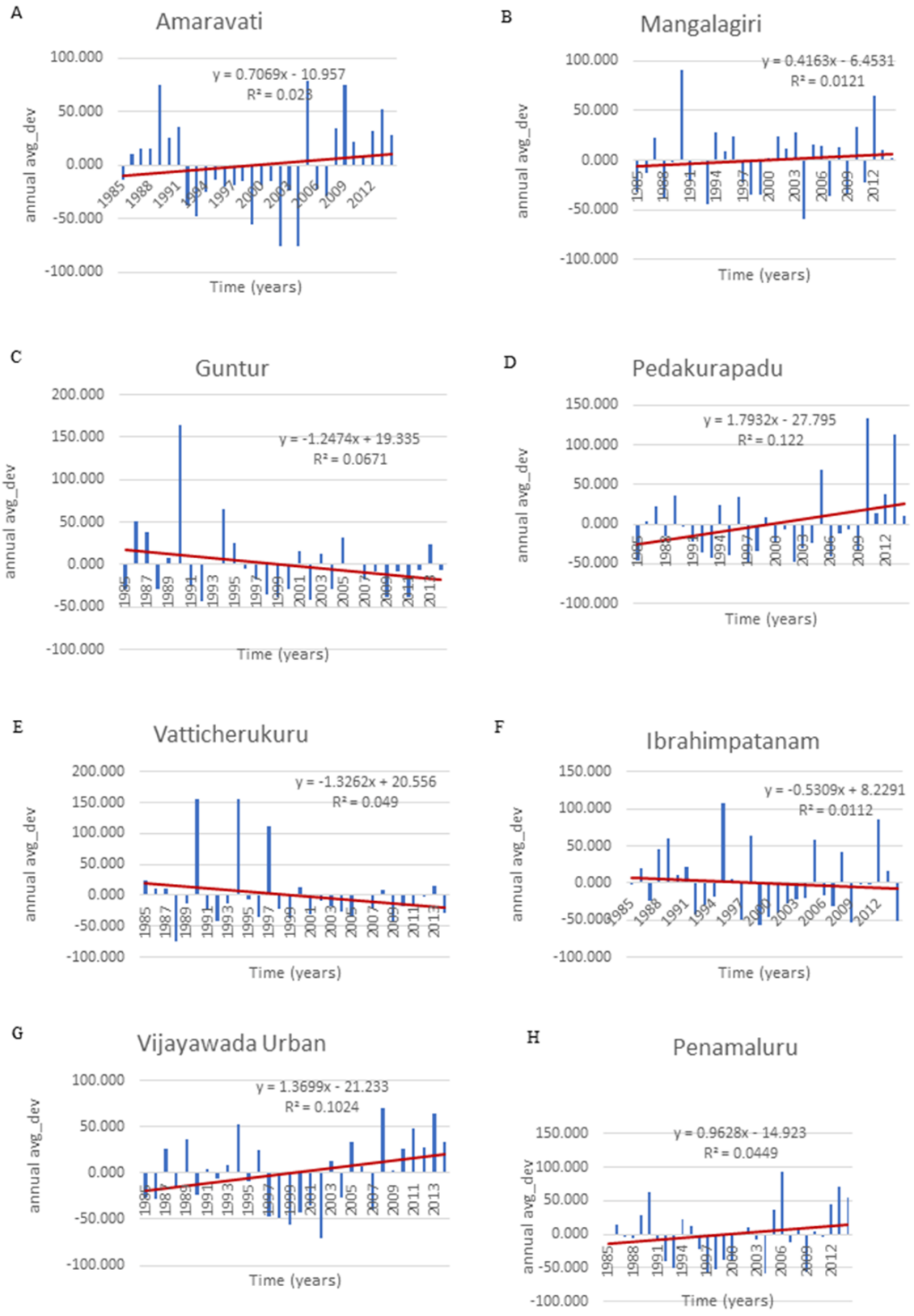

Fig 4. 12 Trends of annual average rainfall series over 30-year period of at 8 gauged precipitation stations (A-H) in and around Kondaveeti Vagu using linear regression

4.3.10. Non-parametric trend test for annual average rainfall

The results of the MK Test and Sen's slope test for annual average rainfall series of 17 gauged rainfall stations are listed in Table 4.8. The parametric statistical MK trend test showed that the rainfall series at Vijayawada Urban has a significant positive trend (Z = 1.71, S=97 and τ=0.223) at 5% significance level (α=0.05). Sen's slope values for a confidence interval of 95% vary from -1.233 (Kanchikacherala) to 1.744 (Vijayawada Urban). Rainfall at gauged stations, Prathipadu, Thadepalli, Amaravati, Phirangipuram, Penamaluru, Mangalagiri and Pedakurapadu showed an insignificant positive trend ($0.09 \leq Z \leq 1.71$) and those at Tadikonda, Guntur, Kanchikacherala, Vatticherukuru, Medikonduru, Duggirala, Ibrahimpatanam, Thullur, Pedakakani showed an insignificant negative trend ($-1.46 \leq Z \leq -0.11$). Fig. 4.13 showed the P-values of the MK test of the annual average rainfall series of the seventeen gauged stations. Annual average rainfall series with the significance of 5% showed that the P-values at Tadikonda, Pedakurapadu and Vijayawada Urban are low indicating a more significant trend.

Table 4. 8 MK Test and Sen's slope test results for annual average precipitation series (1985-2014)

	Annual Average		Annual Maximum	
Station	Z-Value	Sen's slope	Z-Value	Sen's slope
Amaravati	0.54	0.52	0.36	0.28
Thullur	-0.27	-0.257	0.59	0.36
Thadepalli	0.25	0.3	-0.07	-0.25
Mangalagiri	0.95	0.5	0.95	0.5
Tadikonda	-1.46	-0.52	-1.43	-0.54
Medikonduru	-0.68	-0.309	-0.61	-0.24
Guntur	-0.96	-0.585	-0.96	-0.58
Pedakakani	-0.11	-0.079	0.18	0.11
Duggirala	-0.61	-0.414	-0.71	-0.57
Pedakurapadu	1.36	1.222	1.36	1.22
Phirangipuram	0.7	0.56	0.45	0.3
Prathipadu	0.09	0.1	0.16	0.23
Vatticherukuru	-0.82	-0.529	-0.57	-0.29
Ibrahimpatanam	-0.5	-0.467	-0.96	-0.89
Vijayawada Urban	**1.71**	1.744	**1.75**	1.34
Penamaluru	0.88	0.684	0.57	0.63
Kanchikacherala	-0.95	-1.233	-0.8	-0.78

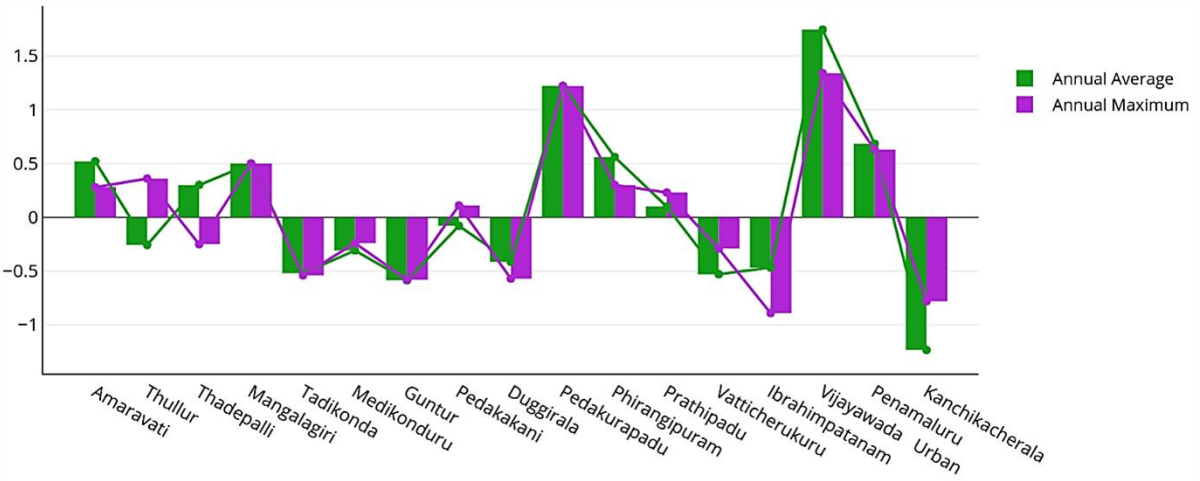

Fig 4. 13 Sen's slope for the annual average and annual maximum precipitation series of gauged stations

4.3.11. Non-parametric trend test for gauged annual maximum rainfall

The results of the MK Test and Sen's slope test for annual maximum rainfall series of the 17 rainfall stations are shown in Table 4.9. The MK test results for the annual maximum rainfall series also showed a significant positive trend only at Vijayawada Urban gauged station, with a Z value of 1.75. Rainfall series at the gauged stations at Amaravati, Thullur, Mangalagiri, Pedakakani, Pedakurapadu, Phirangipuram, Prathipadu and Penamaluru showed insignificant positive trends with Z values ranging from 0.16 to 1.36. Rainfall at the rest of the 8 gauge stations namely Tadikonda, Guntur, Ibrahimpatanam, Kanchikacherala, Duggirala, Medikonduru, Vatticherukuru and Thadepalli showed insignificant negative trends with Z values in the range -1.43 to -0.07. The S values varied from -81 (Tadikonda) to 99 (Vijayawada Urban). The Kendall's Tau (τ) value has the maximum at Vijayawada Urban (0.23) and minimum at Tadikonda (-0.19). With respect to P-value, Vijayawada Urban showed a significant positive trend at 8%. Sen's slope values calculated with a confidence interval of 95% showed positive values ranging from 0.11 to 1.34 and negative values in the range -0.89 to -0.24, which agree with the results of MK Test.

Table 4. 9 Results of the MK test and Sen's slope test for annual maximum rainfall series (1985-2014)

Station	Z-Value	S	P-value	Tau (τ)	Sen's slope
Amaravati	0.36	21	0.72	0.05	0.28
Thullur	0.59	34	0.56	0.08	0.36
Thadepalli	-0.07	-5	0.94	-0.01	-0.25
Mangalagiri	0.95	54	0.34	0.12	0.50
Tadikonda	-1.43	-81	0.15	-0.19	-0.54
Medikonduru	-0.61	-35	0.54	-0.08	-0.24
Guntur	-0.96	-55	0.34	-0.13	-0.58
Pedakakani	0.18	11	0.86	0.03	0.11
Duggirala	-0.71	-41	0.48	-0.09	-0.57
Pedakurapadu	1.36	77	0.18	0.18	1.22
Phirangipuram	0.45	26	0.66	0.06	0.30
Prathipadu	0.16	10	0.87	0.02	0.23
Vatticherukuru	-0.57	-33	0.57	-0.08	-0.29
Ibrahimpatanam	-0.96	-55	0.34	-0.13	-0.89
Vijayawada Urban	1.75	99	0.08	0.23	1.34
Penamaluru	0.57	33	0.57	0.08	0.63
Kanchikacherala	-0.80	-46	0.42	-0.11	-0.78

4.4. Stationarity and Homogeneity Analysis

4.4.1. Stationarity and non-stationarity

The test for stationarity of annual average rainfall series was carried out using ADF, PP and KPSS test for the 17 stations and the results are shown in Table 4.10. PP and ADF tests show non-stationarity in the time-series when the test shows null hypothesis H0, while the KPSS test showed stationarity in the time-series data for null hypothesis H0. A confidence level of 0.05 was considered for the stationarity test in this study. ADF and PP tests showed stationarity for all the gauged stations except for Penamaluru and it corresponded to the maximum P-value (one-tailed) of 0.07 whereas other stations showed relatively lesser P-values. KPSS test showed non-stationarity at Amaravati, Thullur, Pedakurapadu and Vijayawada Urban gauged station having the P-value (one-tailed) as 0.002, 0.015, 0.023 and 0.002 respectively. Rest of the stations showed stationarity, the P-values ranging from 0.055 to 0.94 corresponding to Penamaluru and Tadikonda stations respectively.

Table 4. 10 Stationarity of annual average precipitation series using ADF, PP and KPSS test for the gauged stations

Station	Dickey-Fuller test		Phillips-Perron test		KPSS test	
	P-value (one-tailed)	Stationarity	P-value (one-tailed)	Stationarity	P-value (one-tailed)	Stationarity
Amaravati	0.030	Ha	0.025	Ha	0.002	Ha
Thullur	0.001	Ha	0.001	Ha	0.015	Ha
Thadepalli	0.001	Ha	0.001	Ha	0.195	**H0**
Mangalagiri	< 0.0001	Ha	< 0.0001	Ha	0.729	**H0**
Tadikonda	0.001	Ha	0.001	Ha	0.940	**H0**
Medikonduru	0.000	Ha	0.000	Ha	0.837	**H0**
Guntur	0.000	Ha	0.000	Ha	0.625	**H0**
Pedakakani	0.020	Ha	0.019	Ha	0.260	**H0**
Duggirala	0.001	Ha	0.001	Ha	0.107	**H0**
Pedakurapadu	0.000	Ha	0.000	Ha	0.023	Ha
Phirangipuram	0.002	Ha	0.002	Ha	0.678	**H0**
Prathipadu	0.001	Ha	0.000	Ha	0.871	**H0**
Vatticherukuru	< 0.0001	Ha	< 0.0001	Ha	0.821	**H0**
Ibrahimpatanam	0.001	Ha	0.001	Ha	0.466	**H0**
Vijayawada Urban	0.011	Ha	0.007	Ha	0.002	Ha
Penamaluru	0.070	**H0**	0.094	**H0**	0.055	**H0**
Kanchikacherala	0.007	Ha	0.008	Ha	0.213	**H0**

4.4.2. Homogeneity of rainfall

Table 4.11, shows the results of the test for homogeneity of the annual average rainfall series using SNHT, Pettit's, Buishand's and von Neumann's tests. In SNHT, Pettit's and Buishand's tests, the year of the change points for the annual average rainfall time-series was obtained and shown in the Table, whereas the von Neumann's test only identified the presence of the change point. Pettit's test shows that all the gauged stations are homogeneous for the annual average rainfall series whereas heterogeneity for annual average rainfall series was observed in all the tests.

The year 2004 can be recognised as the year having the greatest number of change points. In SNHT test, the change points that are identified in the year 2007 and 2009 at Vijayawada Urban and Pedakurapadu and the rainfall data were non-homogenous. Similarly, in Buishand's test, the change points that were seen in the year 2004 at the two stations, and the rainfall data was non-homogenous in the year 2009 at Pedakurapadu. In von Neumann's test, data at Amravati and Penamaluru shows non-homogeneity.

Rainfall series at the two rain gauge stations showed non-homogeneity by SNHT and Buishand's test both. Buishand's test and von Neumann's test showed heterogeneity in Amaravati station.

Similar results are obtained in parametric regression analysis and non-parametric Mann Kendall test, with Mann Kendall trend test showing significant trend among the result.

Table 4. 11 Homogeneity of annual average precipitation series using Pettit's, SNHT, Buishand's and von Neumann's test for the gauged stations

Stations	Pettitt's test			SNHT			Buishand's test			von Neumann's test		
	K	t	trend	T0	t	trend	Q	t	trend	N	P-value	trend
Amaravati	115	2007	H0	7.07	2007	H0	6.92	2004	**Ha**	1.41	0.05	**Ha**
Thullur	81	1991	H0	3.58	2004	H0	4.97	2004	H0	2.04	0.55	H0
Thadepalli	80	2002	H0	2.34	2004	H0	4.14	2002	H0	2.00	0.48	H0
Mangalagiri	59	2000	H0	2.02	2011	H0	2.74	2009	H0	2.46	0.90	H0
Tadikonda	76	1998	H0	2.88	1995	H0	4.56	1995	H0	1.98	0.46	H0
Medikonduru	53	2005	H0	5.11	2013	H0	2.26	2013	H0	2.29	0.79	H0
Guntur	81	1996	H0	4.91	1990	H0	5.51	1995	H0	1.97	0.43	H0
Pedakakani	84	2002	H0	4.28	2002	H0	5.65	2002	H0	1.54	0.10	H0
Duggirala	84	1990	H0	4.97	1990	H0	4.97	1990	H0	2.07	0.57	H0
Pedakurapadu	103	2009	H0	11.28	2009	**Ha**	6.97	2009	**Ha**	1.97	0.45	H0
Phirangipuram	63	2011	H0	2.23	2011	H0	2.50	2011	H0	1.94	0.42	H0
Prathipadu	42	1988	H0	1.96	1985	H0	2.66	1997	H0	1.95	0.43	H0
Vatticherukuru	65	1997	H0	3.42	1997	H0	5.11	1997	H0	2.26	0.77	H0
Ibrahimpatanam	74	1998	H0	1.95	1998	H0	3.88	1998	H0	2.09	0.59	H0
Vijayawada Urban	71	2007	H0	9.79	2007	**Ha**	7.38	2004	**Ha**	1.48	0.07	H0
Penamaluru	90	2004	H0	6.71	2011	H0	6.10	2004	H0	1.21	0.01	**Ha**
Kanchikacherala	88	1994	H0	3.41	1985	H0	3.47	1994	H0	1.49	0.07	H0

H0-null hypotheses, Ha- alternate hypotheses.

4.5. Land Use Land Cover Changes

4.5.1. Comparison of Landsat 8 OLI and Sentinel 2

The comparison of Landsat 8 Operational Land Imager (OLI) and Sentinel 2 data has been made for the year 2018 (Fig 4.14). Table 4.12 and Table 4.13 give the comparison of accuracy calculated using the error matrix or confusion matrix. For Landsat data, the average user's accuracy was 82.8%, and the average producer's accuracy was 71.95%. The kappa coefficient for Landsat data was 0.718. For Sentinel data, the average user's accuracy was 82.9%, the average producer's accuracy was 79.8% and the kappa coefficient was 0.77. Comparison of these two data set showed that Sentinel 2 has higher accuracy than Landsat 8.

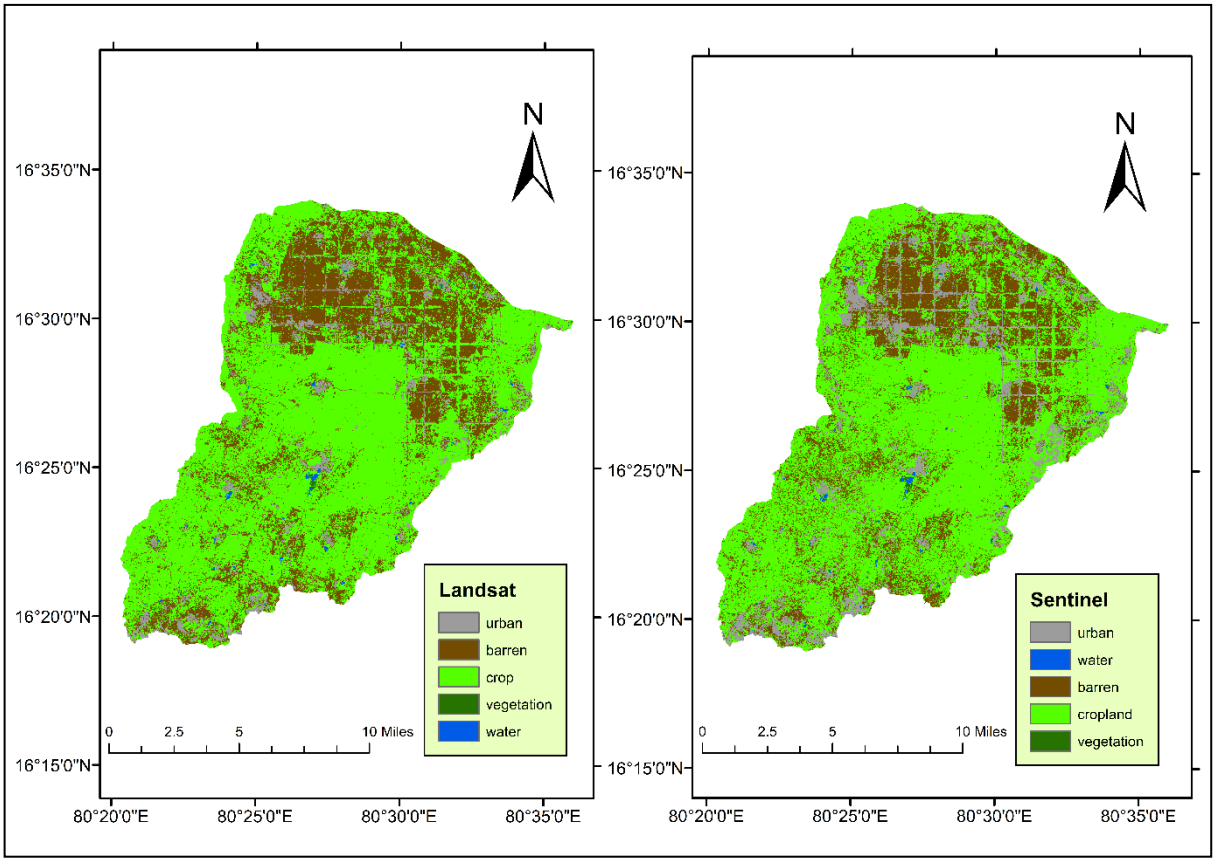

Fig 4. 14 Comparison between Landsat and Sentinel supervised classification for the year 2018

Table 4. 12 Error matrix for Landsat 8 (2018)

		Supervised classification					
		Built-up Area	Barren Land	Cropland	Vegetation	Water	Total
Reference points	Built-up Area	37	9	6			52
	Barren Land		19	2			21
	Cropland	2		78	1		81
	Vegetation		1	9	5	1	16
	Water			5		12	17
	Total	39	29	100	6	13	187

Table 4. 13 Error matrix for Sentinel 2A (2018)

		Supervised classification					
		Built-up Area	Water	Barren Land	Cropland	Vegetation	Total
Reference points	Built-up Area	55		1	2		58
	Water		34				34
	Barren Land	1		27	9		37
	Cropland	2		16	91	3	112
	Vegetation				10	10	20
	Total	58	34	44	112	13	261

4.5.2. Comparison of indices

The trends of different indices have been calculated for Landsat 8 and Sentinel 2. Fig 4.15 showed the maximum value of the indices (NDVI, MNDWI, NDISI and NDBI) using Landsat 8, and Fig 4.16 showed the maximum value of the indices using Sentinel 2.

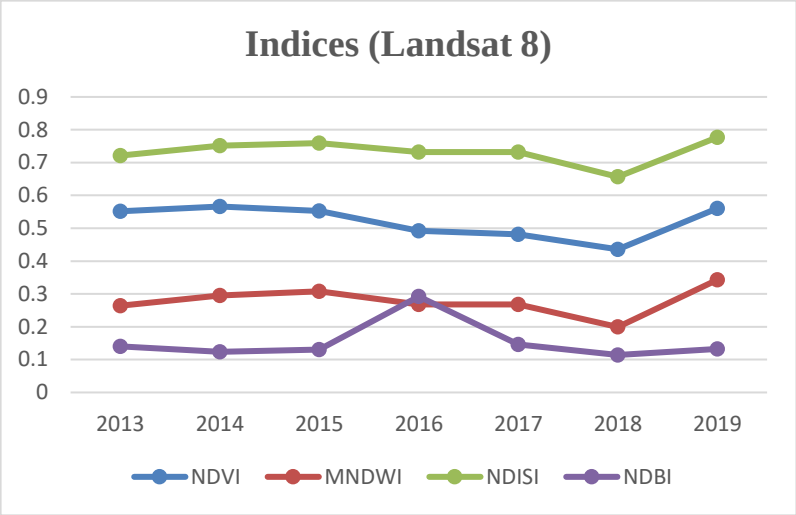

Fig 4. 15 Plots of maximum indices values for Landsat 8 OLI

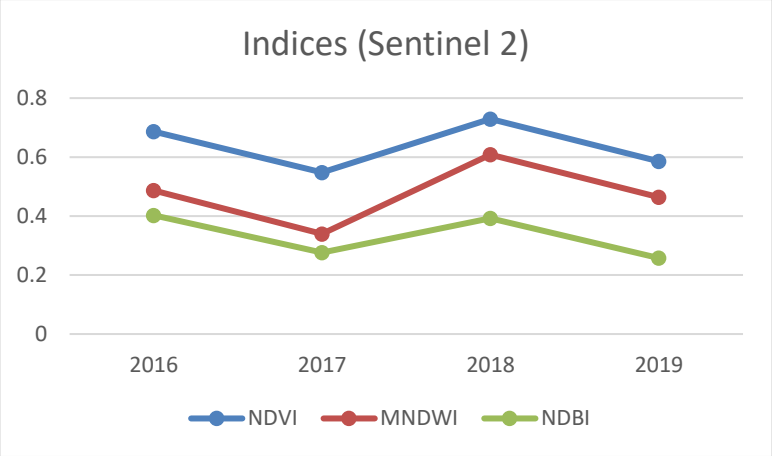

Fig 4. 16 Plots of maximum indices values for Sentinel 2

The trend of indices in Sentinel showed the inconsistency of data. This trend does not tend help to reach any conclusion. The trend should either decrease or increase. If the NDVI decreases, it can be assumed that the construction activities have resulted in the reduction of vegetation. If the NDVI increases, it can be assumed that plantation was being done in the area. Inconsistency in the trend of indices in Sentinel is due to the fact that the data has not undergone atmospheric correction. Sentinel data does not have a thermal infrared band and hence the computation of NDISI was not possible.

Based on the results, it can be concluded that sentinel data is suitable for supervised classification for the years 2016 to 2019. Landsat data is better for the computation of various indices.

Table 4.14 shows the maximum values of the indices calculated using Landsat data. The NDVI, MNDWI, and the NDISI values decrease gradually from the year 2015 till 2018. The increase in the values of these indices in the year 2019 can be justified due to the creation of a new wing under APCRDA for the plantation works, called the Environmental Management Regulatory Authority (EMRA), hence increasing the vegetation. The built-up index does not show a gradual trend but increases in the year 2019. However, there is an anomaly observed in the year 2016. This may be due to the error in collected data as these indices were calculated mathematically using raster calculator without the involvement of any manual operations

Table 4. 14 Maximum values of various indices

Indices	2013	2014	2015	2016	2017	2018	2019
NDVI	0.55	0.57	0.55	0.49	0.48	0.44	0.56
MNDWI	0.26	0.30	0.31	0.27	0.27	0.20	0.34
NDISI	0.72	0.75	0.76	0.73	0.73	0.66	0.78
NDBI	0.14	0.12	0.13	0.29	0.15	0.11	0.13

4.5.3. Land Use and Land Cover changes

Land cover has changed significantly between 2016 and 2019. This is because the new capital city was being constructed with huge infrastructure causing conversion of most of the cropland into urban and barren land. For studying the Land use and land cover details of the area, Landsat 5 TM data was used for the years 1990, 2000, and 2010; Landsat 8 data was used for the period from 2013 to 2016; Sentinel 2 data was used for 2016 to 2019. Sentinel data was used due to its high resolution of 10m. The areas of different classes computed from the supervised classification are shown in Table 4.15. The kappa coefficients for the classification are presented in Table 4.16.

Table 4. 15 Area (Km^2) of different classes.

	1990	2000	2010	2013	2014	2015	2016	2017	2018	2019
Urban	14.49	37.30	17.17	14.95	29.50	33.65	26.19	35.45	41.74	107.25
Barren	18.45	15.90	3.67	0.61	3.92	21.44	8.79	73.04	101.52	71.09
Cropland	367.46	364.75	396.45	407.15	384.73	353.91	376.31	304.95	276.92	218
Vegetation	21.44	4.80	5.21	0.135	4.43	14.041	3.10	9.15	1.80	26.19
Water	1.31	0.399	0.64	0.295	0.55	0.10	1.26	0.56	1.17	0.63

Table 4. 16 Accuracy of supervised classification data

	1990	2000	2010	2013	2014	2015	2016	2017	2018	2019
Users Accuracy (average)	81.9	82	82.1	92.2	81.7	85.2	87.2	83.9	82.9	86.7
Producer Accuracy (average)	78.8	75.2	73.1	50.5	71	73.3	74.2	83.4	79.8	78.01
kappa Coefficient	0.73	0.74	0.75	0.65	0.75	0.76	0.78	0.78	0.77	0.77

The built-up area (urban) had increased from 3.41% to 25.2%, most of which happened between 2016 to 2019. The increased area was historically cropland. The cropland decreased from 86.6% in 1990 to 51.4% in 2019. There was an increase in barren land from 4.3% in 1990 to 16.76% in 2019. This change in the land use was due to the farmers voluntarily donating their lands under the 'Land Pooling Scheme'. There was not much significant change in the vegetation area during this period; it was 5.05% in 1990 and 6.17% in 2019. The water area within the study area boundaries was about 0.3% in 1990, and it changed to 0.1% in 2019. Though artificial canals were built to divert the river water into the new capital region in the study area, it was not detected by the satellites since the data was from the months of April and May. As the Krishna is a seasonal river, the canals might be dry during the summer months. Temporal changes in land use and land cover for the years 1990, 2000, 2010, and 2018 are shown in Fig. 4.17. Supervised classification for the years 1990, 2000, 2010, 2013, 2014, 2015, 2016, 2017, 2018, and 2019 are shown in Fig 4.18 to Fig. 4.27. Details of conversion of land cover from one class to another are shown in Fig 4.28.

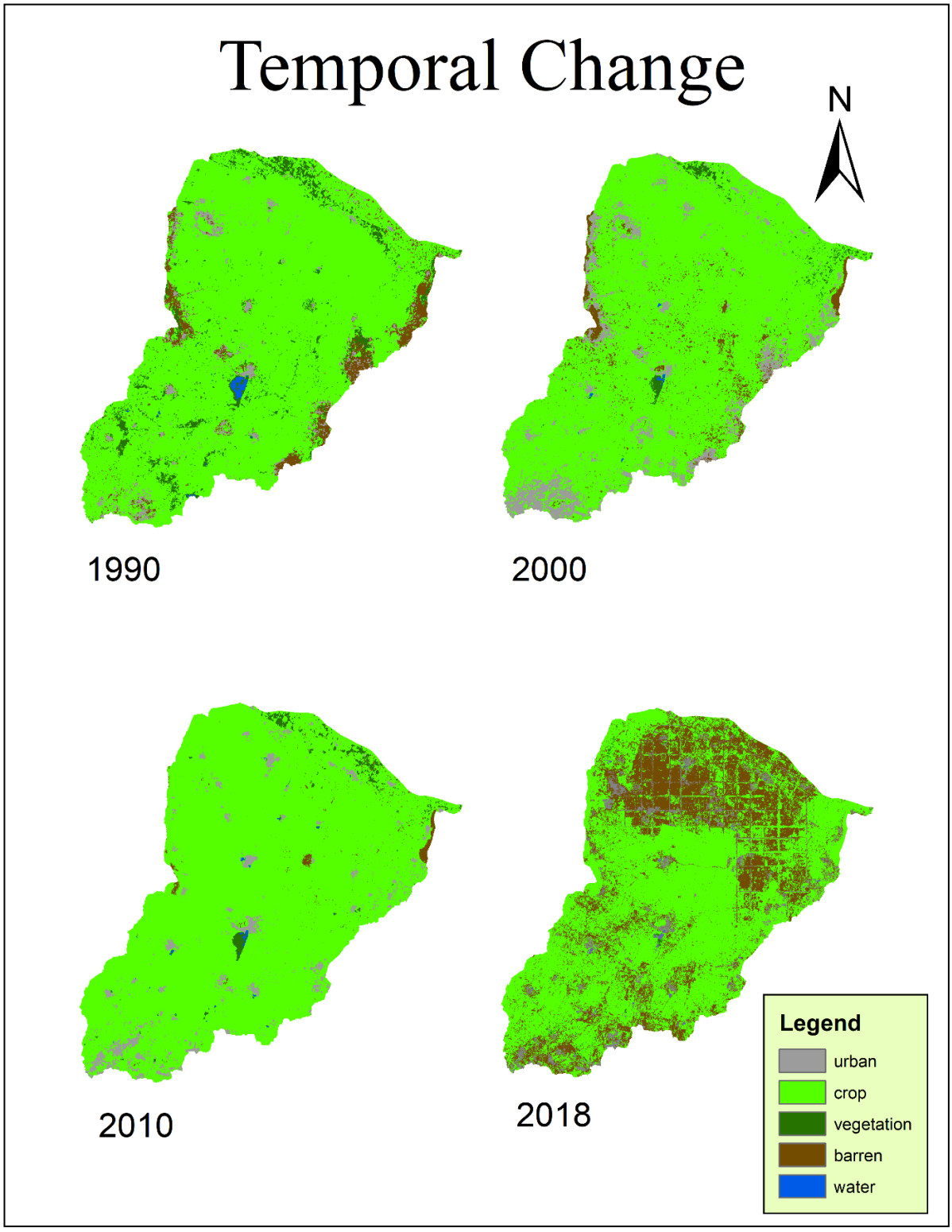

Fig 4. 17 Temporal change in land use and land cover

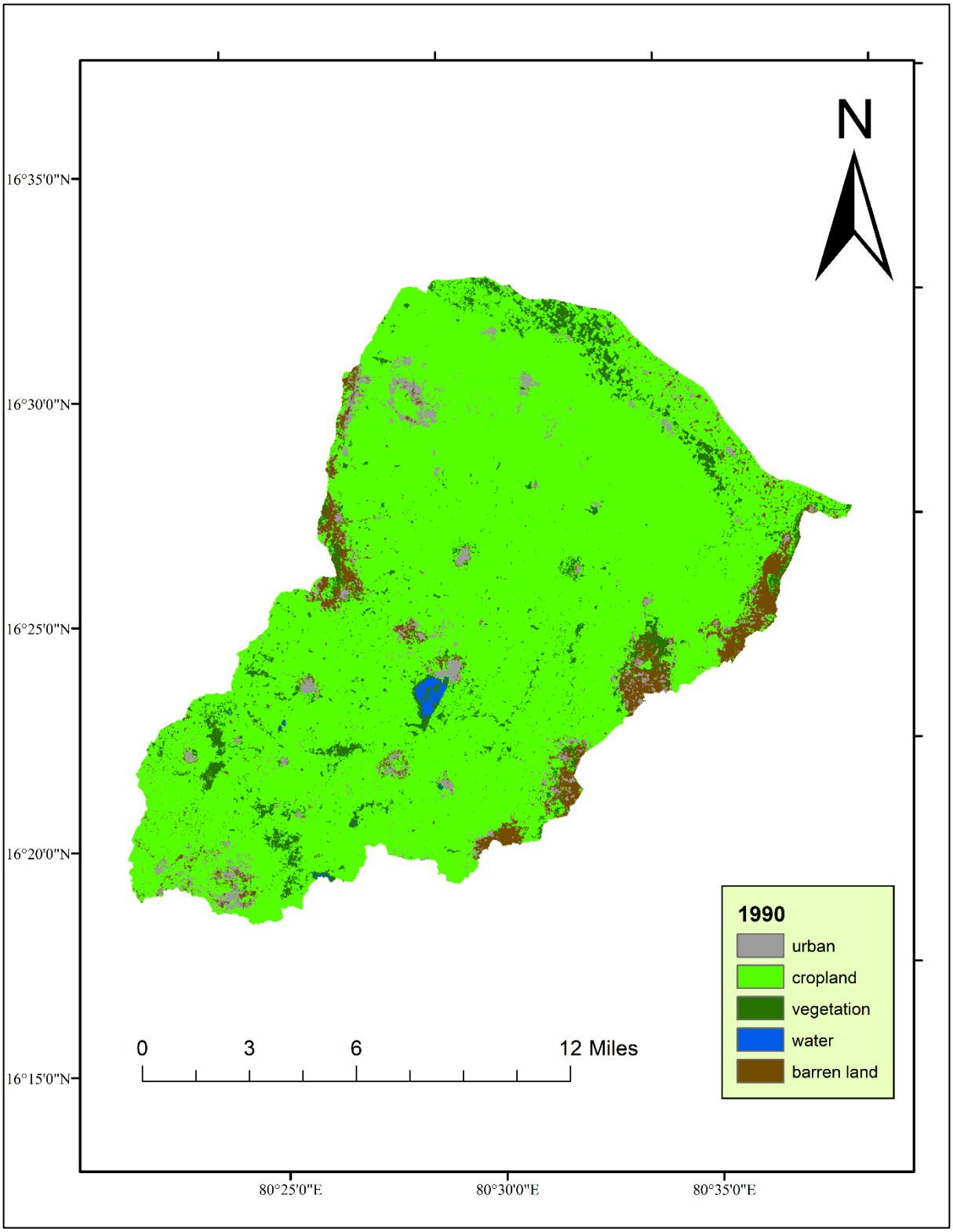

Fig 4. 18 Supervised classification based on 1990 data

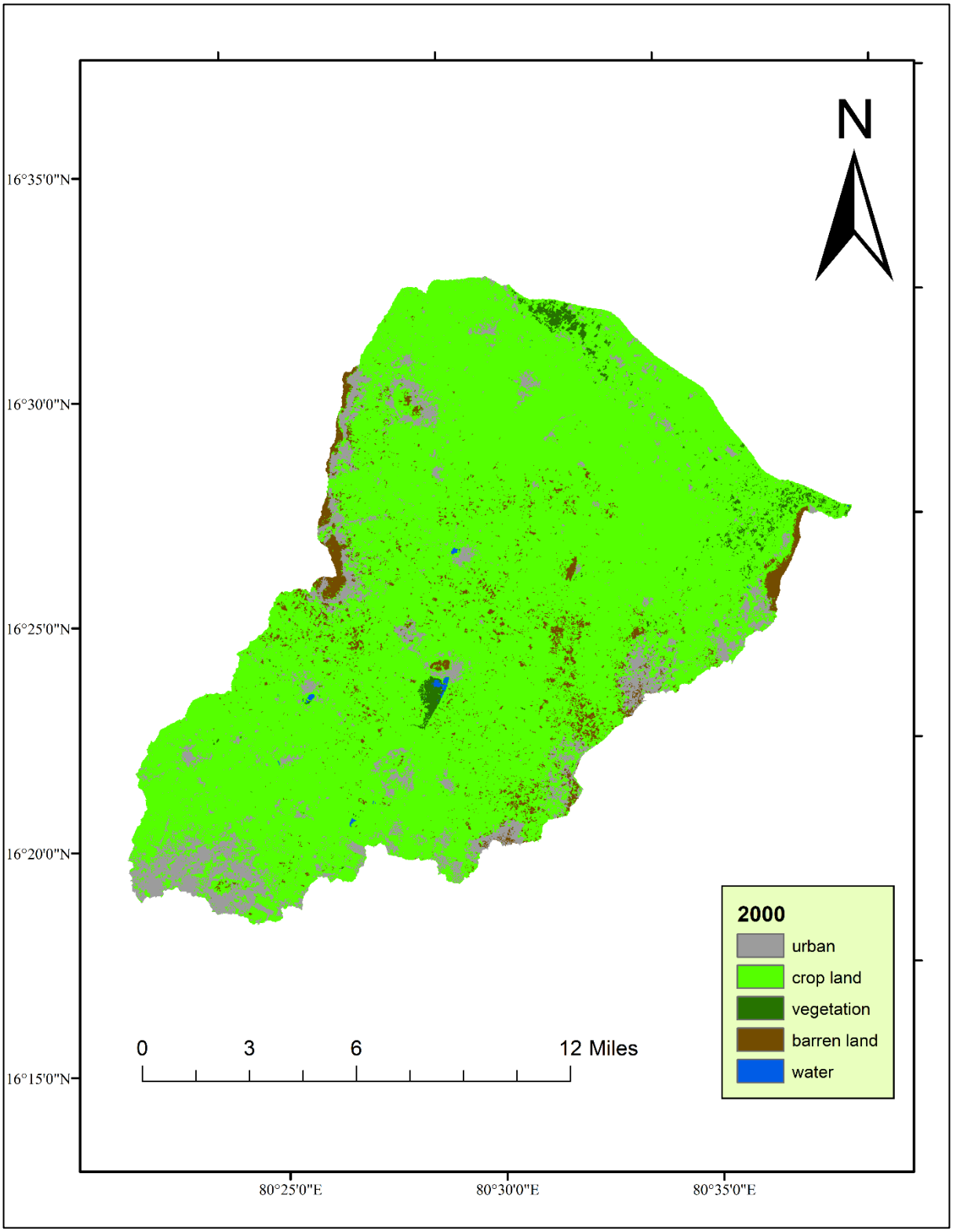

Fig 4. 19 Supervised classification based on 2000 data

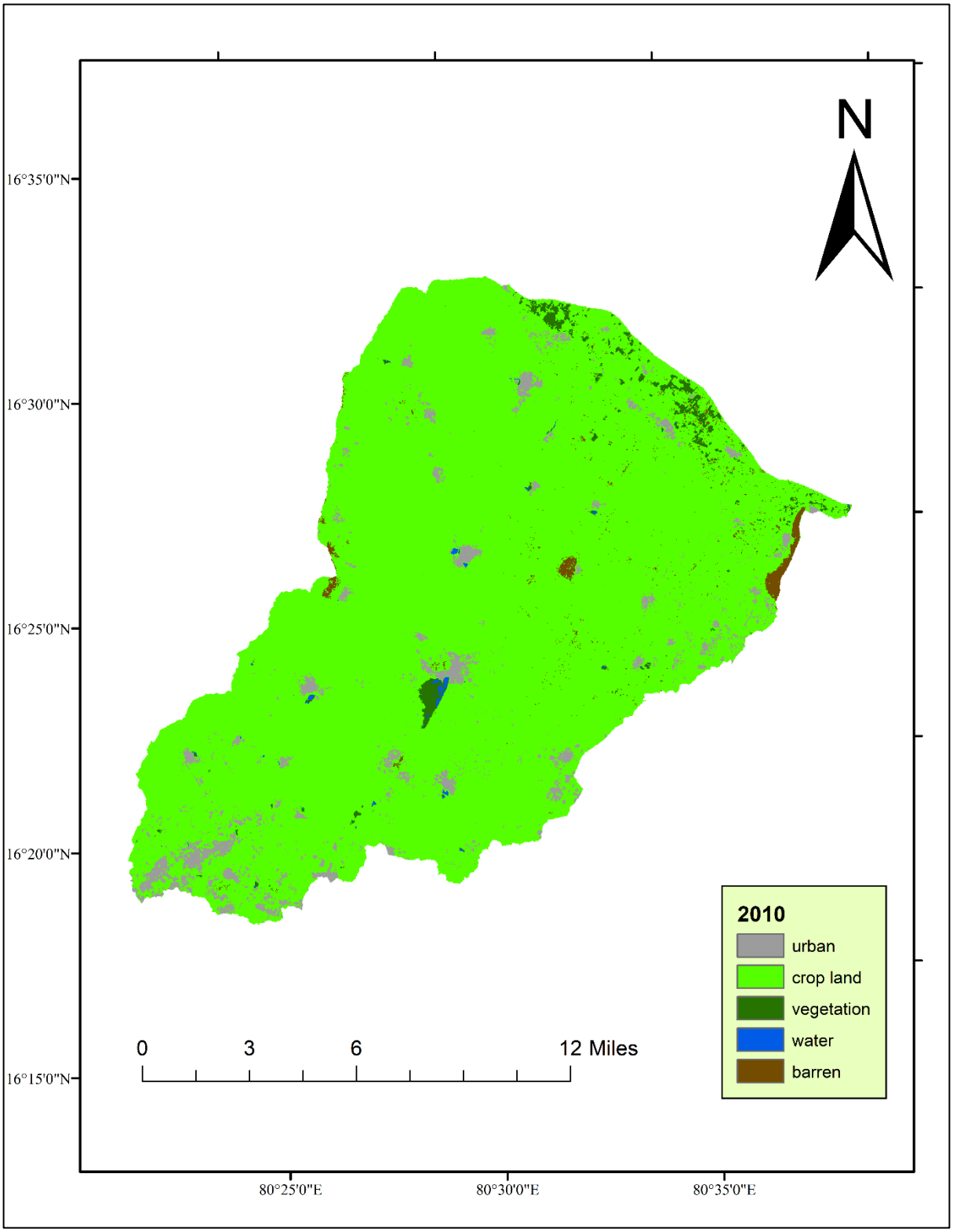

Fig 4. 20 Supervised classification based on 2010 data

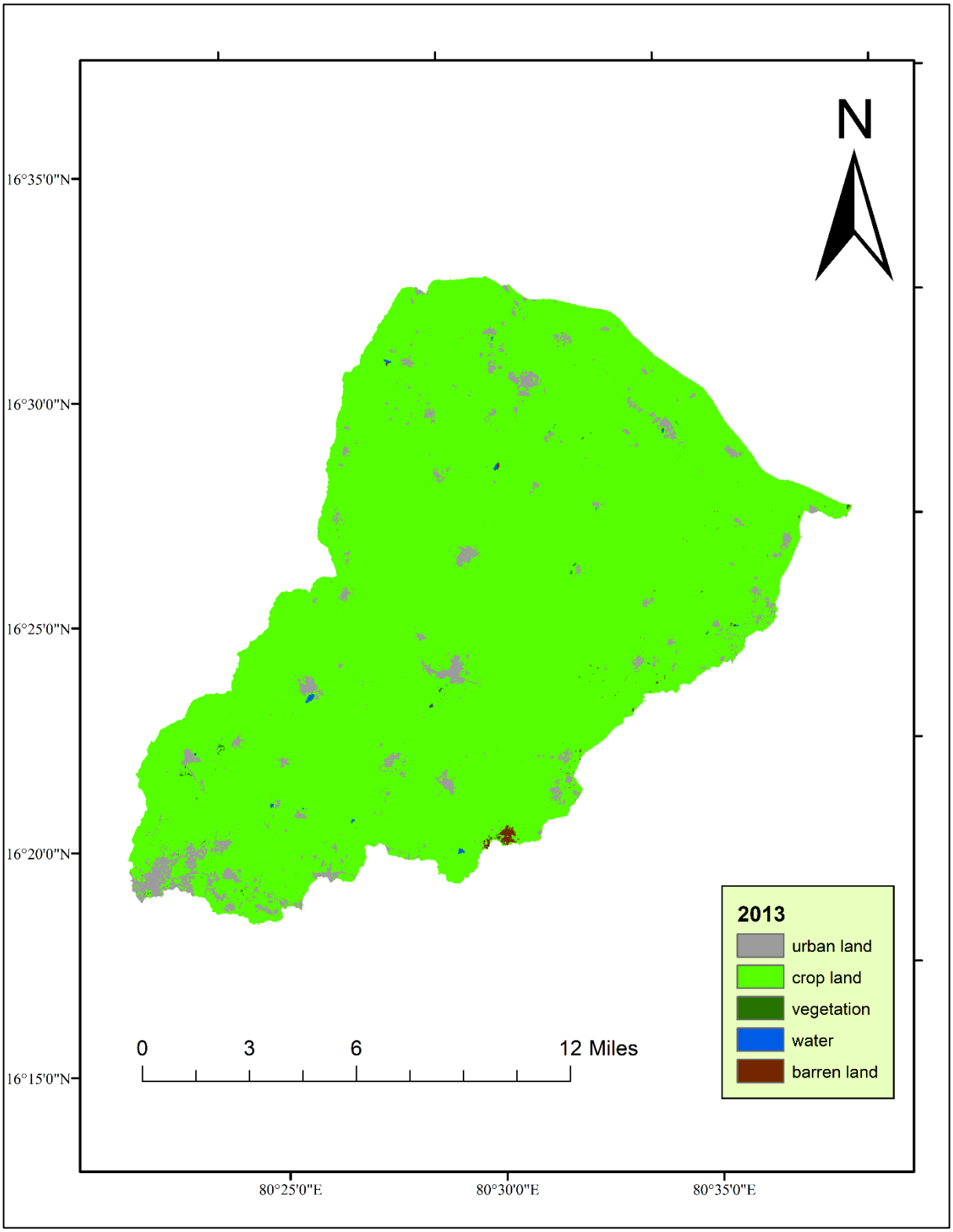

Fig 4. 21 Supervised classification based on 2013 data

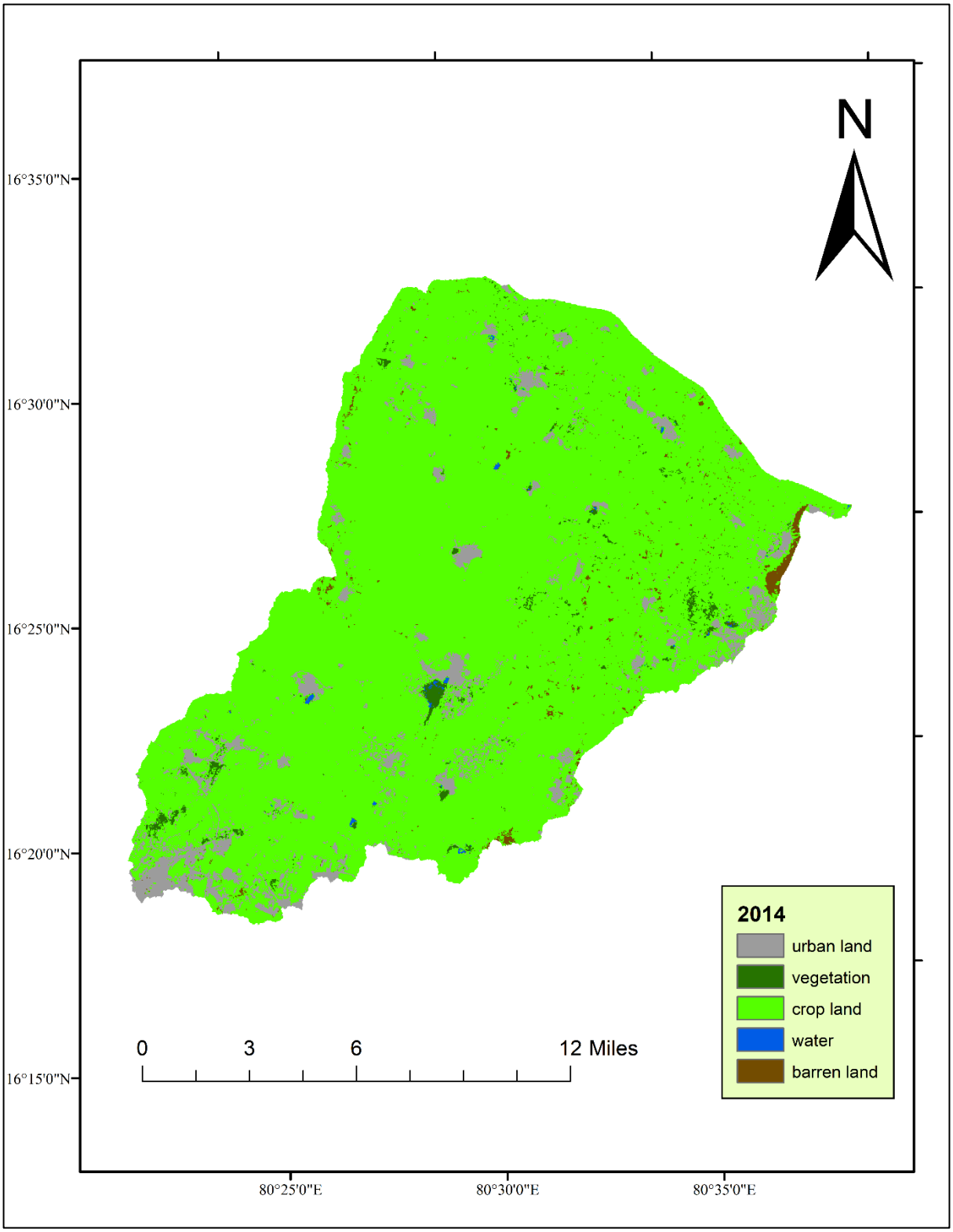

Fig 4. 22 Supervised classification based on 2014 data

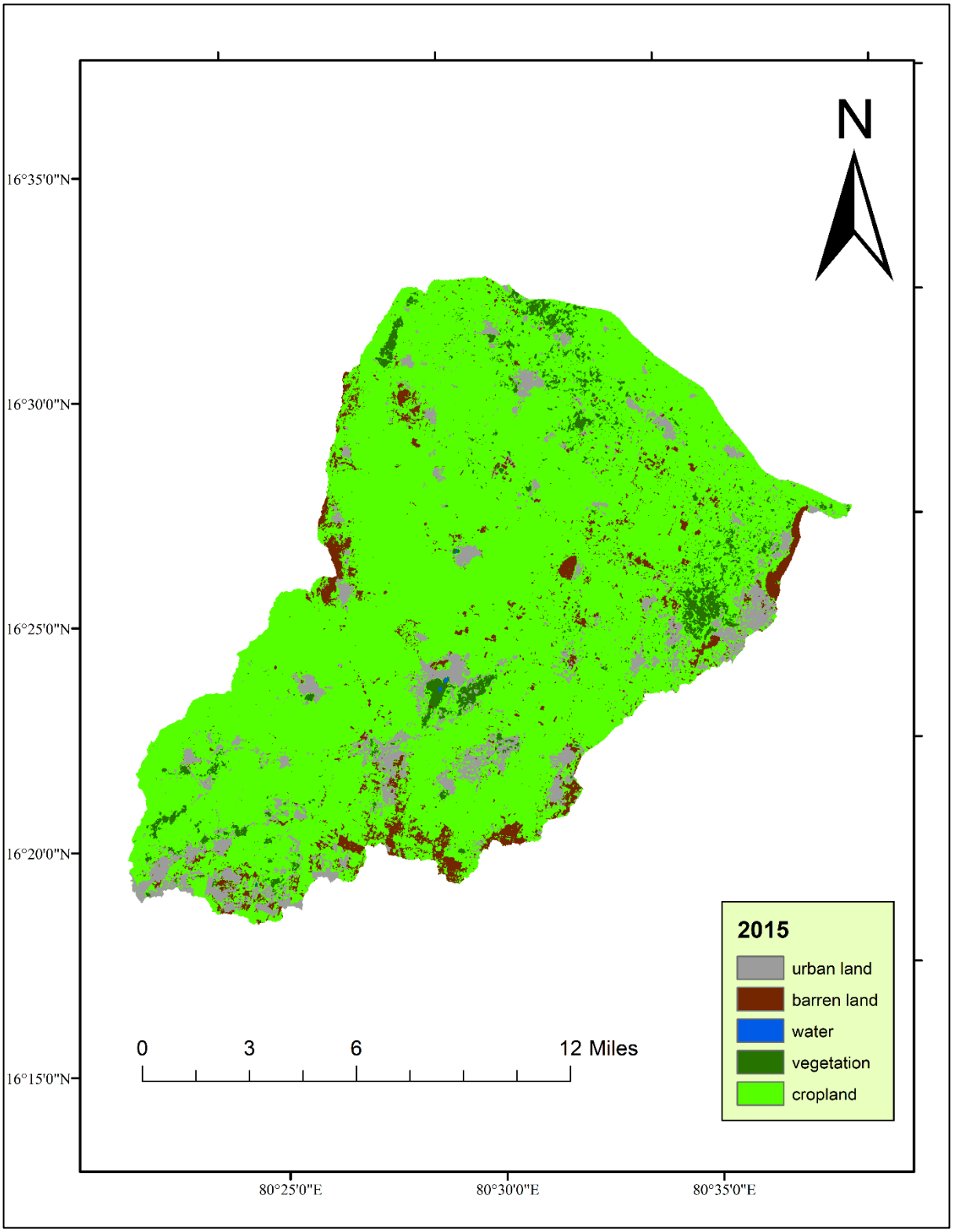

Fig 4. 23 Supervised classification based on 2015 data

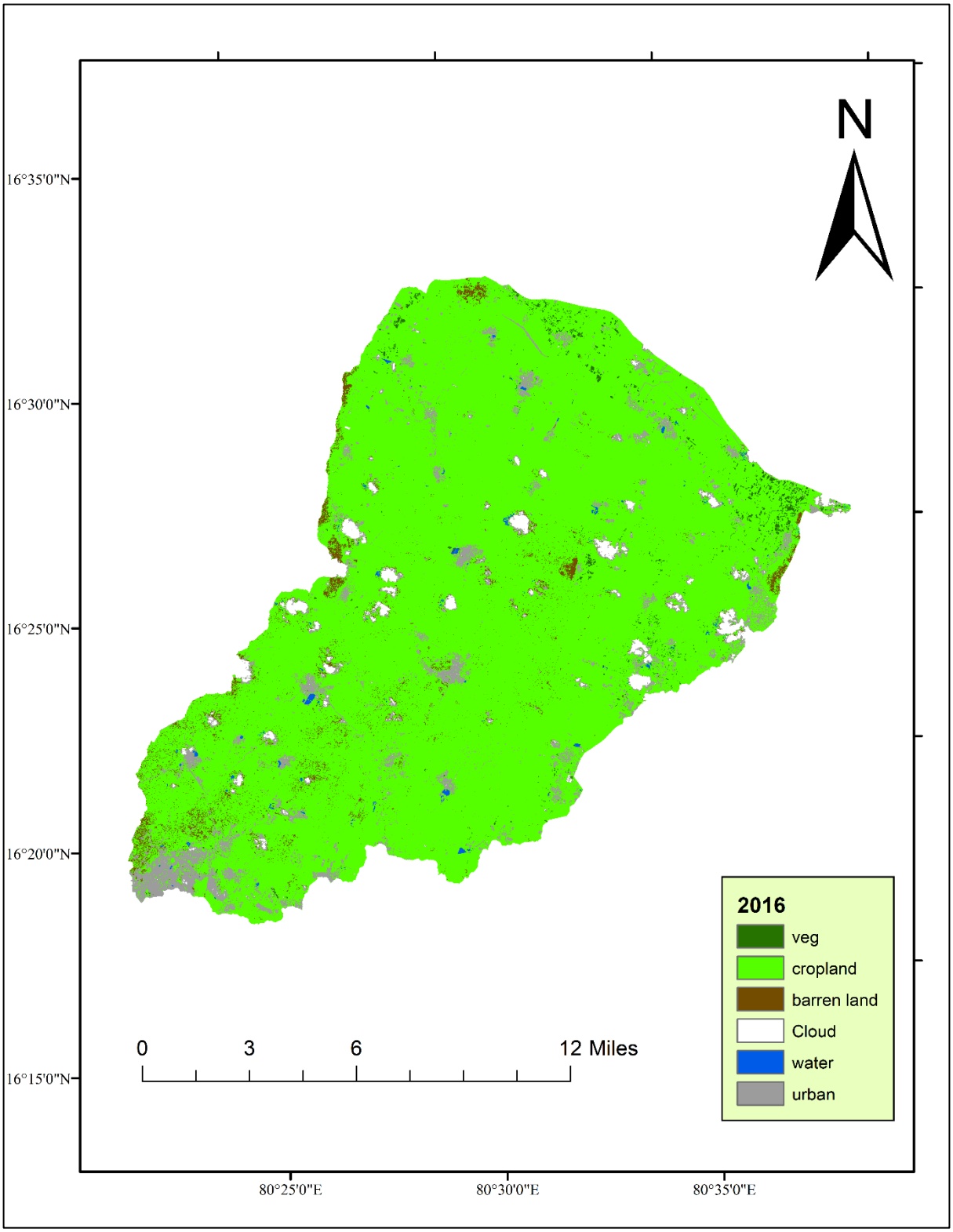

Fig 4. 24 Supervised classification based on 2016 data

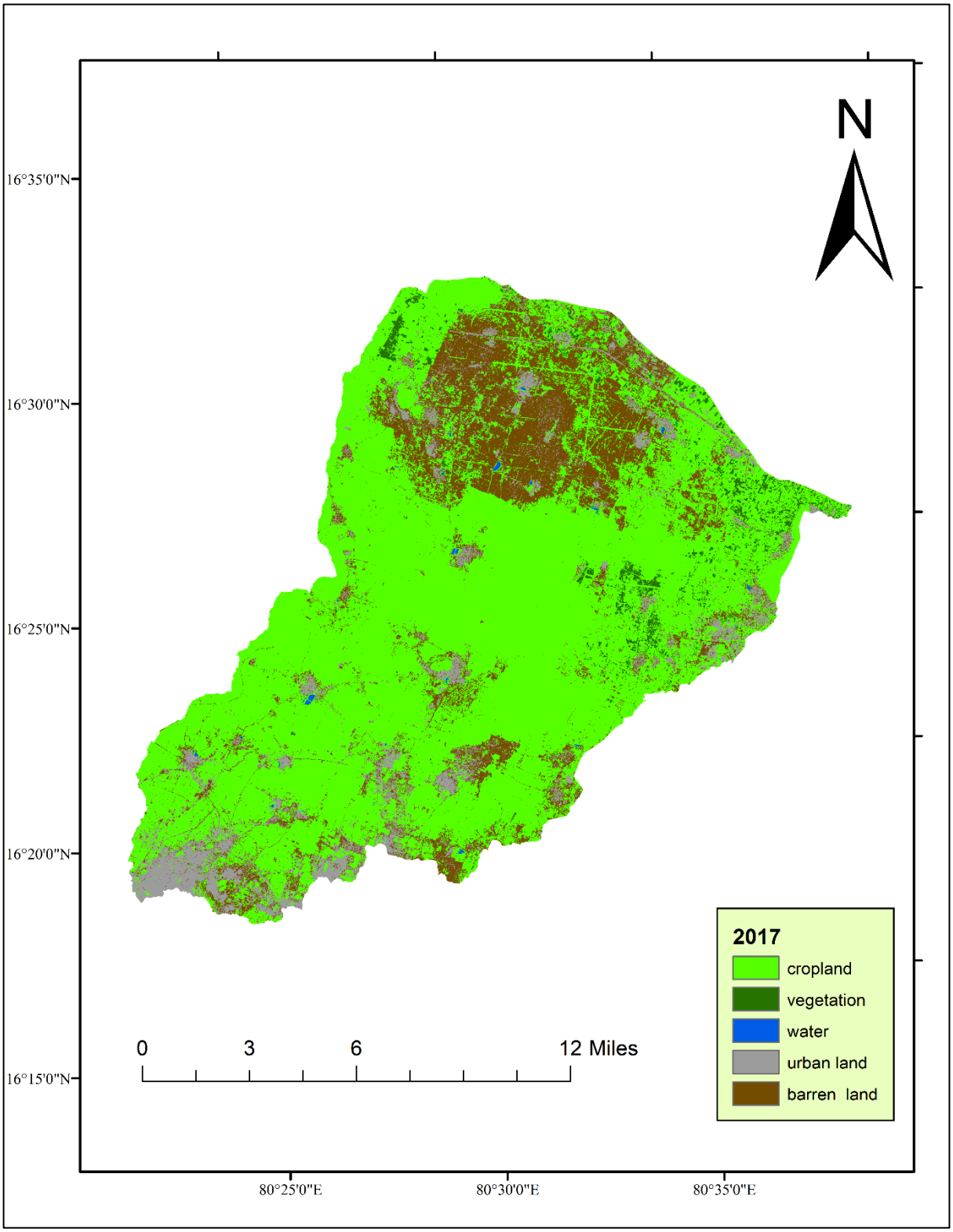

Fig 4. 25 Supervised classification based on 2017 data

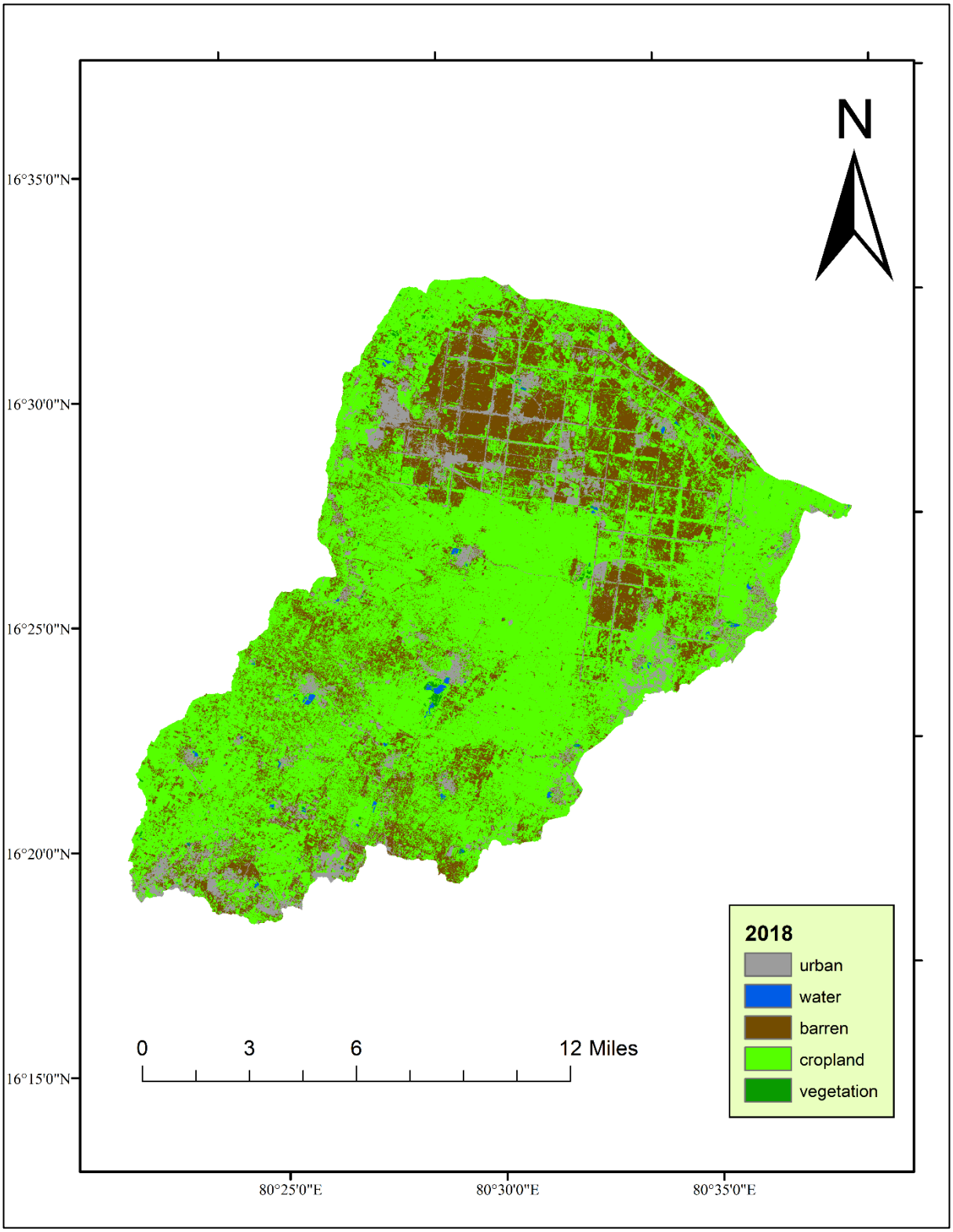

Fig 4. 26 Supervised classification based on 2018 data

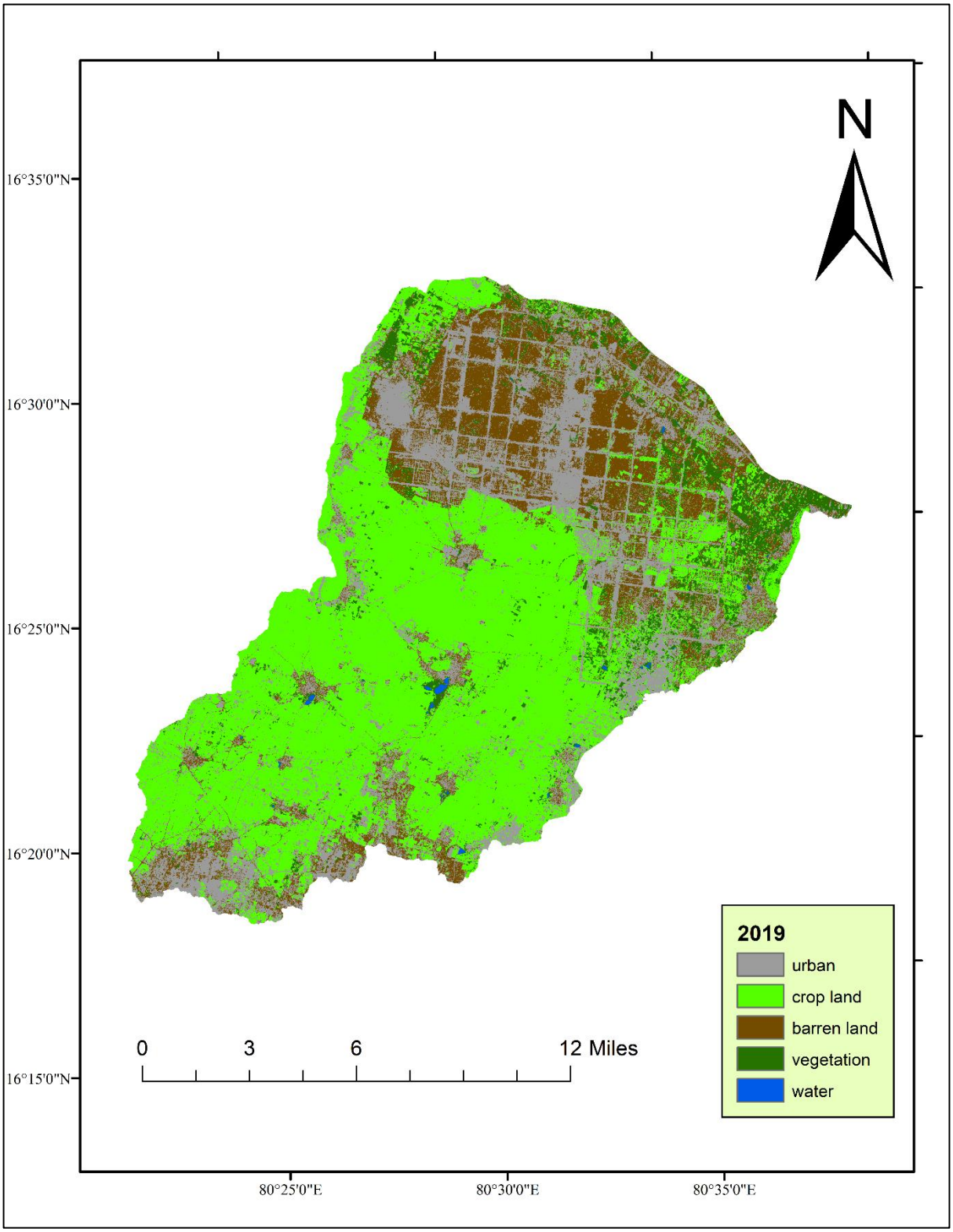

Fig 4. 27 Supervised classification based on 2019 data

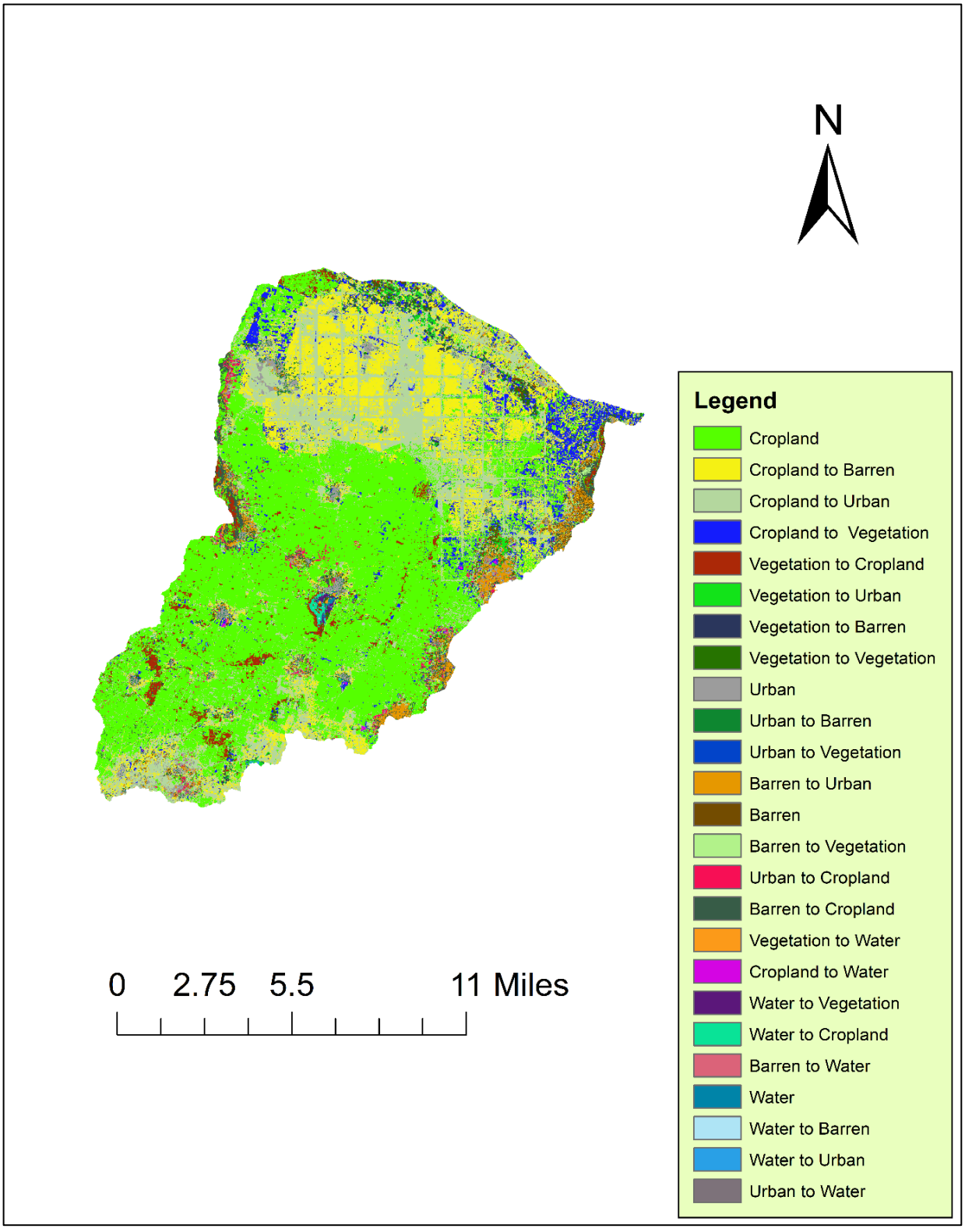

Fig 4. 28 Conversion of land cover

4.6. Flood Inundation Using HEC-RAS

4.6.1. Frequency analysis

Frequency analysis was carried out for the rainfall data. Using the ***Easyfit*** Software, the addition of the rankings of Kolmogorov Smirnov, Anderson Darling and Chi-Squared is done to find the least sum, considering it as a good fit. It is found that the GEV distribution fits well to the data. Table 4.17 shows the rainfall depth for different return periods using GEV. The result indicates that for the return period of 100 years, the rainfall depth will be around 240mm.

Table 4. 17 Rainfall depth for different return periods using GEV

Return Period (years)	P	Xt (mm)
2	0.50	84.47
5	0.80	119.95
10	0.90	145.25
20	0.95	170.96
50	0.98	206.50
100	0.99	234.90
200	0.995	264.81

4.6.2. Watershed delineation

The Kondaveeti Vagu catchment is delineated into 25 sub-basins with the first step of pre-processing using the extension HEC-GeoHMS. The HEC-HMS model was generated in ArcGIS by preparing the basin model, meteorological model and control specifications. The results of pre-processing namely, the maps for fill sinks, flow direction, flow accumulation, stream definition, stream segmentation, catchment processing, and catchment grid delineation are presented in Fig.4.29 and Fig. 4.30. Fig 4.29 shows the layouts of fill sink, flow directions, flow accumulation and stream segmentation. Fig 4.30 shows layout for catchment grid delineation, drainage line, catchment polygon processing and adjoint catchment.

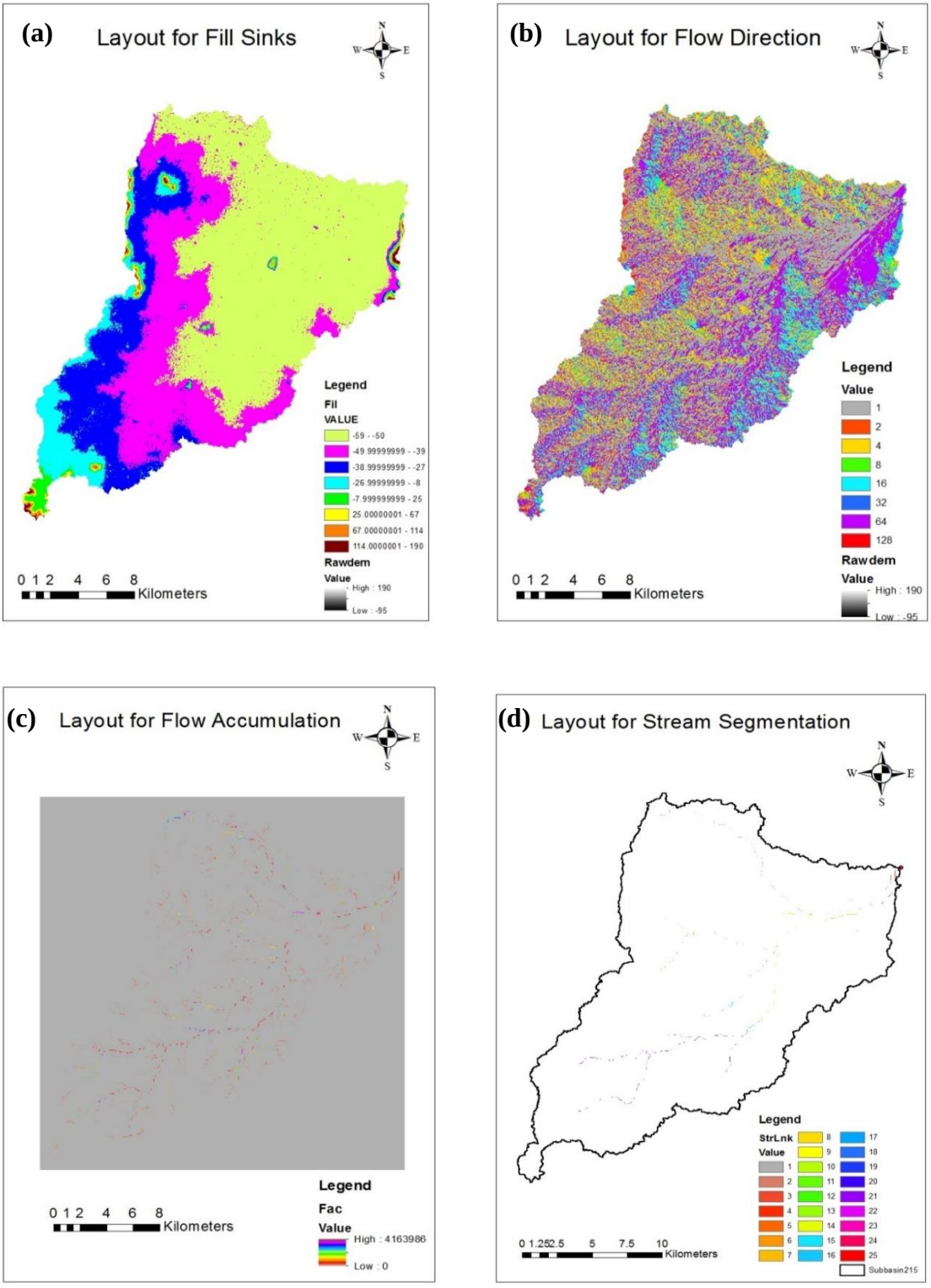

Fig 4. 29 Layouts for (a) fill sink, (b) flow direction, (c) flow accumulation and (d) stream segmentation

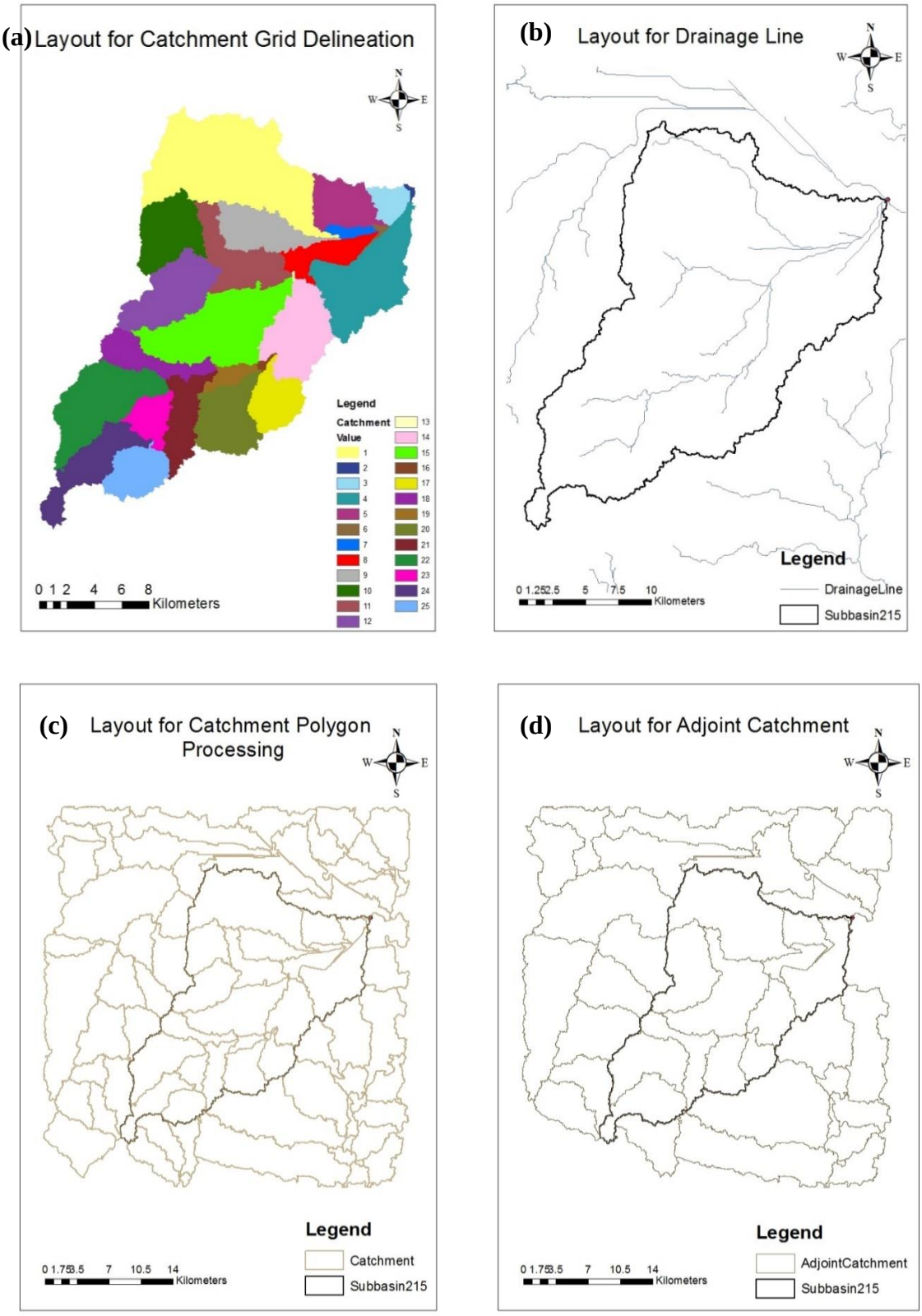

Fig 4. 30 Layout for (a) catchment grid delineation, (b) drainage line, (c) catchment polygon processing and (d) adjoint catchment

Table 4.18 shows the characteristics of area of each delineated sub-basin of the Kondaveeti Vagu catchment. The total area of the watershed is 420 sq km.

Table 4. 18 Attribute table of the sub-basins in the catchment area

Table

Subbasin217

gridcode	Shape_Length	Shape_Area	HydroID	DrainID	Name	Description	PrecipGage	TotStormP
1	75294.8526	68187015.98622	26	26	W260	<Null>	Precip Gage 1	<Null>
2	5327.7514	457056.308292	27	27	W270	<Null>	Precip Gage 2	<Null>
3	16729.9482	5928699.271375	28	28	W280	<Null>	Precip Gage 3	<Null>
4	50270.5664	35268984.690251	29	29	W290	<Null>	Precip Gage 4	<Null>
5	29282.4534	14775268.713419	30	30	W300	<Null>	Precip Gage 5	<Null>
6	9928.9918	762710.767822	31	31	W310	<Null>	Precip Gage 6	<Null>
7	12471.7826	2407461.835001	32	32	W320	<Null>	Precip Gage 7	<Null>
8	29928.2412	10634067.876391	33	33	W330	<Null>	Precip Gage 8	<Null>
9	37031.909	17591423.764255	34	34	W340	<Null>	Precip Gage 9	<Null>
10	32814.1072	20210257.585108	35	35	W350	<Null>	Precip Gage 10	<Null>
11	44599.7402	19505073.432843	36	36	W360	<Null>	Precip Gage 11	<Null>
12	37798.782	24151388.178713	37	37	W370	<Null>	Precip Gage 12	<Null>
13	2058.4494	113525.868454	38	38	W380	<Null>	Precip Gage 13	<Null>
14	40361.7558	25154488.847192	39	39	W390	<Null>	Precip Gage 14	<Null>
15	55134.1566	40057028.705139	40	40	W400	<Null>	Precip Gage 15	<Null>
16	7123.8502	637475.925548	41	41	W410	<Null>	Precip Gage 16	<Null>
17	27748.709	13566396.059548	42	42	W420	<Null>	Precip Gage 17	<Null>
18	38545.4748	12673359.532877	43	43	W430	<Null>	Precip Gage 18	<Null>
19	17476.639	4138350.023559	44	44	W440	<Null>	Precip Gage 19	<Null>
20	35054.1842	20309936.356272	45	45	W450	<Null>	Precip Gage 20	<Null>
21	39736.1464	14492930.364167	46	46	W460	<Null>	Precip Gage 21	<Null>
22	47626.8688	31069035.431494	47	47	W470	<Null>	Precip Gage 22	<Null>
23	24943.564	8980356.954783	48	48	W480	<Null>	Precip Gage 23	<Null>
24	45972.0382	18979697.900904	49	49	W490	<Null>	Precip Gage 24	<Null>
25	27345.0884	13912471.868374	50	50	W500	<Null>	Precip Gage 25	<Null>

1 (0 out of 25 Selected)

The longest flow path of the sub-basins, centroid for the sub-catchments, and centroidal longest flow path for each sub-basin were found out by using HEC-GeoHMS extension in ArcGIS software. Fig. 4.31 shows the layout for longest flow path, centroid and centroidal longest flow path of sub-basins.

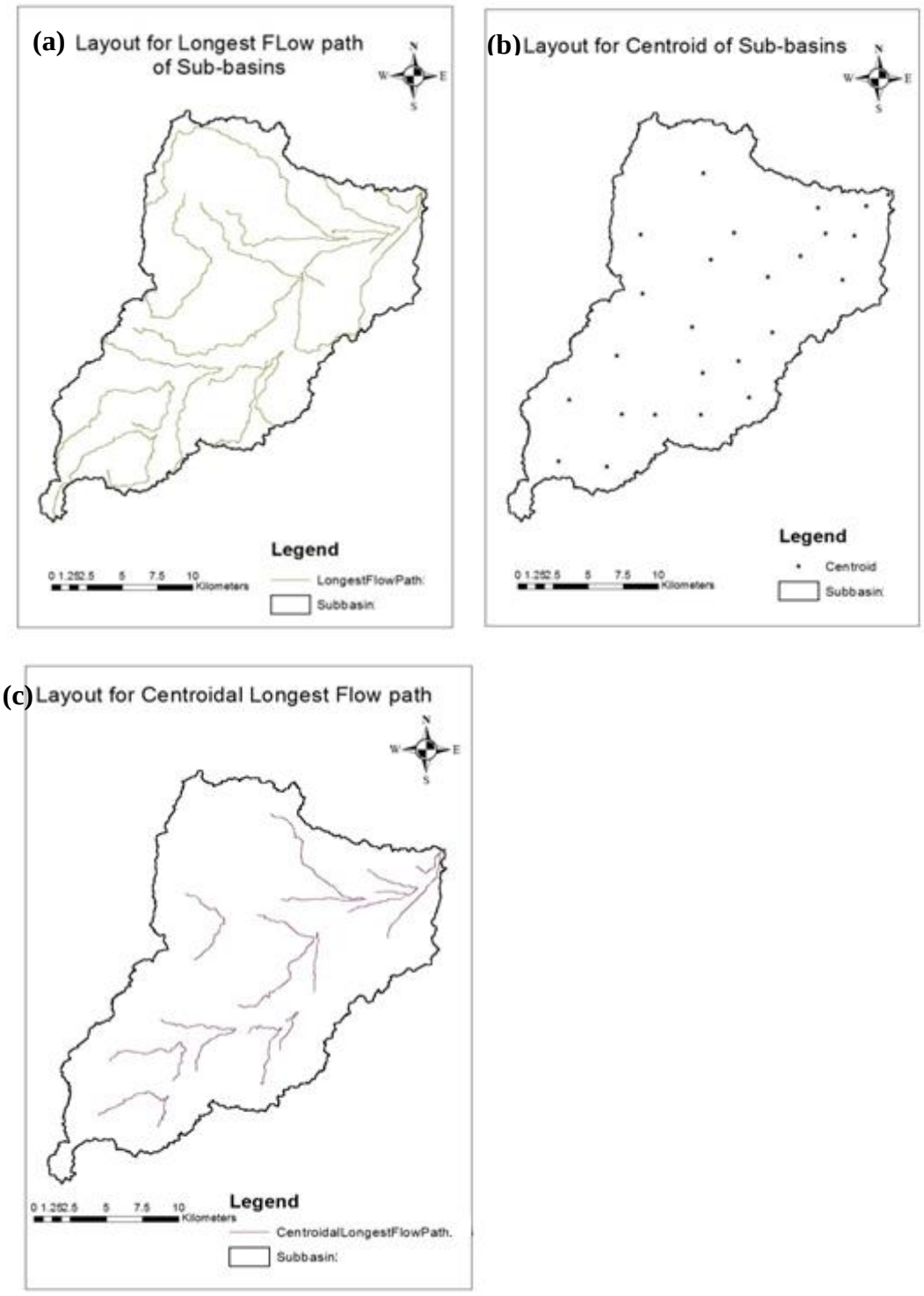

Fig 4. 31 Layout for (a) longest flow path, (b) centroid and (c) centroidal longest flow path of sub-basins

4.6.3. HEC-HMS model

HEC-HMS model with the extension HEC-GeoHMS consists of 25 sub-basins, 12 reaches and 12 junctions. The simulation is carried out for 100-year return period for 24-hrs maximum rainfall of 234 mm (Fig.4.32.)

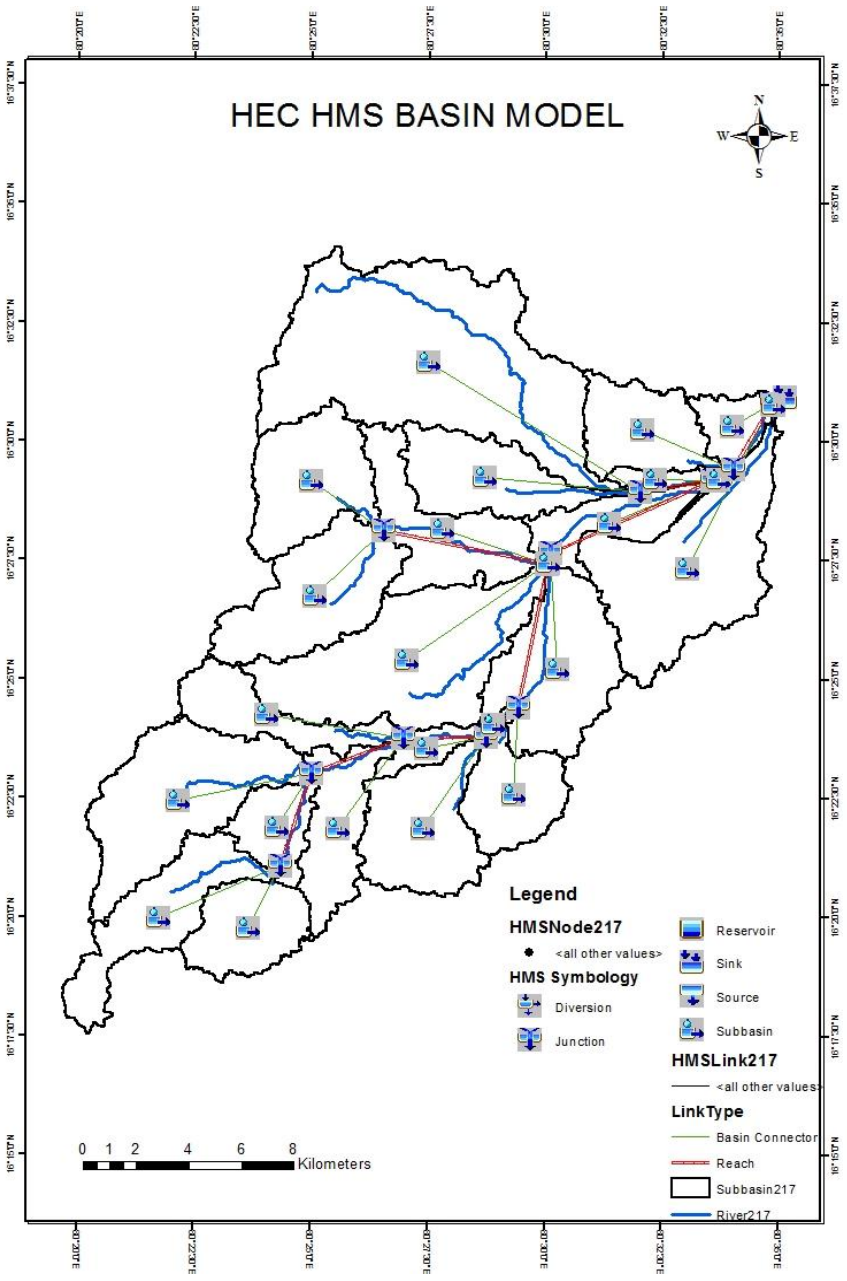

Fig 4. 32 HEC-HMS model generated in ArcMap using HEC-GeoHMS

Since Kondaveeti Vagu catchment is ungauged, no water levels or discharge measurements were available. The only calibration value available was the maximum discharge of 460 m^3/s for 100-year return period, at the confluence point of Kondaveeti Vagu with River Krishna. Manual calibration was carried out by trial-and-error method to simulate the historical flood inundation event and to get an estimate of the average Manning's n value and percent of imperviousness for the study reach. By simulation for one day maximum of 100-year return period, the peak discharge at the outlet of the Kondaveeti Vagu catchment was obtained as 460. 4 m^3/s. The hydrographs are generated at the outlet and junctions. The hydrograph showing peak flow discharge obtained from HEC-HMS is shown in Fig.4.33. These hydrographs obtained were given as input for the unsteady flow analysis by the HEC-RAS model.

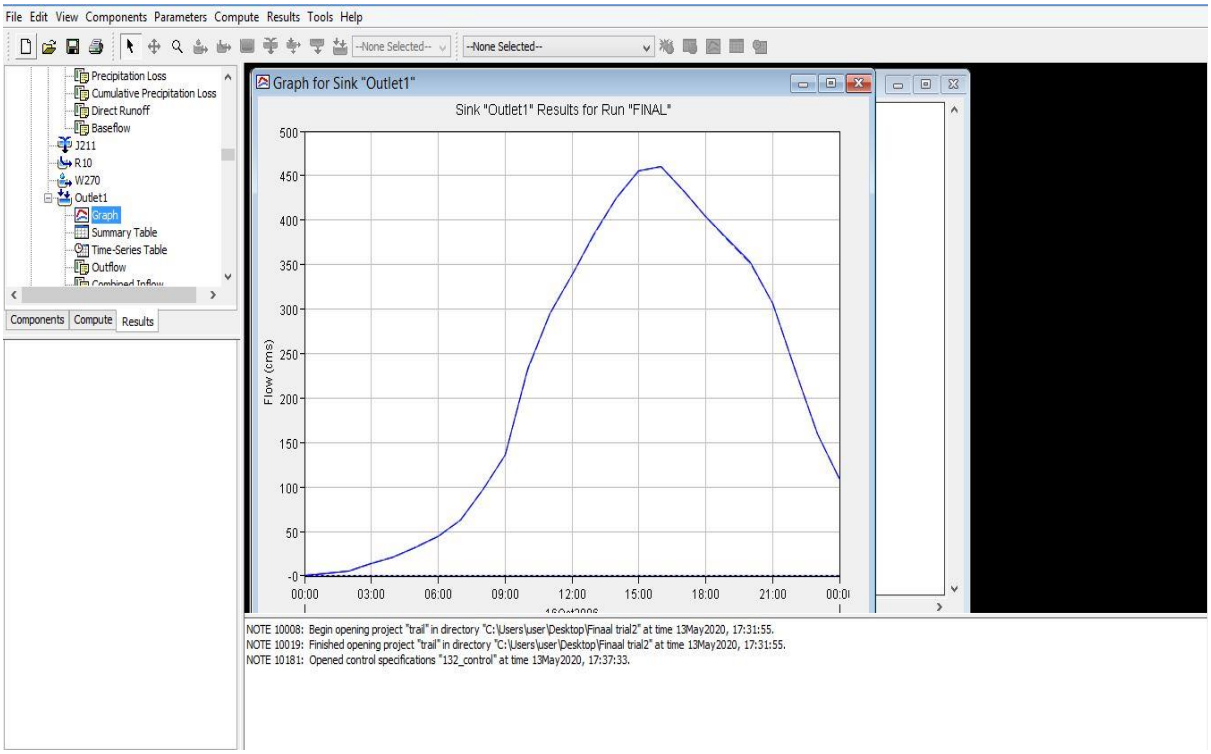

Fig 4. 33 The flow at the outlet of sub-basin for 100-year return period

Table 4.19 shows the peak discharge, time of the peak and volume at every sub-basin, junction, and reaches for the 100-year return period. Highest discharge of 460 m^3/s was observed at the Undavalli outlet. It can be seen from the results that the sub-basins like W260, W350, W370, W430 etc., lying in the upstream region had much lower peak discharge and volume compared to the sub-basins in the downstream low-lying region.

Table 4. 19 Results obtained in simulation of HEC-HMS model for 100- year return period

Hydrologic Element	Drainage area (km^2)	Peak Discharge (m^3/s)	Time of Peak
W490	18.97	21.9	16Oct2006, 15:00
W500	13.91	11.2	16Oct2006, 16:00
J158	32.89	32.7	16Oct2006, 15:00
R230	32.89	32.6	16Oct2006, 16:00
W470	31.06	36.1	16Oct2006, 15:00
W480	8.98	11.7	16Oct2006, 15:00
J163	72.94	79.4	16Oct2006, 15:00
R200	72.94	78.5	16Oct2006, 16:00
W460	14.49	15.1	16Oct2006, 15:00
W430	12.67	15.6	16Oct2006, 15:00
J168	100.10	108	16Oct2006, 15:00
R190	100.10	107	16Oct2006, 16:00
W450	20.31	23.6	16Oct2006, 15:00
W440	4.13	8.5	16Oct2006, 11:00
J171	124.56	135.8	16Oct2006, 16:00
R160	124.56	135.5	16Oct2006, 16:00
W420	13.56	15	16Oct2006, 15:00
W410	0.63	0.5	16Oct2006, 15:00
J178	138.75	150.4	16Oct2006, 16:00
R150	138.75	137.3	16Oct2006, 16:00
W370	24.15	29.3	16Oct2006, 15:00
W350	20.21	23.6	16Oct2006, 15:00
J191	44.36	52.9	16Oct2006, 15:00
R110	44.36	51.8	16Oct2006, 16:00
W400	40.05	46.1	16Oct2006, 15:00
W360	19.50	28.8	16Oct2006, 11:00
J183	103.92	124	16Oct2006, 15:00
R120	103.92	123.8	16Oct2006, 15:00
W380	0.11	0.1	16Oct2006, 15:00
W390	25.15	29.1	16Oct2006, 15:00
J186	267.95	287.5	16Oct2006, 16:00
R100	267.95	286	16Oct2006, 16:00
W260	68.18	102.8	16Oct2006, 10:00
W340	17.59	18.2	16Oct2006, 15:00
J198	85.77	108.4	16Oct2006, 10:00
R60	85.77	102.4	16Oct2006, 11:00
W330	10.63	11.7	16Oct2006, 15:00
W320	2.40	1.9	16Oct2006, 15:00
J201	366.77	395.7	16Oct2006, 16:00

R40	366.77	395.4	16Oct2006, 16:00
W300	14.77	23.3	16Oct2006, 10:00
W310	0.76	0.9	16Oct2006, 15:00
J206	382.30	413.9	16Oct2006, 16:00
R30	382.30	408.4	16Oct2006, 16:00
W290	35.26	54.4	16Oct2006, 10:00
W280	5.92	7.3	16Oct2006, 15:00
J211	423.50	459.9	16Oct2006, 16:00
R10	423.50	459.9	16Oct2006, 16:00
W270	0.45	0.7	16Oct2006, 10:00
Outlet1	423.96	460.4	16Oct2006, 16:00

4.6.3.1. Design flood discharge for different return periods

The calibrated model is simulated in HEC-HMS for the estimation of maximum flood discharge for design event return periods of 2-year, 5-year, 10-year, 50-year, and 100-year. Design storms of 84.48mm, 119.95mm, 145.25mm, 206.5mm, and 234.9mm, which were given as data input for return periods of 2-year, 5-year, 10-year, 50-year, and 100-year into Kondaveeti Vagu, the HMS model generated runoff (peak flood discharges) of 107m^3/s, 192.4 m^3/s, 238.3 m^3/s, 398.7 m^3/s, and 460 m^3/s magnitudes respectively at the Undavalli outlet. The user interface of the simulation results of 5-year, 10-year, and 50-year, which shows the peak discharges, are shown in Fig 4.34 to Fig 4.37.

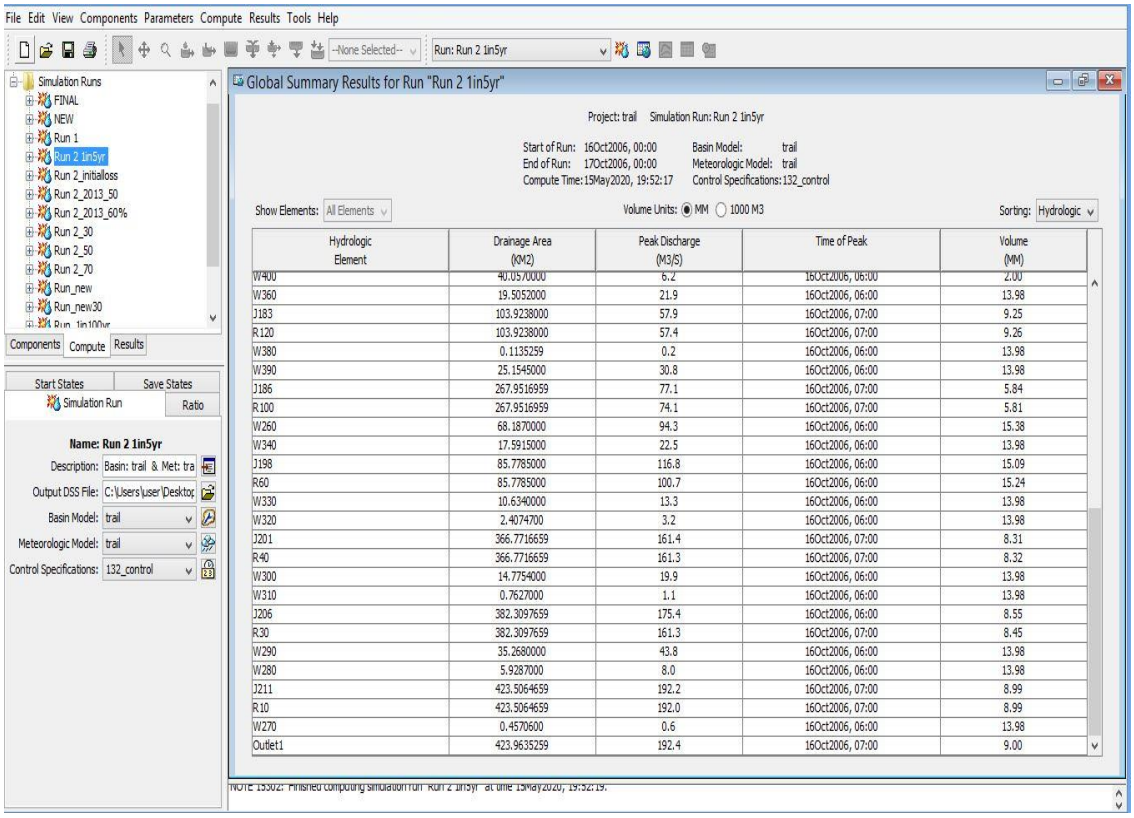

Hydrologic Element	Drainage Area (KM2)	Peak Discharge (M3/S)	Time of Peak	Volume (MM)
W400	40.0570000	6.2	16Oct2006, 06:00	2.00
W360	19.5052000	21.9	16Oct2006, 06:00	13.98
J183	103.9238000	57.9	16Oct2006, 07:00	9.25
R120	103.9238000	57.4	16Oct2006, 07:00	9.26
W380	0.1135259	0.2	16Oct2006, 06:00	13.98
W390	25.1545000	30.8	16Oct2006, 06:00	13.98
J186	267.9516959	77.1	16Oct2006, 07:00	5.84
R100	267.9516959	74.1	16Oct2006, 07:00	5.81
W260	68.1870000	94.3	16Oct2006, 06:00	15.38
W340	17.5915000	22.5	16Oct2006, 06:00	13.98
J198	85.7785000	116.8	16Oct2006, 06:00	15.09
R60	85.7785000	100.7	16Oct2006, 06:00	15.24
W330	10.6340000	13.3	16Oct2006, 06:00	13.98
W320	2.4074700	3.2	16Oct2006, 06:00	13.98
J201	366.7716659	161.4	16Oct2006, 07:00	8.31
R40	366.7716659	161.3	16Oct2006, 07:00	8.32
W300	14.7754000	19.9	16Oct2006, 06:00	13.98
W310	0.7627000	1.1	16Oct2006, 06:00	13.98
J206	382.3097659	175.4	16Oct2006, 06:00	8.55
R30	382.3097659	161.3	16Oct2006, 07:00	8.45
W290	35.2680000	43.8	16Oct2006, 06:00	13.98
W280	5.9287000	8.0	16Oct2006, 06:00	13.98
J211	423.5064659	192.2	16Oct2006, 07:00	8.99
R10	423.5064659	192.0	16Oct2006, 07:00	8.99
W270	0.4570600	0.6	16Oct2006, 06:00	13.98
Outlet1	423.9635259	192.4	16Oct2006, 07:00	9.00

Fig 4. 34 Peak discharges corresponding to 5-year return period

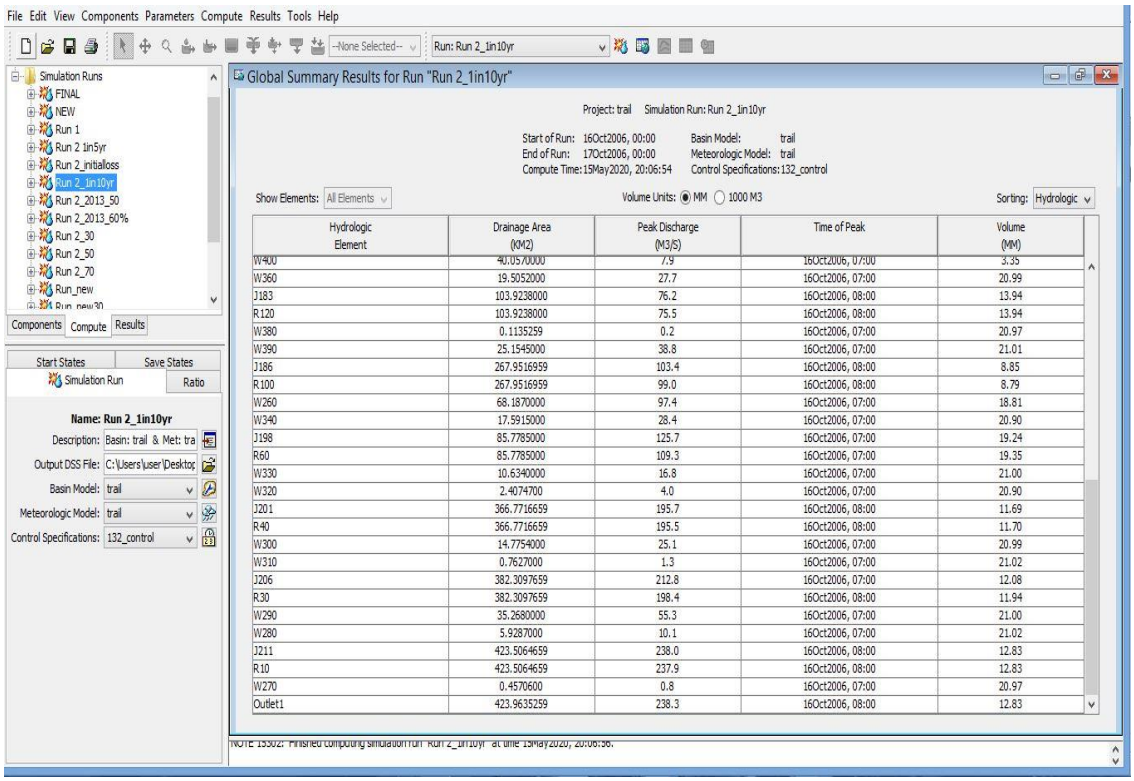

Hydrologic Element	Drainage Area (KM2)	Peak Discharge (M3/S)	Time of Peak	Volume (MM)
W400	40.0570000	7.9	16Oct2006, 07:00	3.35
W360	19.5052000	27.7	16Oct2006, 07:00	20.99
J183	103.9238000	76.2	16Oct2006, 08:00	13.94
R120	103.9238000	75.5	16Oct2006, 08:00	13.94
W380	0.1135259	0.2	16Oct2006, 07:00	20.97
W390	25.1545000	38.8	16Oct2006, 07:00	21.01
J186	267.9516959	103.4	16Oct2006, 08:00	8.85
R100	267.9516959	99.0	16Oct2006, 08:00	8.79
W260	68.1870000	97.4	16Oct2006, 07:00	18.81
W340	17.5915000	28.4	16Oct2006, 07:00	20.90
J198	85.7785000	125.7	16Oct2006, 07:00	19.24
R60	85.7785000	109.3	16Oct2006, 07:00	19.35
W330	10.6340000	16.8	16Oct2006, 07:00	21.00
W320	2.4074700	4.0	16Oct2006, 07:00	20.90
J201	366.7716659	195.7	16Oct2006, 08:00	11.69
R40	366.7716659	195.5	16Oct2006, 08:00	11.70
W300	14.7754000	25.1	16Oct2006, 07:00	20.99
W310	0.7627000	1.3	16Oct2006, 07:00	21.02
J206	382.3097659	212.8	16Oct2006, 07:00	12.08
R30	382.3097659	198.4	16Oct2006, 08:00	11.94
W290	35.2680000	55.3	16Oct2006, 07:00	21.00
W280	5.9287000	10.1	16Oct2006, 07:00	21.02
J211	423.5064659	238.0	16Oct2006, 08:00	12.83
R10	423.5064659	237.9	16Oct2006, 08:00	12.83
W270	0.4570600	0.8	16Oct2006, 07:00	20.97
Outlet1	423.9635259	238.3	16Oct2006, 08:00	12.83

Fig 4. 35 Peak discharges corresponding to 10-year return period

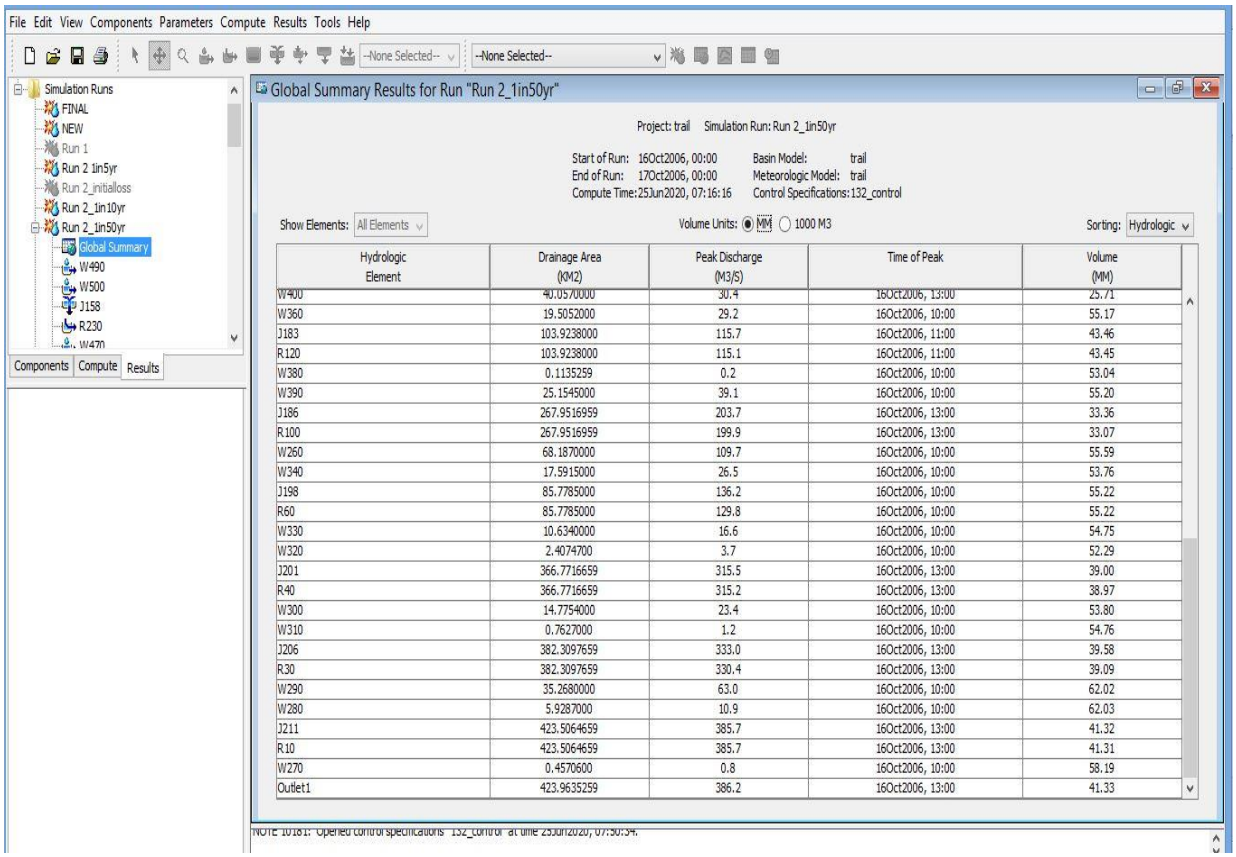

Hydrologic Element	Drainage Area (KM2)	Peak Discharge (M3/S)	Time of Peak	Volume (MM)
W400	40.0570000	30.4	16Oct2006, 13:00	25.71
W360	19.5052000	29.2	16Oct2006, 10:00	55.17
J183	103.9238000	115.7	16Oct2006, 11:00	43.46
R120	103.9238000	115.1	16Oct2006, 11:00	43.45
W380	0.1135259	0.2	16Oct2006, 10:00	53.04
W390	25.1545000	39.1	16Oct2006, 10:00	55.20
J186	267.9516959	203.7	16Oct2006, 13:00	33.36
R100	267.9516959	199.9	16Oct2006, 13:00	33.07
W260	68.1870000	109.7	16Oct2006, 10:00	55.59
W340	17.5915000	26.5	16Oct2006, 10:00	53.76
J198	85.7785000	136.2	16Oct2006, 10:00	55.22
R60	85.7785000	129.8	16Oct2006, 10:00	55.22
W330	10.6340000	16.6	16Oct2006, 10:00	54.75
W320	2.4074700	3.7	16Oct2006, 10:00	52.29
J201	366.7716659	315.5	16Oct2006, 13:00	39.00
R40	366.7716659	315.2	16Oct2006, 13:00	38.97
W300	14.7754000	23.4	16Oct2006, 10:00	53.80
W310	0.7627000	1.2	16Oct2006, 10:00	54.76
J206	382.3097659	333.0	16Oct2006, 13:00	39.58
R30	382.3097659	330.4	16Oct2006, 13:00	39.09
W290	35.2680000	63.0	16Oct2006, 10:00	62.02
W280	5.9287000	10.9	16Oct2006, 10:00	62.03
J211	423.5064659	385.7	16Oct2006, 13:00	41.32
R10	423.5064659	385.7	16Oct2006, 13:00	41.31
W270	0.4570600	0.8	16Oct2006, 10:00	58.19
Outlet1	423.9635259	386.2	16Oct2006, 13:00	41.33

Fig 4. 36 Peak discharges corresponding to 50-year return period

4.6.3.2. Sensitivity analysis of HEC-HMS model

Calibration of the hydrologic model could not be done because of the non-availability of discharge data since Kondaveeti Vagu was ungauged. The sensitivity of the HMS model for the Kondaveeti Vagu catchment was manually checked for 100-year return period by varying the percentage of imperviousness of the basin. As the Amaravati region is still under development, it is assumed that around 60% of the city will be paved surfaces. The imperviousness of the sub-basins in the capital city region was varied by 10% to determine the variation of the discharge at the outlet. HEC-HMS model gave different design event flood discharges for different percentages of imperviousness as given in Table 4.20. With the increment of the percentage of imperviousness by 10%, an increase of 3 to 6 % in the flood discharge values were observed. Amaravati is subjected to rapid developments leading to more impervious cover which will be adding to the existing flooding problems.

Table 4. 20 Design flood discharge corresponding to different percentage of imperviousness

Imperviousness of sub-catchments (%)	Design event flood discharge (m^3/s)
50	443.9
60	460.4
70	487.1

4.6.4. Flood inundation modelling

4.6.4.1. HEC-RAS model

Hydraulic modelling was performed using HEC-RAS software. For the Amaravati region, the simulation was carried out with the 100-year rainfall of 230mm. The hydrographs generated in HEC-HMS for different junctions and the outlet were given as the input for the unsteady flow data of reservoirs and flow area. The upstream and downstream boundary conditions are defined for the region. The simulation was run for every hour. Fig. 4.37 shows the flood inundation in the Amaravati region at three different times of the simulation.

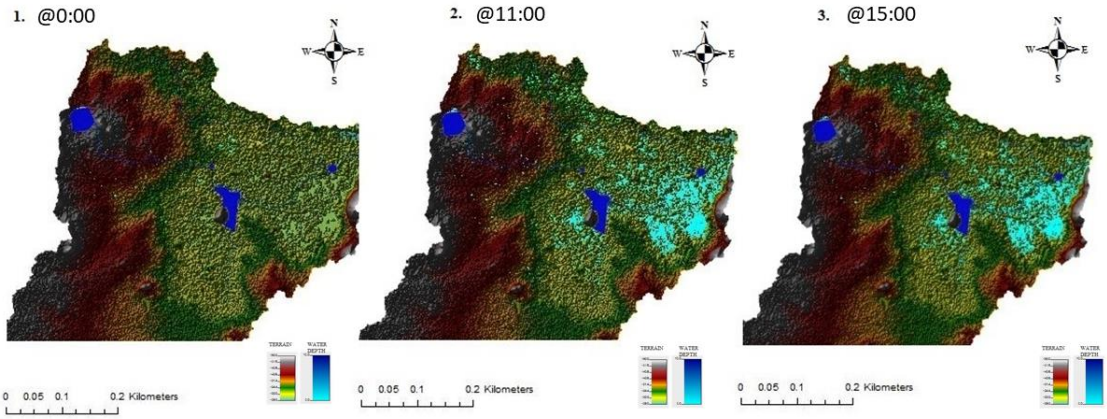

Fig 4. 37 Flood inundation at different times for 24 hour maximum 100-year rainfall

Low-lying areas like Undavalli, Krishnayapalem, Mangalagiri, Dolas Nagar and Nalakapeta are mostly inundated. Some regions around Neerukonda reservoir, inundated including the Thullur regio, are also inundated. For the extreme rainfall event, even the regions near Vaddamanu and Anathavaram, which are the high elevation regions, showed patches of

water, giving the caution that not only the low-lying areas but also the higher elevation regions are also susceptible for flooding.

4.6.4.2. Simulation for past rainfall event

The HEC-RAS model developed for the Kondaveeti Vagu catchment was used for simulating the data of the past flood event that occurred in 2013. The accumulated five-day maximum rainfall event was 321mm. The regions which were mostly inundated were the low-lying regions like Undavalli, Krishnayapalem, Mangalagiri, Dolas Nagar, Nalakapeta and Malkapuram. Water was seen accumulating in Thullur region which is at the upstream of the Kondaveeti Vagu. Flood inundation map is exported to ArcGIS and the area of inundation was found out to be 54.24 sq km. Fig 4.38 shows the maximum extent of flood inundation for past 5-day maximum rainfall event.

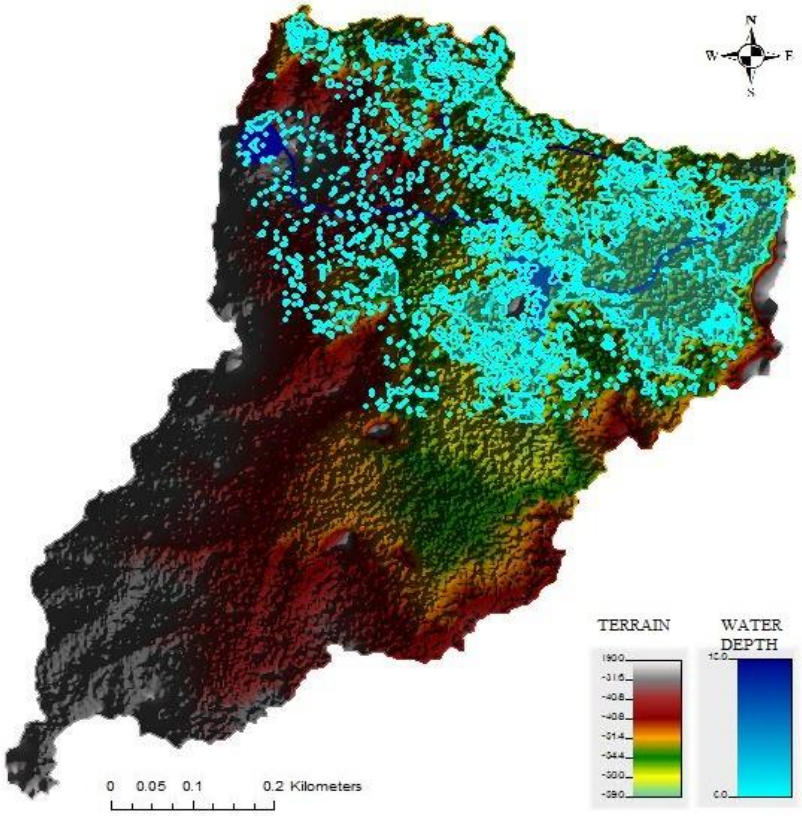

Fig 4. 38 Maximum extent of flood inundation for past 5-day maximum rainfall event

4.7. Bias Correction

Bias correction was carried out for the nine grid points in and around the study area for monthly average and maximum rainfall time series of RCM dataset. Qmap.P, Qmap.S, CDF and linear scaling transformation are used for the bias correction. Standard error, mean absolute error, root mean square error and mean square error were calculated for each grid point of all the six bias corrected RCMs. As the methodology applied to all RCMs were similar, as an example, results from the CNRM-CM5 RCM dataset are only explained further.

Standard error and mean square error (MSE) calculated for the bias-corrected results using Qmap.P, Qmap.S, CDF and linear scaling transformation for average and maximum monthly series are shown in Table 4.21. Highest standard error for monthly average series using these methods were 0.44, 0.62, 0.71 and 1.52 respectively. Correspondingly, the maximum MSE values for monthly average series are respectively 9.09, 12.87, 13.61 and 31.54. The lowest values in standard errors calculated for monthly average series are 0.32, 0.43, 0.43 and 0.72 respectively, while the lowest MSE values for monthly average series are 6.60, 8.89, 8.83 and 41.97 respectively. It is evident from the analysis that the linear scaling technique showed higher values of error compared to the other three methods and hence it can be concluded that this method is not efficient for correcting bias. Similarly, for maximum monthly series the standard error and MSE obtained for Qmap.P, Qmap.S and CDF methods had error values much higher when compared to average monthly series. The highest MSE value for average monthly series was obtained as 31.54 using linear scaling method, whereas the lowest MSE value was 6.60 using Qmap.P transformation. Standard error and MSE were very high for the monthly maximum series, which show that bias correction techniques are poor for the extreme events.

Fig 4.39 shows the mean absolute error (MAE) calculated for the bias-corrected results using the four methods for average monthly series for nine grid points. Root mean square error (RMSE) calculated for the bias-corrected results using these methods for average and maximum monthly series of nine grid points are shown in Fig 4.40. Higher MAE and RMSE values were present in the linear scaling transformation method, which show the inability of linear scaling approach in correcting the bias compared to Qmap.P, Qmap.S transformation and CDF. Out of these four methods, Qmap.P gave the least MAE and RMSE, and hence it is the best among the four methods for bias correction.

The bias correction methods are spatially independent, since the error in each grid points vary. Due to higher error values for the monthly maximum bias corrected series, bias correction methods are inadequate in preserving the extremes.

Table 4. 21 Standard error (SE) and mean square error (MSE) for the bias-corrected results using Qmap.P, Qmap.S transformation, CDF and linear transformation for average and maximum monthly series

Error	Grid	For average monthly series				For maximum monthly series		
		Qmap.P	Qmap.S	CDF	Linear scaling	Qmap.P	Qmap.S	CDF
SE	1	0.42	0.43	0.44	0.98	66.91	85.00	90.37
	2	0.44	0.50	0.51	1.08	47.17	58.92	61.04
	3	0.37	0.53	0.54	1.52	67.84	83.58	120.23
	4	0.44	0.46	0.48	0.82	60.08	79.51	83.36
	5	0.36	0.44	0.43	1.10	51.03	69.89	62.97
	6	0.42	0.62	0.71	1.49	61.71	75.80	112.59
	7	0.37	0.44	0.47	0.72	71.98	106.99	135.79
	8	0.32	0.43	0.43	0.89	25.86	42.67	42.85
	9	0.42	0.61	0.59	1.29	42.55	59.97	61.67
MSE	1	8.68	8.96	9.09	20.36	1387.62	1762.68	1873.95
	2	9.06	10.29	10.64	22.40	978.14	1221.76	1265.70
	3	7.61	10.96	11.26	31.54	1406.84	1733.13	2493.14
	4	9.09	9.55	9.88	17.01	1245.91	1648.78	1728.55
	5	7.47	9.08	8.91	22.88	1058.33	1449.20	1305.73
	6	8.81	12.87	13.61	30.99	1279.79	1571.79	2334.71
	7	7.75	9.05	9.66	14.97	1492.66	2218.61	2815.79
	8	6.60	8.89	8.83	18.42	536.292	884.78	888.64
	9	8.76	12.63	12.13	26.72	882.438	1243.55	1278.75

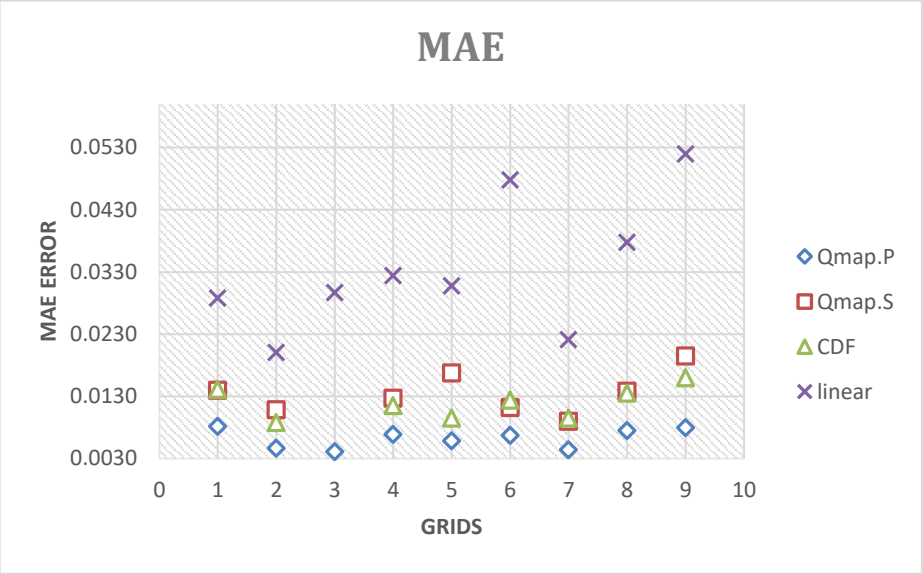

Fig 4. 39 Mean absolute error (MAE) for the bias-corrected result using Qmap.P, Qmap.S transformation, CDF transformation and linear transformation for average monthly series for nine grid points

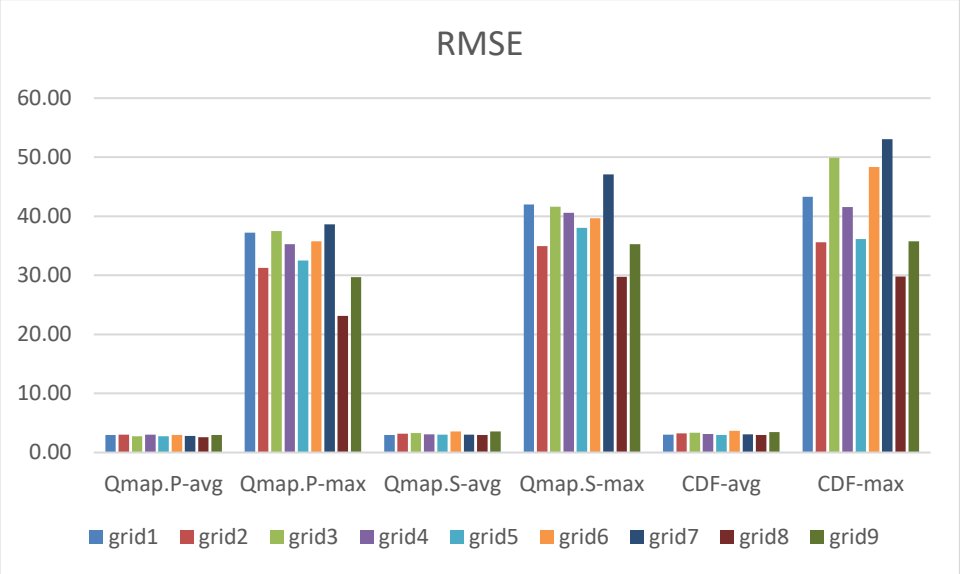

Fig 4. 40 Root mean square error (RMSE) for the bias-corrected result using Qmap.P, Qmap.S transformation, CDF transformation for average and maximum monthly series of nine grid points

4.8. Climate Change Impact on Urban Flood

Bias corrected RCM was used for the analysis of climate change impact. Ensemble of climate models was made after bias correction. RCM ensemble was done for the six RCM models with 2 different parameters using multi-model mean method. Historic (1970 – 2005), RCP 4.5 future 1 (2014-2056), RCP 4.5 future 2 (2057-2099), RCP 8.5 future 1 (2014-2056) and RCP 8.5 future 2 (2057-2099) are the ensemble RCM time series. Rainfall depths for different return periods using GEV for historic data (RCM), RCP 4.5 future 1, RCP 4.5 future 2, RCP 8.5 future 1 and RCP 8.5 future 2 were calculated for different probability of exceedance (P) and shown in Table 4.22. Peak discharges were calculated for the rainfall corresponding to the four scenarios and shown in Table 4.23. HEC-HMS model was used for the calculation of peak discharge for different return periods. Peak discharges for different return periods are shown in the Fig. 4.41. It was found that RCP 8.5 future 1 shows maximum peak discharge.

Table 4. 22 Rainfall depth for different return periods using GEV for historic data (RCM), RCP 4.5future 1, RCP 4.5future 2, RCP 8.5 future 1 and RCP 8.5 future 2

Return Period (Years)	P	Rainfall depth Xt (mm) for historic data (RCM)	Rainfall depth Xt (mm) for RCP 4.5future 1	Rainfall depth Xt (mm) for RCP 4.5future 2	Rainfall depth Xt (mm) for RCP 8.5 future 1	Rainfall depth Xt (mm) for RCP 8.5 future 2
2	0.50	30.142	25.7	28.2	34.5	33.4
5	0.80	37.114	36.5	40.2	50.5	49.0
10	0.90	40.99	45.3	50.8	63.0	60.6
20	0.95	44.236	55.0	63.4	76.5	72.8

Table 4. 23 Peak discharge for different return periods for historic data (RCM), RCP 4.5future 1, RCP 4.5future 2, RCP 8.5 future 1 and RCP 8.5 future 2

Return Period (Years)	Peak Discharge (m^3/s) for historic data (RCM)	Peak Discharge (m^3/s) for RCP 4.5future 1	Peak Discharge (m^3/s) for RCP 4.5future 2	Peak Discharge (m^3/s) for RCP 8.5 future 1	Peak Discharge (m^3/s) for RCP 8.5 future 2
2	129.9	109.4	120.7	150.6	145.4
5	161.5	158.7	176.1	231.0	223.0
10	180.0	201.5	232.5	315.9	298.7
20	197.0	260.5	319.0	431.0	396.2

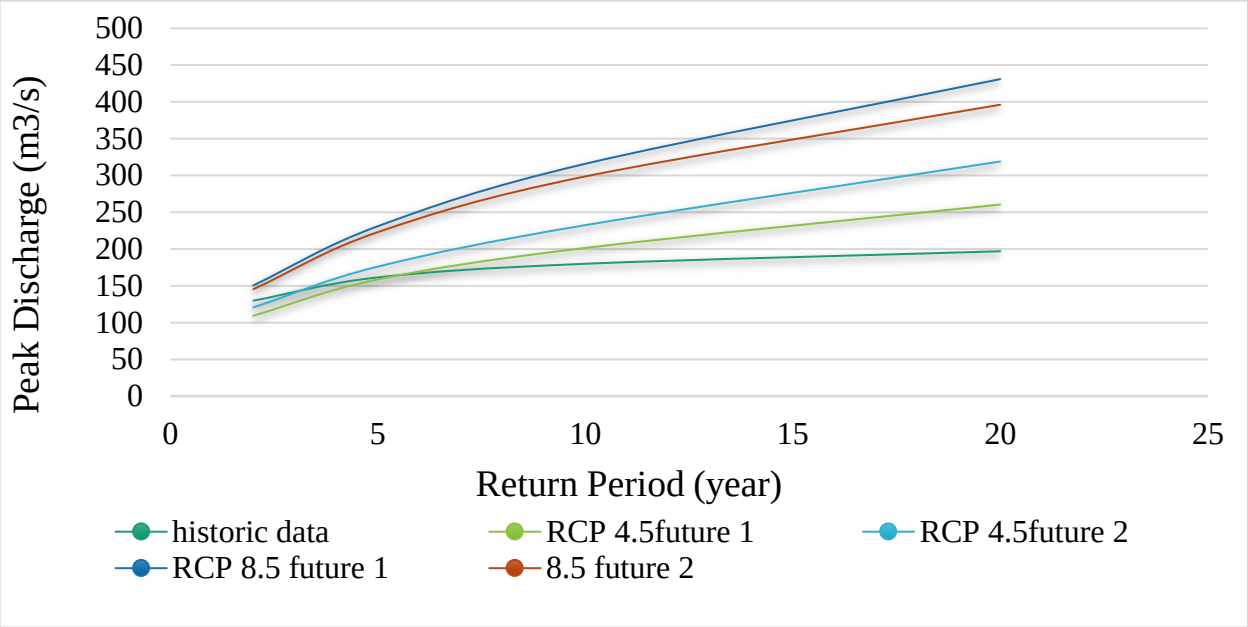

Fig 4. 41 Peak discharge for different return periods

4.9. Urban Flood Mitigation (BMP)

SWMM V5.1 was used to design the different LID scenarios. Biological BMPs, Structural BMPs and Combination of biological and structural BMPs were the three scenarios considered. Biological BMPs are Bioretention, Rain Garden and Grass swale. Structural BMPs considered are permeable pavement, infiltration trench and rain barrel. The introduction of different LID units is expected to improve the infiltration capability of the selected area by reducing the surface runoff. The SWMM model was set up using the input data collected from APCRDA and the use of ArcGIS. 25 sub-basins were obtained after the delineation of the Kondaveeti Vagu watershed. The longest flow path in the sub-basins, centroid for the sub-catchments, and centroidal longest flow path for each sub-basin have already been calculated.

As already mentioned, the Kondaveeti Vagu catchment is ungauged, and the maximum discharge of 460 m^3/s for 100-years return period, at the confluence point of Kondaveeti Vagu with River Krishna was available from records. Initially, the model is simulated for 100-year return period for 24-hour maximum rainfall of 234 mm. The simulation for one day maximum of 100-year return period, the peak discharge at the outlet of the Kondaveeti Vagu catchment is obtained as 459. 6 m^3/s. Simulation process displayed the continuity errors for runoff and flow routing, which show the net flow (outflow-inflow) for the entire drainage system. If the continuity error is more than 10%, the input parameters need to be changed. Too

long computational steps or too short conduits cause excess continuity error. In this study, continuity error obtained was less than 10%.

The SWMM model was developed for the study area as shown in Fig. 4.42. Flow in the channels is dependent on its slope and dimensions. Runoff hydrographs for sub-catchments were calculated. The peak discharges were determined at the outlet of each of the sub-catchment and it was found that the maximum peak runoff was observed at the outlet of sub-catchment S1.

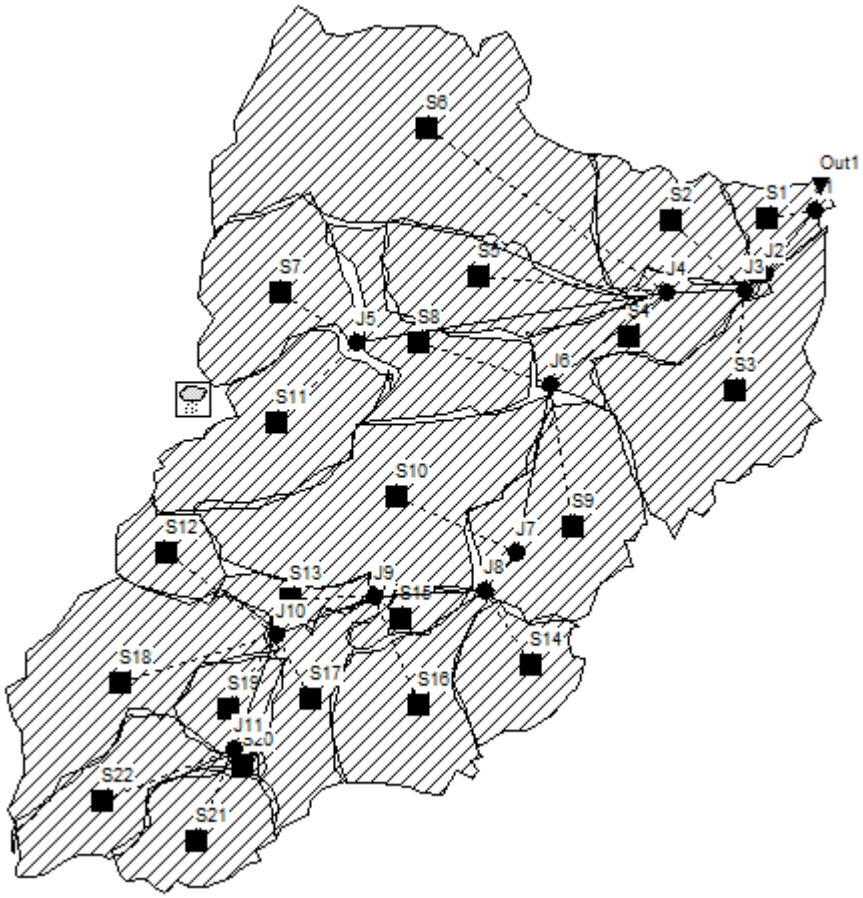

Fig 4. 42 SWMM model for Kondaveeti Vagu catchment

From the results from SWMM, it can be seen that, similar to the HEC-HMS results, the low-lying areas like Undavalli, Krishnayapalem, Mangalagiri, Dolas Nagar and Nalakapeta were inundated. Some regions around Neerukonda reservoir were also inundated

including the Thullur region. In the extreme rainfall event, even the regions near Vaddamanu and Anathavaram, which are the high elevation regions, showed patches of water.

This study mainly concentrated on the results of flood control measures using LID techniques in the urbanising area of the Amaravati region. Specifically, the effect of six LID types and their combinations are simulated for a 10-year return period rainfall. The effects on peak runoff for different LID approaches are shown in Table 4.24 to Table 4. 26.

Table 4. 24 Comparison of runoff (m^3/s) of biological BMPs

Sub-catchment	No LID (m^3/s)	Bioretention (m^3/s)	% reduction	Rain garden (m^3/s)	% reduction	Grass swale (m^3/s)	% reduction
S16	12.6	11.9	5.56	12.1	3.97	11.5	8.73
S14	10.1	8.9	11.88	9.5	5.94	9.3	7.92
S10	7.9	7.3	7.59	7.5	5.06	7.2	8.86
S6	28.7	27.1	5.57	26.7	6.97	27.2	5.23
S2	23.4	22.8	2.56	23.1	1.28	22.7	2.99

Table 4. 25 Comparison of runoff (m^3/s) of structural BMPs

Sub-catchment	No LID (m^3/s)	Permeable pavement (m^3/s)	% reduction	Infiltration trench (m^3/s)	% reduction	Rain barrel (m^3/s)	% reduction
S16	12.6	12.4	1.59	12.0	4.76	11.7	7.14
S14	10.1	9.6	4.95	9.4	6.93	9.8	2.97
S10	7.9	7.6	3.80	7.5	5.06	7.8	1.27
S6	28.7	27.3	4.88	27.4	4.53	27.8	3.14
S2	23.4	22.8	2.56	23.2	0.85	22.9	2.14

Table 4. 26 Comparison of runoff (m^3/s) of combined BMP

Sub-catchment	No LID (m^3/s)	Combination (m^3/s)	% reduction
S16	12.6	11.8	6.35
S14	10.1	9.1	9.90
S10	7.9	7.2	8.86
S6	28.7	26.9	6.27
S2	23.4	22.5	3.85

It can be observed that the sub-catchment S14 has the highest percentage reduction in peak runoff (11.88%) using bioretention structures. Grass swales have the best controlling and reducing potential to reduce the runoff volume for S16 (8.73%), S10 (8.86%), and S2 (3.85%).

S2 has the lowest effect on peak runoff using infiltration trench. Based on the results obtained, it can be concluded that the performance and potential of biological BMPs are higher in controlling and reducing the runoff volume comparing to those of structural BMPs. Biological BMPs are environmental friendly and cost effective.

CHAPTER 5

SUMMARY AND CONCLUSIONS

5.1. Summary

Flood is one of the severe natural disasters, which causes huge damage annually including loss of human lives. Studies on urban flooding show that the effects of urban flooding are intensifying as a result of anthropogenic activities as well as climate change impacts. With the expansion in urbanization, people are relocating to the urban areas at a very rapid rate. There is an increase in impervious and impenetrable surface due to the infrastructure development to cater to the needs of the dense urban population. Assessment of the change in flood characteristics under the context of climate change plays a significant role in managing the flood risk. Identifying the vulnerable areas associated with the projected changes in climate allows the local authorities to plan for the future development. This study, therefore, focusses on the impact of climate change on flood and the mitigation of flood in urbanizing area.

Amaravati city, in the state of Andhra Pradesh, is under rapid development with increased impervious surfaces due to the construction of infrastructure like new buildings, roads, path walks, parking lots, etc. Kondaveeti Vagu and Pala Vagu, both flowing through the city, have seasonal flood extremities every year. Low lying areas are inundated even in a matter of a few hours during extreme rainfall events. Thus, the study and modelling of the flood are required for the proper management to reduce the losses as much possible. The relief from flood risks can be effectively provided when detailed information are obtained about the frequency, character, and magnitude of the flood in the area.

The maximum of monthly, seasonal and annual trends for rainfall are obtained using MK1, MK2 and ITA techniques and the trend magnitudes are calculated using Sen's slope estimator for 15 grid points in the study area. Using the Kolmogorov–Smirnov test, the normality of maximum monthly and seasonal rainfall data series was checked for the entire study period. None of the rainfall series used in this study was following a normal distribution. Results of the MK1, MK2 and Sen's slope approaches are presented for the 15 grid points.

ITA technique was employed for annual and seasonal rainfall for the period 1961-2018. Trend detection using the ITA technique was carried out, without any assumptions, to get the sub-series of the dataset. Results from the ITA technique are compared with those obtained from MK1 and MK2 tests. Results for monthly maximum trends for rainfall and comparison of seasonal and annual trends are presented.

The Z statistics of monthly maximum rainfall data obtained from MK1 and MK2 were calculated. Out of 180 cases, 21 cases (11.6%) displayed significant positive trends in MK1 while 22 cases (12%) displayed significant positive trends in MK2 considering the three significant levels. In this study, no significant negative trends were observed for monthly maximum rainfall. For MK1 test, positive significant trends were detected for the months of January, February, May, August and November, whereas for MK2 test, most of the positive trends were observed in the months of May, August, November and December. Compared to MK1 test, MK2 test exhibited similar significant positive trends. From MK1 and MK2 tests, more significant positive trends were seen in the month of May followed by the months of August and November.

Rainfall trend showed large variability in ITA technique compared to other two trend tests (MK1 and MK2) considered in the study. For annual series, using MK1 and MK2 tests, trends were detected only for grid point G8, whereas, in the case of ITA technique, trends were detected for all the grid points. ITA technique will not consider any prior conditions like that of MK tests, due to which, the graphical ITA technique is more appropriate in detecting monotonic and non-monotonic trends.

In pre-monsoon season, similar trends were detected by both MK1and MK2 tests compared to ITA technique. But, for the ITA technique, all trends were limited to only the low phase. In the monsoon season, no trends were noticed for MK1 and MK2 whereas, by ITA techniques, increasing trends were observed at G4, G7, G8, G13 and G14. During the post-monsoon season, no trends were detected for all grid points using MK1 and MK2, while increasing trends were observed for G4, G13 and G14 by ITA technique. In the winter season, positive trends were detected for all the 15 grid points using MK1 and MK2 tests, whereas positive trends were noticed for all 15 grid points in low phase using ITA technique. ITA technique, thus, showed a tendency to detect more trends compared to MK1 and MK2 tests.

The study of stationarity of annual average precipitation series was carried out using ADF, PP and KPSS tests for the 17-gauge stations. The null hypothesis (H0) was considered

for the study, when the confidence level is lower than the P-value. PP and ADF tests showed non-stationarity in the time-series when the test showed null hypothesis H0, while the KPSS test showed stationarity in the time-series data for null hypothesis H0. A confidence level of 0.05 was considered for the stationarity test in this study. Dickey-Fuller test and Phillips-Perron test showed stationarity for all the gauged stations except for Penamaluru corresponding to the maximum P-value of 0.07 whereas the other stations showed relatively lower P-values. KPSS test showed non-stationarity at Amaravati, Thullur, Pedakurapadu and Vijayawada Urban gauging stations having the P-value as 0.002, 0.015, 0.023 and 0.002 respectively. Rest of the stations showed stationarity by KPSS test, the P-value ranging from 0.055 to 0.94 corresponding to Penamaluru and Tadikonda stations respectively.

In SNHT, Pettit's and Buishand's tests, the year of the change points for the annual average precipitation time-series was obtained. The von Neumann's test only identified the presence of the change point. Pettit's test showed that the annual average precipitation series were homogeneous for all the gauge stations whereas heterogeneity for annual average precipitation series was observed by SNHT, Buishand's and von Neumann's tests. The year 2004 can be recognised as the year having the greatest number of change points. In SNHT test, the change points were identified in the year 2007 and 2009 at Vijayawada Urban and Pedakurapadu. Similarly, in Buishand's test, the change points were observed in the year 2004 at two stations, namely, Amravati and Vijayawada Urban and in the year 2009, non-homogeneity was observed at Pedakurapadu. Data at Amravati and Penamaluru showed non-homogeneity while performing von Neumann's test. Two rain gauge stations, i.e., Vijayawada Urban and Pedakurapadu showed non-homogeneity by SNHT and Buishand's test. Buishand's test and von Neumann's test showed heterogeneity in Amaravati station.

The comparison of the accuracy of Landsat 8 OLI and Sentinel 2 data, using the error matrix or confusion matrix, was done for the year 2018. For Landsat and Sentinel data, average user's accuracy, average producer's accuracy and the kappa coefficient were computed. Comparison of these two data showed that Sentinel 2 had higher accuracy than Landsat 8.

The trend of different indices was calculated for Landsat 8 and Sentinel 2. The trend of indices in Sentinel showed inconsistency of data. No conclusions could be arrived at from this. If the NDVI decreases, it can be assumed that the construction activities have resulted in decrease in vegetation. If the NDVI increases, it can be assumed that plantation was being done in the area. But that is not the case in the study area. This inaccuracy might be due to the

reason that the data had not undergone atmospheric correction. Moreover, Sentinel data does not have Thermal infrared band which makes it impossible to compute NDISI.

Land cover in the study area had changed significantly between the years 2016 and 2019. This is due to the fact that a new capital city was being constructed, converting most of the cropland into urban and barren land. Landsat 5 TM data was used for the years 1990, 2000, and 2010, Landsat 8 data for the period 2013 – 2016; and Sentinel 2 data for the period 2016 – 2019. Sentinel data was used due to its high resolution of 10m. The areas under different classes were computed using supervised classification.

The built-up area increased significantly between the years 2016 and 2019. The increased built-up area was historically cropland. Significant decrease in cropland and increase in barren land were noticed during the period from 1990 to 2019, while the vegetation area did not show much changes during this period. Though the study area is located on the banks of Krishna River, it does not include any part of it. Artificial canals that were built to divert the river water into the new capital region, were not detected by the satellites since the data were for the months April and May. Since Krishna Ris a seasonal river, the canals might be dry during these months.

Frequency analysis was carried out for the rainfall data for the period from 1961 to 2018. The addition of the rankings of Kolmogorov Smirnov, Anderson Darling and Chi-Squared was done to find the least sum, considering the rainfall series follow the GEV distribution which was found as a good fit. The rainfall depths for different return periods using GEV were calculated. For a 100-year return period, the rainfall depth worked out to be around 240mm.

Kondaveeti Vagu catchment being ungauged, no water levels or discharge measurements were available. The only calibration value available was a maximum discharge of 460 m^3/sec for a return period of 100 years at the confluence point of Kondaveeti Vagu with River Krishna. Manual calibration was carried out by trial-and-error method to simulate the historical flood inundation event and to get an estimate of the average Manning's n value and percentage of imperviousness for the study reach.

As the Amaravati region is still under development, it is assumed that around 60% of the city will be paved surfaces. The imperviousness of the sub-basins in the capital city region was varied in steps of 10% to determine the variation of the discharge at the outlet. HEC-HMS model gave different design flood discharges for different percentage of imperviousness. With

every increment of 10% in imperviousness, the increase in flood discharges was found to be in the range of 3% to 6 %.

Hydraulic modelling was performed using HEC-RAS software. For the Amaravati region, the simulation is carried out for the 100-year rainfall of 230mm. The hydrographs generated in HEC-HMS for different junctions and the outlet were given as the input for the unsteady flow data of reservoirs and flow area. The upstream and downstream boundary conditions were defined for the region and hourly simulation was run.

Mostly, the low-lying areas like Undavalli, Krishnayapalem, Mangalagiri, Dolas Nagar and Nalakapeta were inundated. Some regions around Neerukonda reservoir, including the Thullur region, were also inundated. For the extreme rainfall event, even the regions near Vaddamanu and Anathavaram which are the high elevation regions showed patches of water, giving the caution that not only the low-lying areas but also the higher elevation regions were susceptible for flooding.

The HEC-RAS model developed for the Kondaveeti Vagu catchment was simulated for the past flood event that occurred in 2013. The accumulated five-day maximum rainfall was computed to be 321mm. The regions in the catchment which were inundated were the low-lying region like Undavalli, Krishnayapalem, Mangalagiri, Dolas Nagar, Nalakapeta and Malkapuram. Water was seen accumulated in Thullur region which is at the upstream of the Kondaveeti Vagu. Flood inundation map was exported to ArcGIS, from which, the area of inundation was found out to be 54.24 km^2.

RCMs show critical biases in precipitation and therefore, it is mandatory that bias correction is to be carried out so that they can be used for further research. Six RCMs were considered in this study. Bias correction techniques were applied to reduce the errors in RCMs. Four statistical bias correction techniques, namely, linear scaling, cumulative distributive transformation, quantile mapping using parametric transformation and quantile mapping using smooth spline methods were used. The bias corrected datasets were compared with observed datasets using different relative errors, viz., standard error, mean absolute error, root mean square error and mean square error. Relative errors compare the simulated data with observed data.

The results showed that quantile mapping using parametric transformation technique gave minimum error compared to the other three methods. As the linear scaling method was designed only to correct the mean, its bias correction results are very poor and not satisfactory.

The most effective bias correction method was the quantile mapping using parametric transformation method, which integrates information frequency distribution for the observed and modelled precipitations. It was found that the efficiency of bias correction depended on the spatial variations since the error was varying at each grid point.

RCM ensemble was done for the six RCM models with 2 different parameters using multi-model mean method. Historic (1970 – 2005), RCP 4.5 future 1 (2014-2056), RCP 4.5 future 2 (2057-2099), RCP 8.5 future 1 (2014-2056) and RCP 8.5 future 2 (2057-2099) are the ensemble RCM time series. Rainfall depths for different return periods using GEV for historic data (RCM), RCP 4.5future 1, RCP 4.5future 2, RCP 8.5 future 1 and RCP 8.5 future 2 were calculated. For the respective rainfall depth, peak discharges were calculated and it was found that RCP 8.5 future 1 showed maximum peak discharge.

Low Impact Development (LID) is a stormwater management strategy that seeks to mitigate the impacts of increased runoff and stormwater pollution by managing runoff as close to its source as possible. LID comprises a set of site design strategies that minimises runoff. LIDs are small scale structural practices that mimic natural or predevelopment hydrology through the processes of infiltration, evapotranspiration, harvesting, filtration and detention of stormwater. These practices can effectively reduce the volume and rate of stormwater flows. Various LID controls are available for implementation. Each LID control, with their respective level of implementation, creates different scenarios.

Three LID scenarios were considered for the study, biological BMPs, structural BMPs and combination of biological and structural BMPs. Biological BMPs are Bioretention, Rain Garden and Grass swale. Structural BMPs are Permeable pavement, Infiltration trench and Rain barrel. The three scenarios are simulated for 5-year return period in five sub-catchments for 50% of the catchment area. Based on the results obtained, it was observed that the performance and potential of biological BMPs were higher in controlling and reducing the runoff volume compared to those of structural BMPs.

5.2 Conclusion

The research reported in this thesis contributes towards assessing the impact of climate change on urban flood and flood inundation model for the study area with mitigation measures using Best Management Practices. The conclusions from the study are:

- Parametric linear regression analysis of annual precipitation displayed a positive trend in 53% of the stations and at 30% of the stations, a negative trend was observed. From

the analysis of extreme monthly rainfall using Sen's slope, it was observed that Sen's slope had the lowest magnitude in October i.e., nearly -0.08 mm/year whereas the highest magnitude occurred in May (nearly 0.17 mm/year). MK2 test exhibited similar significant positive trends compared to MK1 for extreme monthly rainfall. For MK1 and MK2 tests, the extreme rainfall during the winter seasons exhibited significant positive trends for the 15 grids.

- Pettitt's test showed homogeneity in the annual precipitation series at all the stations. SNHT and Buishand's tests showed heterogeneity at Pedakurapadu and Vijayawada Urban stations. Change points were observed more frequently in 2004. von Neumann's test showed heterogeneity at Amaravati and Penamaluru. ADF test and PP test showed stationarity at 90% of annual precipitation. 76% of annual time-series showed stationarity using the KPSS test.
- It is observed that ITA technique detected trend better than MK tests. The graphical representation is a novelty as it shows hidden sub-trends of the dataset series. The ITA technique overcomes the assumptions of dependency of the dataset, distribution normality and dataset length.
- The construction activities in Amaravati has made sharp changes in the land cover and land use. The built-up area (urban) increased from 3.41% to 25.2%, most of which happened between 2016 to 2019. The increase in the values of indices, viz NDVI, MNDWI, NDISI and NDBI, in the year 2019 may be due to the creation of Environmental Management Regulatory Authority (EMRA), for the plantation works, which fucussed on increasing the vegetation.
- Frequently inundated regions in the Amaravati city, even with the heavy rainfall for small durations, are the low-lying areas, viz., Undavalli, Krishnayapalem, Mangalagiri, Dolas Nagar, Nalakapeta and Malkapuram. For heavy rainfall events, water fills can be noticed in the upstream region of the study and in the regions around Ananthavaram reservoir. The flood inundation maps developed can be used for the planning and management of an early warning system and public awareness.
- Quantile mapping using parametric transformation technique gave optimum values for the bias correction with minimum error compared to the linear scaling, cumulative distributive transformation and quantile mapping using smooth spline method.

- Rainfall depths for different return periods using GEV for historic data (RCM), RCP 4.5future 1, RCP 4.5future 2, RCP 8.5 future 1 and RCP 8.5 future 2 and the peak discharges were calculated. It was found out that RCP 8.5 future 1 gave maximum peak discharge.
- The performance and potential of biological BMPs (LID), were higher in controlling and reducing the runoff volume compared to those of structural BMPs.

5.3. Contribution from the Research Study

- Climate change impact on flooding in the study area is analysed. The results can be used for planning the infrastructure in a developing city considering the effect of climate change.
- The flood inundation maps developed can be used for the planning and management of an early warning system for the floods and for creation of public awareness.
- Mitigation of urban flood using best management techniques, developed in this study, can reduce the vulnerability in the study area.
- The methodology developed in this study can be used for the similar urbanising cities.

5.4. Challenges Encountered

- Better resolution DEMs, which would have given improved results for flood inundation mapping, were not available for the study.
- One of the biggest hurdles encountered was the observed flow data not being available for the Kondaveeti Vagu and tributaries, since these streams were ungauged. The only calibrated value known at the outlet point that is at the Undavalli was the 100-year discharge data.

5.5. Scope for future study

The study can be taken forward further by linking the models to weather forecasting systems to develop real time flood inundation maps.

References

Adnan, M. S. G., Abdullah, A. Y. M., Dewan, A., and Hall, J. W. (2020). "The effects of changing land use and flood hazard on poverty in coastal Bangladesh." *Land Use Policy*, 99, 104868. https://doi.org/10.1016/j.landusepol.2020.104868

Ahmad, B., Kaleem, M. S., Butt, M. J., and Dahri, Z.H. (2010). "Hydrological Modelling and Flood Hazard Mapping of Nullah lai." *Proceedings of Pakistan Academy of Sciences*, 47(4) pp. 215-226.

Ahmad, H. F., Alam, A., Bhat, M. S., and Ahmad, S. (2016). "One Dimensional Steady Flow Analysis Using HECRAS – A case of River Jhelum, Jammu and Kashmir." *European Scientific Journal, ESJ*, 12(32), 340. https://doi.org/10.19044/esj.2016.v12n32p340

Al Balasmeh, O., Babbar, R., and Karmaker, T. (2019). "Trend analysis and ARIMA modeling for forecasting precipitation pattern in Wadi Shueib catchment area in Jordan." *Arabian Journal of Geosciences*, 12(2), 27. https://doi.org/10.1007/s12517-018-4205-z

Alahacoon, N., Matheswaran, K., Pani, P., and Amarnath, G. (2018). "A Decadal Historical Satellite Data and Rainfall Trend Analysis (2001–2016) for Flood Hazard Mapping in Sri Lanka." *Remote Sensing*, 10(3):16–23. https://doi.org/10.3390/rs10030448

Alain, M., and Sophie, D. (2010). "Design Criteria of Urban Drainage Infrastructures under Climate Change." *Journal of Water Resources Planning and Management*, American Society of Civil Engineers, 136(2), 201–208. https://doi.org/10.1061/(ASCE)WR.1943-5452.0000023

Alberti, M., Marzluff, J. M., Shulenberger, E., Bradley, G., Ryan, C., and Zumbrunnen, C. (2003). "Integrating Humans into Ecology: Opportunities and Challenges for Studying Urban Ecosystems." *BioScience*, 53(12), 1169–1179. https://doi.org/10.1641/0006-3568(2003)053[1169:IHIEOA]2.0.CO;2

Alexandersson, H. (1986). "A homogeneity test applied to precipitation data." *Journal of Climatology, John Wiley & Sons*, Ltd, 6(6), 661–675. https://doi.org/10.1002/joc.3370060607

Ali, M., Khan, S. J., Aslam, I., and Khan, Z. (2011). "Simulation of the impacts of land-use change on surface runoff of Lai Nullah Basin in Islamabad, Pakistan." *Landscape and Urban Planning*, 102(4), 271–279. https://doi.org/10.1016/j.landurbplan.2011.05.006

Anderson, M. L., Chen, Z.-Q., Kavvas, M. L., and Feldman, A. (2002). "Coupling HEC-HMS with Atmospheric Models for Prediction of Watershed Runoff." *Journal of Hydrologic Engineering*, American Society of Civil Engineers, 7(4), 312–318. https://doi.org/10.1061/(ASCE)1084-0699(2002)7:4(312)

Andersson, E. (2006). "Urban Landscapes and Sustainable Cities." *Ecology and Society*, Resilience Alliance Inc., 11(1). http://www.jstor.org/stable/26267821

Arnbjerg-Nielsen, K. (2012). "Quantification of climate change effects on extreme precipitation used for high resolution hydrologic design." *Urban Water Journal*, 9(2), 57–65. https://doi.org/10.1080/1573062X.2011.630091

Arora, A. S., and Reddy, A. S. (2013). "Multivariate analysis for assessing the quality of stormwater from different Urban surfaces of the Patiala city, Punjab (India)." *Urban Water Journal*, Taylor & Francis, 10(6), 422–433. https://doi.org/10.1080/1573062X.2012.739629

Asfaw, A., Simane, B., Hassen, A., and Bantider, A. (2018). "Variability and time series trend analysis of rainfall and temperature in northcentral Ethiopia: A case study in Woleka sub-basin." *Weather and Climate Extremes*, 19, 29–41. https://doi.org/10.1016/j.wace.2017.12.002

Ay, M., and Kisi, O. (2015). "Investigation of trend analysis of monthly total precipitation by an innovative method." *Theoretical and Applied Climatology*, 120(3), 617–629. https://doi.org/10.1007/s00704-014-1198-8

Bartels, R. J., Black, A. W., and Keim, B. D. (2020). "Trends in precipitation days in the United States." *International Journal of Climatology*, John Wiley & Sons, Ltd, 40(2), 1038–1048. https://doi.org/10.1002/joc.6254

Bates, P. D., and De Roo, A. P. J. (2000). "A simple raster-based model for flood inundation simulation." *Journal of Hydrology*, 236(1), 54–77. https://doi.org/10.1016/S0022-1694(00)00278-X

Beighley, R. E., Melack, J. M., and Dunne, T. (2003). "Impacts of California's climatic regimes and coastal land use change on streamflow characteristics1." *JAWRA Journal of the American Water Resources Association*, John Wiley & Sons, Ltd, 39(6), 1419–1433. https://doi.org/10.1111/j.1752-1688.2003.tb04428.x

Bewket, W., and Conway, D. (2007). "A note on the temporal and spatial variability of rainfall in the drought-prone Amhara region of Ethiopia." *International Journal of Climatology*, John Wiley & Sons, Ltd, 27(11), 1467–1477. https://doi.org/10.1002/joc.1481

Bisht, D. S., Chatterjee, C., Kalakoti, S., Upadhyay, P., Sahoo, M., and Panda, A. (2016). "Modeling urban floods and drainage using SWMM and MIKE URBAN: a case study." *Natural Hazards*, 84(2), 749–776. https://doi.org/10.1007/s11069-016-2455-1

Bisht, D. S., Chatterjee, C., Raghuwanshi, N. S., and Sridhar, V. (2018). "An analysis of precipitation climatology over Indian urban agglomeration." *Theoretical and Applied Climatology*, 133(1), 421–436. https://doi.org/10.1007/s00704-017-2200-z

Brunner, M. I., Sikorska, A. E., and Seibert, J. (2018). "Bivariate analysis of floods in climate impact assessments." *Science of The Total Environment*, 616–617, 1392–1403. https://doi.org/10.1016/j.scitotenv.2017.10.176

Buishand, T. A. (1982). "Some methods for testing the homogeneity of rainfall records." *Journal of Hydrology*, 58(1), 11–27. https://doi.org/10.1016/0022-1694(82)90066-X

Burger, G., Sitzenfrei, R., Kleidorfer, M., and Rauch, W. (2014). "Parallel flow routing in SWMM 5." *Environmental Modelling & Software*, 53, 27–34. https://doi.org/10.1016/j.envsoft.2013.11.002

Burrel, B. C., Davar, K., and Hughes, R. (2007). "A Review of Flood Management Considering the Impacts of Climate Change." *Water International*, Routledge, 32(3), 342–359. https://doi.org/10.1080/02508060708692215

Byakatonda, J., Parida, B. P., Kenabatho, P. K., and Moalafhi, D. B. (2018). "Analysis of rainfall and temperature time series to detect long-term climatic trends and variability over semi-arid Botswana." *Journal of Earth System Science*, 127(2), 25. https://doi.org/10.1007/s12040-018-0926-3

Caloiero, T. (2020). "Evaluation of rainfall trends in the South Island of New Zealand through the innovative trend analysis (ITA)." *Theoretical and Applied Climatology*, 139(1), 493–504. https://doi.org/10.1007/s00704-019-02988-5

Carrivick, J. L. (2006). "Application of 2D hydrodynamic modelling to high-magnitude outburst floods: An example from Kverkfjöll, Iceland." *Journal of Hydrology*, 321(1), 187–199. https://doi.org/https://doi.org/10.1016/j.jhydrol.2005.07.042

Castellarin, A., Kohnova, S., Gaal, L., Fleig, A., Salinas, J.L., Toumazis, A., Kjeldsen, T.R., Macdonald, N. (2012) "Review of applied-statistical methods for flood-frequency analysis in Europe." *NERC/Centre for Ecology & Hydrology*, 122pp.

Cayan, D. R., Maurer, E. P., Dettinger, M. D., Tyree, M., and Hayhoe, K. (2008). "Climate change scenarios for the California region." *Climatic Change*, 87(1), 21–42. https://doi.org/10.1007/s10584-007-9377-6

Chatterjee, C., Kumar, R., Kumar, S., Jain, S. K., Lohani, A. K., and Singh R.D. (2001). "Intercompression of responses of HEC-1 package and Nash model." *Journal of Hydrology*, 3 pp. 13-24.

Chebana, F. (2001). "Multivariate Analysis of Hydrological Variables." *Encyclopedia of Environmetrics*, Major Reference Works. https://doi.org/10.1002/9780470057339.vnn044

Chen, Y., Xu, Y., and Yin, Y. (2009). "Impacts of land use change scenarios on storm-runoff generation in Xitiaoxi basin, China." *Quaternary International*, 208(1–2), 121–128. https://doi.org/10.1016/j.quaint.2008.12.014

Christensen, J. H., Boberg, F., Christensen, O. B., and Lucas-Picher, P. (2008). "On the need for bias correction of regional climate change projections of temperature and

precipitation." *Geophysical Research Letters*, John Wiley & Sons, Ltd, 35(20). https://doi.org/10.1029/2008GL035694

Costa, A. C., and Soares, A. (2009). "Homogenization of Climate Data: Review and New Perspectives Using Geostatistics." *Mathematical Geosciences*, 41(3), 291–305. https://doi.org/10.1007/s11004-008-9203-3

Cui, L., Wang, L., Lai, Z., Tian, Q., Liu, W., and Li, J. (2017). "Innovative trend analysis of annual and seasonal air temperature and rainfall in the Yangtze River Basin, China during 1960–2015." *Journal of Atmospheric and Solar-Terrestrial Physics*, 164, 48–59. https://doi.org/10.1016/j.jastp.2017.08.001

Cunderlik, J.M., and Donald, H. B. (2004). "Linkages between Regional Trends in Monthly Maximum Flows and Selected Climatic Variables." *Journal of Hydrologic Engineering*, American Society of Civil Engineers, 9(4), 246–256. https://doi.org/10.1061/(asce)1084-0699(2004)9:4(246)

Cunge, J. A., Holly, F. M., and Verwey, A. (1980). "Practical aspects of computational river hydraulics." *Boston: Pitman Advanced Pub. Program*.

Dabanlı, İ., Şen, Z., Yeleğen, M. Ö., Şişman, E., Selek, B., and Güçlü, Y. S. (2016). "Trend Assessment by the Innovative-Şen Method." *Water Resources Management*, 30(14), 5193–5203. https://doi.org/10.1007/s11269-016-1478-4

Dasgupta, S., Gosain, A. K., Rao, S., Roy, S., and Sarraf, M. (2013). "A megacity in a changing climate: the case of Kolkata." *Climatic Change*, 116(3), 747–766. https://doi.org/10.1007/s10584-012-0516-3

Deepesh, M., and Jha, M. K. (2012) "Hydrologic time series analysis: theory and practice." *Springer*, New York

Devia, G. K., Ganasri, B. P., and Dwarakish, G. S. (2015). "A Review on Hydrological Models." *Aquatic Procedia*, 4, 1001–1007. https://doi.org/https://doi.org/10.1016/j.aqpro.2015.02.126

Dickey, D. A., and Fuller, W. A. (1979). "Distribution of the Estimators for Autoregressive Time Series with a Unit Root." *Journal of the American Statistical Association*, Taylor & Francis, 74(366a), 427–431. https://doi.org/10.1080/01621459.1979.10482531

Duhan, D., and Pandey, A. (2013). "Statistical analysis of long term spatial and temporal trends of precipitation during 1901–2002 at Madhya Pradesh, India." *Atmospheric Research*, 122, 136–149. https://doi.org/10.1016/j.atmosres.2012.10.010

Ekström, M., Fowler, H. J., Kilsby, C. G., and Jones, P. D. (2005). "New estimates of future changes in extreme rainfall across the UK using regional climate model integrations. 2. Future estimates and use in impact studies." *Journal of Hydrology*, 300(1), 234–251. https://doi.org/https://doi.org/10.1016/j.jhydrol.2004.06.019

El Adlouni, S., Bobée, B., and Ouarda, T. B. M. J. (2008). "On the tails of extreme event distributions in hydrology." *Journal of Hydrology*, 355(1), 16–33. https://doi.org/10.1016/j.jhydrol.2008.02.011

Elliott, A. H., and Trowsdale, S. A. (2007). "A review of models for low impact urban stormwater drainage." *Environmental Modelling & Software*, 22(3), 394–405. https://doi.org/10.1016/j.envsoft.2005.12.005

EPA. (2013). U.S. Environmental Protection Agency (EPA) International Decontamination Research and Development Conference . Research Triangle Park, NC, November 05 - 07, 2013. U.S. Environmental Protection Agency, Washington, DC, EPA/600/R-14/210, 2014.

Erdas Inc. (1999). Erdas Field Guide. Erdas Inc., Atlanta, Georgia.

Farrokhi, A., Farzin, S., and Mousavi, S.-F. (2020). "A New Framework for Evaluation of Rainfall Temporal Variability through Principal Component Analysis, Hybrid Adaptive Neuro-Fuzzy Inference System, and Innovative Trend Analysis Methodology." *Water Resources Management*, 34(10), 3363–3385. https://doi.org/10.1007/s11269-020-02618-0

Feidas, H., Makrogiannis, T., and Bora-Senta, E. (2004). "Trend analysis of air temperature time series in Greece and their relationship with circulation using surface and satellite data: 1955–2001." *Theoretical and Applied Climatology*, 79(3), 185–208. https://doi.org/10.1007/s00704-004-0064-5

Fosu, C., Forkuo, K. E., and Asare, Y. M. (2012). "River Inundation and Hazard Mapping – a Case Study of Susan River – Kumasi." Department of Geomatics Engineering, Kwame Nkrumah University of Science &Technology, Private Mail Bag, Kumasi, Ghana, *proceedings of global geospatial conference* 2012 Quebec City, Canada, 14-17 May-2012.

Frei, C., Christensen, J. H., Déqué, M., Jacob, D., Jones, R. G., and Vidale, P. L. (2003). "Daily precipitation statistics in regional climate models: Evaluation and intercomparison for the European Alps." *Journal of Geophysical Research: Atmospheres*, John Wiley & Sons, Ltd, 108(D3). https://doi.org/10.1029/2002JD002287

Fuller, W. A. (1996). "Introduction to statistical time series." Second edn. *John Wiley & Sons*, Inc., New York.

Gilbert, R. O. (1987). "Statistical Methods for Environmental Pollution Monitoring." *Van Nostraud Reinhold*, New York, 320 pp

Güçlü, Y. S., Şişman, E., and Dabanlı, İ. (2020). "Innovative triangular trend analysis." *Arabian Journal of Geosciences*, 13(1), 27. https://doi.org/10.1007/s12517-019-5048-y

Gwet, K. L. (2002). "Kappa Statistic is not Satisfactory for Assessing the Extent of Agreement Between Raters."

Hallegatte, S., Ranger, N., Mestre, O., Dumas, P., Corfee-Morlot, J., Herweijer, C., and Wood, R. M. (2011). "Assessing climate change impacts, sea level rise and storm surge risk in port cities: a case study on Copenhagen." *Climatic Change*, 104(1), 113–137. https://doi.org/10.1007/s10584-010-9978-3

Hamed, K. H., and Ramachandra Rao, A. (1998). “A modified Mann-Kendall trend test for autocorrelated data.” *Journal of Hydrology*, 204(1), 182–196. https://doi.org/10.1016/S0022-1694(97)00125-X

Han, J.-Y., Baik, J.-J., and Lee, H. (2014). “Urban impacts on precipitation.” *Asia-Pac. J. Atmos. Sci.*, 50, 17–30. https://doi.org/10.1007/s13143-014-0016-7

Hardy, M. J., Kuczera, G., and Coombes, P. J. (2005). “Integrated urban water cycle management: the UrbanCycle model.” *Water Science and Technology*, 52(9), 1–9. https://doi.org/10.2166/wst.2005.0276

Hawkins, D. M. (1977). “Testing a Sequence of Observations for a Shift in Location.” *Journal of the American Statistical Association*, Taylor & Francis, 72(357), 180–186. https://doi.org/10.1080/01621459.1977.10479935

Hay, L. E., Wilby, R. L., and Leavesley, G. H. (2000). “A comparison of delta change and downscaled gcm scenarios for three mountainous basins in the united states.” *JAWRA Journal of the American Water Resources Association*, John Wiley & Sons, Ltd, 36(2), 387–397. https://doi.org/10.1111/j.1752-1688.2000.tb04276.x

Hosseinzadehtalaei, P., Tabari, H., and Willems, P. (2020). “Climate change impact on short-duration extreme precipitation and intensity–duration–frequency curves over Europe.” *Journal of Hydrology*, 590, 125249. https://doi.org/https://doi.org/10.1016/j.jhydrol.2020.125249

Hostetler, S. W., Alder, J. R., and Allan, A. M. (2011). “Dynamically downscaled climate simulations over North America: Methods, evaluation, and supporting documentation for users.” *Open-File Report*, Reston, VA. . https://doi.org/10.3133/ofr20111238

Hou, J., Zhou, N., Chen, G., Huang, M., and Bai, G. (2021). “Rapid forecasting of urban flood inundation using multiple machine learning models.” *Natural Hazards*, 108(2), 2335–2356. https://doi.org/10.1007/s11069-021-04782-x

Huang, Y. F., Puah, Y. J., Chua, K. C., and Lee, T. S. (2015). "Analysis of monthly and seasonal rainfall trends using the Holt's test." *International Journal of Climatology*, John Wiley & Sons, Ltd, 35(7), 1500–1509. https://doi.org/10.1002/joc.4071

Huss, M., Bauder, A., and Funk, M. (2009). "Homogenization of long-term mass-balance time series." *Annals of Glaciology*, Cambridge University Press, 50(50), 198–206. https://doi.org/10.3189/172756409787769627

Idowu, D., and Zhou, W. (2021). "Land Use and Land Cover Change Assessment in the Context of Flood Hazard in Lagos State, Nigeria." *Water* . 13(8):1105. https://doi.org/10.3390/w13081105

Ipcc. (2014). "Climate change 2014: Impacts, Adaptations, and Vulnerability."

Jain, M. K., and Ramshastri, K. S. (1990). "Application of HEC-1 to Hemavati river (upto Sakleshpur) basin." NIH Report No. CS-55

Jain, S. K., and Kumar, V. (2012). "Trend analysis of rainfall and temperature data for India." *Current Science* 102:37-49

Jain, S. K., Kumar, V., and Saharia, M. (2013). "Analysis of rainfall and temperature trends in northeast India." *International Journal of Climatology*, John Wiley & Sons, Ltd, 33(4), 968–978. https://doi.org/10.1002/joc.3483

Jaiswal, R. K., Lohani, A. K., and Tiwari, H. L. (2015). "Statistical Analysis for Change Detection and Trend Assessment in Climatological Parameters." *Environmental Processes*, 2(4), 729–749. https://doi.org/10.1007/s40710-015-0105-3

Jamali, B., Löwe, R., Bach, P. M., Urich, C., Arnbjerg-Nielsen, K., and Deletic, A. (2018). "A rapid urban flood inundation and damage assessment model." *Journal of Hydrology*, 564, 1085–1098. https://doi.org/10.1016/j.jhydrol.2018.07.064

Janssen, V. (2009). "Understanding coordinate reference systems, datums and transformations." *International Journal of Geoinformatics*, 5(4), 41–53.

Javari, M. (2017). “Spatial variability of rainfall trends in Iran.” *Arabian Journal of Geosciences*, 10(4), 78. https://doi.org/10.1007/s12517-017-2857-8

Jayasuriya, L. N. N., Kadurupokune, N., Othman, M., and Jesse, K. (2007). “Contributing to the sustainable use of stormwater: the role of pervious pavements.” *Water Science and Technology*, 56(12), 69–75. https://doi.org/10.2166/wst.2007.753

Jeffrey, M., and Edward, B. (2019). “Flood Frequency Hydrology with Limited Data for the Weser River Basin, Germany.” *Journal of Hydrologic Engineering*, American Society of Civil Engineers, 24(3), 5019002. https://doi.org/10.1061/(ASCE)HE.1943-5584.0001713

Jia, H., Lu, Y., Yu, S. L., and Chen, Y. (2012). “Planning of LID-BMPs for urban runoff control: The case of Beijing Olympic Village.” *Separation and Purification Technology*, Elsevier B.V., 84, 112–119. https://doi.org/https://doi.org/10.1016/j.seppur.2011.04.026

Kang, D.-H., Nam, D.-H., Jeung, S.-J., and Kim, B.-S. (2021). “Impact Assessment of Flood Damage in Urban Areas Using RCP 8.5 Climate Change Scenarios and Building Inventory.” *Water* . 13(6):756. https://doi.org/10.3390/w13060756

Kang, H. M., and Yusof, F. (2010). “Homogeneity tests on the daily rainfall series in Peninsular Malaysia.” *International Journal of Contemporary Mathematical Sciences* 7(1):9– 22.

Kanji, G. K. (2006). “100 statistical tests.” SAGE Publications, London.

Karpouzos, D., Kavalieratou, S., Babajimopoulos, C. (2010). “Trend analysis of precipitation data in Pieria Region (Greece).” *European Water* 31–40.

Kendall, M. G. (1975). “Rank Correlation Methods.” 4th Edn, *Charles Griffin*, London, 272 pp.

Kisi, O. (2015). “An innovative method for trend analysis of monthly pan evaporations.” *Journal of Hydrology*, 527, 1123–1129. https://doi.org/10.1016/j.jhydrol.2015.06.009

Knebl, M. R., Yang, Z.-L., Hutchison, K., and Maidment, D. R. (2005). "Regional scale flood modeling using NEXRAD rainfall, GIS, and HEC-HMS/RAS: a case study for the San Antonio River Basin Summer 2002 storm event." *Journal of Environmental Management*, 75(4), 325–336. https://doi.org/10.1016/j.jenvman.2004.11.024

Krishnakumar, K. N., Prasada Rao, G. S. L. H. V., and Gopakumar, C. S. (2009). "Rainfall trends in twentieth century over Kerala, India." *Atmospheric Environment*, 43(11), 1940–1944. https://doi.org/10.1016/j.atmosenv.2008.12.053

Kug, J.-S., and Ahn, M.-S. (2013). "Impact of urbanization on recent temperature and precipitation trends in the Korean peninsula." *Asia-Pacific Journal of Atmospheric Sciences*, 49(2), 151–159. https://doi.org/10.1007/s13143-013-0016-z

Kumar, A. C., and Reshma, T. (2017). "4D Applications of GIS in Construction Management." *Advances in Civil Engineering*, (D. Tapete, ed.), Hindawi, 2017, 1048540. https://doi.org/10.1155/2017/1048540

Kumar, K. S., and Rathnam, E. V. (2019). "Analysis and Prediction of Groundwater Level Trends Using Four Variations of Mann Kendall Tests and ARIMA Modelling." *Journal of the Geological Society of India*, 94(3), 281–289. https://doi.org/10.1007/s12594-019-1308-4

Kumar, V., and Jain, S. K. (2011). "Trends in rainfall amount and number of rainy days in river basins of India (1951–2004)." *Hydrology Research*, 42(4), 290–306. https://doi.org/10.2166/nh.2011.067

Kumar, V., Jain, S. K., and Singh, Y. (2010). "Analysis of long-term rainfall trends in India." *Hydrological Sciences Journal*, Taylor & Francis, 55(4), 484–496. https://doi.org/10.1080/02626667.2010.481373

Kumar, Y., and Kumar, A. (2020). "Spatiotemporal analysis of trend using nonparametric tests for rainfall and rainy days in Jodhpur and Kota zones of Rajasthan (India)." *Arabian Journal of Geosciences*, 13(15), 691. https://doi.org/10.1007/s12517-020-05687-y

Kwiatkowski, D., Phillips, P. C. B., Schmidt, P., and Shin, Y. (1992). "Testing the null hypothesis of stationarity against the alternative of a unit root: How sure are we that economic time series have a unit root?" *Journal of Econometrics*, 54(1), 159–178. https://doi.org/10.1016/0304-4076(92)90104-Y

Lamb, R., Crossley, M., and Waller, S. (2009). "A fast two-dimensional floodplain inundation model." *Proceedings of the Institution of Civil Engineers - Water Management*, 162(6), 363–370. https://doi.org/10.1680/wama.2009.162.6.363

Lambin, E. F. (1997). "Modeling and monitoring land cover change processes in tropical regions." *Progress in Physical Geography,* 21(3):375–393.

Langat, P. K., Kumar, L., and Koech, R. (2017). "Temporal Variability and Trends of Rainfall and Streamflow in Tana River Basin, Kenya." *Sustainability*. https://doi.org/10.3390/su9111963

Lee, S.-B., Yoon, C.-G., Jung, K. W., and Hwang, H. S. (2010). "Comparative evaluation of runoff and water quality using HSPF and SWMM." *Water Science and Technology*, 62(6), 1401–1409. https://doi.org/10.2166/wst.2010.302

Leonard, M., Metcalfe, A., and Lambert, M. (2008). "Frequency analysis of rainfall and streamflow extremes accounting for seasonal and climatic partitions." *Journal of Hydrology*, 348(1), 135–147. https://doi.org/10.1016/j.jhydrol.2007.09.045

Li, C., Zwiers, F., Zhang, X., Chen, G., Lu, J., Li, G., Norris, J., Tan, Y., Sun, Y., and Liu, M. (2019). "Larger Increases in More Extreme Local Precipitation Events as Climate Warms." *Geophysical Research Letters*, John Wiley & Sons, Ltd, 46(12), 6885–6891. https://doi.org/10.1029/2019GL082908

Li, H., Wang, D., Singh, V. P., Wang, Y., Wu, J., Wu, J., Liu, J., Zou, Y., He, R., and Zhang, J. (2019). "Non-stationary frequency analysis of annual extreme rainfall volume and intensity using Archimedean copulas: A case study in eastern China." *Journal of Hydrology*, 571, 114–131. https://doi.org/10.1016/j.jhydrol.2019.01.054

Liu, L., Liu, Y., Wang, X., Yu, D., Liu, K., Huang, H., and Hu, G. (2015). "Developing an effective 2-D urban flood inundation model for city emergency management based on cellular automata." *Natural Hazards and Earth System Sciences*, 15(3), 381–391. https://doi.org/10.5194/nhess-15-381-2015, 2015.

López, E., Bocco, G., Mendoza, M., and Duhau, E. (2001). "Predicting land-cover and land-use change in the urban fringe: A case in Morelia city, Mexico." *Landscape and Urban Planning*, 55(4), 271–285. https://doi.org/1016/S0169- 2046(01)00160-8

Lørup, J. K., Refsgaard, J. C., and Mazvimavi, D. (1998). "Assessing the effect of land use change on catchment runoff by combined use of statistical tests and hydrological modelling: Case studies from Zimbabwe." *Journal of Hydrology*, 205(3), 147–163. https://doi.org/10.1016/S0168-1176(97)00311-9

Lucas, G. R. (1995). "Remote sensing and image interpretation, 3rd edn, by T. M. Lillesand and R. W. Kiefer, 1994. Wiley, Chichester. No. of pages: 750. Price: £19.95 (paperback); £67.00 (cloth). ISBN 0471 305 758." *Geological Journal*, John Wiley & Sons, Ltd, 30(2), 204. https://doi.org/10.1002/gj.3350300217

Lundholm, J. T., and Richardson, P. J. (2010). "MINI-REVIEW: Habitat analogues for reconciliation ecology in urban and industrial environments." *Journal of Applied Ecology*, John Wiley & Sons, Ltd, 47(5), 966–975. https://doi.org/https://doi.org/10.1111/j.1365-2664.2010.01857.x

Machiwal, D., and Jha, M. K. (2012). "Hydrologic Time Series Analysis. Theory and Practice." *Springer*, Netherlands.

Machiwal, D., Kumar, S., Dayal, D., and Mangalassery, S. (2017). "Identifying abrupt changes and detecting gradual trends of annual rainfall in an Indian arid region under heightened rainfall rise regime." *International Journal of Climatology*, John Wiley & Sons, Ltd, 37(5), 2719–2733. https://doi.org/10.1002/joc.4875

Maidment, D. R., and Seth, Ahrens. (1999). "Introduction to HEC – HMS: CE 394k.2" Surface Water hydrology, electronic document. Retrieved from

http://www.ce.utexas.edu/prof/maidment/grad/tate/research/RASExercise/webfiles/hecras.html. Accessed 17 September 2012.

Malamud, B. D., and Turcotte, D. L. (2006). "The applicability of power-law frequency statistics to floods." *Journal of Hydrology*, 322(1), 168–180. https://doi.org/10.1016/j.jhydrol.2005.02.032

Malik, A., and Kumar, A. (2020). "Spatio-temporal trend analysis of rainfall using parametric and non-parametric tests: case study in Uttarakhand, India." *Theoretical and Applied Climatology*, 140(1), 183–207. https://doi.org/10.1007/s00704-019-03080-8

Mann, H. B. (1945). "Non-parametric tests against trend." *Econometrica* 13:245–259

Marak, J. D. K., Sarma, A. K., and Bhattacharjya, R. K. (2020). "Innovative trend analysis of spatial and temporal rainfall variations in Umiam and Umtru watersheds in Meghalaya, India." *Theoretical and Applied Climatology*, 142(3), 1397–1412. https://doi.org/10.1007/s00704-020-03383-1

Maraun, D., Wetterhall, F., Ireson, A. M., Chandler, R. E., Kendon, E. J., Widmann, M., Brienen, S., Rust, H. W., Sauter, T., Themeßl, M., Venema, V. K. C., Chun, K. P., Goodess, C. M., Jones, R. G., Onof, C., Vrac, M., and Thiele-Eich, I. (2010). "Precipitation downscaling under climate change: Recent developments to bridge the gap between dynamical models and the end user." *Reviews of Geophysics*, John Wiley & Sons, Ltd, 48(3). https://doi.org/10.1029/2009RG000314

Mark, O., Weesakul, S., Apirumanekul, C., Aroonnet, S. B., and Djordjević, S. (2004). "Potential and limitations of 1D modelling of urban flooding." *Journal of Hydrology*, 299(3), 284–299. https://doi.org/https://doi.org/10.1016/j.jhydrol.2004.08.014

Marko, K., Elfeki, A., Alamri, N., and Chaabani, A. (2019). "Two Dimensional Flood Inundation Modelling in Urban Areas Using WMS, HEC-RAS and GIS (Case Study in Jeddah City, Saudi Arabia) BT - Advances in Remote Sensing and Geo Informatics Applications." H. M. El-Askary, S. Lee, E. Heggy, and B. Pradhan, eds., Springer

International Publishing, Cham, 265–267. https://doi.org/10.1007/978-3-030-01440-7_62

Martin, O., and Ovcharovichova, A. R. J. (2012). "Application of HEC HMS/RAS and GIS Tools in Flood Modeling: A Case Study for River Sironko@ Uganda." *Global Journal of Engineering, Design and Technology*.

Martínez-Solano, F. J., Iglesias-Rey, P. L., Saldarriaga, J. G., and Vallejo, D. (2016). "Creation of an SWMM Toolkit for Its Application in Urban Drainage Networks Optimization." *Water*. https://doi.org/10.3390/w8060259

Maurer, E. P., and Hidalgo, H. G. (2008). "Utility of daily vs. monthly large-scale climate data: an intercomparison of two statistical downscaling methods." *Hydrology and Earth System Sciences*, 12(2), 551–563. https://doi.org/10.5194/hess-12-551-2008

Meehl, G. A., and Thomas, F. S. (2007). "Global climate projections, in Climate Change 2007: The Physical Science Basis." Contribution of working Group I to the Fourth Assessment Report of the Intergovernmental Panel on Climate Change. edited by S. Solomon et al, pp. 749–845, Cambridge Univ. Press, New York

Meena, Y. R., and Anil, K. G. (2018). "Evaluation of Stormwater BMPs Performances for Flood Volume Reduction in Bengaluru City, Karnataka, India." *SSRG International Journal of Civil Engineering* 5.7: 5-10. https://doi.org/10.14445/23488352/IJCE-V5I7P102

Mei, C., Liu, J., Wang, H., Li, Z., Yang, Z., Shao, W., Ding, X., Weng, B., Yu, Y., and Yan, D. (2020). "Urban flood inundation and damage assessment based on numerical simulations of design rainstorms with different characteristics." *Science China Technological Sciences*, 63(11), 2292–2304. https://doi.org/10.1007/s11431-019-1523-2

Melesse, A. M., and Shih, S. F. (2002). "Spatially distributed storm runoff depth estimation using Landsat images and GIS." *Computers and Electronics in Agriculture*, 37(1), 173–183. https://doi.org/10.1016/S0168-1699(02)00111-4

Meshram, S. G., Singh, S. K., Meshram, C., Deo, R. C., and Ambade, B. (2018). "Statistical evaluation of rainfall time series in concurrence with agriculture and water resources of Ken River basin, Central India (1901–2010)." *Theoretical and Applied Climatology*, 134(3), 1231–1243. https://doi.org/10.1007/s00704-017-2335-y

Metcalf and Eddy, Inc., University of Florida and Water Resources Engineers, Inc. (1971). "Storm water management model, vol 1-final report." EPA Report No. 11024DOV07/71 (NITS PB-203289), Environmental Protection Agency, Washington, D.C

Michelangeli, P.-A., Vrac, M., and Loukos, H. (2009). "Probabilistic downscaling approaches: Application to wind cumulative distribution functions." *Geophysical Research Letters*, John Wiley & Sons, Ltd, 36(11). https://doi.org/10.1029/2009GL038401

Modarres, R., and Ouarda, T. B. M. J. (2013). "Modeling rainfall–runoff relationship using multivariate GARCH model." *Journal of Hydrology*, 499, 1–18. https://doi.org/10.1016/j.jhydrol.2013.06.044

Mohorji, A. M., Şen, Z., and Almazroui, M. (2017). "Trend Analyses Revision and Global Monthly Temperature Innovative Multi-Duration Analysis." *Earth Systems and Environment*, 1(1), 9. https://doi.org/10.1007/s41748-017-0014-x

Mokhtar, E. S., Pradhan, B., Ghazali, A. H., and Shafri, H. Z. M. (2018). "Assessing flood inundation mapping through estimated discharge using GIS and HEC-RAS model." *Arabian Journal of Geosciences*, 11(21), 682. https://doi.org/10.1007/s12517-018-4040-2

Nair, S. C., and Mirajkar, A. B. (2021). "Spatio–temporal rainfall trend anomalies in Vidarbha region using historic and predicted data: a case study." *Modeling Earth Systems and Environment*, 7(1), 503–510. https://doi.org/10.1007/s40808-020-00928-1

NDMA. (2012). "National disaster management guidelines." National disaster management authority, government of India, February.

Neumann, J. von. (1941). “Distribution of the Ratio of the Mean Square Successive Difference to the Variance.” *The Annals of Mathematical Statistics*, 12(4), 367–395. https://doi.org/doi:10.1214/aoms/1177731677

Nguyen, H. D., Fox, D., Dang, D. K., Pham, L. T., Viet Du, Q. V, Nguyen, T. H., Dang, T. N., Tran, V. T., Vu, P. L., Nguyen, Q.-H., Nguyen, T. G., Bui, Q.-T., and Petrisor, A.-I. (2021). “Predicting Future Urban Flood Risk Using Land Change and Hydraulic Modeling in a River Watershed in the Central Province of Vietnam.” *Remote Sensing.* 13(2):262. https://doi.org/10.3390/rs13020262

Núñez-González, G. (2020). “Analysis of the trends in precipitation and precipitation concentration in some climatological stations of Mexico from 1960 to 2010.” *Natural Hazards*, 104(2), 1747–1761. https://doi.org/10.1007/s11069-020-04244-w

Palizdan, N., Falamarzi, Y., Huang, Y. F., and Lee, T. S. (2017). “Precipitation trend analysis using discrete wavelet transform at the Langat River Basin, Selangor, Malaysia.” *Stochastic Environmental Research and Risk Assessment*, 31(4), 853–877. https://doi.org/10.1007/s00477-016-1261-3

Palizdan, N., Falamarzi, Y., Huang, Y. F., Lee, T. S., and Ghazali, A. H. (2014). “Regional precipitation trend analysis at the Langat River Basin, Selangor, Malaysia.” *Theoretical and Applied Climatology*, 117(3), 589–606. https://doi.org/10.1007/s00704-013-1026-6

Panofsky, H. A., and Brier, G. W. (1968). “Some Application of Statistics to Meteorology.” 224 pp, Pa. State Univ, University Park

Papaioannou, G., Loukas, A., Vasiliades, L., and Aronica, G. T. (2016). “Flood inundation mapping sensitivity to riverine spatial resolution and modelling approach.” *Natural Hazards*, 83(1), 117–132. https://doi.org/10.1007/s11069-016-2382-1

Papaioannou, G., Vasiliades, L., Loukas, A., and Aronica, G. T. (2017). “Probabilistic flood inundation mapping at ungauged streams due to roughness coefficient uncertainty in hydraulic modelling.” *Advances in Geosciences*, 44, 23–34. https://doi.org/10.5194/adgeo-44-23-2017

Patel, D. P., Ramirez, J. A., Srivastava, P. K., Bray, M., and Han, D. (2017). "Assessment of flood inundation mapping of Surat city by coupled 1D/2D hydrodynamic modeling: a case application of the new HEC-RAS 5." *Natural Hazards*, 89(1), 93–130. https://doi.org/10.1007/s11069-017-2956-6

Pathak, A. A., and Dodamani, B. M. (2020). "Trend analysis of rainfall, rainy days and drought: a case study of Ghataprabha River Basin, India." *Modeling Earth Systems and Environment*, 6(3), 1357–1372. https://doi.org/10.1007/s40808-020-00798-7

Patra, J. P., Mishra, A., Singh, R., and Raghuwanshi, N. S. (2012). "Detecting rainfall trends in twentieth century (1871–2006) over Orissa State, India." *Climatic Change*, 111(3), 801–817. https://doi.org/10.1007/s10584-011-0215-5

Patro, S., Chatterjee, C., Mohanty, S., Singh, R., and Raghuwanshi, N. S. (2009). "Flood inundation modeling using MIKE FLOOD and remote sensing data." *Journal of the Indian Society of Remote Sensing*, 37(1), 107–118. https://doi.org/10.1007/s12524-009-0002-1

Peterson, E. W., and Wicks, C. M. (2006). "Assessing the importance of conduit geometry and physical parameters in karst systems using the storm water management model (SWMM)." *Journal of Hydrology*, 329(1), 294–305. https://doi.org/10.1016/j.jhydrol.2006.02.017

Pettitt, A. N. (1979). "A Non-Parametric Approach to the Change-Point Problem." *Journal of the Royal Statistical Society. Series C (Applied Statistics)*, [Wiley, Royal Statistical Society], 28(2), 126–135. https://doi.org/10.2307/2346729

Phien, H. N., and Fang, T.-S. E. (1989). "Maximum likelihood estimation of the parameters and quantiles of the general extreme-value distribution from censored samples." *Journal of Hydrology*, 105(1), 139–155. https://doi.org/10.1016/0022-1694(89)90100-5

Phillips, P. C. B., and Xiao, Z. (1998). "A Primer on Unit Root Testing." *Journal of Economic Surveys*, John Wiley & Sons, Ltd, 12(5), 423–470. https://doi.org/10.1111/1467-6419.00064

Piani, C., Weedon, G. P., Best, M., Gomes, S. M., Viterbo, P., Hagemann, S., and Haerter, J. O. (2010). "Statistical bias correction of global simulated daily precipitation and temperature for the application of hydrological models." *Journal of Hydrology*, 395(3), 199–215. https://doi.org/10.1016/j.jhydrol.2010.10.024

Potter, K. W. (1991). "Hydrological impacts of changing land management practices in a moderate-sized agricultural catchment." *Water Resources Research*, John Wiley & Sons, Ltd, 27(5), 845–855. https://doi.org/10.1029/91WR00076

Praskievicz, S., and Chang, H. (2009). "A review of hydrological modelling of basin-scale climate change and urban development impacts." *Progress in Physical Geography: Earth and Environment*, SAGE Publications Ltd, 33(5), 650–671. https://doi.org/10.1177/0309133309348098

Prescott, P., and Walden, A. T. (1983). "Maximum likeiihood estimation of the parameters of the three-parameter generalized extreme-value distribution from censored samples." *Journal of Statistical Computation and Simulation*, Taylor & Francis, 16(3–4), 241–250. https://doi.org/10.1080/00949658308810625

Rabori, A. M., and Ghazavi, R. (2018). "Urban Flood Estimation and Evaluation of the Performance of an Urban Drainage System in a Semi-Arid Urban Area Using SWMM." *Water Environment Research*, John Wiley & Sons, Ltd, 90(12), 2075–2082. https://doi.org/10.2175/106143017X15131012188213

Rai, P. K., Dhanya, C. T., and Chahar, B. R. (2018). "Coupling of 1D models (SWAT and SWMM) with 2D model (iRIC) for mapping inundation in Brahmani and Baitarani river delta." Natural Hazards, 92(3), 1821–1840. https://doi.org/10.1007/s11069-018-3281-4

Ranaee, E., Shoushtari, M. M., and Quchani, S. R. (2009). "The Combination of HEC-Geo-HMS, HEC-HMS and MIKE11 Software Utilize in a Two Branches River Flood Routing Modeling." *2009 Second International Conference on Environmental and Computer Science*, 317–321. https://doi.org/10.1109/ICECS.2009.62

Ranger, N., Hallegatte, S., Bhattacharya, S., Bachu, M., Priya, S., Dhore, K., Rafique, F., Mathur, P., Naville, N., Henriet, F., Herweijer, C., Pohit, S., and Corfee-Morlot, J. (2011). "An assessment of the potential impact of climate change on flood risk in Mumbai." Climatic Change, 104(1), 139–167. https://doi.org/10.1007/s10584-010-9979-2

Riahi, K., Rao, S., Krey, V., Cho, C., Chirkov, V., Fischer, G., Kindermann, G., Nakicenovic, N., and Rafaj, P. (2011). "RCP 8.5—A scenario of comparatively high greenhouse gas emissions." *Climatic Change*, 109(1), 33. https://doi.org/10.1007/s10584-011-0149-y

Riebsame, W. E., Meyer, W. B., and Turner, B. L. (1994). "Modeling land use and cover as part of global environmental change." *Climatic Change*, 28(1), 45–64. https://doi.org/10.1007/BF01094100

Rojas, R., Feyen, L., Dosio, A., and Bavera, D. (2011). "Improving pan-European hydrological simulation of extreme events through statistical bias correction of RCM-driven climate simulations." *Hydrology and Earth System Sciences*, 15(8), 2599–2620. https://doi.org/10.5194/hess-15-2599-2011

Rong, Y., Zhang, T., Zheng, Y., Hu, C., Peng, L., and Feng, P. (2020). "Three-dimensional urban flood inundation simulation based on digital aerial photogrammetry." *Journal of Hydrology*, 584, 124308. https://doi.org/10.1016/j.jhydrol.2019.124308

Rosenberg, E. A., Keys, P. W., Booth, D. B., Hartley, D., Burkey, J., Steinemann, A. C., and Lettenmaier, D. P. (2010). "Precipitation extremes and the impacts of climate change on stormwater infrastructure in Washington State." *Climatic Change*, 102(1), 319–349. https://doi.org/10.1007/s10584-010-9847-0

Rossman, L. (2010). "Storm Water Management Model User's Manual Version 5.0." Cincinnati: U.S. Environmental Protection Agency.

Rossman, L. A., and Huber, W. C. (2016). "Storm water management model reference manual." EPA/600/R-15/162A.

Rossman, L.A. (2014). “Storm Water Management Model User’s Manual Version 5.1.” USEPA: Washington, DC, USA.

Rubin, D. B. (1987). “Multiple imputation for non-response in surveys.” New York: Wiley.

Rubin, D. B. (1988). “An overview of multiple imputation. In Proceedings of the survey research methods section of the American statistical association.” *American Statistical Association,* pp 79–84.

Saghafian, B., Farazjoo, H., Bozorgy, B., and Yazdandoost, F. (2008). “Flood Intensification due to Changes in Land Use.” *Water Resources Management*, 22(8), 1051–1067. https://doi.org/10.1007/s11269-007-9210-z

Sahoo, S. N., and Sreeja, P. (2016). “Relationship between peak rainfall intensity (PRI) and maximum flood depth (MFD) in an urban catchment of Northeast India.” *Natural Hazards: Journal of the International Society for the Prevention and Mitigation of Natural Hazards*, *Springer; International Society for the Prevention and Mitigation of Natural Hazards*, vol. 83(3), pages 1527-1544, September. https://doi.org/10.1007/s11069-016-2374-1

Sarchani, S., Seiradakis, K., Coulibaly, P., and Tsanis, I. (2020). “Flood Inundation Mapping in an Ungauged Basin.” *Water* . 12(6):1–21. https://doi.org/10.3390/W12061532

Scheffer, J. (2002). “Dealing with missing data.” *Research Letters in the Information and Mathematical Sciences* 3:153–160. http://hdl.handle.net/10179/4355

Schiermeier, Q. (2011). “Increased flood risk linked to global warming.” *Nature*, 470(7334), 316. https://doi.org/10.1038/470316a

Schmidli, J., Frei, C., and Vidale, P. L. (2006). “Downscaling from GCM precipitation: a benchmark for dynamical and statistical downscaling methods.” *International Journal of Climatology*, John Wiley & Sons, Ltd, 26(5), 679–689. https://doi.org/10.1002/joc.1287

Sen, A. K., and Niedzielski, T. (2010). "Statistical Characteristics of Riverflow Variability in the Odra River Basin, Southwestern Poland." *Polish Journal of Environmental Studies*, 19(2), 387–397.

Sen, D. (2013). "Real-time rainfall monitoring and flood inundation forecasting for the city of Kolkata." *ISH Journal of Hydraulic Engineering*, Taylor & Francis, 19(2), 137–144. https://doi.org/10.1080/09715010.2013.787718

Sen, P. K. (1968). "Estimates of the Regression Coefficient Based on Kendall's Tau." *Journal of the American Statistical Association*, Taylor & Francis, 63(324), 1379–1389. https://doi.org/10.2307/2285891

Serencam, U. (2019). "Innovative trend analysis of total annual rainfall and temperature variability case study: Yesilirmak region, Turkey." *Arabian Journal of Geosciences*, 12(23), 704. https://doi.org/10.1007/s12517-019-4903-1

Shahid, S., Wang, X.-J., Harun, S. Bin, Shamsudin, S. B., Ismail, T., and Minhans, A. (2016). "Climate variability and changes in the major cities of Bangladesh: observations, possible impacts and adaptation." *Regional Environmental Change*, 16(2), 459–471. https://doi.org/10.1007/s10113-015-0757-6

Silva, F. V, Bonumà, N. B., and Uda, P. (2014). "FLOOD MAPPING IN URBAN AREA USING HEC-RAS MODEL SUPPORTED BY GIS." *Proceedings of the 6th International Conference on Flood Management*, Sao Paulo, Brazil.

Singh, G., Panda, R. K., and Nair, A. (2020). "Regional scale trend and variability of rainfall pattern over agro-climatic zones in the mid-Mahanadi River basin of eastern India." Journal of Hydro-environment Research, 29, 5–19. https://doi.org/10.1016/j.jher.2019.11.001

Singh, R. N., Sah, S., Das, B., Potekar, S., Chaudhary, A., and Pathak, H. (2021). "Innovative trend analysis of spatio-temporal variations of rainfall in India during 1901–2019." *Theoretical and Applied Climatology*, 145(1), 821–838. https://doi.org/10.1007/s00704-021-03657-2

Sovilj, D., Eirola, E., Miche, Y., Björk, K.-M., Nian, R., Akusok, A., and Lendasse, A. (2016). "Extreme learning machine for missing data using multiple imputations." *Neurocomputing*, 174, 220–231. https://doi.org/10.1016/j.neucom.2015.03.108

Spearman, C. (1987). "The Proof and Measurement of Association between Two Things." *The American Journal of Psychology*, University of Illinois Press, 100(3/4), 441–471. https://doi.org/10.2307/1422689

Stow, D. A., and Chen, D. M. (2002). "Sensitivity of multitemporal NOAA AVHRR data of an urbanizing region to land-use/land-cover changes and misregistration." *Remote Sensing of Environment*, 80(2), 297–307. https://doi.org/https://doi.org/10.1016/S0034-4257(01)00311-X

Subramanya, K. (2018) "Engineering Hydrology," 4th Edition, Tata McGraw-Hill Publishing, New Delhi

Suklitsch, M., Gobiet, A., Leuprecht, A., and Frei, C. (2008). "High Resolution Sensitivity Studies with the Regional Climate Model CCLM in the Alpine Region." *Meteorologische Zeitschrift*, Schweizerbart Science Publishers, Stuttgart, Germany, 17(4), 467–476. https://doi.org/10.1127/0941-2948/2008/0308

Suklitsch, M., Gobiet, A., Truhetz, H., Awan, N. K., Göttel, H., and Jacob, D. (2011). "Error characteristics of high-resolution regional climate models over the Alpine area." *Climate Dynamics*, 37(1), 377–390. https://doi.org/10.1007/s00382-010-0848-5

Sun, Q., Miao, C., AghaKouchak, A., and Duan, Q. (2017). "Unraveling anthropogenic influence on the changing risk of heat waves in China." *Geophysical Research Letters*, John Wiley & Sons, Ltd, 44(10), 5078–5085. https://doi.org/https://doi.org/10.1002/2017GL073531

Suriya, S., and Mudgal, B. V. (2012). "Impact of urbanization on flooding: The Thirusoolam sub watershed – A case study." *Journal of Hydrology*, 412–413, 210–219. https://doi.org/10.1016/j.jhydrol.2011.05.008

Tabari, H., and Willems, P. (2015). “Investigation of streamflow variation using an innovative trend analysis approach in northwest Iran.” *E-proc of the 36th IAHR World Cong*., The Hague.

Talukdar, G., Swain, J. B., and Patra, K. C. (2021). “Flood inundation mapping and hazard assessment of Baitarani River basin using hydrologic and hydraulic model.” *Natural Hazards*, 109(1), 389–403. https://doi.org/10.1007/s11069-021-04841-3

Tan, X., and Gan, T. Y. (2015). “Nonstationary Analysis of Annual Maximum Streamflow of Canada.” *Journal of Climate*, American Meteorological Society, Boston MA, USA, 28(5), 1788–1805. ttps://doi.org/10.1175/JCLI-D-14-00538.1

Teng, J., Jakeman, A. J., Vaze, J., Croke, B. F. W., Dutta, D., and Kim, S. (2017). “Flood inundation modelling: A review of methods, recent advances and uncertainty analysis.” *Environmental Modelling & Software*, 90, 201–216. https://doi.org/10.1016/j.envsoft.2017.01.006

Teutschbein, C., and Seibert, J. (2012). “Bias correction of regional climate model simulations for hydrological climate-change impact studies: Review and evaluation of different methods.” *Journal of Hydrology*, 456–457, 12–29. https://doi.org/10.1016/j.jhydrol.2012.05.052

Theil, H. (1950). “A rank-invariant method of linear and polynomial regression analysis.” *Proc. of the Royal Netherlands Academy of Sciences*, Series A 53:386–392.

Thomson, A. M., Calvin, K. V, Smith, S. J., Kyle, G. P., Volke, A., Patel, P., Delgado-Arias, S., Bond-Lamberty, B., Wise, M. A., Clarke, L. E., and Edmonds, J. A. (2011). “RCP4.5: a pathway for stabilization of radiative forcing by 2100.” *Climatic Change*, 109(1), 77. https://doi.org/10.1007/s10584-011-0151-4

Thrasher, B., Maurer, E. P., McKellar, C., and Duffy, P. B. (2012). “Technical Note: Bias correcting climate model simulated daily temperature extremes with quantile mapping.” *Hydrology and Earth System Sciences*, 16(9), 3309–3314. https://doi.org/10.5194/hess-16-3309-2012

Timbadiya, P., Patel, P., and Porey, P. (2014). "A 1D–2D Coupled Hydrodynamic Model for River Flood Prediction in a Coastal Urban Floodplain." *Journal of Hydrologic Engineering*, American Society of Civil Engineers, 20(2), 5014017. https://doi.org/10.1061/(ASCE)HE.1943-5584.0001029

Tomozeiu, R., Stefan, S., and Busuioc, A. (2005). "Winter precipitation variability and large-scale circulation patterns in Romania." *Theoretical and Applied Climatology*, 81(3), 193–201. https://doi.org/10.1007/s00704-004-0082-3

Tsubaki, R., and Fujita, I. (2010). "Unstructured grid generation using LiDAR data for urban flood inundation modelling." *Hydrological Processes*, John Wiley & Sons, Ltd, 24(11), 1404–1420. https://doi.org/10.1002/hyp.7608

Turco, M., Llasat, M. C., Herrera, S., and Gutiérrez, J. M. (2017). "Bias correction and downscaling of future RCM precipitation projections using a MOS-Analog technique." *Journal of Geophysical Research: Atmospheres*, John Wiley & Sons, Ltd, 122(5), 2631–2648. https://doi.org/10.1002/2016JD025724

US Army Corps of Engineers (USACE). (2010). "River Analysis System HEC-RAS: Applications Guide." *Hydrologic Engineering Center*, Davis, CA – United States of America.

USACE. (2010). "HEC-RAS River analysis system, Hydraulic reference manual, Version 4.1." *USACE, Davis*, CA, USA

van Gelder, P., Wang, W., and Vrijling, J.K. (2006). "Statistical estimation methods for extreme hydrological events." In: Vasiliev O., van Gelder P., Plate E., Bolgov M. (eds) Extreme Hydrological Events: New Concepts for Security. *NATO Science Series*, vol 78. Springer, Dordrecht. https://doi.org/10.1007/978-1-4020-5741-0_15

Vemula, S., Raju, K. S., Veena, S. S., and Kumar, A. S. (2019). "Urban floods in Hyderabad, India, under present and future rainfall scenarios: a case study." *Natural Hazards*, 95(3), 637–655. https://doi.org/10.1007/s11069-018-3511-9

Verma, M. K., and Swain, S. (2016). "Statistical Analysis of Precipitation over Seonath River Basin." *International Journal of Applied Engineering Research* 11(4):2417–2423. https://doi.org/10.22161/ijaers.5.1.20

Viera, A. J., and Garrett, J. M. (2005). "Understanding inter-observer agree- ment: the kappa statistic." Family Med. 37, 360–363.

Villarini, G., Smith, J. A., Serinaldi, F., Bales, J., Bates, P. D., and Krajewski, W. F. (2009). "Flood frequency analysis for nonstationary annual peak records in an urban drainage basin." *Advances in Water Resources*, 32(8), 1255–1266. https://doi.org/10.1016/j.advwatres.2009.05.003

Vorosmarty, C. J., Pamela, G., Joseph, S., and Lammers. R. (2000). "Global Water Resources: Vulnerability from Climate Change and Population Growth." *Science*, American Association for the Advancement of Science, 289(5477), 284–288. https://doi.org/10.1126/science.289.5477.284

Wang, G., Liu, J., Kubota, J., and Chen, L. (2007). "Effects of land-use changes on hydrological processes in the middle basin of the Heihe River, northwest China." *Hydrological Processes*, John Wiley & Sons, Ltd, 21(10), 1370–1382. https://doi.org/10.1002/hyp.6308

Wang, Q. J. (1990). "Estimation of the GEV distribution from censored samples by method of partial probability weighted moments." *Journal of Hydrology*, 120(1), 103–114. https://doi.org/10.1016/0022-1694(90)90144-M

Wang, Q. J. (1996a). "Using partial probability weighted moments to fit the extreme value distributions to censored samples." *Water Resources Research*, John Wiley & Sons, Ltd, 32(6), 1767–1771. https://doi.org/10.1029/96WR00352

Wang, Q. J. (1996b). "Direct Sample Estimators of L Moments." *Water Resources Research*, John Wiley & Sons, Ltd, 32(12), 3617–3619. https://doi.org/10.1029/96WR02675

Wang, Q., Xu, Y., Wang, Y., Zhang, Y., Xiang, J., Xu, Y., and Wang, J. (2020). "Individual and combined impacts of future land-use and climate conditions on extreme hydrological

events in a representative basin of the Yangtze River Delta, China." Atmospheric Research, 236, 104805. https://doi.org/10.1016/j.atmosres.2019.104805

Wang, W., van Gelder, P. H. A. J. M., and Vrijling, J. K. (2005). "Trend and stationarity analysis for stream flow processes of rivers in western Europe in the 20th century." *IWA International Conference on Water Economics, Statistics, and Finance*, International Water Association (IWA), London, U.K.

Wang, W., Vrijling, J. K., Van Gelder, P. H. A. J. M., and Ma, J. (2006). "Testing for nonlinearity of streamflow processes at different timescales." *Journal of Hydrology*, 322(1), 247–268. https://doi.org/10.1016/j.jhydrol.2005.02.045

Wang, Y., Xu, Y., Tabari, H., Wang, J., Wang, Q., Song, S., and Hu, Z. (2020). "Innovative trend analysis of annual and seasonal rainfall in the Yangtze River Delta, eastern China." *Atmospheric Research*, 231, 104673. https://doi.org/10.1016/j.atmosres.2019.104673

Wheater, H., Sorooshian, S., and Sharma, K. (Eds.). (2007). "Hydrological Modelling in Arid and Semi-Arid Areas." *International Hydrology Series*, Cambridge University Press, Cambridge. https://doi.org/10.1017/CBO9780511535734

Wibig, J., and Glowicki, B. (2002). "Trends of minimum and maximum temperature in Poland." *Climate Research*. 20:123–133. https://doi.org/10.3354/cr020123

Widmann, M., Bretherton, C. S., and Salathé, E. P. (2003). "Statistical Precipitation Downscaling over the Northwestern United States Using Numerically Simulated Precipitation as a Predictor." *Journal of Climate*, American Meteorological Society, Boston MA, USA, 16(5), 799–816. https://doi.org/10.1175/1520-0442(2003)016<0799:SPDOTN>2.0.CO;2

Wijngaard, J. B., Klein Tank, A. M. G., and Können, G. P. (2003). "Homogeneity of 20th century European daily temperature and precipitation series." *International Journal of Climatology*, John Wiley & Sons, Ltd, 23(6), 679–692. https://doi.org/10.1002/joc.906

Willems, P., Arnbjerg-Nielsen, K., Olsson, J., and Nguyen, V. T. V. (2012). "Climate change impact assessment on urban rainfall extremes and urban drainage: Methods and

shortcomings." *Atmospheric Research*, Elsevier B.V., 103, 106–118. https://doi.org/10.1016/j.atmosres.2011.04.003

Winkler, J. A., Guentchev, G. S., Liszewska, M., Perdinan, , and Tan, P.-N. (2011). "Climate Scenario Development and Applications for Local/Regional Climate Change Impact Assessments: An Overview for the Non-Climate Scientist." *Geography Compass*, John Wiley & Sons, Ltd, 5(6), 301–328. https://doi.org/10.1111/j.1749-8198.2011.00426.x

Wu, H., Li, X., and Qian, H. (2018). "Detection of Anomalies and Changes of Rainfall in the Yellow River Basin, China, through Two Graphical Methods." *Water*. https://doi.org/10.3390/w10010015

Xu, H. (2006). "Modification of normalised difference water index (NDWI) to enhance open water features in remotely sensed imagery." *International Journal of Remote Sensing*, Taylor & Francis, 27(14), 3025–3033. https://doi.org/10.1080/01431160600589179

Xu, H. (2010). "Analysis of impervious surface and its impact on urban heat environment using the normalized difference impervious surface index (NDISI)." *Photogrammetric Engineering & Remote Sensing*, vol. 76(5), pp. 557-565,. https://doi.org/10.14358/PERS.76.5.557

Xu, T., Jia, H., Wang, Z., Mao, X., and Xu, C. (2017). "SWMM-based methodology for block-scale LID-BMPs planning based on site-scale multi-objective optimization: a case study in Tianjin." *Frontiers of Environmental Science & Engineering*, 11(4), 1. https://doi.org/10.1007/s11783-017-0934-6

Yalcin, E. (2020). "Assessing the impact of topography and land cover data resolutions on two-dimensional HEC-RAS hydrodynamic model simulations for urban flood hazard analysis." *Natural Hazards*, 101(3), 995–1017. https://doi.org/10.1007/s11069-020-03906-z

Yan, Z.-W., Wang, J., Xia, J.-J., and Feng, J.-M. (2016). "Review of recent studies of the climatic effects of urbanization in China." *Advances in Climate Change Research*, 7(3), 154–168. https://doi.org/https://doi.org/10.1016/j.accre.2016.09.003

Yoo, S.-H. (2007). "Urban Water Consumption and Regional Economic Growth: The Case of Taejeon, Korea." *Water Resources Management*, 21(8), 1353–1361. https://doi.org/10.1007/s11269-006-9087-2

Yozgatligil, C., and Yazici, C. (2016). "Comparison of homogeneity tests for temperature using a simulation study." *International Journal of Climatology*, John Wiley & Sons, Ltd, 36(1), 62–81. https://doi.org/10.1002/joc.4329

Yue, S., Pilon, P., and Phinney, B. O. B. (2003). "Canadian streamflow trend detection: impacts of serial and cross-correlation." *Hydrological Sciences Journal*, Taylor & Francis, 48(1), 51–63. https://doi.org/10.1623/hysj.48.1.51.43478

Zamir, F., Hanif, F., and Naz, S. (2021). "Extreme rainfall frequency analysis for Balakot, Pakistan, using Gumbel's distribution." *Arabian Journal of Geosciences*, 14(13), 1283. https://doi.org/10.1007/s12517-021-06780-6

Zekâi, Ş. (2012). "Innovative Trend Analysis Methodology." *Journal of Hydrologic Engineering*, American Society of Civil Engineers, 17(9), 1042–1046. https://doi.org/10.1061/(ASCE)HE.1943-5584.0000556

Zha, Y., Gao, J., and Ni, S. (2003). "Use of normalized difference built-up index in automatically mapping urban areas from TM imagery." *International Journal of Remote Sensing*, Taylor & Francis, 24(3), 583–594. https://doi.org/10.1080/01431160304987

Zhang, S., and Pan, B. (2014). "An urban storm-inundation simulation method based on GIS." *Journal of Hydrology*, 517, 260–268. https://doi.org/10.1016/j.jhydrol.2014.05.044

Zhao, G., Xu, Z., Pang, B., Tu, T., Xu, L., and Du, L. (2019). "An enhanced inundation method for urban flood hazard mapping at the large catchment scale." *Journal of Hydrology*, 571, 873–882. https://doi.org/10.1016/j.jhydrol.2019.02.008

Zhou, Z., Wang, L., Lin, A., Zhang, M., and Niu, Z. (2018). “Innovative trend analysis of solar radiation in China during 1962–2015.” *Renewable Energy*, 119, 675–689. https://doi.org/10.1016/j.renene.2017.12.052

Zhu, Z., Chen, Z., Chen, X., and He, P. (2016). “Approach for evaluating inundation risks in urban drainage systems.” *Science of The Total Environment*, 553, 1–12. https://doi.org/10.1016/j.scitotenv.2016.02.025

Zimmermann, E., Bracalenti, L., Piacentini, R., and Inostroza, L. (2016). “Urban Flood Risk Reduction by Increasing Green Areas for Adaptation to Climate Change.” *Procedia Engineering*, 161, 2241–2246. https://doi.org/10.1016/j.proeng.2016.08.822

Zope, P. E., Eldho, T. I., and Jothiprakash, V. (2017). “Hydrological impacts of land use–land cover change and detention basins on urban flood hazard: a case study of Poisar River basin, Mumbai, India.” *Natural Hazards*, 87(3), 1267–1283. https://doi.org/10.1007/s11069-017-2816-4

Publications from the thesis:

In Peer Reviewed Journals

- **Seenu P Z**, Venkata Rathnam E, and Jayakumar K V (2019) "Visualisation of urban flood inundation using SWMM and 4D GIS." Spatial Information Research. doi:10.1007/s41324-019-00306-9 (ESCI)
- **Seenu P Z** and Jayakumar K V (2020) "Optimisation of Bias Correction Methods for RCM Precipitation Data and their Effects on Extremes." Advances in Intelligent Systems and Computing https://doi.org/10.1007/978-981-15-3215-3_9 (SCOPUS)
- **Seenu P Z** and Jayakumar K V (2021) "Comparative study of innovative trend analysis technique with Mann-Kendall tests for extreme rainfall" Arabian Journal of Geosciences. https://doi.org/10.1007/s12517-021-06906-w (SCIE)

In Conference Proceedings

- **Seenu P Z**, E V Rathnam and K V Jayakumar, "Flood inundation study of part of Hyderabad city using SWMM AND GIS" Hydro-2017, Ahmedabad, India
- **Seenu P Z** and K V Jayakumar, "Statistical trend, homogeneity and stationarity analysis of annual rainfall for Amaravati - Andhra Pradesh" TSSC-2018, NIT Warangal.
- **Seenu P Z** and K V Jayakumar, "Optimisation of Bias Correction Methods for RCM Precipitation Data and their Effects on Extremes" NOIEAS-2019, NIT Warangal.
- **Seenu P Z**, Rashmi Yadav and K V Jayakumar, "2D Urban Flood Inundation Model Using HEC-RAS – Case Study" APHW-2019, IIT Roorkee.

- **Seenu P Z** and K V Jayakumar, "Flood Mitigation using Low Impact Development in Urbanising Area – A Case Study" ITHES2021, NIT Warangal.

ACKNOWLEDGEMENT

First and foremost, I would like to express immense gratitude to my supervisor ***Prof. K V Jayakumar***. It has been a great learning experience working with him, and a lot of credit for my achievements and accomplishments goes to my supervisor. His constant support and guidance have always motivated me to work and aided me to channelize my energy on the correct path. I have learned a lot of new things, both in my career as well as in life, during the time I spent with my supervisor.

I would like to express my sincere thanks to the members of the Doctoral Scrutiny Committee, Prof. N V Umamahesh, Dr K Venkat Reddy, Prof. Y N Reddy and Chairman Prof. P. Rathish Kumar, for their kind suggestion on the research. I am also very grateful to my teachers Prof. P. Anand Raj, and Late. Prof. E.Venkata Rathnam for the encouragement and support.

I am thankful to many researcher scholars and friends who have directly or indirectly helped me in this journey. I should point out the immense support offered by Ms J S S Vani, Dr Uday Kumar, Ms Soumyashree Dixit, Ms Sreelatha, and Mr Satheesh Kumar. Their continuous support during my research work in making impactful research observations and publishing papers. I am also blessed to have Mr Nikhil Thoppil and Mr Kavin Kumar as my best companions during my life at NIT Warangal and share all our happiness and worries. I

am also thankful to my batch mates at NIT Warangal, all PG and UG friends, for the joyful moments at NIT Warangal Campus.

On a special note, I would like to acknowledge my father, Mr A Peerumohammed, and my mother, Mrs A Zahira. I am always thankful for their prayers and belief in me. Their prayers helped me to move forward in life. I am also thankful to my in-laws, especially Mrs Razeena, for her encouragement and support. I thank my brother Mr Ajeesh Mohammed for the countless help he gave me to achieve my goals. I am grateful to my supportive husband, Mr Aneesh Latheef. I am eternally grateful to my son, Master Ahaan S Aneesh, who patiently bore with me throughout the period of thesis writing.

Above all, I thank Lord Almighty for his immense blessings showered upon me, without which this work would not have become successful.

Seenu P Z